An Investigation in Optimising RF MEMS Switching for Integrated Mobile Wireless Systems

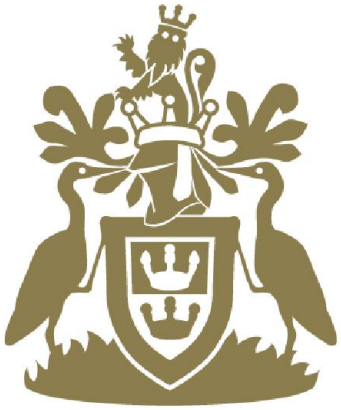

Mohammed Abdullah Al-Amin

Department of Engineering and Built Environment

Anglia Ruskin University

This dissertation is submitted for the degree of

Doctor of Philosophy

Faculty of Science and Technology

August 2017

I would like to dedicate this thesis to my parents

Fatema Akthar

and

Ayub Ali

Declaration

I declare that this thesis is my own original work, except for references. This thesis has not been submitted, in whole or in part, to any universities, except for the qualification of Doctor of Philosophy (PhD) at Anglia Ruskin University.

Mohammed Abdullah Al-Amin

August 2017

Acknowledgements

I would like to express my sincere gratitude to my supervisors:

Dr. Sufian Yousef for his extra support and encouragement during my PhD. I am also grateful for his guidance and motivation, throughout this thesis.

A very special thanks to Barry Morris for his industrial experience, technical knowledge and expertise in the field of electronics engineering and nano technology. I would also like to thank him for providing essential guidance and encouragement in understanding RF MEMS technology and inspiring me to innovate.

I would like to also thank Professor Hassan Shirvani for encouraging me to critically think.

Finally, I would like to thank my parents for their moral and financial support during the course of this PhD, and providing me with encouragement throughout my whole life.

Abstract

Radio Frequency Micro Electromechanical Systems (RF MEMS) technology is used to help switch, filter or tune signals from Direct Current to RF. RF MEMS switches are known to provide good isolation with low insertion loss and can be applied to a wide range of frequencies with almost no power consumed to drive them, which provides an advantage for integrated mobile wireless systems. Despite the benefits, RF MEMS switches have not seen a rapid development for commercialisation in the integrated mobile wireless systems market because of reliability issues and high actuation voltage requirements, which makes additional voltage drive circuitry necessary. This in turn makes the overall switch larger in size. Due to these shortfalls, this research undertakes an investigation by optimising RF MEMS switches.

This thesis presents an RF MEMS switch for use in mobile systems, based on the optimisation of a cantilever, ohmic type switch. The optimisation resulted in five major iterations, each providing improvements over the cantilever. The final optimised iteration researched is the 'S' Shaped, Split Pivot, Seesaw, Double-Pole Double-Throw (DPDT) switch. This optimised design provides capabilities of high RF isolation. It provides low actuation voltages (by using 'Delta Plates'). The switch takes advantage of an 'S' Shaped, Split Pivot, allowing the pivot to flex with less force, which reduces actuation voltage. The optimised designs provide a selection of switches, which take advantage of low voltages used by mobile systems (i.e. $\leq$ 5V). The 'S' shaped pivot has a lower von mises stress (15MPa), which is below the yield strength of copper (70 MPa), allowing the design to return to its original state without deforming. This proved a 97.8% reduction in von mises stress over the cantilever and a reduction of actuation voltage from 30V down to 1.13V. The functionality of the switch is increased by 4 times to provide DPDT switching over the cantilever's Single-Pole Single-Throw (SPST) switching. Also, the 'S' Shaped, Split Pivot, Seesaw DPDT switch, maintains a higher isolation over its predecessor (cantilever) with an average isolation of -102.89 dB over a frequency range from 5GHz to 45GHz. This provides a 246% improvement to that of the cantilever's isolation.

A Finite Element Analysis approach was used, with mathematical analysis to validate the Intellisuite simulation tool. A secondary validation was conducted, with known practical cantilever results against the Intellisuite Simulation tool for the electromechanical characteristics of the switch. The electromagnetics (EM) characteristics of the switch were also validated, with the Computer Simulation Technology (CST) electromagnetic simulation tool, against the cantilever's practical results. The optimisation followed a linear approach, with each component of the switch having incremental improvements, such as: Contacts, Beam, Electrostatic Parallel Plates and Pivots. The research has discovered that RF MEMS switches (i.e. cantilevers) are larger than the micro size, require high actuation voltages and have increased von mises stress. The optimisations focused on four areas of improvements to the characteristics of the switch and addressed them as follows: reducing actuation voltage, decreasing von mises stress, increasing isolation of the contacts and expanding functionality.

Key words: RF MEMS, Switching, Seesaw, DPDT, Actuation Voltage, Von mises

Contents

Contents i

List of Figures v

List of Tables xi

Abbreviations xiii

1 Introduction 1

1.1 MEMS Technology Overview 2

1.1.1 Dr. Richard Phillips Feynman 3

1.1.2 The Growth of MEMS Technology 4

1.2 RF MEMS 6

1.2.1 Present Status of RF MEMS 6

1.2.2 Ohmic Type Switches 7

1.2.3 Capacitive Type Switch 7

1.3 Methodology 8

1.4 Research Questions 10

1.5 Aims and Objectives 12

1.6 Summary of Current Technology 13

1.7 Thesis Structure 16

2 Literature Review 18

2.1 Materials 18

2.2 Stress and Reliability 21

2.2.1 Stress 21

2.2.2 Reliability 23

2.2.3 Temperature Reliability 26

2.2.4 Contact Reliability 27

2.2.5 Hermetic Sealing 28

2.3 Simulation 28

2.3.1 Electromagnetic Simulation 30
2.3.2 Modelling 31
2.3.3 Design Optimisation 33
2.4 Actuation Voltage Levels 37
2.5 Switching Methods 39
2.6 Contact Analysis 42
3 Mathematical Modelling 45
3.1 Electrostatic Actuation 45
3.2 Theoretical Modelling of a Cantilever Beam 46
3.2.1 Moment of Inertia of a beam 47
3.2.2 Displacement of the beam 47
3.2.3 Extension of the beam 48
3.2.4 Stress and Strain of the beam 48
3.2.5 Spring Constant (Elastic Recovery) of the beam 49
3.3 Resonant Frequency 50
3.3.1 Resonant Frequency of a Beam 50
3.4 Electromagnetics Two Port Network Analysis 53
3.4.1 Two Port Network 53
3.5 Finite Element Modelling 57
4 Engineering Design Process 59
4.1 Selection of Software Modelling and Simulation Tools 59
4.2 Preliminary Sketch Modelling 62
4.3 Experimental Methodologies 63
4.3.1 Implementing Design to Intellisuite 3DBuilder 63
4.3.2 Setting Up Intellisuite TEM Simulation Analysis 64
4.3.3 Simulation Processes 69
5 RF MEMS Switch Design 94

5.1 RF MEMS 94
5.1.1 RF MEMS within Mobile Systems Communication: Advantages and Disadvantages 96
5.1.2 Real World use of RF MEMS Switches 97
5.2 Initial Design 98
5.3 Straight Pivot Seesaw RF MEMS Switch 102
5.4 'S' Shaped Pivot Seesaw RF MEMS Switch 105
5.5 'S' Shaped Pivot with Delta Electrostatic Plates RF MEMS Switch 106
5.6 'S' Shaped Split Pivot with Delta Electrostatic Plates RF MEMS Switch 108
6 Results and Validation 109
6.1 Grid Independency 109
6.2 Simulation Against Mathematical Analysis 110
6.2.1 Electrostatic Force 111
6.2.2 Displacement of the Beam 112
6.2.3 Resonant Frequency 114
6.3 Validation of the HRL Cantilever Against Simulation 116
6.3.1 Validation of Experimental Results Against Simulation 116
6.4 Design Results 118
6.4.1 Stress and Electrostatic Characteristics 118
6.4.2 EM Characteristics 120
7 Discussion and Results Analysis 122
7.1 Validation 122
7.1.1 Grid Independency 123
7.1.2 Validation of Simulation against Mathematical Analysis 125
7.1.3 Validation of Simulation against Experimental Results 135
7.2 Design Result Analysis 136
7.2.1 Stress and Electrostatic Characteristics 137

7.2.2 Electromagnetic Characteristics 162
8 Conclusion 168
8.1 Future Work 173
References 174
Self-Publications 183
Appendix A 184
Appendix B 187
MEMS Fabrication Techniques 187
Conventional IC Fabrication process 187
Bulk Micromachining 188
Surface Micromachining 188
Fusion Bonding 189
LIGA and Sacrificial LIGA 190
Appendix C 191
Result Tables 191

List of Figures

Figure 1.1: (label added for this reprint) Log2 of the number of components per integrated function versus year (G. E. Moore 2006) 4
Figure 1.2: Intel Logic Transistor Density prediction (Intel and Mistry, K 2017) 5
Figure 1.3: Ohmic Type Switch circuit 7
Figure 1.4: Capacitive type Switch circuit 7
Figure 1.5: Methodology Process 9
Figure 1.6: Diagram of the thesis structure 17
Figure 3.1: Schematic diagram of the electrostatic force on parallel plates 46
Figure 3.2: Image (Ansari, Cho 2009) , of a fixed-free beam but edited to illustrate the Equation 3.12 51
Figure 3.3: (Ansari, Cho 2009) Step Profile Cantilever 52
Figure 3.4: Two Port Network diagram 54
Figure 3.5: Two Port Network analysis setup for S11 parameters when Port 1 is active and port 2 is 0 (short), Port 1 is reflected 55
Figure 3.6: Two Port Network analysis setup for S21 parameters when Port 1 is active and port 2 is 0, Port 1 to 2 is pass though. 55
Figure 3.7: Two Port Network analysis setup for S22 parameters when Port 2 is active and port 1 is 0. Port 2 is reflected 55
Figure 3.8: Two Port Network analysis setup for S22 parameters when Port 2 is active and port 1 is 0. Port 2 to 1 is passed though 56
Figure 3.9: Example of a Meshed Structure with Elements and Nodes indicated 58
Figure 3.10: Example of Mesh Structure with Highlighted Nodes on a Surface Wire Mesh View 58
Figure 4.1: Preliminary sketch of initial RF MEMS design 62
Figure 4.2: Implementation of sketches to a simulated model 63
Figure 4.3: Validation options on 3DBuild 64
Figure 4.4: Validation error results 64
Figure 4.5: VisualEase representation of the RF MEMS switch simulation displacement 64
Figure 4.6: Example of the assignment to the seesaw model 66
Figure 4.7: Intellisuite Materials database within TEM Simulator 67

Figure 4.8: Boundary assignment which is shown in red for TEM 67
Figure 4.9: Applying loads to the switch for TEM simulation 68
Figure 4.10: Static Simulation Settings.....70
Figure 4.11: Simulation Set Up of Static Analysis with Contact analysis enabled ...72
Figure 4.12: Z axis Displacement vs Voltage (Result shown using 2DViewer) 72
Figure 4.13: Simulation Set Up for maximum mode contribution at the pull-in voltage.....73
Figure 4.14: Setting of strain energy calculation for mode 1.....74
Figure 4.15: Setting of strain energy calculation for mode 2.....74
Figure 4.16: Simulation Set Up of Capacitance Analysis.....75
Figure 4.17: Device property 76
Figure 4.18: Wiring A circuit.....77
Figure 4.19: Simulation Setup (Press OK button to start simulation) 78
Figure 4.20: Chart Template Set Up 79
Figure 4.21: Capacitance vs Voltage 79
Figure 4.22: Simulation Setting for Frequency Response 81
Figure 4.23: Example of Natural Frequency Result Displayed in Intellisuite 82
Figure 4.24: Graphical representation of dynamic voltage used for contact release simulation.....84
Figure 4.25: Simulation Setting for Dynamic Contact Release 84
Figure 4.26: Tabular Voltage selection.....85
Figure 4.27: Setting the Tabular Voltages 85
Figure 4.28: Flow Diagram of the CST Simulation Process.....88
Figure 4.29: Setup of the simulation for High Frequency 88
Figure 4.30: Frequency Domain Solver Parameters 89
Figure 4.31: Simulation setting options available on the Simulation tab ribbon.....89
Figure 4.32: Frequency Range Settings for CST to run analysis within.....89
Figure 4.33: Background Properties (left) and Boundary Conditions (right) used for all designs.....90
Figure 4.34: Waveguide Port setup window 91
Figure 4.35: Setting up E-Field monitors using the Field Monitor setup window 92
Figure 4.36: Example of Results from CST S-Parameters 93
Figure 5.1: Radant MEMS RMSW221 SPDT switch DC to 20 GHz 97
Figure 5.2: Radant MEMS RMSW240 SP4T Switch DC to 20 GHz.....98

Figure 5.3: Simplified Block Diagram of a transceiver setup.....98
Figure 5.4: HRL RF MEMS Switch from Gabriel M. Rebeiz, RF MEMS Theory, Design and Technology, 2003, p 135.....99
Figure 5.5: Daniel Hyman et al, 1999, HRL Cantilever SPST Switch.....100
Figure 5.6: Modelled on Intellisuite TEM Simulation tool.....100
Figure 5.7: (Left) Single Straight Pivot Seesaw DPDT Switch with pivot width of 5 μm, (Right) Split Pivot Seesaw DPDT Switch with Pivot width 2 μm each and a spacing of 1 μm between them.....102
Figure 5.8: Stress for various pivot thicknesses to achieve a 1 μm displacement...103
Figure 5.9: Actuation Voltage for various pivot thicknesses to achieve a 1 μm displacement.....103
Figure 5.10: Model of the Straight Pivot Seesaw RF MEMS Switch v1.....104
Figure 5.11: Model of the Straight Pivot Seesaw RF MEMS Switch v2.....104
Figure 5.12: ‘S’ Shaped Spring Pivot showing the Link Segments.....105
Figure 5.13: ‘S’ Shaped Pivot Seesaw RF MEMS Switch.....106
Figure 5.14: ‘S’ Shaped Pivot with Delta Electrostatic Plates RF MEMS Switch..107
Figure 5.15: 'S' Shaped Split Pivot View.....108
Figure 6.1: Diagram of the electrostatic plates and its dimensions (Left) and the beam and its dimensions (Right).....111
Figure 6.2: Fixed Electrostatic plates on Intellisuite TEM.....111
Figure 6.3: (Left) Visual Representation of the model prior to simulation, (Right) Visual representation of the beam model after simulation, with colour coded results information.....113
Figure 6.4: Dimension of the HRL cantilever beam from Daniel Hyman et al, 1999 116
Figure 7.1: Grid Independency comparison of different mesh sizes.....124
Figure 7.2: Dimensions of two parallel electrostatic plates.....125
Figure 7.3: 3D Representation of two parallel plates.....127
Figure 7.4: Electrostatic Force Equation vs Simulated Average force on face vs Simulated average force on centre nodes on face.....127
Figure 7.5: Force Pressure distribution though the cross section of X and Y axis..128
Figure 7.6: Pressure distribution of force in MPa on one side of the plate.....129

Figure 7.7: Dimensions of the Fixed-Free Beam used for the ‘Displacement of a Beam’ Simulation 131
Figure 7.8: Results of the ‘Displacement of a Beam’ Simulation verses Mathematical 131
Figure 7.9: Fixed-Free Beam Dimensions with variable length from 10 µm to 20 µm 133
Figure 7.10: Simulated verses Mathematical Frequency response of a beam with varied length 134
Figure 7.11: Displacement vs Voltage of HRL Cantilever Beam Switch 135
Figure 7.12: Bar Graph Results of the Actuation Voltage of the switches 137
Figure 7.13: Bar Graph Results of the Displacement of the switches for total Air Gap 138
Figure 7.14: Bar graph of von mises Stress of the switches (rounded to the closest 1 MPa) 139
Figure 7.15: von Mises Stress for HRL Cantilever SPST Switch 140
Figure 7.16: von Mises Stress for Scaled Down Version of the HRL Cantilever SPST Switch 140
Figure 7.17: von Mises Stress for Straight Pivot Seesaw Switch DPDT Switch v1 141
Figure 7.18: von Mises Stress for Straight Pivot Seesaw DPDT Switch v2 141
Figure 7.19: von Mises Stress for 'S' Shaped Pivot Seesaw DPDT Switch 142
Figure 7.20: von Mises Stress for 'S' Shaped Pivot Seesaw DPDT Switch with Delta Plates 142
Figure 7.21: Graph form representation of the Voltage vs Displacement of HRL Cantilever SPST Switch 143
Figure 7.22: Graph form representation of the Voltage vs Displacement of Scaled Down version of HRL Cantilever SPST Switch by 10 times 144
Figure 7.23: Graph form representation of the Voltage vs Displacement of Straight Pivot Seesaw DPDT Switch v1 145
Figure 7.24: Graph form representation of the Voltage vs Displacement of Straight Pivot Seesaw DPDT Switch v2 145
Figure 7.25: Graph form representation of the Voltage vs Displacement of ‘S’ Shaped Pivot Seesaw DPDT Switch 146
Figure 7.26: Graph form representation of the Voltage vs Displacement of ‘S’ Shaped Pivot with Delta Angled Electrostatic Plates DPDT Switch 146

Figure 7.27: Graph form representation of the Voltage vs Displacement of ‘S’ Shaped Split Pivot with Delta Angled Electrostatic Plates DPDT Switch 147
Figure 7.28: Contact Analysis for the HRL Cantilever SPST Switch 148
Figure 7.29: Contact Analysis for the Scaled Down version of HRL Cantilever SPST Switch by 10 times 149
Figure 7.30: Contact Analysis for the Straight Pivot Seesaw DPDT Switch, v1 149
Figure 7.31: Contact Analysis for the Straight Pivot Seesaw DPDT Switch, v2 150
Figure 7.32: Contact Analysis for the Straight Pivot Seesaw DPDT Switch, v2, with shorter reaction time.....150
Figure 7.33: Zoomed in overshoot and undershoot from Figure 7.32 151
Figure 7.34: Zoomed in contact bounce from Figure 7.32 151
Figure 7.35: Contact Analysis for the ‘S’ Shaped Pivot Seesaw DPDT Switch.....152
Figure 7.36: Contact Analysis for the ‘S’ Shaped Pivot with Delta Angled Electrostatic Plates DPDT Switch.....152
Figure 7.37: Contact Analysis for the ‘S’ Shaped Split Pivot with Delta Angled Electrostatic Plates DPDT Switch.....153
Figure 7.38: Example of Set Timing for the Elastic Recovery Experiment 155
Figure 7.39: Elastic Recovery analysis result for the HRL Cantilever SPST Switch 156
Figure 7.40: Elastic Recovery analysis result for the Scaled Down version of the HRL Cantilever SPST Switch by 10 times 156
Figure 7.41: Elastic Recovery analysis result for the Straight Pivot Seesaw DPDT Switch, v1, with upper and lower contact release.....157
Figure 7.42: Elastic Recovery analysis result for the Straight Pivot Seesaw DPDT Switch, v2, with upper and lower contact release.....158
Figure 7.43: Elastic Recovery analysis result for the ‘S’ Shaped Pivot Seesaw DPDT Switch with upper and lower contact release.....158
Figure 7.44: Elastic Recovery analysis result for the ‘S’ Shaped Pivot with Delta Angled Electrostatic Plates DPDT Switch with upper and lower contact release ...159
Figure 7.45: Elastic Recovery analysis result for the ‘S’ Shaped Split Pivot with Delta Angled Electrostatic Plates DPDT Switch with upper and lower contact release 159
Figure 7.46: Resonant Frequencies of the different types of switches 160
Figure 7.47: CST simulation S21 parameter analysis result for switch contacts.....162

Figure 7.48: Graph of the S11 simulated results from CST for the different designs 163
Figure 7.49: Overall contact model view of Design 1 164
Figure 7.50: Overall contact model view of Design 2 165
Figure 7.51: Overall contact model view of Design 3 165
Figure 7.52: Overall contact model view of Design 4 165
Figure 7.53: Overall contact model view of Design 5 165
Figure 7.54: Close up view of Design 1.....166
Figure 7.55: Close up view of Design 2.....166
Figure 7.56: Close up view of Design 3.....166
Figure 7.57: Close up view of Design 4.....166
Figure 7.58: Close up view of Design 5.....167

List of Tables

Table 3.1: Example of parameters for Governing Equations.....57
Table 4.1: Comparison of the Simulation Software.....61
Table 4.2: Material Properties.....66
Table 5.1: Performance Characteristics of RF MEMS, PIN Diodes and FETs referenced from Gabriel M. Rebeiz, RF MEMS Theory, Design and Technology, p 5 (Rebeiz 2003).....95
Table 5.2: Comparison of Actuation Voltage Requirement of Single and Split, Straight Pivot Seesaw, DPDT Switch.....102
Table 6.1: Results of the average force applied between two plates 110
Table 6.2: Comparison of simulated and calculated forces 112
Table 6.3: Displacement of the beam Comparison Between Simulation and Mathematical Model 113
Table 6.4: Copper Beam Parameters.....113
Table 6.5: Resonant Frequency of the beam with simulated and mathematical results 115
Table 6.6: Voltage verses displacement of HRL Cantilever beam switch.....116
Table 6.7: Characteristics of practical verses simulated results.....117
Table 6.8: Results of the different types of RF MEMS switches (rounded to the closest 1 MPa).....118
Table 6.9: Resonant Frequency of the RF MEMS switches 119
Table 6.10: CST Comparison of results for the different designs at S21 120
Table 6.11: CST Comparison of results for the different designs at S11 120
Table 7.1: Node requirement for the test per mesh size.....123
Table 7.2: Percentage difference of accuracy from 50 μm 124
Table 7.3: Pressure exerted at the centre nodes along the X and Y axis.....128
Table 7.4: Comparison of Resonant Frequency of the HRL Cantilever SPST Switch-Experimental Verses Simulated 136
Table 7.5: Switches activation and deactivation speed.....154
Table 7.6: Error comparisons between simulations of the HRL Cantilever contacts against the measured 163

Table 8.1: List of Objectives linked to Achievements addressed in Chapters and Sections 170
Table 9.1: HRL Cantilever SPST Switch..... 191
Table 9.2: Scaled Down version of HRL Cantilever SPST Switch by 10 times 192
Table 9.3: Straight Pivot Seesaw DPDT Switch v1 193
Table 9.4: Straight Pivot Seesaw DPDT Switch v2 193
Table 9.5: ‘S’ Shaped Pivot Seesaw DPDT Switch 196
Table 9.6: ‘S’ Shaped Pivot with Delta Angled Electrostatic Plates DPDT Switch 196
Table 9.7: ‘S’ Shaped Split Pivot with Delta Angled Electrostatic Plates DPDT Switch..... 200
Table 9.8: HRL Cantilever SPST Switch..... 203
Table 9.9: Scaled Down version HRL Cantilever SPST Switch by 10 times..... 212
Table 9.10: Straight Pivot Seesaw DPDT Switch v1 (Lower Release Contact)..... 216
Table 9.11: Straight Pivot Seesaw DPDT Switch v1 (Upper Release Contact) 219
Table 9.12: Straight Pivot Seesaw DPDT Silicon and Copper v2 (Lower Contact Release) 221
Table 9.13: Straight Pivot Seesaw DPDT Silicon and Copper v2 (Upper Contact Release) 224
Table 9.14: ‘S’ Shaped Pivot Seesaw DPDT Switch (Lower Contact Release)..... 226
Table 9.15: ‘S’ Shaped Pivot Seesaw DPDT Switch (Upper Contact Release) 228
Table 9.16: ‘S’ Shaped Pivot with Delta Angled Electrostatic Plates DPDT Switch (Upper Contact Release) 231
Table 9.17: ‘S’ Shaped Pivot with Delta Angled Electrostatic Plates DPDT Switch (Lower Contact Release)..... 235
Table 9.18: ‘S’ Shaped Split Pivot with Delta Angled Electrostatic Plates DPDT Switch (Upper Contact Release) 240
Table 9.19: ‘S’ Shaped Split Pivot with Delta Angled Electrostatic Plates DPDT Switch (Lower Contact Release)..... 249

Abbreviations

µm	Micrometre
µN	Micro Newtons
µs	Micro Seconds
1D	One Dimension
1P6M	One-Poly-Six-Metal
2D	Two Dimension
2G	Second Generation (Wireless communication system)
2P4M	Two-Poly-Four-Metal
3D	Three Dimension
3G	Third Generation (Wireless communication system)
4G	Fourth Generation (Wireless communication system)
ADS	Advanced Design System
Al	Aluminium
ANNs	artificial neural networks
ANSYS	Analysis System
ASIC	Application-Specific Integrated Circuit
ASlC file	ASIC language Source Code file
Au	Gold
BiCMOS	Bipolar Complementary Metal Oxide Semiconductor
BP	Back Propagation
C Band	C Band Frequencies (4 to 8 GHz)
CAD	Computer Aided Design
Caltech	California Institute of Technology
CMOS	Complementary Metal Oxide Semiconductor
CMUT	Cap Active Micro-Machined Ultrasonic Transducer
CNES	The Centre National D'études Spatiales
CPW	Co Planar Wave
CST	Computer Simulation Technology
Cu	Copper
DARPA	Defence Advanced Research Projects Agency
dB	Decibels
dBm	Decibel-Milliwatts
DC	Direct Current
DC-DC	Direct-Current to Direct-Current
DPDT	Double-Pole Double-Throw
DUT	Device Under Test
E-Field	Electromagnetic Field
EM	Electromagnetic
EM3DS	Electro Magnetic 3D Simulator
ESD	Electro-Static-Discharge
FEA	Finite Element Analysis
FEM	Finite Element Modelling
FET	Field-Effect Transistor

fF	Femtofarad
GaN	Gallium Nitride
Gbps	Giga-Bits or Giga-Bytes per Second
GHz	Gigahertz
GPa	Gigapascals
GSM	Global System for Mobile
GUI	Graphical User Interface
HFSS	High Frequency Structural Simulator
HRL	Hughes Research Laboratories
Hz	Hertz
i.e.	exempli gratia
IC	Integrated Circuit
IEEE	Institute of Electrical and Electronics Engineers
Ir	Iridium
JEDEC	Joint Electron Device Engineering Council Solid State Technology Association
K Band	K Band Frequencies (18 to 27 GHz)
Ka Band	Ka Band Frequencies (27 to 40 GHz)
kPa	Kilo Pascal
kV	Kilo Volts
LC	Inductor Capacitor
m	metre
mA	Milliamps
MEMS	Micro Electro-Mechanical Systems
MHz	Megahertz
mm	Millimetre
MOEMS	Micro Opto Electro-Mechanical Systems
MPa	MegaPascal
MPST	Multi-Pole Single-Throw
MTSP	Multi-Throw Single-Pole
MUMPS	Multi-User MEMS Processing System
mV	Millivolt
mW	Milliwatt
N	Newton
nA	Nanoamp
NEMS	Nano Electro-Mechanical Systems
nm	Nanometre
ns	Nanosecond
^{o}C	Degree Celsius
PA	Power Amplifier
Pa	Pascal
PECVD	Plasma Enhanced Chemical Vapor Deposition
PHM	Prognostic and Health Management
PIN	Positive Intrinsic Negative
Pt	Platinum

PTC	Parametric Technology Corporation
Q Factor	Quality Factor
RF	Radio Frequency
RF MEMS	Radio Frequency Micro Electro-Mechanical Systems
RLC	Resistor Inductor Capacitor
ROM	Reduced Order Macro
Rx	Receive
s	second
S11	Scatter Parameter Reflection Coefficient at port 2
S12	Scatter Parameter Isolation
S21	Scatter Parameter Insertion Loss
S22	Scatter Parameter Reflection Coefficient at port 2
SAT	Standard ACIS Text
Si	Silicon
SiN	Silicon Nitride
SMA	Shape Memory Alloy
SOIMUMPS	Silicon-On-Insulator Multi-User MEMS Processing System
SP11T	Single-Pole Eleven-Throw
SP3T	Single-Pole Three-Throw
SP4T	Single-Pole Four-Throw
SP6T	Single-Pole Six-Throw
SP7T	Single-Pole Seven-Throw
SP8T	Single-Pole Eight-Throw
SPDT	Single-Pole Double-Throw
SPMT	Single-Pole Multi-Throw
SPST	Single-Pole Single-Throw
SPxT	Single-Pole X Number-Throw
T/R	Transmit / Receive
TDR	Time Domain Reflectometry
TEM	Thermo Electro-Mechanical
THz	Tera Hertz
TSMC	Taiwan Semiconductor Manufacturing Company
TV	Television
Tx	Transmit
UK	United Kingdom
USA	United States of America
V	Volts
v1	Version 1
v2	Version 2
VNA	Vector Network Analyser
W	Watts
Wi-Fi	Wireless Fidelity
WYSIWYG	What You See Is What You Get
X Band	X Band Frequencies (8 to 12 GHz)
Ω	Ohms

Chapter 1

1 Introduction

In today's information era, the use of microelectronics has been a success with the use of miniaturisation and integration to other microelectronics at high volume productions, which has decreased the cost of each microchip allowing it to be used in almost every aspect of our lives.

Micro-Electro Mechanical Systems, also known as MEMS, are a technology using miniaturised electro-mechanical components within a structure or device. This technology helped to revolutionise the electronic sensor market allowing devices to be smaller than their counterparts and provide improved performance. MEMS devices in electronics can be used either actively or passively to interact with its surrounding such as light, motion, radio frequencies, etc. Although MEMS technology is relativity new compared to solid state semiconductor technology, it has helped to revolutionise different markets such as the sensor or optical markets by allowing devices to be smaller than their counterparts and provide an improved performance. The potential of MEMS is further increased due to MEMS fabrication being based on conventional semiconductor Integrated circuit (IC) fabrication processes.

The ability of miniaturisation provides an advantage, for device performance and circuit integration which allows devices to become smaller to incorporate and fabricate into a larger system, which results to a significant decrease on the price per unit.

The sectors in which MEMS high volume manufacturing has been successful has been: sensors, optical and audio products other sectors are close to commercialisation or is limited due to the intrinsic designs of MEMS devices, reliability problems and specialised packaging procedures. Semiconductor manufacturers have invested

increase efforts into MEMS productions which will eventually see a decrease in cost per unit and availability in other sectors of electronics.

Radio Frequency Micro-Electro Mechanical Systems (RF MEMS) are devices which are used to interact with radio frequencies. The area of interest are RF MEMS switches, which are mechanically moving parts which performs either as a variable capacitor and a three-dimensional inductor or a fixed resistor/capacitor and a three-dimensional inductor also, compared to their solid-state counterparts' RF MEMS switches provides a superior performance. The recent growth of wireless technologies and research has shown to provide massive potential for integration of RF MEMS devices in to high volume consumer and commercial markets systems, but due to the reliability and difficulty of integration of these devices the progression laboratory research to commercial use has been restricted to high end, military and space applications.

The thesis motivations focus is on RF MEMS switching by presenting a new micro switch design which has been developed from an optimisation of a cantilever switch. The new design addresses the need for reliability for RF MEMS by reducing the von mises stress of the device during switching periods, which in-turn reduces the actuated voltage requirements allowing direct use of the design in common voltage levels used in low voltage and battery powered devices.

1.1 MEMS Technology Overview

Micro-Electro Mechanical Systems, also known as MEMS, are a technology using miniaturised electro-mechanical components within a structure or device. This technology helped to revolutionise the electronic sensor market allowing devices to be smaller than their counterparts and provide improved performance.

1.1.1 Dr. Richard Phillips Feynman

The introduction of micro components was first envisioned by Physicist and Noble Prize Winner Dr. Richard Phillips Feynman, who presented a lecture at the California Institute of Technology (Caltech) called ‘There’s Plenty of Room at the Bottom’. He envisioned the use of machines at the micro and molecular level.

At the time of the lecture he acknowledges that there was technical limitation in creating devices or systems at the micro scale. However, Feynman explored options for miniaturization without the need of particular sizes, such as values, data storage and processing and compared it to machinery which is effected by miniaturization.

He considered miniaturising material volume required memory capacity to represent an element of information. Dr. Feynman estimated that by using a reduction factor of 25000 for an ordinary printed letter it would need an equivalent volume of 100 atoms, which would allow to provide a capacity of 1015 bits of data in a dust particle.

Feynman envisioned the need for increased computing power, by scaling down the electronic circuity parasitic capacitance can be reduced, therefore this simultaneously increase speed, processing and reduces power consumption, which in-turn allows denser packaging of components. However, Feynman did not take in to consideration leakage currents which occurs when electronic circuitry is scaled down.

Feynman considered miniaturisation of machinery, that the effect of forces, materials magnetic behaviour and friction. He observed that during downscale of mechanical elements, weight and inertia is irrelevant compared to strength of the material, but he noted that the material characteristics for metals change at the nanoscale which makes it not ideal for repetitive designs, on the other hand amorphous materials such as plastics and glass provide homogeneous characteristics making it ideal for repetitive designs at the nanoscale.

Feynman reasoned that when scaled down the lubrication of component create unnecessary friction without the use of lubrication it provides the ability for rapid heat transfer.

His first practical example of a micro machine, was the electric micro motor, which would be constructed using a process of thin-film deposition and be operated via electrostatic actuation (R. Feynman 1993).

1.1.2 The Growth of MEMS Technology

With the advent of the Integrated Circuit (IC), allowing fabrication of small objects onto a silicon substrate (wafer), using technological processes such as photographic and chemical etching. It was realised that the circuits could be scaled down and retain similar characteristics to their larger counter parts. This in turn created an increased rush of development in ways to print more circuits onto a silicon wafer, providing greater economic benefit and increase in profit, which spurred the increase for integration and miniaturisation.

This has been demonstrated by the increase from 10 circuits in 1960 to 10 million circuits in 1990, which is in accordance with Moore's Law (G. E. Moore 2006); this is shown in Figure 1.1 and further shown in Figure 1.2 as a record of the last 10 years.

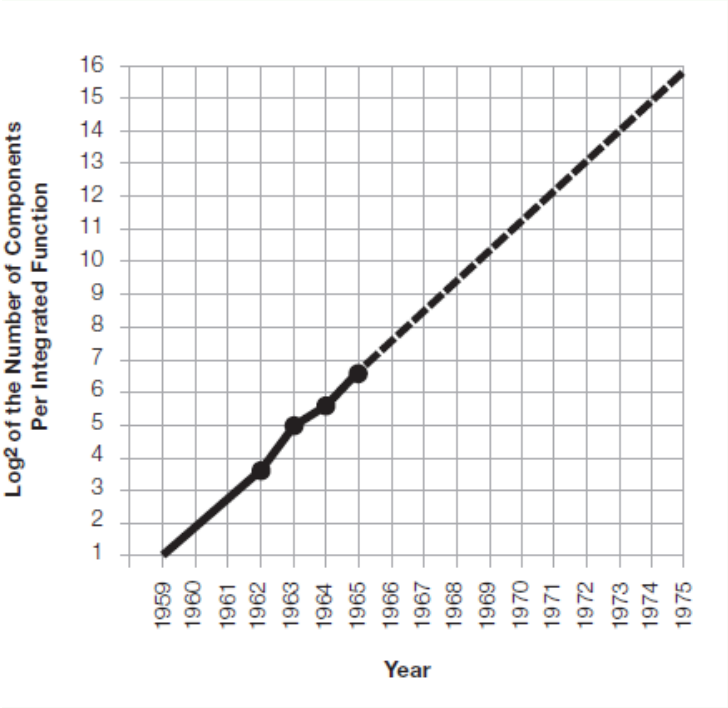

Figure 1.1: (label added for this reprint) Log2 of the number of components per integrated function versus year (G. E. Moore 2006)

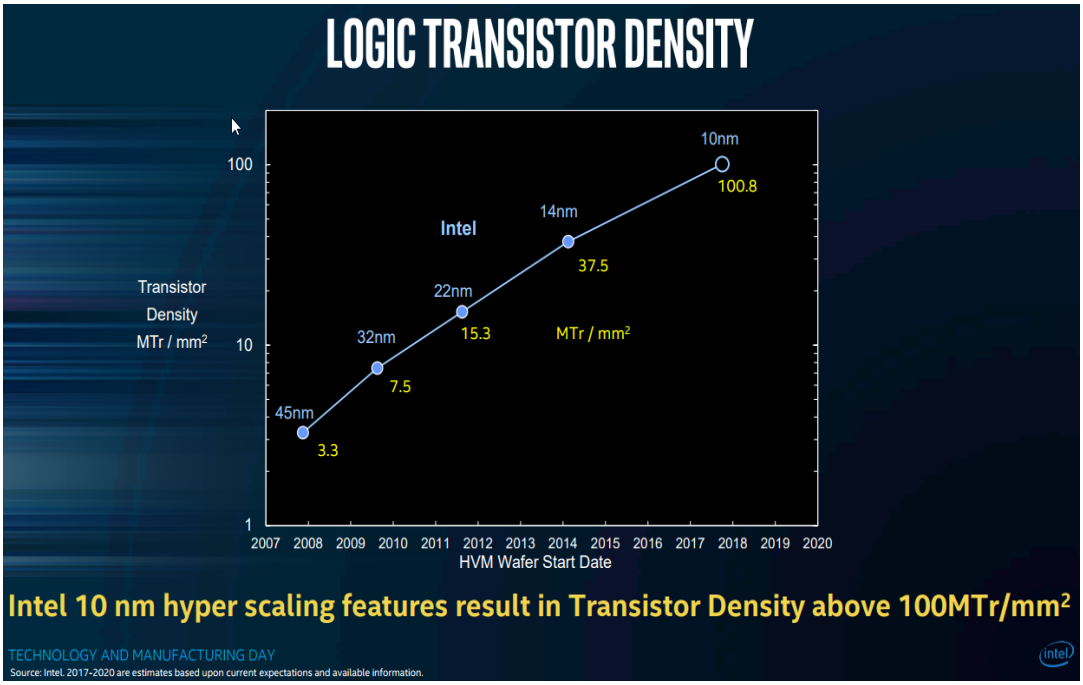

Figure 1.2: Intel Logic Transistor Density prediction (Intel and Mistry, K 2017)

The IC industries success in mass production, spurred researchers and engineers to apply similar concepts of electronics manufacturing to mechanical, optical and fluidic technologies hoping to achieve similar performances and cost improvements. To achieve these goals, it was realised that fabrication techniques would need to be assessed, due to the IC fabrication being two-dimensional and require development in fabrication techniques for three-dimensional structures (Varadan et al. 2003).

1.2 RF MEMS

1.2.1 Present Status of RF MEMS

Radio Frequency Micro-Electro Mechanical Systems, also known as its acronym 'RF MEMS'. In today's world, there demand for increased functionality, which can be implemented by miniaturisation. RF MEMS are known to be ideal for low power consumption due to the use of voltage only, which is known as electrostatic actuation. The RF MEMS switch also provides good insertion loss and isolation while being highly linear because of the direct mechanical contacts of the switch.

The high density of current technology has reached a point where leakage current is becoming more significant, which would mean an increase requirement of power. However, with RF MEMS, the use of electrostatics actuation provides a solution to this issue, because of its innate use of voltage rather than current for actuation.

Ohmic type RF MEMS switches have been known to be large in its size and usually reaching millimetre sizes (Pranonsatit et al. 2006) .

Currently the present status of MEMS devices is at a disadvantage when it comes to size constraints as most RF MEMS switches are too large to be implemented into an integrated circuit and are packaged separately, which causes difficulty when creating smaller mobile devices (Seki et al. 2013). RF MEMS are commonly known for reliability issues due to the moving components, which causes a high chance of material fatigue and breakage. MEMS devices are also known to have a high voltage actuation (10 – 100V) as shown in the work carried out by (Pranonsatit et al. 2006) and (Jongseok Kim et al. 2007a). This is due to electrostatic actuation and design size, and requires the device to provide a separate voltage source to be stepped up from a low voltage to a high voltage, this causes extra requirement of components to achieve designated voltage levels. This research takes these into account for the design of the RF MEMS switch in order to overcome these problems.

1.2.2 Ohmic Type Switches

An electrostatic ohmic switch, also known as series switches, uses metal-to-metal contacts, which normally is in the off-state until an actuation voltage is supplied to switch it on. In the on-state, a metal bar is used to short circuit the gap between the input and output lines; this type of switch has the capability of switching from DC to RF signals. However, it also has fabrication and reliability challenges.

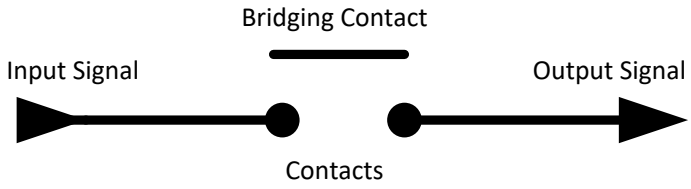

Figure 1.3: Ohmic Type Switch circuit

1.2.3 Capacitive Type Switch

Electrostatic capacitive switches are shunt type switches which consists of a metal bridge connected to an RF ground. This bridge moves vertically above an isolated signal line. The switch is normally in its on-state until the actuation voltage moves the bridge to its down position, which in-turn short circuits the signal line to RF ground via capacitive coupling. This type of switch is not suitable for low frequency signals however it is relatively simple to fabricate, with fast switching speed of a few microseconds. Compared to ohmic switches the footprint is relatively small.

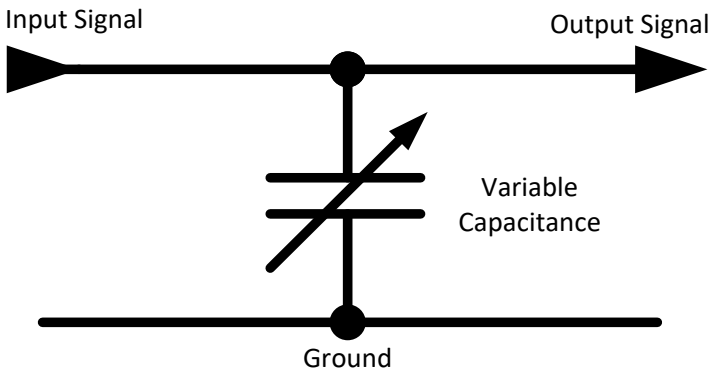

Figure 1.4: Capacitive type Switch circuit

1.3 Methodology

The methodology involves the use of mathematics and simulations to characterise RF MEMS switches. The mathematical methodology was used to characterise the mechanical and electrical elements of the switch. The mathematical analysis of switch is then compared to simulated counterpart, to identify the accuracy of the simulation.

As for the simulation, it involves the use of design optimisation of a cantilever beam eventually creating a unique design which provides a lower actuation voltage than the original. Other optimisations can be considered as an added benefit, which can then be compared to designs that may fall within the same design class.

The simulations will be conducted on Intellisense software called Intellisuite, where by the models will be first created on Intellisuite's 3DBuilder. The models will then be simulated using the Thermo-Electro-Mechanical (TEM) simulation tool from Intellisense. Here the materials, fixed boundary conditions, voltage and contact characteristics with quad-edge meshing will be applied for mechanical analysis and triangular meshing for electrical analysis on the switch design (Triangular meshing allows for electrostatic force analysis). The results from this analysis provides information concerning: stress, displacement and force of the device, static and dynamic results. The models are then passed onto the SYNPLE simulation package (from Intellisense), whereby the simulation results will then provide modal analysis for dynamic contact release.

The models will then be subjected to Electromagnetic (EM) simulation using a software tool called 'Computer Simulation Technology' (CST). Here the designs will be applied with material characteristics and a hexahedral or tetrahedral meshing, ready for analysis. Once completed, the results will be correlated to provide two port scatter parameters.

With these results, they will then be tabulated and compared to see if design optimisations could improve them over a cantilever RF MEMS switch. This methodology is shown in Figure 1.5. The optimisations focused on four areas of improvements to the characteristics of the switch and addressed them as follows:

- Reducing actuation voltage
- Decreasing von mises stress
- Increasing isolation of the contacts
- Expanding functionality

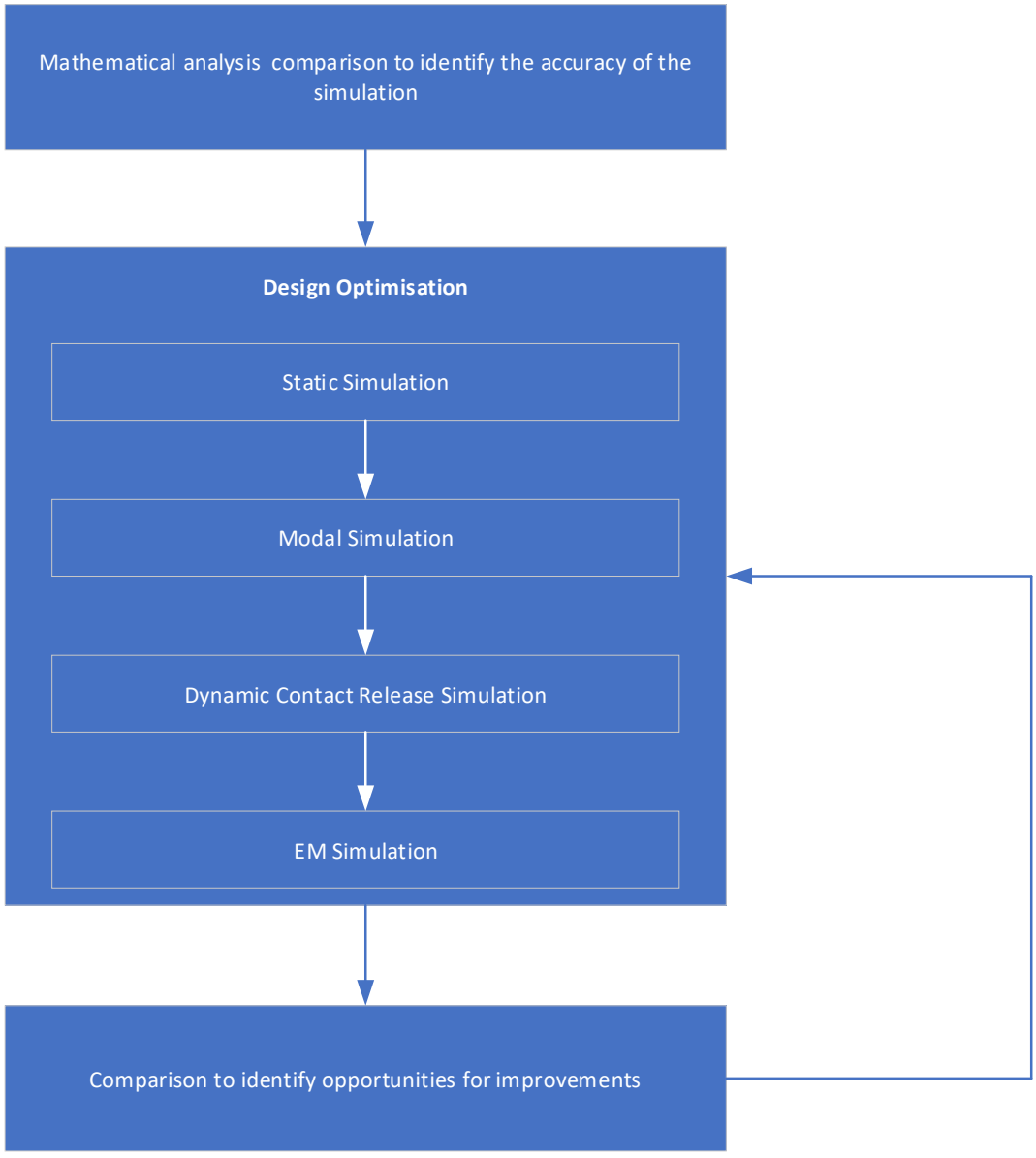

Figure 1.5: Methodology Process

1.4 Research Questions

In this research thesis, the fundamental questions to be asked, are:

What are the reasons for using RF MEMS switches in mobile communications?

The development of mobile technologies is a rapidly growing field, with researchers finding new and innovative ways to develop mobile systems for increased functionality. Due to the advances in silicon manufacturing, the use of three dimensional designs such as RF MEMS are now possible for mass production. RF MEMS switches provide advantages for isolation over solid-state switches, with its physical disconnection of the contacts, it is less likely to leak compared to solid-state switches. A comparison of existing solid-state and RF MEMS switching technology is made in this research.

What are the challenges in existing MEMS switches?

At the time of writing the reliability of RF MEMS switching is relatively poor and the voltage requirements are relatively high. To achieve the high voltage requirements, the RF MEMS switch require step up Direct Current to Direct Current (DC-DC) converters, this in turn requires extra area on the silicon chip and would require a more complex design.

At the time of writing the average minimum feature size of MEMS manufacturing is only between 1.5 - 2 μm, whereas advance RF MEMS switches require feature sizes of less than 40 nm. Although CMOS (Complementary metal–oxide–semiconductor), as of 2017, 7 nm was achieved for mass production by Intel, but this CMOS technology is for two dimensional (2D) designs only. As MEMS manufacturing improves, RF MEMS switches, which require small feature sizes, would then be manufacturable.

Can the proposed methodology be used to validate the hypothesis?

Since the time of Professor Larry Larson (L. E. Larson et al. 1991a) with the invention of the first RF MEMS switch (varactor), the advancement of switches has been

facilitated with the use of computers, this allows for fast simulations of designs at the micro and nano scales using Finite Element Analysis (FEA).

The research is to be conducted via simulation, with the use of validating against an existing design, the simulation would need to be validated with a grid independency study. This would be to prove the accuracy of the results obtained from the simulation. The simulation is also compared with known mathematical equation for validation.

What is the practical frequency range for use of RF MEMS with mobile communications?

Practical frequency ranges for this research are to be used with protocols and frequencies common to mobile phone communications, such as Bluetooth, Wi-Fi, GSM, 2G, 3G, 4G. Therefore, the frequency range would need to encompass the frequencies of all the protocols mobile phones use. These frequency ranges are to be included in a design range from DC to 45 GHz.

What are the required driving voltages of RF MEMS Switches?

The research will conduct a study of the current voltage requirements of existing RF MEMS switches, this would be the starting point from which other parameters would be found.

An example of a tool that facilitates the development of RF MEMS, such as the understanding of maths formulas, is the use of MathCAD. This software provides the user an easy and expedient way of calculating complex equations.

1.5 Aims and Objectives

The aim of this research is to explore the performance of RF MEMS active switching. This includes the use of modelling, simulation and mathematical analysis. The goal is to provide active switching, which increases reliability and lowers consumption by using voltages that are closer to battery voltage levels ranging up to 5V. This in turn helps to reduce the complexity of creating extra complementary components to communicate with the rest of the circuit which therefore reduces circuit size. To accomplish the goal, a list of objectives has been developed to guide the study:

1. Explore the types of RF MEMS switches
2. Explore the voltage requirements and dimensions for RF MEMS switches
3. Explore the stress, reliability and materials used in existing RF MEMS switches
4. Analyse the characteristics of electrostatics attraction of two parallel plates
5. Develop mathematical analysis of switch components (using MathCAD)
6. Comparison of commercial FEA/FEM tools for mechanical and electromagnetic properties of the switch
7. Develop switch design on FEM tools
8. Develop boundary condition and meshing setup of switch on a mechanical FEA tool
9. Develop boundary condition and meshing setup of switch on an electromagnetic FEA tool
10. Study the differences of mathematical analysis and FEA simulations and study the differences of an existing design against a FEA modelled simulation
11. Optimise and improve functionality of the design using the same FEA simulation settings
12. Compare all major iteration of the FEA modelled designs against existing design

1.6 Summary of Current Technology

The vision towards nano and micro scale technology, was theorised by physicist Richard Feynman in a series of lectures entitled 'There's Plenty of Room at the Bottom' at an American Physical Society meeting at Caltech on December 26th, 1959 (R. P. Feynman 1992). The lectures envisioned ideas of manipulating individual atoms to form machines at the micro and nano scale.

MEMS (Micro-Electro-Mechanical Systems) was invented by Harvey C. Nathanson in 1965 which served as a tuner for microelectronic radios. It was developed with Robert A. Wickstorm and William E. Newell at Westinghouse Research Lab in Pittsburgh. This was originally patented as a Micro-Electric Frequency Selective Apparatus. A later revision of the device was then patented as the Resonant Gate Transistor (H. C. Nathanson et al. 1965).

The first RF MEMS (and MEMS varactor) switch was developed by Dr. Larry Larson in 1991 with Hughes Research Labs in Malibu with the support of DARPA (Defence Advanced Research Projects Agency) the initial switch was created to operate at frequencies from DC to 50 GHz with a voltage requirement of 50 – 100 V. The design was a basic single pole single throw (SPST) cantilever switch which demonstrated the mechanical functionality at a micro level. The initial design presented reliability issues due to mechanical failure with material fatigue, stiction and tribology issues (L. E. Larson et al. 1991) .

RF MEMS is a relatively new technology that has rapidly been developed, because of the demand of smaller portable devices which require less power consumption for longer battery life. RF MEMS has the advantage over conventional solid-state devices due to being voltage driven and requiring little current for reduced battery consumption.

RF MEMS switch research has been rapidly changing due to advances with software simulation. This provides researchers an essential tool for rapid simulation testing of designs and theories. Also, advances in fabrication techniques has facilitated the progress of nano structures of RF MEMS designs.

There are different ways of creating an RF MEMS structure, two main contact methods are capacitive and ohmic.

Capacitive contacts use a dielectric also known as an insulating layer between the contacts. This prevents the contacts from touching each other. Unlike ohmic switches, capacitive RF MEMS switches have high pass filtering. Also, capacitive switching does not suffer from stiction caused by hot switching, which allows capacitive switches to switch at higher peak voltages compared to ohmic RF MEMS devices. This makes capacitive switching favoured for high power equipment (IEEE 2013) .

Ohmic switching uses direct contact to the transmission line. This method has become highly favoured by DARPA and industry (e.g. Texas Instruments, Hughes Research Laboratories and Analog Devices), this is due to the high isolation during the off state and low resistance in the on state for providing better signal compared to capacitive switching. The disadvantages of ohmic switching is the use of high RF power which causes stiction during hot switching. Ohmic switching is favoured in low voltages and signal power, for portable use. The research conducted here uses ohmic contact switching because of the advantages described above.

Common designs of ohmic RF MEMS switches include cantilever, rotary, comb drive and seesaw switching.

Cantilever switching is the very first type of RF MEMS switch, which was designed by Dr. Larry Larson at Hughes Research Laboratories. The first cantilever design proved the concept of RF MEMS switching with capabilities of switching from DC to 50 GHz. The advantages of the design are the simplicity and effectiveness of achieving high frequency switching, with ease of fabrication. The disadvantages of the cantilever are its limited switch capabilities i.e. single-pole single-throw (SPST) operation.

Rotary Switching is based on the principles of the wobble motor. This type of switching was designed by Suneat Pranonsatit at the Imperial College London, UK (Pranonsatit et al. 2006). The switch had the ability to provide a single-pole eight-throw (SP8T), providing a greater connectivity of different signals. Unfortunately, rotary switching is more complex to fabricate as three components are required to be fabricated separately and assembled together. Also, due to size, the switch is beyond the micrometre scale with a diameter of 1 mm and an air gap of 10 μm, causing the switch to require higher voltages (100 V).

Comb Drive switching uses a set of combed teeth to contact with a second set, this is to provide greater contact area for reduced resistance for low signal loss. The

characteristics of the comb drive provides a greater advantage over other designs. However, this characteristic also has the disadvantage of size and higher probability of mechanical failure due to stiction (Akiba et al. 2010) .

Seesaw Switching uses a balanced beam on a central pivot to provide single-pole single-throw (SPST) contacting using pull-up and pull-down electrostatic forces. The first seesaw type design for RF MEMS was published at IEEE MELECON 2006 by Jorge M. Cabral and Andrew S. Holmes (Cabral, Holmes 2006). The concept design proved to provide low actuation voltages range from 5 V to 80 V with a large air gap of 10 μm providing improved isolation, within a small space envelope. Seesaw RF MEMS designs were initially only proving SPST or SPDT switching.

To summarise all design, have a common layout structure where they are limited to single pole switching. Also, the limitation of using a single plane for contacting, limits the switching functionality. Size is an important factor for mobile communication systems as integrated circuits are becoming increasingly smaller. Most of the above designs have dimensions exceeding the micrometre scale. Although typical RF MEMS switch designs require electrostatic voltages from 5 V to 100V, this is outside the operating voltages found in mobile communication logic voltage standards, which are governed by JEDEC (JEDEC 2007a) (JEDEC 2007b).

The research conducted here provides multiple RF MEMS switch advancements into a seesaw structure. There are several aspects of the design that have been improved since the initial concept, including the pivot, electrostatic plates, beam and structural materials.

The innovative, empirical approach in the research, is analysis by improving each area of the RF MEMS seesaw switch using multiple iterations. This yields lower voltages and von mises stress levels, with improved isolation after each iteration.

The contribution to knowledge of research is an innovative RF MEMS seesaw switch with increased connectivity to multiple protocols. The use of an upper and lower set of contacts at each side of the beam, with increased multi-pole functionally takes advantage of the three-dimensional area. This enables the switch to fit within a micro space envelope (i.e. within 0 to 100 micrometres). The innovative seesaw structure has a lower von mises stress for extended reliability with reduced voltage, for allowing direct implementation into mobile communications equipment.

1.7 Thesis Structure

The thesis is sectioned into eight main chapters.

Chapter 2 comprises the literature review on topics involving RF MEMS switching. It starts off with exploring the previous research in the materials used for MEMS, which it goes on to explaining the past research into stress and reliability, with an understanding of the simulation software that has been used. Other areas of past research include Actuation voltage levels, switching methods and contact analysis.

Chapter 3 the 'Theoretical Background' chapter, summarises the theory and mathematical modelling for determining the characteristics of electrostatic actuation, displacement of a beam, resonant frequency and electromagnetic two port analysis.

Chapter 4 is the 'Engineering design process' this chapter describes the approach taken for the research and development of the RF MEMS switch designs. The chapter later describes the implementation of the use of Intellisuite and CST for simulating the design, which include all the associated parameters required to start a simulation.

Chapter 5 is the 'RF MEMS Switch Design'. This chapter describes the development of the RF MEMS switch from the original HRL Cantilever developed by (Hyman et al. 1999) from Hughes Research Laboratories, which is used as a benchmark from where advancements were made, to achieve a unique design. It also describes the stages which made a significant impact to the performance of the switch.

Chapter 6 provides the Results and Validation section. In this chapter, the initial validation is described with the use of Grid Independency and mathematical analysis of the HRL cantilever, this is to provide an understanding of the accuracy of the simulation, this was followed by the results of the unique designs, which reveals the finding from Intellisuite TEM simulation tool and CST EM Simulation tool. This includes Electrostatic characteristics, stress and EM characteristics.

Chapter 7 contains the discussion and results analysis section, where details of the results are explained and compared to existing research. It also shows the contributing factors on reducing the actuation voltages of the design.

Chapter 8 is the conclusion from the results obtained from this research, with recommended options of topics for future work studies.

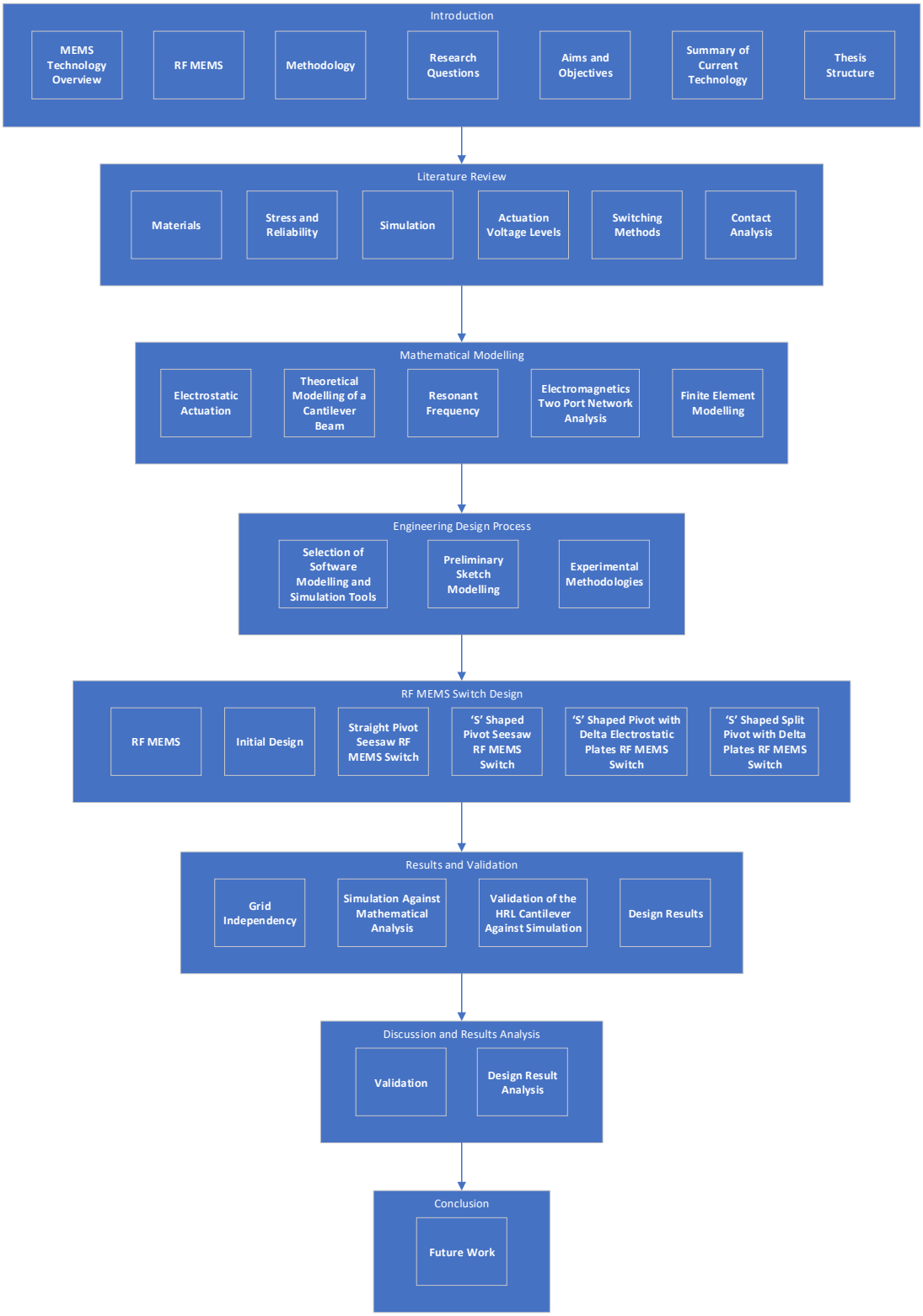

Figure 1.6: Diagram of the thesis structure

Chapter 2

2 Literature Review

This literature review provides critical analysis of a comprehensive set of papers, applicable to the RF MEMS seesaw design. The review is structured in to the following:

- Materials
- Stress and Reliability
- Simulation
- Actuation Voltage Levels
- Switching Methods
- Contact Analysis
- Manufacturing

2.1 Materials

Multiple mechanical properties studies of MEMS materials have been conducted to provide a comprehensive, usable list of materials for RF MEMS manufacturing, with a group of test methods such as: tensile, bend, resonant structure, bulge and indentation testing.

A report was published (Sharpe et al. 2004) on the mechanical properties of MEMS materials, which include laboratory level stress testing of materials and their properties. These new techniques and procedures were developed for thin film structures. During testing, the author found electroplated nickel to be highly reliable for the manufacturing processes compared to Polysilicon, silicon, nitride or silicon carbide. The report is a comprehensive listing of results for MEMS materials and considered to be a 'Handbook', due to the number of significant times the materials have been tested. This method of testing is considered the first of its kind, as all the materials were being tested equally within the same laboratory. A study published by (Pratap, Arunkumar 2007) , in India, on material selection for MEMS components was

conducted for MEMS researchers and designers to help choose the correct materials for optimum performance of the switch. The study is inspired by the Ashby approach. This approach provides the designer an index table of material properties such as: elastic modulus, failure strength, thermal conductivity, coefficient of thermal expansion, specific heat, density and fracture toughness. The report explains that multiple design parameters are usually required rather than a single parameter. Examples of a MEMS gyro and CMUT (cap active micro-machined ultrasonic transducer) were used to prove this concept. Exotic materials, such as diamond, were proven to have a better performance over silicon using the Ashby approach. This exhibits a clear case for developing exotic materials for MEMS, due to the performance indices of the materials used (Ashby 2000).

Other studies published on the mechanical properties of MEMS materials study on the characterises of four areas; elastic properties, internal stress, strength and fatigue (Stanimirović, Stanimirović 2009). Materials used for testing are commonly employed in MEMS fabrication today, such as, polysilicon, gold, copper aluminium, titanium, nickel and iron. The study provides an overview of the basic test methods used, with a definition of the mechanical properties of common MEMS materials. However, the lack of international standards for MEMS materials, and their properties, with a lack of standardisation of measurement methods or tests may hamper the ability of growth for MEMS development. Although other research has been conducted with the testing MEMS materials (W. N. Sharpe 2001), there are noticeable similarities on the method of testing, which could provide a solid foundation for designers and researchers to decide the correct material for optimum performance of the RF MEMS device.

Research goes on to further studies of metal-to-metal contacting of materials. (McGruer et al. 2006) published a report on the thermal, mechanical and material influences on ohmic type RF MEMS switches. The report examines the performance and reliability of contacting on MEMS switch. All materials were tested for several days and were exposed to air, which caused some materials to be far susceptible to contamination (oxidisation). A simulated test was run, to calculate intermodulation distortion of a MEMS switch. This was conducted with finite element analysis using ANSYS. It was observed, that by increasing the percentage of gold within an alloy, it helps to decrease contamination problems. Also, with hermetically sealed packaging, contamination problems can be nullified. This study justifies the requirement for

hermetically sealed packaging of RF MEMS devices. Another study compares gold and gold nickel alloys for use as a contact material, because of their non-corrosive properties (Zhenyin Yang et al. 2009). This study conducted an experiment using a commercially available MEMS switch. The device was calibrated to apply twice the force required, to increase wear rates of the switch. This helped to penetrate any contaminated film formed to ensure a metal-to-metal contact. The experiment is tested during hot switching conditions and shows a correlation between material properties and micro-contacting performance. It also shows a correlation between both material volume and surface properties. It is noted from the author, that further optimisation of the alloy properties need to be researched for MEMS switching applications.

A later introduction of nano scaling of materials, such as carbon for RF MEMS switches, provides MEMS designs with increased material flexibility, while allowing MEMS devices to require low actuation voltages. (Mafinejad et al. 2013), in Iran, published a report on the use of Carbon Materials in RF MEMS switches. The paper conducts a comparative study of RF MEMS switches, created using materials such as; gold, aluminium and graphene. Due to the structure of graphene, MEMS designs can be created at the nano scale, hence the term NEMS (Nano Electro-Mechanical Systems). Actuation voltages of beams, using aluminium and gold, required 37 V compared to graphene, which required only 7.7 V. Switching times were greatly improved using graphene, providing switching speeds of approximately 3.5 ns, compared to aluminium and gold switching speeds of 6.56 μs and 17.4 μs respectively. Although the performance characteristics of graphene/carbon based MEMS/NEMS are impressive, the materials are still in their early stages of research.

2.2 Stress and Reliability

2.2.1 Stress

Stress and strain of RF MEMS switches are important factors, as they improve reliability during fabrication and long-term operation. (Shea Jan 21, 2006), in Switzerland, published a report on the reliability of MEMS devices for space applications. The report focuses on key environmental impacts such as vibration, thermal shock and radiation, which are likely to occur within space. The report explains common mechanical and electrical failure modes of MEMS devices, which are carefully examined. The author notes MEMS devices have a higher tolerance to ionisation and atomic displacement from radiation, but failure could occur with high doses of radiation, which causes the accumulation of charge to occur within the dielectric layers that can increase the actuation drive voltage. Thermal shock to MEMS devices can cause a severe impact to the reliability of the materials used within the device. The research needs to consider more material options to provide greater robustness against heat radiation (Infra-Red Radiation). MEMS are considered to be highly reliable during high shock levels, due to the mass of the switch being negligible from Newton's second law (shown in Equation 2.1) (IL Kofsky 1951).

Equation 2.1

$$Force = mass\ x\ acceleration$$

With this formula, a standard MEMS device can withstand a shock in excess of 1000 G, as this will only result in forces within the mN scale. It is concluded from the study, that for MEMS to survive extreme conditions, hermetically sealed packaging is required for increased reliability and longevity. Although this may be costly, due to the limited number of devices fabricated, it is also concluded that the cost is negligible compared to the reliability and performance requirements.

Residual stress can occur at the end of manufacturing and is defined as "those stresses that remain in a material or body after manufacturing and processing in the absence of external forces or thermal gradient" (Leondes 2006). (J. T. Huang, S. Y. Li 2006), in Taiwan, published a study on developing CMOS compatible RF MEMS switches using residual stress. The study demonstrates a novel approach to fabricating MEMS switches with TSMC (Taiwan Semiconductor Manufacturing Company) CMOS 0.35

µm 2P4M process and post-process techniques. The author used an RF MEMS metal-to-metal contact switch, for the CMOS fabrication process. Residual stress is identified as a common fabrication problem of MEMS with CMOS, as it produces large deflections on the beam. To compensate for this problem, the author conducted a design optimisation of the switch with the use of a FEM (Finite Element Modelling) software tool called Coventorware. Also, (Ur Rahman et al. 2009), in Australia, published a report on the investigation of residual stress. The author specifically focuses on the effects on RF MEMS switches and modelling of the spring constant. The report investigates the stresses generated during the fabrication process when gold material is used. The practical designs are analysed to model the spring constant of the beam using the Euler-Bernoulli equation. The author notes that changes to pressure and RF power can change compressive stress into tensile stress. Another example of residual stress has been carried out by (K. Y. Chan, R. Ramer 2009), on a novel low stress sensitivity and low actuation RF MEMS switch. The switch is designed using Coventorware design and simulation, FEM software tool and HFSS for simulating RF characteristics of the device. They compared the electrical requirements of the actuation voltages of both the simulated and the fabricated switch, which showed a significant increase of the simulated voltage of 14 V to the fabricated voltage of 20 V. The difference of the two designs were due to the effects of residual stress on the fabricated beam. Although the authors conclude that the simulation and testing were in accordance with the measured results, the values of the voltages prove to show a large difference.

(Niu, Rebeiz 2012), in the USA, published a paper on a RF MEMS switch with high biaxial and stress gradient tolerances. The report presents a design, simulation and fabrication of a miniaturised RF MEMS switch, with high tolerance to stress during actuation. The fabricated design had been tested using a standard probe tip method within a nitrogen filled chamber, and was visually scanned using Wyko to see if the switch conformed to design size specifications. It is noted that the design of the switch was to allow direct implementation and compatibility with CMOS backend systems to allow for reduced fabrication costs.

Also, (Parsediya 2016), in India, published a paper on the deflection and stresses of effective micro cantilever beam designs under low mass loading. The paper studies on five different types of cantilever beams with the rectangular beam being the standard

version on which to compare. The study uses the FEM simulation tool called ANSYS for stress and displacement results. The author concludes that BEAMS 2, 3, 4 and 5 provides improved deflection for use with nano bio sensing. Although the stress for these improved designs are better than the first proposed beam and conventional rectangular beam, the stresses are far greater, but the author concludes that the stress values are negligible. (Boldeiu et al. 2015), had published a paper on the study of the von mises stress in RF MEMS which anchors. The paper delved into the aspects of the RF MEMS switch anchoring of the switch and the understanding of stress influences with the area, the paper demonstrated different types of the anchors and compared the stress levels between them, while later optimising the design to reduce stress affected directly at the anchor. It was proved that the optimisation helped to decrease stress between 45% to 82% and obtained a maximum stress level of 67 MPa, which was lower than the young's modulus of gold. Although the paper proved an importance for reducing stress at the anchor, it does come to question if the resonant frequency of the device would change due to the optimisation.

2.2.2 Reliability

(J. C. M. Hwang 2007),conducted a study on the reliability of actuated electrostatic RF MEMS switches. The study reviews two types of actuated RF MEMS, ohmic and capacitive switches.

Ohmic type MEMS switches have shown to have a higher probability of failure, due to either mechanical or electrical stress. Mechanical stress can be deformation, fatigue and wear of the material. As for electrical stress, this can be considered as arching, welding, melting and electro-migration. These failures depend heavily on the material characterisation chosen for the design, which if not chosen correctly can cause vulnerabilities on the surfaces of the materials such as contamination.

As for capacitive switches, the study references improvements to help overcome dielectric charging, for example; improving dielectric material, reducing actuation voltages, reducing dielectric contact area or optimising the control voltage waveforms. It is acknowledged that capacitive switching failures are better understood than ohmic switching. The study describes ways of mitigating failures of capacitive switches,

using accelerated test models, which were developed in the study to predict the lifetime of the switch. (P. G. Steeneken, O. Wunnicke 2012), in the Netherlands, published a report conducting an experiment using MEMS switches for power electronics. The report took performance comparisons of transistor type switches, to see the potential of MEMS switching by examining the physical performance capabilities. Using semi-empirical modelling, it was proven in this study that MEMS switches were capable of outperforming silicon based transistors with actuation voltages of less than 30 V and may stand an even ground against Gallium Nitride (GaN) transistors, if large actuation voltages are applied (i.e. more than 1000 V).

Further studies on the techniques for modelling the mechanical stress of RF MEMS capacitive switches were examined by (C. Palego et al. 2008). The author presented a novel technique of using microwave intermodulation. This is to measure the mechanical resonance directly from a packaged or unpackaged (devices open to the air) RF MEMS capacitive switch, with a quality factor approaching unity while air damping is present. The techniques proved to be an effective and suitable solution to differentiate the long-term reliability of mechanical and electrical effects.

A study on the electro-static discharge (ESD) and cycling effects for ohmic and capacitive RF MEMS switches (A. Tazzoli et al. 2007), identifies the dynamic responses of both RF MEMS type switches within different conditions of bias and actuation time. The study found that there is a trade-off between switching quality and voltage. As voltage was increased, switching speed was increased, but resulted with contact bounce, which reduced contact quality. The authors conclude, more extensive studies are required on ESD sensitivity. A published study from (S. Sangameswaran et al. 2010), in Belgium, on the behaviour of RF MEMS switches with ESD stress helped to understand the procedure of ESD testing on capacitive switches, under different ambient pressure and environmental conditions. Compared to CMOS, MEMS are far more susceptible to ESD. This approach to testing provides an insight of ESD and how it critically affects the reliability of a MEMS devices. Also, (Y. Huang et al. 2012), presented a report on a novel electrostatic RF MEMS switch, using prognostics functions. For conducting the test, a capacitive RF MEMS bridge electrostatic actuation switch was used. The fabricated switch was tested for RF characterisation using a network analyser. This provided time domain reflectometry (TDR) analysis of the MEMS switch. Unfortunately, the authors did not list the results

of the insertion loss from the TDR analysis. For ESD testing, the authors used a Human body model approach. This resulted with the capacitive RF MEMS switch to handle up to 2 kV of static discharge. The switch had shown to burn out when higher static discharge voltages were applied. With these ESD results, the authors created a Prognostic and Health Management (PHM) of the switch, which provided a way to calculate the remaining life of the device before failure. By comparing the results to the lab test, this provided reasonable accuracy of the lifetime of a capacitive RF MEMS switch.

Studies on the long-term reliability of RF MEMS tuneable capacitors, conducted by (E. Ogawa et al. 2011), in Japan, studied on creep induced deformation of tuneable RF MEMS capacitors, which are commonly caused due to ductile metal used for beams. The authors mention overcoming this problem in a previous report, by using a brittle material called silicon nitride (SiN) for the spring. Using the design, the authors conduct a long-term analysis of the structure with a Finite Element Modelling simulation tool (ANSYS). The study uses an accelerated analysis on the deformation of the structure (at the down state) for 3 years at 85 ^{o}C. The SiN spring type tuneable RF MEMS capacitor had no fatal creep deformations when released from the depressed down state after three years. From the authors' previous report, the structure of the design had long-term immunity from creeping whilst retaining performance. (R. Behielt et al. 2014), presented a paper on the long-term investigation of RF MEMS switches on failure mechanisms induced by dielectric charging. The experiment conducted for the paper explains a way to provide quantitative statements about the amount of charge sent to the dielectric layers. It resulted from the long-term recording of changes in the switching voltages of the device under test, using a novel purpose-built measurement setup, which enables the investigation of temperatures. The experiment could extract information of the shift of the pull-in voltage, and calculate the amount of charge, in order to investigate the narrowing effect. With the finding of the narrowing effects, it is then possible to identify failure caused by accumulated charge, and therefore allow designs to be more robust. This experimental methodology can be implemented with other electrostatically actuated devices and can be considered a tool for improving designs to exhibit a higher robustness against dielectric charging. Other area papers were published in this field including (M. L. Ya et al. 2016), where the authors proposed the use of proving (R. Behielt et al. 2014)

theatrical investigation of charging effect in the dielectric. The paper the uses Comsol multiphysics 4.3, with the use of electro-mechanics module within Comsol. The experiment uses a triangular voltage input to simulate the pull-in voltages to obtain the actuation time. With this, the parasitic charge effects can then be analysed using the time-domain dynamic simulation. The results concluded that the pull-in voltage required would need to be small in the area of 2V. Also, an effective bias voltage with an improved waveform would drastically reduce the parasitic charges and therefore increase the lifetime of the device. The author concluded that dialectics, with rougher surfaces, would produce stronger electric fields, but the switches with these types of characteristics would require lower actuation voltages, but would compromise the RF performance.

2.2.3 Temperature Reliability

Stress can be caused by temperature, which hampers the RF MEMS switching reliability and longevity. A study by (I. Reines et al. 2009) in the USA, presented a report on a stress tolerant and temperature stable RF MEMS switch capacitor. The report presents a reduced sensitivity to residual stress and temperature, due to the circular symmetric geometry of the structure. The device was mechanically simulated using CoventorWare software simulation tool and then fabricated using Raytheon RF MEMS capacitive switch process. The paper compared the circular switch design to a design created by Raytheon, with graphical results displaying a far stable voltage slope (range) from -5 ºC to 95 ºC. It is noted that the design improves the uniformity for a wafer scale, which increased yield and manufacturability of wafer-to-wafer lots. Other studies on stress related to temperature, such as (R. Mahameed, G. M. Rebeiz 2011), provides an RF MEMS switch for use with wide temperature ranges. The RF MEMS switch design is of a single pole single throw (SPST) switch, with the use of a capacitive membrane for contact. The switch was tested to be temperature stable with a variation of less than 50 mV/ºC from 25 ºC to 125 ºC, with a Q-factor of approximately 8. The study proves a working thin film fabrication process, which can be used at a smaller scale for Ka band. Although not emphasised much in the report, the design requires a high voltage to drive the actuation.

2.2.4 Contact Reliability

Areas of reliability are also noted for concern in metal-to-metal contacting, which is commonly used in ohmic RF MEMS switches. (A. Broue et al. 2010), in France, published a report on the multi-physical characterisation of micro contact materials for RF MEMS switches. The report explains a comparison between several types of material uses for the contacts. The author uses a methodology of testing, which was developed by NOVA MEMS. The testing technique uses a commercial nano-indenter, which is coupled with electrical measurements. This type of technique was originally created for testing vehicles to investigate the underlying physics for surface related failure modes. The test uses an RF MEMS ohmic switch, which actuates at 40 V. The experiments conducted provide a better understanding of contact physics, which will help to increase improvements of the micro contact reliability. (J. Pal et al. 2016) presented a paper on the creation of high power and reliable SPST and SP3T RF MEMS switches for wireless applications. The paper demonstrated the development of a circular type RF MEMS switch, which implemented SOIMUMPS (Silicon-On-Insulator Multi-User MEMS Processes) fabrication process. The fabricated design was capable of hot switching with power up to 2W at ten million cycles (for SPST switch) and 1W at seven million cycles (for SP3T switch). Both the SPST and SP3T switches provided good isolation with -29 dB and -37dB respectively and results were validated using a Keysight FieldFox RF network vector analyser (N9923A). Although the voltage requirement of the switch is not implied in writing within the paper, it is shown on the graphs and tables that the device would require actuation voltages from 43V to 63V. A comparison of the switch from other previous work has shown that the switch outperforms all other research on hot switching cycles, but actuation voltage requirements and isolation is mainly below the other designs. The author does conclude the switch can be implemented for use with dual band antennas such as the ones used for Wi-Fi for smart antennas.

2.2.5 Hermetic Sealing

Other studies have focused on increasing reliability on silicon wafers such as, (A. Menz, R. Hper 2012), in Germany, where the authors published a report on increasing the reliability of a silicon-based RF MEMS switch, with the use of a zero level hermetically sealed package to avoid contamination of the contacts. The prototype design is originally for an SPST switch with the use of a lateral CPW (Co-Planar Wave) feed though (characteristic impedance of 50 Ω). The device has been tested for reliability during hot switching, which it was able to achieve i.e. 300 mA for 100000 cycles without failure. The author expresses that further extensive durability tests would be necessary to prove the reliability of the switches and future development a SP4T (Single pole four throw) version of the switch is to be created. Studies such as (F. Souchon et al. 2013), which examines dielectric free designs of MEMS to increase reliability by reducing dielectric charging. The study uses time predictive modelling tool to examine charge accumulation. The study acknowledges that further increases in reliability can be achieved through wafer level packaging and hermetically sealed packaging as this improves the durability of the material from charging and contact degradation.

2.3 Simulation

Due to the advances in computing computational speed, software simulation for RF MEMS has been rapidly developed and has become an integral part of designing RF MEMS switches, as it allows researchers and designers to create and simulate designs ready for real world fabrication with high accuracy and low cost. This chapter presents studies and papers with the use of software simulation, such as (Yonghua Zhang et al. 2005) , in China, which presents a report on the design and analysis of micromechanical structures for an electromagnetic bi-stable RF MEMS switch, where electromagnetic driving forces were obtained using magnetic interaction. The authors explain the calculations for the electromagnetic specifications and provide mechanical force information, but the report is limited without the understanding of RF characteristics of the switching contacts and its voltage and current requirements.

Simulations provide designers and researchers with the ability to test novel structures quickly. (L. Liu 2007), published a report on high performance RF MEMS series contact switches. The report presents a new and novel cantilever beam switch with metal-to-metal contact switching. This proved a switch design for allowing high contact pressure to occur with the same electrostatic force, which in turn, reduced the overall contact resistance and provided a broader voltage range for actuation switching, while improving reliability. (M. Spasos et al. 2010), in Greece, published a report on the simulated analysis and design of an RF MEMS switch. The design of the switch is an all metal, in line series type ohmic RF MEMS switch, which is a novel Hammerhead design. The author explains that the switch is suitable for many applications but mentions there is more research work required on the control of the ohmic switching using stochastic (PSO) and Taguchi statistic optimisation.

Other design simulation examples occur in papers such as (S. Lakshmi et al. 2014), where it was presented on the design and simulation of multi-beam RF MEMS varactor. The paper proposes a novel design of implementing multiple fixed-fixed beams to increase the capacitance of the beam structure. The experimentation was conducted using Coventorware simulation tool, in order to find results of voltage requirements of the beam, which in turn provides the capacitance information of the structure. The observation discovered that if the number of beams rose then it would have increased the affected area, which therefore increases the capacitance range. It is noted that the structure of the switch would require a synchronised activation of electrostatic voltage, which may be considered a disadvantage, but with the use of different length of beams would overcome the disadvantage. (N. Saba et al. 2015), presented a paper on the simulation and analysis of actuation voltage of electrostatically actuated RF MEMS cantilever switch, the authors present a simulated concept design of a cantilever beam switch, which was originally designed by (H. Jaafar et al. 2011) (Design and simulation of high performance RF MEMS series switch). The simulation software used for the analysis was COMSOL Multiphysics, with the materials used from its own database. A comparison of four different types of materials were conducted and Aluminium was chosen to be the best choice. Also, a test on thicknesses of the beams and contact air gaps was conducted. The author then decided that the thinnest beam thickness, with a combination of the smallest air gap, would provide the optimum beam displacement for low voltage electrostatic actuation.

The paper presents the mechanical aspects of the cantilever beam switch, which also complies to the mathematical theory reported in the paper, but it does not explain the RF characteristics of the design, which in turn, does not provide grounds to prove the advantage of the switch for its own class within RF MEMS. Therefore, a comparison of how well it does against other cantilever beam switches is not applicable.

2.3.1 Electromagnetic Simulation

Simulation and modelling of EM (Electro- Magnetic) on RF MEMS switches provides an understanding of the characteristics of the devices ability to switch frequencies and provide isolation between switching. (L. Vietzorreck 2006), in Germany, published a study on the electro-magnetic modelling of RF MEMS devices. The study discusses the availability of modelling tools and techniques used for the creation of MEMS devices. It goes on to explain the two main types of full-wave analysis methods, e.g. frequency domain analysis and time domain analysis. The authors note that with the use of correct modelling and simulation software tools, MEMS components can be created efficiently with accurate performance results. As for (M. Wietstruck et al. 2013), in Germany, a report was presented on the electro-thermo and mechanical analysis of BiCMOS embedded RF MEMS switches. The report explains the significant influences of temperature on actuation voltages and on-state capacitance for BiCMOS embedded RF MEMS switches. The authors studied the effects of temperature on RF performance, the analysis results had shown a 0.1 dB change for insertion loss at 80 GHz. This proves small changes in RF performance is due to temperature. The analysis proved that with higher temperatures, the membrane begins to buckle and causes the actuation voltage to increase. The authors conclude the analysis proves that temperature significantly influences the pull-in actuation voltage and that this analysis is a vital step in providing an efficient process for design optimisation for temperature robust designs.

2.3.2 Modelling

With these advancements in simulation software, researchers are able to implement new methods of modelling and analysis. (D. Peyrou et al. 2008) , in France, presented a study on a novel methodology of simulating RF MEMS contacts. This new method allows the designer to improve the behaviour of the system at the surface level. The study examines two methods of generating surface roughness of the contact. The first method uses the original shape of the material and incorporates a novel reverse engineering method. The second method uses parametric design language to generate the normally distributed rough surface of the material. The author discusses that the simulated methodology helps to analyse roughness and provides a guideline for material choices for future MEMS designs. (Chuang et al. 2009) presented a paper on the electro-mechanical behaviour of the curled cantilever beam. The paper explains an analytical solution, in which the pull-in voltage of a micro curled cantilever beam can be approximated. The model takes into consideration the fringe field capacitance of the electrostatic plates and is used at the wafer level for extracting the young's modulus of the thin film used on the cantilever beam. The approximated analytical solution model is based on the Euler's beam model and minimum energy method. The author then verifies the analytical solution has improved accuracy over other published papers of similar models, where it compares the experimental data against the authors solution and other solution presented previously. Also, (Ansari, Cho 2009) presented their paper on the deflection, frequency and stress characteristics of rectangular, triangular and step profile micro cantilevers for biosensors. The cantilevers' characteristics were taken into consideration with consideration to surface stress. This study used the effects of 6 different types of cantilever structures and using Stoney's equation to mathematically model them. Three of the designs are standard designs and the other three as modified versions of the standard. The modified version would prove increased displacement over the originals. The study used ANSYS for finite element modelling and analysis to achieve results of the designs and demonstrated the comparison between the modified and standard. The authors proved this by increasing deflection and frequency characteristics. The micro-cantilevers can be a viable option for use within biosensors. The paper also showed good correspondence between analytical models and simulated results, which validated the conformity of both analysis. It was noted on the paper that although the triangular cantilever profile

presented the best deflection and frequency characteristics over the other two profiles, it would have manufacturing difficulties due to the angular design and therefore the step profile micro-cantilever beam would be a practical option for fabrication.

(T. Kim et al. 2013) , presented a paper using a novel method of approach on the modelling of an RF MEMS capacitive shunt switch, using artificial neural networks (ANNs). The scattering parameters (also known as s-parameters) and the structure resonant frequency are simulated using ANNs with high accuracy and a 1% difference from real world values. The ANNs models are based on a full-wave numerical simulation software called ADS Momentum. The authors mentioned that further research is required to reduce any predictive errors and to provide mechanical and electrical input and output parametric results of the switch. Also, a published report at IEEE, on the review of mechanical modelling of fixed-to-fixed beam for RF MEMS switches, which uses a cantilever beam as an example to describes the mechanical principles and functions for simulation of models. The mathematical analysis of the MEMS switch uses MATLAB as the simulation software. It is noted that the use of MATLAB helps to provide a complete analysis of the mechanics of a fixed-to-fixed beam, RF MEMS switch (T. Sharma, A. Tyagi 2013) .

Other studies in understanding the modelling has been researched by (M. Niessner et al. 2010), in Germany, with a published study on the experimental analysis and modelling of mechanical impact during dynamic pull-in of the RF MEMS switch activation. The experiment uses three models to analyse the simulated results to a physical result. The author concluded that no macro-model at the time the study was written, could provide correct physics during initial contact between the membrane and the contact pads. This is due to the higher Eigen-modes during initial impact and further research is required to understand the contact related Eigen-mode impacts. (M. Asaduzzaman et al. 2010), in Germany, presented a report on the electro-thermal and mechanical analysis of an RF MEMS switch. The switch is simulated and analysed using CST Microwave Studio software tool. The author proposed, in designing a RF MEMS switch, for NB Technology in Germany, with the use of two hot actuated armatures. Unfortunately, no other information of the RF and stress characteristics of the device were provided, although the author had noted much further analysis is required for the behaviour and performance of the switch.

(K. Said et al. 2016) presented a paper on the testing and characterisation of a MEMS micro cantilever system. The paper runs two types of practical testing on the cantilever array, the first testing is a static deflection test, where the cantilevers are validated via observation, using a novel optical workstation with a combination of both a surface profiler and a laser vibrometer. This test is to see the working order of the cantilever beam. The test recorded two sets of results, one at 10.2V and the other at 56.4V, with a displacement reading of 150 nm and 760nm, respectively. The dynamic test, which was used to determine the functionality while monitoring the resonant frequency was conducted for both piezo and electrostatic excitation. Although both results were similar, the piezo excitation analysis had a small discrepancy, which the author explains to be due to the background noise vibrations of the piezo disk itself, which interfered with the detected resonance signal. Both experiments were conducted under non-vacuum conditions and the author concludes the device would work ideally for frequency tuning applications. Although the paper describes in detail the mechanical characteristics of the cantilever switch, the paper doesn't take into account the RF performance of the switch.

2.3.3 Design Optimisation

Software simulation helps research to further optimise designs quickly and efficiently. (S. C. Roy, K. J. Rangra 2010) , in India, presented a report that explained the use of simulation software, such as HFSS, to simulate a design optimisation of RF MEMS switches, specifically single-pole four-throw and single-pole six-throw devices, with added optimisations to their Co-Planar Wave (CPW) transmission lines to provide a 50 Ω impedance on the line. These improvements were designed to improve a single SPST (single-pole single-throw) switch, which is used in an array to create SP4T and SP6T devices. These minimum changes have resulted in improvements to the insertion loss and isolation of both devices. (A. F. Malik et al. 2008) , in Pakistan, presented a study on modelling and design of an RF MEMS switch using simulation. The study presents an idea of optimising an RF MEMS switch by using shape memory alloy (SMA) to increase flexibility of the design and reduce the voltage to a desired voltage of approximately 5 V. A static and dynamic simulation was conducted using ANSYS

simulation software, which showed that the use of SMA materials required 30 V for actuation, but with the double membrane technique it was achievable down to 12.5 V. This had shown software simulation to provide a rapid approach to optimisation. Another study of this approach is from (Y. Gong et al. 2009) , in China, who conducted an optimal simulation design for an RF MEMS cantilever beam switch. The switch is based on a broadside MEMS switch created by Hughes Laboratory (HRL), which created a single-pole single-throw cantilever switch. The design was created using finite element modelling and analysis from ANSYS software with an orthogonal experimental approach. As for the simulation, it uses two layer back-propagation (BP) neural network, trained in Levenberg-Marquardt rule. Also, genetic algorithms are used to help optimise the design by random population of encoded candidates, called chromosomes. The simulation optimisations were calculated using MATLAB. The simulated optimisation has resulted in a 42.6% increase in the resonant frequency, which reduced the likelihood of damage to the beam, due to stress. This in turn displayed an improvement for the dynamic stiffness of the design. Random vibration has been taken into account with the use of ANSYS. After further optimisation of the random vibration simulation, the results generated an 85% improvement over the original design. Although the paper is about improving an original design though simulation, there is no written detail of any materials used or if they were taken into consideration for the simulations. However, the software simulation has shown to help increase the performance of the device. Another study has been carried out by (J. T. Huang et al. 2010) , in Taiwan, on the design and fabrication of an RF MEMS switch using CMOS fabrication. This study demonstrates an RF MEMS switch using 1P6M 0.18 μm CMOS fabrication process. For the designing of the RF characteristics, the authors used Coventorware modelling and simulation software tool. The switch showed a low voltage requirement of 2.8 V and an isolation of -75.8 dB at 2.4 GHz, from the simulation software. This paper is an improvement over the authors' previous paper in 2006. One of the noticeable differences between the studies are the improvements in the fabrication from the TSMC (Taiwan Semiconductor Manufacturing Company) CMOS 0.35 μm 2P4M process to the TSMC CMOS 0.18 μm 1P6M process.

Software simulation provides researchers with the ability to validate the design of the switch, allowing a precise example of the switch for real world testing. (C. Do et al.

2011) , in Ireland, presented their report on RF MEMS contact switch modelling, simulation and validation of SPST dynamic performance. The report takes into consideration the theories used for the geometry of a MEMS device such as Euler-Bernoulli beam theory, squeeze-film dampening and Hertz theory. This is to create an accurate dynamic analysis of an SPST RF MEMS switch. The analysis provides results of the device's switch closing times, number and duration of contact bounce, contact deformation and settling times. The comparison between the simulation and the physical experiment proved that the results of the simulation are closely related. The report shows a consistency between simulation and experimentation, for both controlled and uncontrolled actuation. Small discrepancies were observed within the electro-plastic contact mechanics and process, where further development is necessary.

Software simulation packages provide researchers a comprehensive set of tools to design, analyse and understand the characteristics of RF MEMS switches. (H. Jaafar et al. 2011) , in Malaysia, published a study of a design and simulation of a series of RF MEMS switches. The paper conducts a physical level design using Intellisuite 3D builder. Once the design had been created, it was simulated using Thermo-electro mechanical (TEM) simulator to provide stress and strain results. The authors were then able to obtain the optimum voltage levels required for the electrostatic plates. After this was completed, the design was simulated using the electro-magnetic (eMag) simulation. The authors were able to obtain the RF characteristics of the model and noted that the simulation results would help with the designs of future parameters for RF MEMS switches. There was another study by (C. A. Muley, S. A. Naveed 2013) , on the modelling of a cantilever RF MEMS switch. The study proposed a design and simulation using Coventorware modelling and simulation software tool. It conducted a purely simulated modelling and analysis with equations to support the theory. The electromagnetic model used a two-port theory for providing s-parameters. Although the design is a miniaturised example of a common cantilever, the switch proved to have a faster switching speed of 600 ns compared to conventional cantilevers, to date. This shows a unique advantage over existing cantilever designs.

Studies have been conducted in the optimisation of voltage levels with the use of software simulations. (Mafinejad et al. 2013) , in Australia, published a study on the RF techniques for reducing actuation voltages of RF MEMS capacitive shunt switches.

The study describes two options for reducing actuation voltages. The first option is to reduce the LC resonance from the micro-millimetre wave onto the X band frequency, using an inductive bridge. The second option is to use two short high impedance transmission lines for both ends of the co-planar wave line. The study establishes these options for reducing actuation voltages by proving the theory via software simulation. The authors conclude the design is able to use for wide bandwidth from C to K band with a reduction of the capacitive ratio from 50 to 21.4 compared to existing designs.

Another type of design optimisation has been carried out by (F. Ivaldi et al. 2016) , with a paper on a new approach for a multi-cantilever array sensor system with an advance MOEMS readout. The paper shows an overview of a general sensor system and examples of the performance results and compares them to the multi cantilever array, for which several vibrational modes are recorded. The paper presents an innovative way of sensing large arrays of cantilevers with the use of a single laser and a small sized position sensitive detector. The design proves its capability of performing high resolution and sensitivity measurements of the resonant frequencies and increased deflection. The design is a proof of concept, and further research and development is required to increase functionality. (S. B. Asutkar, P. Ghutke 2016) , proposed a paper on the novel approach for optimisation of an RF MEMS capacitive switch. The proposed design was of a fixed – fixed beam type capacitive switch, which requires minimal fabrication of layers, in order to reduce manufacturing cost while using nano scaled components to increase the yield per wafer. The design was created and simulated using Comsol Multiphysics version 5. The design itself used aluminium, due to its young modulus and was used for the fixed anchors and for the flexible membrane. This enables the stiffness of the device to be increased. Although the paper proposed a novel design, it only focused on the mechanical aspects of the switch and further information is not given for the RF characteristics. (J. Lin 2016) , presented a paper in Japan, about an ultra-wideband RF MEMS single pole four throw (SP4T) switch. The paper demonstrates the use of four shunt-configured cantilever switches with the use of resistive-contacts. The switches performance has proven to provide an isolation of less than -40 dB over a range of frequencies between 1 GHz to 5 GHz, with a voltage actuation requirement of 35-45 volts. Although the author has provided the RF characteristics of the switch, there is no mention of the design

software used, but there is a comparison of the RF performance from practical vs the simulated, in which the results came out similar.

Another design optimisation was to alter the cantilever beam to improve displacement while reducing the actuation voltage (R. Raman, T. Shanmuganantham 2016) , presented a paper on the design and analysis of RF MEMS switch with π-shaped cantilever beam for wireless application. The switch presents an operational range from 4 GHz to 12 GHz, while requiring an actuation voltage of 10 volts to pull the cantilever, with isolation of -90.80 dB at 12 GHz. The stress on the cantilever has proven to be low with 30.2695 MPa with an air gap of 1μm. Although the authors have explained the air gap distance there are discrepancies with the results they achieved on Intellisuite, as the displacement they have written was of 1.99581 10-5 μm. It is also noted that the paper is purely simulation based and does not compare other cantilevers directly and is considered as a novel design concept only.

2.4 Actuation Voltage Levels

Reducing voltage levels for RF MEMS has become an ever-increasing need, as it allows reduction of the number of components required that are normally used to step up voltages. This facilitates integration with other devices. (Hee-Chul Lee et al. 2005) , in Korea, presented a paper on the design and fabrication of a piezo actuated, RF MEMS contact switches for low voltage operation. The design operates at either 2.5 V or 3.5 V. The switch uses piezo-electrical actuation in order for the cantilever beam to deform to make contact. It is a single-pole single-throw switch, fabricated with an area of 1.3542 mm2 (i.e. 1.1 x 1.2 mm). HFSS 3D Momentum is used as a software analysis tool and the designing of the switch. The switch presents a compatibility advantage with CMOS fabrication processes, to allow low cost fabrication and enhanced integration to semiconductor circuitry. Also, (Mingxin Song et al. 2008) , in China, presented a paper on the design and analysis of a low actuation voltage, capacitive RF MEMS switch. The switch uses a long length and a thin width, folded-suspension beam. The fabrication process of the switch is done via simulation using a four-mask process. The switch was simulated to actuate below 5 V, with no disturbance from the resonant frequency. The switch was designed and analysed using Intellisuite, with an air gap of 2.5 μm. The authors note the design to be compatible

with CMOS control circuitry and improves the lifetime of the device, although there is no proof of real compatibility and reliability of the device.

(Y. Mafinejad et al. 2009) , in Australia, published a report on the design and simulation of a wide band RF MEMS switch with low voltage. The authors explain the different options of creating RF MEMS switches, which inevitably has complexities with fabrication processing. Also, an explanation into the problems RF MEMS suffers, such as ability of not achieving 0 dB compared to coaxial cable switches, with the inability of RF MEMS to withstand high power transmission handling. The report goes on to explain the desired outcome of the simulation (using EM3DS from MEMS Research) with an expected 6 V for actuation. This resulted in a working switch with frequency range from 2 GHz to 50 GHz. Although the authors explain that the simulation worked, there was no explanation of the resultant simulated parameters of the switch. Therefore, a comparison of the desired outcome and the simulated results cannot be made. Another study by (A. Akiba et al. 2010) , in Japan, presented a design concept of an RF MEMS switch mm-wave for 10 Gbps or greater. The RF MEMS switch incorporates an electrostatic comb drive actuation, to create a single-pole double-throw (SPDT) switch in which dual single-pole single-throw switches are fitted on the silicon interposer chip. The comb drive switch, with mm-wave, uses lateral actuation to avoid contact sticking, which ensures good reliability of the device. The device is driven using a 5 V electrostatic force, with an average actuation switching time of 10.3 μs, with no recorded ringing. The switch has shown a fast release time of 6 μs with a pressure of 2.5 kPa. The actuator had leaked 10 nA of current and the authors conclude that the combination of the MEMS technologies provides great value for mm-wave front-end circuitry.

Further studies published by (M. L. Ya et al. 2013) , in Malaysia, was conducted on the design and analysis of low voltage RF MEMS switches, which describe the use of low voltage electrostatic actuation for complementary metal oxide semiconductor (CMOS) MEMS switches. The study takes into account the drive voltage, von mises stress, displacement of the membrane and the capacitances of the up state and down state of the device. The RF MEMS switch is designed and simulated using COMSOL multiphysics simulation tool. As for the characteristics of the impedance of the Co-Planar Wave (CPW) lines, Agilent AppCAD analysis software tool was used. The drive voltage used for the design did not exceed 3 V, which proved a very low

actuation that is compatible with CMOS drive voltages for seamless integration of the switch without the implementation of any on-chip power source or charge pump. The author demonstrates that the combination of CMOS technology with RF MEMS switch technology provides low cost manufacturing and simplified fabrication techniques for RF MEMS switches.

2.5 Switching Methods

There are studies on the different methods of switching that allow RF MEMS to be configured for various applications and environments. (A. Fukuda et al. 2005) , in Japan, published a report for a reconfigurable power amplifier (PA) for mobile triple band protocol using RF MEMS switching, providing adequate isolation for a frequency range from 900 MHz to 2000 MHz. The authors were not able to explain details of the SPST switch. However, there is an explanation of the reconfigurable power amplifier, which would contribute to 'band-free' use of mobile terminals in the future. Also, (C. T. C. Nguyen 2005) , in the USA, presented a paper at the 42nd Design Automation Conference, on the architectures of RF MEMS. The report reviews the future of RF MEMS and the discussions of research up to the date of the report. The report explains the performance characteristics and applications of the devices. Also, the authors mention the research issues for each of the devices but concludes that changes in the architecture of the device can provide positive outcomes. The authors go on to explain that further advancements of automation for MEMS circuitry is required to gain benefits of the new architecture.

Novel designs in RF MEMS structures provide the switch with added functionality within a limited space envelope. (S. Pranonsatit et al. 2006) , in the UK, presented a paper on the design and fabrication of a rotary RF MEMS switches using the wobble motor principle. The switch is designed as a cartwheel, which is balanced by using a bearing at the centre. The cartwheel rotor is fabricated separately and manually fixed onto the stator with a bonded cap to keep the cartwheel rotor in place. The switch works by 'wobbling' at its pivot, using electrostatic pulling forces to make contact. The rotary switch is an SP8T (Single-Pole 8-Throw), which can provide switching for eight connections, using a single pole. The prototype has been tested to require a relatively high voltage of 100 V, using rectangular pulse widths of 10 ms. Although

the air gap has not been clearly stated, it can be roughly estimated to be 10 μm from the side view of the design. The authors have presented a highly innovative design for an 8-way switch, but due to the size of the cartwheel rotor, it requires a large electrostatic voltage and has a slow switching speed, with fabrication complexities. Also, (Jaewoo Lee et al. 2005a) fabricated design, of a Single-pole six-throw (SP6T) RF MEMS switch for use in multi band applications. The design of the switch is comprised of 6 individual single-pole single-throw (SPST) switches that are configured as two transmitters (Tx) and four receivers (Rx), which is designed for use in quad-band telecommunication applications. (Jaewoo Lee et al. 2005b) , later improved the design in a later report by increasing the frequency range from 0.5 GHz to 20 GHz, with the use of ANSYS multiphysics simulation package.

Other novel studies include the use of seesaw structures for use with RF MEMS switching. (J. M. Cabral, A. S. Holmes 2006) , in the UK, designed and fabricated a novel seesaw type SPST RF MEM switch, which included the implementation of a capacitive shunt across a CPW transmission line, providing switching operation from 0.1 GHz to 60 GHz. The design required no elastic recovery force which provided an advantage as it will not have problems with material stress and fatigue for prolonged use. With the use of a 'tower' to act as a pivot; this has the disadvantage of requiring power in order to function an 'off state'. The height of the tower has been set to a default of 10 μm and can be altered depending on the fabrication needs. This is to allow for a reduced contact distance, which results for lower voltage requirements. The disadvantage to this is that the switch isolation is degraded. The electrostatic drive voltage for the design states a requirement of 80 V but can be reduce down to 5 V by reducing the tower height. The manufacturing process complexity is a common disadvantage of this switch, which the authors state will be rectified over the coming years, due to advances in fabrication techniques. Another study from (Jongseok Kim et al. 2007b) , in Korea, conducted an experiment to design and fabricate of a SPST, variable pivot, seesaw RF MEMS switch for use in reconfigurable system applications. The design uses a seesaw motion in order to activate and deactivate the switch. It is fabricated using a silicon wafer, with a CPW signal line. To drive the electrostatic plates requires a voltage pull of 10 to 12 V. Using a fixed pivot, this has disadvantages for long term use, as it would cause the material at the pivot to crack and fatigue. It is acknowledged that the ohmic contacts could cause stiction due to

degradation. Also, (S. Kang et al. 2006), in Korea, designed and fabricated a seesaw type RF MEMS switch. The switch uses a fine Gap vertical comb drive. ANSYS software simulation tool was used for designing and HFSS for the electromagnetic simulation of the structure. The authors proposed the design to be used with wireless applications which run at 6V. The design is a metal-to-metal contact type using aluminium for the contact. The switch comprises of three parts, the bottom substrate, the movable silicon plate and the capping substrate for the packaging. The authors had noted that the design requires a considerably higher voltage to actuate the comb (40 V was required); this was realised due to the torsion bar of the practical design, which uses 10 μm compared to the simulated design of 3 μm. The authors were able to prove the new process in order to overcome aligning limitation of the seesaw comb-drive. Also, (Sungchan Kang et al. 2008), in Korea, presented a study on a working prototype of a SP4T RF MEMS switch using a double-stop comb drive configuration. The design works by using four sets of comb drive switches, which move laterally to allow switching between four distinct frequencies or bands. The design is simulated using Ansoft HFSS electromagnetic simulation software. The other software used is ANSYS, for creation of the mechanical design. The study requires further research to enhance the uniform characteristics of the switch and further examination of the measurements of the RF properties of the switch when packaged.

(H. H. Yang et al. 2015) created a switch and presented a paper on the symmetric and compact single pole multiple throw RF MEMS switches. This demonstrated the unique design of both a SP7T and SP11T type circular switch, which both use just a single pole to switch between either 7 contacts or 11. Although both designs demonstrated a large functionality, the switches' average isolation was approximately -19 and -17 dB, respectively, while requiring large actuation voltages ranging from 75 to 100 volts. Also, the size of the switches went beyond the micrometre scale. (I. C. Ghosekar et al. 2015), presented a paper on the SPMT, MPST RF MEMS switch using a multiplexing approach. The paper proposed the use of a single-pole multiple-throw (SPMT) and a multiple-throw single-throw (MTSP) type switches within a multiplexer. These cantilever type switches used electrostatic pulling forces to actuate the beam of the switch and used Intellisuite simulation software to analyse the design. The authors' do explain that the multiplexed approach of the system helps to provide a simpler selection of multiple switches and cascading the switches would make the

approach more efficient. The design materials of the switch beam and contacts are of Aluminium (Al), which proved to provide better response times as well as low actuation voltages. The pull-in voltages of the switches are 2.3V with a response time of 40 µs, with a current handling capacity of 20 mA and the switch itself is also within the microscale. Although the switches are shown to provide a great amount of advantages, the author has not explained the RF characteristics of the switch nor images, which directly shows the design of the switch.

Another design method was the use of multi metals for the contacts. A paper was presented by (Z. Jiang et al. 2016) on the use of Copper based multi metal contacts for RF MEMS switches. The design used a standard cantilever type beam switch, which uses three layers of metals, stacked on each other (Gold/Copper/Gold); this method was used to increase the overall contact hardness for the switch. The results had indicated that the multi metal layer configuration had provided seven times more hardness over a single metal type cantilever. The mechanical characteristics of the switch was shown to have a switching speed of 39 µs with an actuation voltage of 36.6 volts and the measured isolation of the switch was -25 dB up to 20 GHz. This cantilever design is a novel approach by using multiple metals for the fabrication of the beam.

2.6 Contact Analysis

As RF MEMS is a mechanical moving component, ohmic contact switches require direct contact, also known as metal-to-metal contacting. This, over time, causes wear of the RF contacts and eventual failure of the device. (J. Oberhammer, G. Stemme 2006), in Sweden, published a paper on the active and passive forces on electrostatic switches for soft metal contacts. The design is a mechanically bi-stable, electrostatic actuation switch mechanism using a large active opening force with a small passive closing force. This is to accommodate soft type metals, such as gold for the contacts. The authors note that the design helps to prove the use of low force actuation for increased reliability of the gold contacts.

Contact analysis is taken into consideration when it comes to stiction as it causes the switch to respond in an improper manner. (Lingbo Zhu et al. 2005), in the USA, published a report of the lotus effects on surfaces. The report aimed to prevent stiction

on MEMS devices. Two types of stiction are identified, ‘release-related stiction’, which occurs within the sacrificial layer removal processes, due to capillary forces. The other type of stiction is ‘in-use stiction’, which normally happens due to the microstructure being exposed to a humid environment. The authors propose an answer to this problem using super-hydrophobic surfaces at the contacts. This can help to avoid stiction of the capillary forces due to the reduced van der Waals forces from the MEMS substrate. The super-hydrophobic surface provided a low surface energy coating with little contact angle hysteresis. The authors noted that super-hydrophobic coatings can effectively avoid stiction due to capillary and van der Waals forces. (A. Hariri et al. 2007), in the USA, also, published a report on the modelling of wet stiction on MEMS devices. The report presents a newly developed model for predicting stiction for uncharged micro components interacting within a humid environment. The theoretical model results are compared to existing practical experiments. The results have concluded that hydrophilic surfaces provide a dominant capillary force, compared to rough surfaces. The new model is based on a novel n-point asperity modelling. The authors compare other theoretical predictions to the new model and conclude the new model provides results that are closer to experimental data. However, the comparison is only based on a single source of experiments and further work would be required to verify the accuracy. The new model demonstrated a powerful and easy-to-use approach for approximating values of stiction within wet conditions.

Contact analysis is used to analyse the reliability of switching high power RF. (Hyouk Kwon et al. 2007), in Japan, published a report for the reliability of high power RF MEMS switches for contact materials. The paper conducted an experiment using gold (Au), platinum (Pt), iridium (Ir) and AuPt alloy, to find which contact material would be most suitable for providing greater reliability for high power RF MEMS switches. The experiment resulted with Au-to-Pt and Au-to-Ir providing enhanced reliability for metal-to-metal contact switching for high power RF MEMS switching applications.

Contact analysis is also used to analyse the transmission of RF though the contacts. (Pennec et al. 2009), in the USA, presented a study on the electrical contact resistance of RF MEMS. The study conducts a computer simulation using ANSYS finite element modelling to simulate the interaction between asperities (roughness of the surface of the contacts), bulk deformations and electro-plastic deformations. A unique reverse

engineering method was created to be implemented with ANSYS, in order to generate rough surfaces of the contacts. For the simulation, the authors used a metal-to-metal, ohmic type switch with gold-to-gold contacts. The practical simulation was fabricated and conducted at NovaMEMS / CNES laboratories. The authors' results had displayed limitation of the software simulation due to ANSYS only allowing a resolution of up to 0.9 μm. This caused inaccuracies when conducting contact roughness simulations of less than 25 μm x 25μm. This method provides RF MEMS ohmic type switches with a guideline for choosing materials and fabrication processes to minimise the resistance at the contact.

In this literature review, the research on reliability and performance has shown to be a key link between the different areas of research (i.e. materials, types of simulation, actuation voltage levels and contact analysis). For example, the choice of material, actuation voltage and size can all affect reliability and performance.

RF MEMS switches require their existing actuation voltages to be reduced in order to be successfully integrated within current mobile technologies. To meet customer demands, RF MEMS switches also need improved performance and reliability.

Chapter 3

3 Mathematical Modelling

The mathematical modelling provides an analysis of the switch design, providing a theoretical analysis of the results. For RF MEMS designs, the following models are based on a cantilever design, which was chosen to evaluate the performance using mathematical analysis, giving analytical results in specific areas of the structures, such as:

- Electrostatic Actuation
- Theoretical Modelling of a Cantilever Beam: Displacement of a Beam Structure
- Resonant Frequency
- Electromagnetics Two Port Network Analysis

3.1 Electrostatic Actuation

When a potential difference is applied between two parallel plates, where electrons accumulate on one plate, and holes accumulate on the other. The positive and negative charges on these plates causes a force to be developed due to the attraction of the charges. The force is known as an electrostatic force, which is dependent upon the voltage applied, the area of the plates, distance between the plates and the dielectric between them. This force is defined by the following Equation (Rebeiz 2003):

Equation 3.1

$$F = \frac{V^2 \varepsilon_0 A}{2d^2}$$

Where,

V = Supply voltage

ε0 = Permittivity of free space

A = Area of the electrostatic plate

d = Distance between the electrostatic plates

F = Force between the electrostatic plates

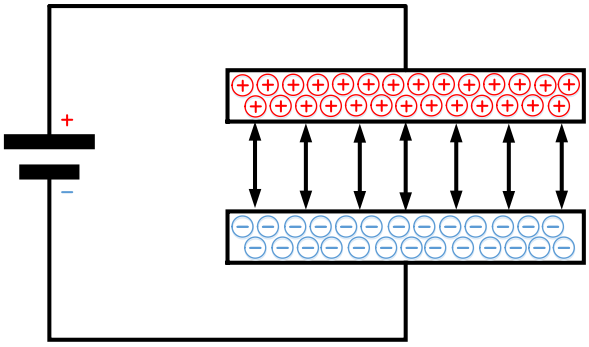

Figure 3.1: Schematic diagram of the electrostatic force on parallel plates

3.2 Theoretical Modelling of a Cantilever Beam

There are several parameters associated with the modelling of a cantilever beam, which include:

- Moment of Inertia of a beam
- Displacement of the beam
- Extension of the beam
- Stress and Strain of the beam
- Spring Constant (Elastic Recovery) of the beam

3.2.1 Moment of Inertia of a beam

With a given cantilever beam with a thickness, t, and width, w, its moment of inertia is defined by the following Equation 3.2 (KUBBY, J.A. 2011).

Equation 3.2

$$I = \frac{(w.t^3)}{12}$$

3.2.2 Displacement of the beam

When a given, force is applied to the cantilever beam its displacement is defined by Equation 3.3 (KUBBY, J.A. 2011.

Equation 3.3

$$\delta = F.\left(\frac{L^3}{3.E.I}\right)$$

Where:

F = Force

L = Length of the beam

E = Young's Modulus of the material

I = Moment of Inertia (As defined in Equation 3.2)

3.2.3 Extension of the beam

As the cantilever extended when a force is applied this can be calculated using Equation 3.4 (KUBBY, J.A. 2011).

Equation 3.4

$$\Delta L = F.\left(\frac{L}{E.A}\right)$$

Where:

E = Young's Modulus

A = Cross-sectional area of the beam

F = Force

L = Length of the beam

3.2.4 Stress and Strain of the beam

Strain is the deformation of a material to an applied force. If the stress or strain is small the beam will return to its original state. This is known as elastic deformation, whereby the material stress is below the yield strength. If the stress of the beam goes beyond the yield strength after the force is removed, this will cause plastic deformation whereby the beam would not recover to its original state.

Stain is defined as the ratio of the beam's extension to its length after a force is applied, which is shown in Equation 3.5 (KUBBY, J.A. 2011):

Equation 3.5

$$\varepsilon = \frac{\Delta L}{L}$$

Where:

ΔL = Extension of the beam

L = Length of the beam

Once the strain is known the stress can then be calculated using Equation 3.6 (KUBBY, J.A. 2011).

Equation 3.6

$$\sigma = E \,.\, \varepsilon$$

Where:

E = Young's Modulus of the beam

ε = Strain of the beam

3.2.5 Spring Constant (Elastic Recovery) of the beam

In the 17th century Robert Hooke discover the relationship in the stress verses strain curves for a number of materials with the linear region. The force required to stretch a material is directly proportional to its extension within a limited range. This relationship is known as Hooke's Law, as defined in Equation 3.7 (KUBBY, J.A. 2011).

Equation 3.7

$$F = k \,.\, \delta$$

Where:

k = Spring Constant

δ = Displacement of the beam (extension/compression)

By rearranging Equation 3.7, the spring constant is defined in Equation 3.8 (KUBBY, J.A. 2011).

Equation 3.8

$$k = \frac{F}{\delta}$$

By rearranging and expanding the equation gives:

Equation 3.9

$$\frac{1}{\delta} = \frac{3 \,.\, E \,.\, I}{L^3} \,.\, F$$

Therefore

Equation 3.10

$$\frac{F}{\delta} = \frac{3 \,.\, E \,.\, I}{L^3}$$

Where $\frac{F}{\delta}$ is the spring constant also known as *k*.

The spring constant can be fully realised as:

Equation 3.11

$$k = \frac{F}{\delta} = \frac{3 . E . I}{L^3} = \left(\frac{3 . E}{L^3}\right)\left(\frac{w . t^3}{12}\right)$$

3.3 Resonant Frequency

Resonant frequency occurs in all materials, resonance change with the structure.

Resonant frequency also known as resonance, is the phenomenon which occurs when vibration from an external source induces an oscillation of the structure or system. Resonance can occur using either mechanical, electrical, acoustic or electromagnetic waves. When the energy of these waves is used as a stimulus on a structure or system with the same natural frequency, it can cause catastrophic effects. However, when it is controlled, resonance serves a useful purpose in many disciplines.

An example of mechanical resonance are environmental chambers, which contain vibrators that induce vibrations within a range of frequencies to the mechanical structure under test, in order to locate the natural frequency of the design. Electronics circuits use resonance to amplify electrical signals; such as radios, TV's and Wi-Fi etc. A tuning fork uses acoustic resonance to create a reference frequency for the purpose of tuning musical instruments. Antennas use resonance to create and receive high frequency electromagnetic waves for communication.

It is important to understand the resonate frequency of the structure, so that we avoid frequencies which would be detrimental to the design.

3.3.1 Resonant Frequency of a Beam

As mentioned previously, all structures have their own natural frequencies which the resonant frequency can affect it.

In order to avoid these frequencies, it is required to find them using the resonant frequency beam equation. This allows the designer to create a beam with a resonant frequency that avoids the switching frequency, in order to prevent damage to the cantilever structure.

The cantilever design described by Daniel Hyman et al. (Hyman et al. 1999) uses the following equation:

Equation 3.12

$$f_0 = 0.16\frac{d}{L^2}\sqrt{\frac{E}{\rho}}$$

Where:

E = Young's Modulus of the material for the beam

ρ = Density of the material for the beam

d = Thickness of the beam

L = Length of the beam

Note: 0.16 used in the Equation 3.12 represents $\frac{1}{2\pi}$

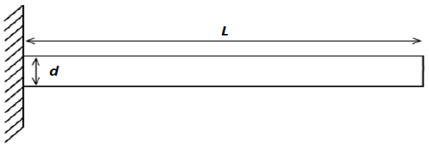

Figure 3.2: Image (Ansari, Cho 2009) , of a fixed-free beam but edited to illustrate the Equation 3.12

Also, as a comparison a second resonant frequency equation can be found in can be found in their journal paper (Ansari, Cho 2009).

Equation 3.13

$$f_0 = \frac{1}{2\pi}\sqrt{\frac{E{t_0}^3}{\rho(l_0 t_0 + lt)(l_0 + l)^3}}$$

Where:

E = Young's Modulus of the material for the beam

ρ = Density of the material for the beam

l_0 = Length of part of the beam closest to the anchor point

l = Length of part of the beam furthest from the anchor point

t_0 = Thickness of part of the beam closest to the anchor point

t = Thickness of part of the beam furthest from the anchor point

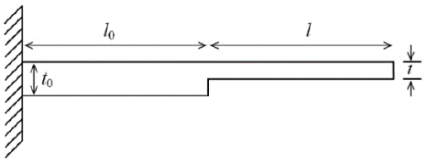

Figure 3.3: (Ansari, Cho 2009) Step Profile Cantilever

Since t_0 and t are the same in the cantilever beam the equation can be simplified to equate to Daniel Hyman's (Hyman et al. 1999) equations as follows:

Equation 3.14

$$f_0 = \frac{1}{2\pi}\sqrt{\frac{Et^3}{\rho t(l_0+l)(l_0+l)^3}}$$

$$f_0 = \frac{1}{2\pi}\sqrt{\frac{Et^2}{\rho(l_0+l)(l_0+l)^3}}$$

$$f_0 = \frac{1}{2\pi}\sqrt{\frac{Et^2}{\rho(l_0+l)^4}}$$

$$f_0 = \frac{t}{2\pi}\sqrt{\frac{E}{\rho(l_0+l)^4}}$$

$$f_0 = \frac{t}{2\pi(l_0+l)^2}\sqrt{\frac{E}{\rho}}$$

It can be seen from Equation 3.12 is similar to Equation 3.14. Also, $l_0 + l$ is the same as L as it is the total length of the beam.

The equation used here, when simulated on Intellisuite provides an exact resonant frequency of the beam, on the condition.

3.4 Electromagnetics Two Port Network Analysis

Electromagnetics (EM) is used to understand the RF capabilities of the RF MEMS switch. This allows the engineer to identify the frequency range in which the design can be used for.

3.4.1 Two Port Network

Two port networks are used to provide the electromagnetic information of any device under test (DUT). The information required for this research are the scatter parameters. Scattering matrix also known as S-matrix is a mathematical quantification of how RF energy would propagate in port networks providing the scatter parameters alternatively known as s-parameters. Port networks can be considered multiple ports but for this instance the use of two port network is used due to the switching nature provided as an input and an output.

As two port networks are used, the terminals are split into two pairs, with each pair consisting of an input and an output. Four parameters can be set from this S11, S12, S22 and S21.

S11 is the reflection coefficient at port 1, whereby the signal sent from port 1 has been reflected through the port. S22 is considered the same but is the reflection coefficient at port 2 (HRANAC, R 2005).

Equation 3.15

$$Return\ Loss\ (RL(dB)) = S_{11} = \Gamma = \frac{V_r}{V_i}$$

Where:

V_r=Reflective Wave Voltage

V_i = Incident (input) wave ratio

Γ (Gamma) can be converted from a ratio to decibels (dB) using the following equation.

Equation 3.16

$$RL\ (dB) = -20\ log_{10}\ \Gamma$$

S12 is the isolation, other names given are; reverse gain and reverse isolation, this is where it can be identified if the DUT has an isolation or gain between the two ports when the signal is transmitted from port 2.

S21 is the insertion loss. This is the loss of signal power resulting from the device under test. These parameters are shown in Figure 3.4.

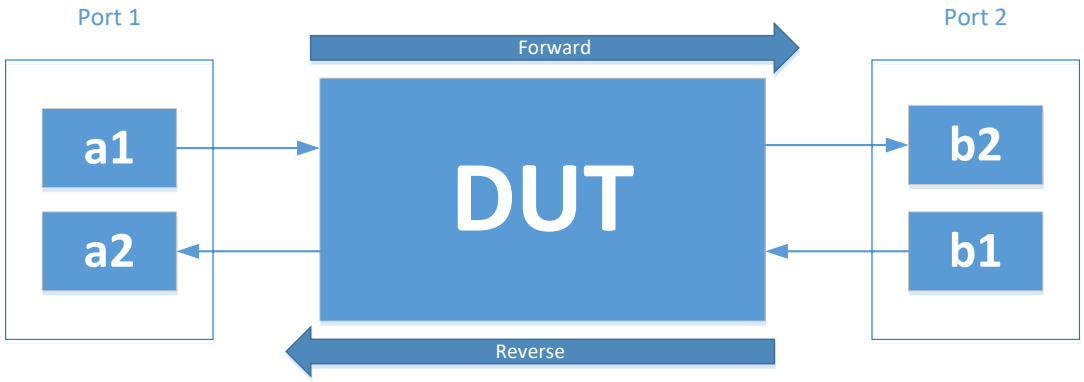

Figure 3.4: Two Port Network diagram

Note: a1 and a2 are input and outputs, respectively, for port 1 and b1 and b2 are input and output, respectively, for port 2. The S-parameters are defined by the following equations (https://www.microwaves101.com/encyclopedias/438-s-parameters-microwave-encyclopedia-microwaves101-com, viewed 11/02/18):

$$S_{11} = \frac{b1}{a1}$$

$$S_{12} = \frac{b1}{a2}$$

$$S_{21} = \frac{b2}{a1}$$

$$S_{22} = \frac{b2}{a2}$$

S_{11} and S_{21} are derived from network measurements when the incident signal value is set for a2 at 0 and solving them as a function of a1. The same is considered for S_{12} and S_{22}, which are derived by setting the incident value of a1 to 0 and solving the ratios as a function of a2. These are shown diagrammatically in Figure 3.5, Figure 3.6, Figure 3.7 and Figure 3.8.

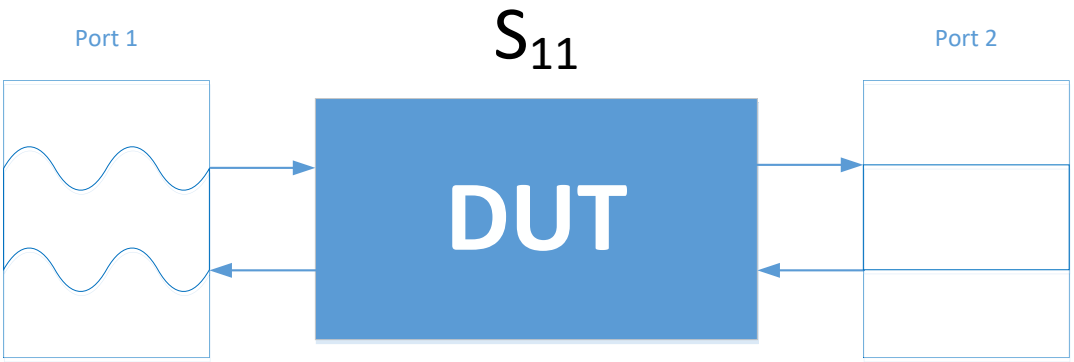

Figure 3.5: Two Port Network analysis setup for S11 parameters when Port 1 is active and port 2 is 0 (short), Port 1 is reflected

Figure 3.6: Two Port Network analysis setup for S21 parameters when Port 1 is active and port 2 is 0, Port 1 to 2 is pass though.

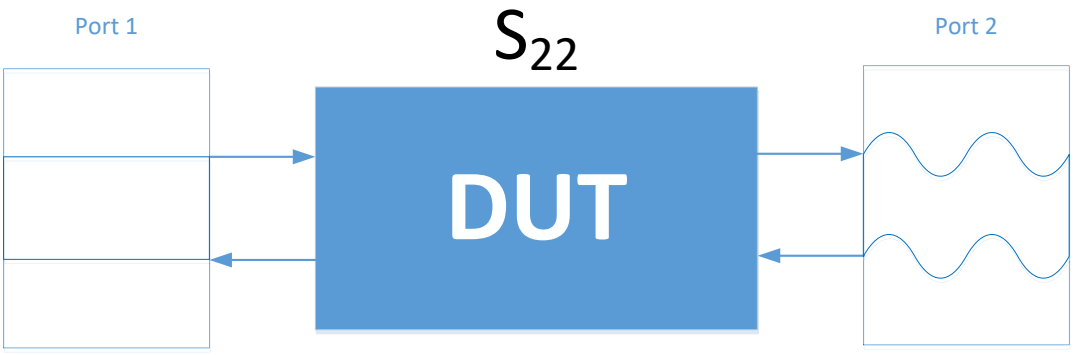

Figure 3.7: Two Port Network analysis setup for S22 parameters when Port 2 is active and port 1 is 0. Port 2 is reflected

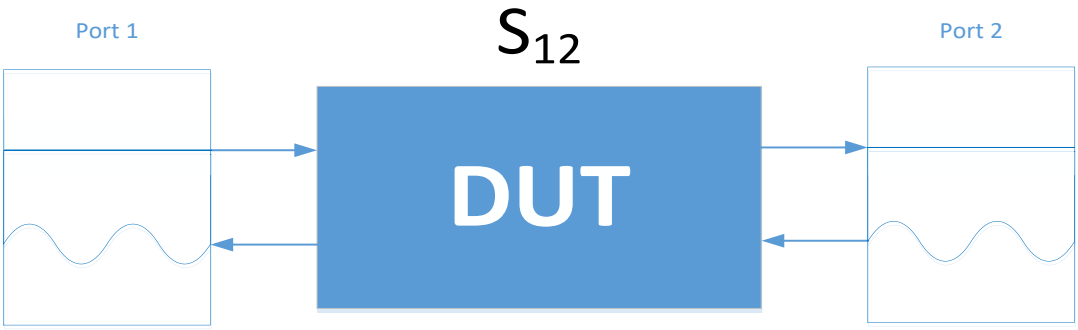

Figure 3.8: Two Port Network analysis setup for S22 parameters when Port 2 is active and port 1 is 0. Port 2 to 1 is passed though

S-parameters integrates the use of real and imaginary or the magnitude and phase parts as they are changed by the network. These input and output parameters can be obtained via practical method using a Vector Network Analyser (VNA) or by simulation. For pragmatic reasons simulation, has been used to generate and obtain these parameters via CST (Computer Simulation Technology) Electromagnetic Simulation software.

3.5 Finite Element Modelling

Finite Element Modelling (FEM), also known as Finite Element Analysis (FEA) is a numerical method. FEM is used to solve engineering problems relating to problems which include structural analysis, electromagnetics and electro-mechanics. This method results in a set of simultaneous algebraic equations, which require boundary parameters to be applied to the governing equation (Equation 3.17) in order for it to be solved (Nielsen, C. V et al 2013).

Equation 3.17

$$K.U = F$$

Where:

K = Property

U = Behaviour

F = Action

Table 3.1: Example of parameters for Governing Equations

	Property (K)	**Behaviour (U)**	**Action (F)**
Elastic	Stiffness	Displacement	Force
Electrostatic	Dielectric Permittivity	Electric Potential	Charge

Figure 3.9 shows a structure, which is made up of a group of elements and nodes to create a mesh. Shared nodes provide an assembly of elements for the global equation shown in Equation 3.17. Where K is the property of the material, U is the behaviour and F is the action or the consequence of the applied load to the material. These can change depending on the type of analysis required, either elastic (to find the movement or force exerted onto the material) or electrostatic (to find the resultant charge).

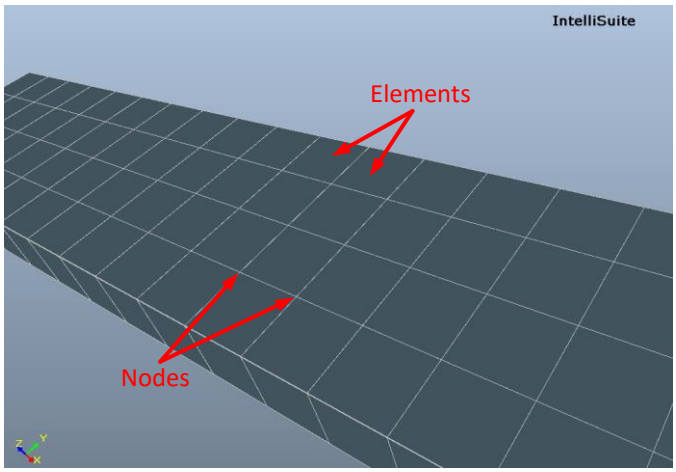

Figure 3.9: Example of a Meshed Structure with Elements and Nodes indicated

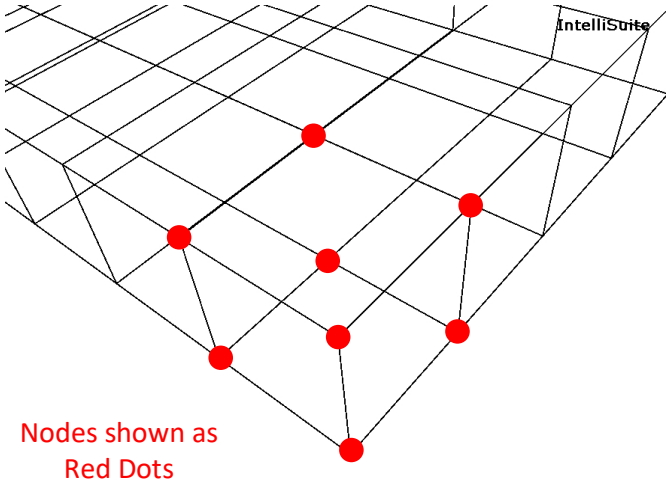

Figure 3.10: Example of Mesh Structure with Highlighted Nodes on a Surface Wire Mesh View

The algebraic equation for each element is defined by Equation 3.17 and all the element equation within the structure are combined together. Intellisuite is a purely 3D finite element analysis, which is controlled by the 3D governing equations (Equation 3.17). This analysis is a non-linear process, which approximates complex structures. Due to the complexity of the structure a linear mathematical approach is not practical.

This chapter provides mathematical modelling of the fundamental parameters a cantilever switch. It also provides a theoretical background of the methods employed for electromagnetics (i.e. two port analysis), resonant frequency, finite element modelling and electrostatic actuation.

Chapter 4

4 Engineering Design Process

This chapter describes the approach taken for the research and development of the RF MEMS switch designs. It later describes the implementation of the use of Intellisuite and CST for simulating the designs, using Finite Element Modelling (FEM) for designing and Finite Element Analysis (FEA) for simulation. Both these methods provide a significant contribution to the development of the RF MEMS switch, which include all the associated parameters required to start a simulation.

The FEM modelling focuses on a two-dimensional (2D) layout of the structure with the intent of creating a three-dimensional (3D) design model. The FEA simulation uses the FEM design to provide stress, displacement and electromagnetic outcomes of the structure, for a given voltage input.

The use of FEA and FEM software tools provides an expedient approach to design and simulation, while reducing cost to a minimum. These software tools can be used on a high specification computer to provide computational data of the structure for a MEMS device. The software tools provide high precision analysis with regular updates.

4.1 Selection of Software Modelling and Simulation Tools

For improving the RF MEMS switch, a modelling and simulation tool, also known as Finite Element Modelling (FEM) and Finite Element Analysis (FEA), is required for computer aided design (CAD) with computational analysis. The FEM and FEA simulation tools provide the user with a rapid method for designing, simulating and optimising. This approach reduces cost for analysis due to being highly accurate virtual simulation (with respect to the physical design).

The following modelling and simulation tools were reviewed to select the optimum tool suitable for design and analysis of the switch:

Intellisense

Intellisuite provide a graphical user interface (GUI) tool for users to develop and analyse MEMS devices. The software is designed for MEMS development only but provides a simple CAD FEM tool with a validation tool to detect any errors in the mesh. Intellisuite uses an intuitive method for designing, allowing the user to draw the shape on a grid using a mouse. Also, during analysis for assigning the boundaries, the user can again use the mouse to point and click on the MEMS structure to assign the boundary conditions.

Coventor

Coventor, with their software called Coventorware, is similar as Intellisuite, but requires more time during CAD FEM designs due to the complexity of drawing, requiring the user to plot the shape of the design using the x, y and z axis. Also, all boundaries are required to be assigned before analysis, with the use of a table. This causes mistakes as the user cannot see the design while assigning the boundaries and the boundary number needs to be noted before being assigned.

Comsol

Comsol is considered an all-in-one tool with a module specifically for MEMS design and analysis. The software requires the user to assign the correct module for analysis before creating the RF MEMS structure. This method can overwhelm the user due to the variety of modules available; the principles of design and analysis are similar to Coventorware.

ANSYS

ANSYS is very similar to Comsol but is considered one of the most popular FEA and FEM tools in the market with a large online community of people to help with most problems. ANSYS is installed as modules and the concept of the software is the same as Comsol, with a larger range of analysis modules to cover various types of analysis. This again causes problems for the user as it will require a steep learning curve of the software.

Computer Simulation Technology (CST)

Computer Simulation Technology, also known as CST, is predominantly a FEA and FEM design and simulation tool for electromagnetic (EM) design and analysis. However, it can also be used for particle physics. CST, provides a range of plugins to allow imports of geometries created from other software tools. CST EM design and analysis is intuitive allowing the use of port analysis with a simple GUI interface.

With the choices of software, more value is given to the software supplier in providing efficient and reliable customer support, with initial training to provide rudimentary skills for operating the software tools. The learning curve of the software is also given special significance in the decision making, as this helps increase productivity, since the user will be able to start promptly on the simulation project.

Table 4.1: Comparison of the Simulation Software

	GUI Interface	Types of Simulation	Customer Support	Learning Curve
Intellisuite	User Friendly – 5/5 Intuitive – 5/5	MEMS Only Simulation	Free Support - Within 1 day Regular Updates from customer response	4/5
Coventor	User Friendly – 2/5 Intuitive – 3/5	MEMS Only Simulation	Support – Within 7 days Updates available	3/5
Comsol	User Friendly – 1/5 Intuitive – 2/5	Comprehensive set of Simulations	No Support available unless paid for Updates available	2/5
Ansys	User Friendly – 1/5 Intuitive – 1/5	Comprehensive set of Simulations	No Support available unless paid for Updates available	2/5
CST	User Friendly – 5/5 Intuitive – 5/5	RF and Physics Simulations Only	Support – Within 7 days Updates available	5/5

Note: 1 = lowest score and 5 = highest score

For this research, Intellisuite from Intellisense was chosen, due to the intuitive 3D FEM modelling tool, providing a WYSIWYG (What-You-See-Is-What-You-Get) outcome of the design with a user-friendly GUI (Graphical User Interface), a gentle learning curve compared to the other FEM and FEA packages and reliable customer support, which provides a fast response to problems with emails and software updates. This gives the user a speedy implementation to the modelling of the RF MEMS switch structure. The other software tool chosen for the research is CST, for its powerful yet intuitive importing of geometries and its EM port simulation for MEMS devices. A comparison table between the different software packages is shown in Table 4.1.

4.2 Preliminary Sketch Modelling

Before starting modelling on the FEM tool, a number of hand drawn outline designs were sketched (as shown in Figure 4.1). This approach provides an expedient means of planning and preparing the design before implementing it to a model.

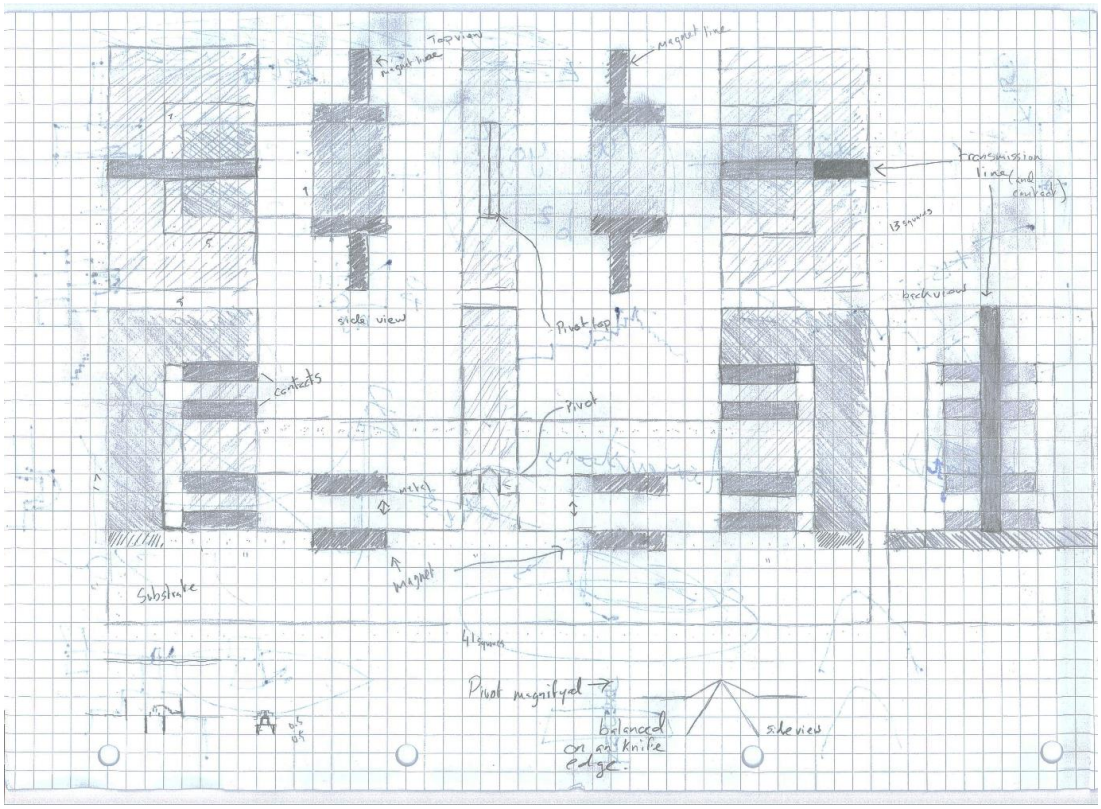

Figure 4.1: Preliminary sketch of initial RF MEMS design

4.3 Experimental Methodologies

The experimental methodologies are in accordance with the Aims and objectives described in sub chapter 1.5.

4.3.1 Implementing Design to Intellisuite 3DBuilder

With the use of Intellisuite FEM package. The outline sketches were manually drawn as a model within 3DBuilder (shown in Figure 4.2).

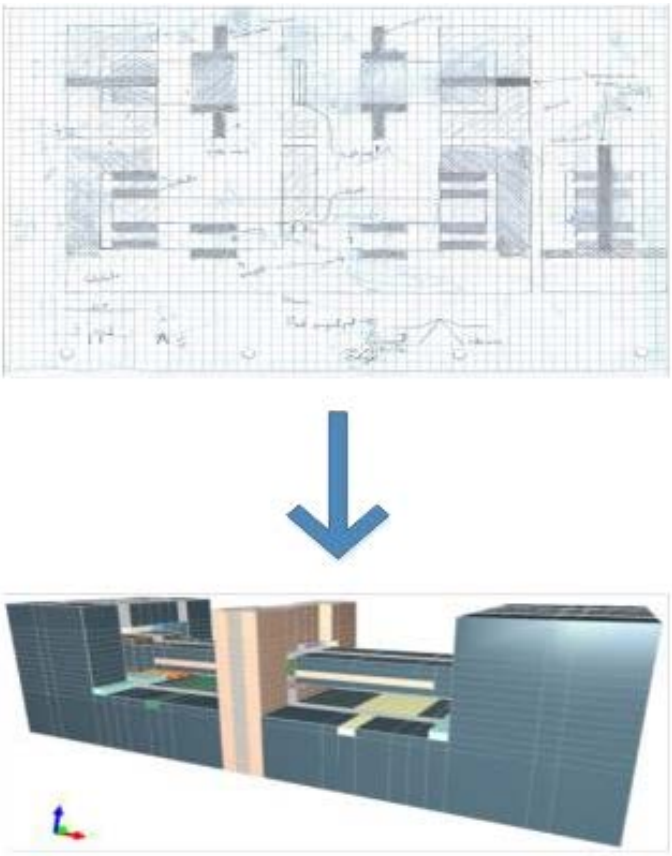

Figure 4.2: Implementation of sketches to a simulated model

Once the model is completed initial validation tests are applied to see if it complied with the simulation package. These are the mesh connectivity and conformity shown in Figure 4.3 and Figure 4.4. The mesh connectivity verifies that all nodes of the mesh are connected correctly on the x, y and z axes without any overlapping or misalignments. If an error occurs the tool will highlight the area. The mesh conformity validates if any illegal elements have been applied to the model which will again be highlighted.

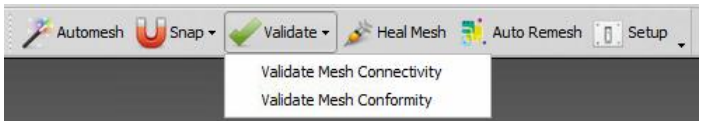

Figure 4.3: Validation options on 3DBuild

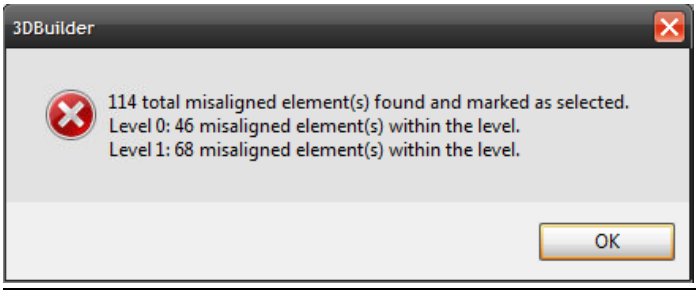

Figure 4.4: Validation error results

4.3.2 Setting Up Intellisuite TEM Simulation Analysis

Once the 3Dbuilder model is designed and validated it is then passed on to the Thermo Electro-Mechanical (TEM) simulation module. This allows a fast-analytical analysis of stress, displacement, force and speed, within the structure of the design. The results can then be transferred to VisualEase which can then visually interpret the results (shown in Figure 4.5).

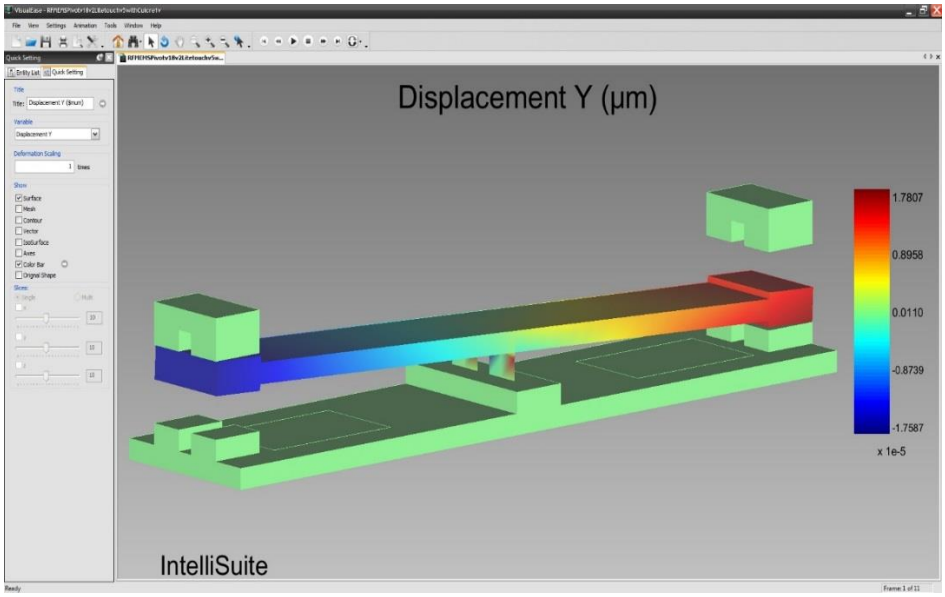

Figure 4.5: VisualEase representation of the RF MEMS switch simulation displacement

For analysis to occur using Intellisuite simulation software tool, such as Thermo-Electro Mechanical (TEM), parameters are required to be set, i.e.:

- Mesh size
- Material Characteristics
- Boundary conditions
- Voltage Loads

These are also explained in the following sub-chapters.

4.3.2.1 Meshing

One of the important factors for analysis is the mesh, each point of the mesh is known as the node. Each mesh provides the FEA tool information of the material and structural properties, in order to define the structural reaction during different loading conditions. For this method with the use of Intellisuite, a small mesh size is applied using Intellisense's auto-mesh tool, this tool applies a user-defined quadrature mesh to the whole RF MEMS structure. For specific applications, a further mesh is applied, these meshes are used for the mechanical structure of critical points of the design to provide improved resolution of the area in question. The electrical mesh is applied to define the materials, which will activate the electrostatic plates, to, again, provide a better resolution of how the structure will react. Figure 4.6 shows the assignment of the mesh.

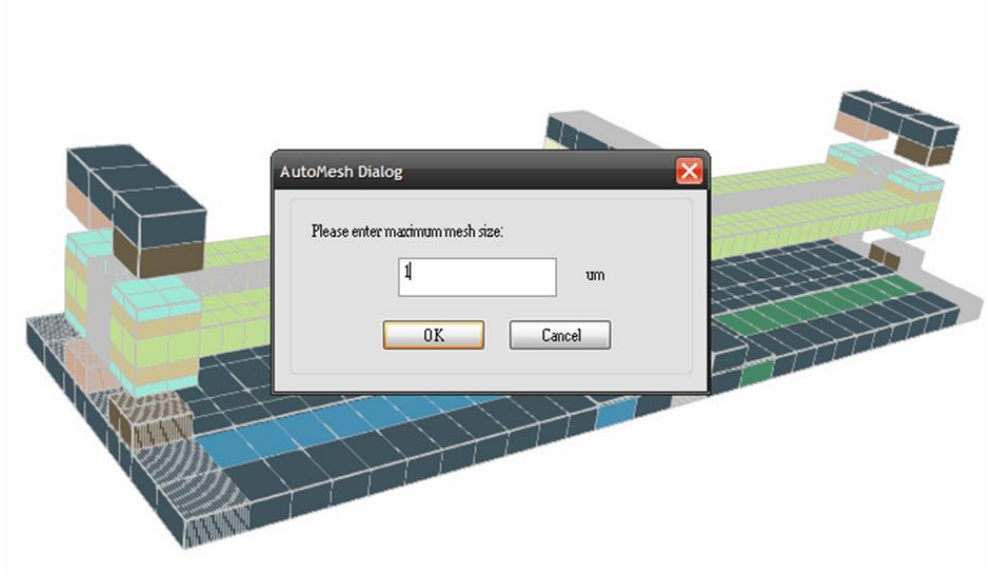

Figure 4.6: Example of the assignment to the seesaw model

4.3.2.2 Material properties

In order to decide the correct material for analysis, the material properties are required to be studied, (Sharpe et al. 2004), (McGruer et al. 2006), (Pratap, Arunkumar 2007), (Stanimirović, Stanimirović 2009), Material characteristics, such as flexibility with elastic recovery, are decided with Young's Modulus and Tensile Strength (shown in Table 4.2). During simulation, the material will require to be sufficiently flexible to make contact with a low Young's modulus with sufficient tensile strength to withstand stress while being flexed and provide elastic recovery to return to its original state without deforming permanently. Material properties can be applied using Intellisuite's Material Database, which take in to account common materials used for MEMS applications. This is shown in Figure 4.7.

Table 4.2: Material Properties

	Materials				
	Copper	Aluminium	Silver	Gold	Tungsten
Young's Modulus (GPa)	117	69	83	79	411
Yield Strength (MPa)	70	7 - 11	0	0	0
Ultimate Yield Strength (MPa)	210	40 - 50	170	120	1510

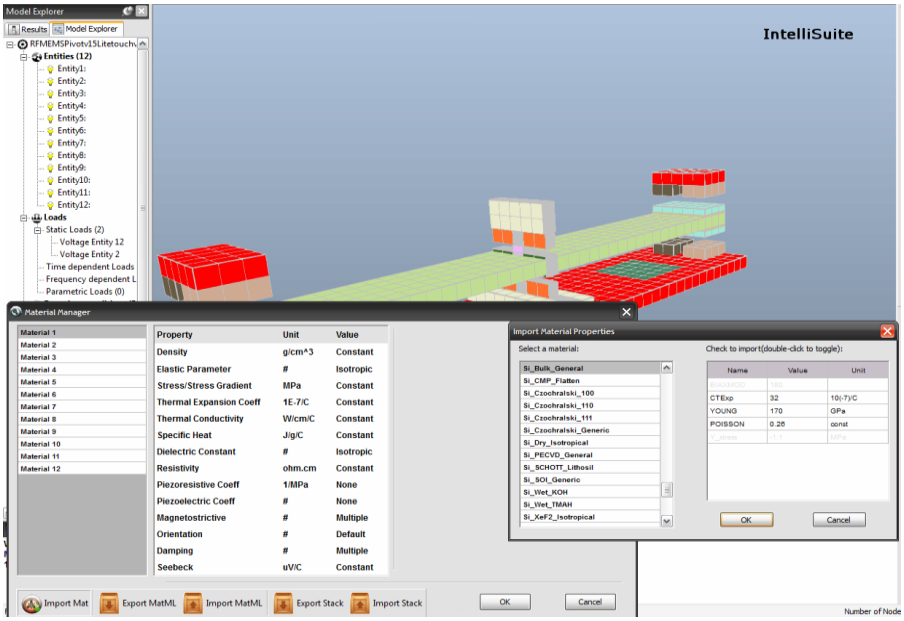

Figure 4.7: Intellisuite Materials database within TEM Simulator

4.3.2.3 Boundaries

Boundaries provide the simulation tool information of the model, by providing parameters of the areas of the model which will be either fixed or moving on each direction of the axis. This in turn helps the simulation with a reference point to anchor from. An example of applying a fixed boundary is shown in Figure 4.8, which is highlighted.

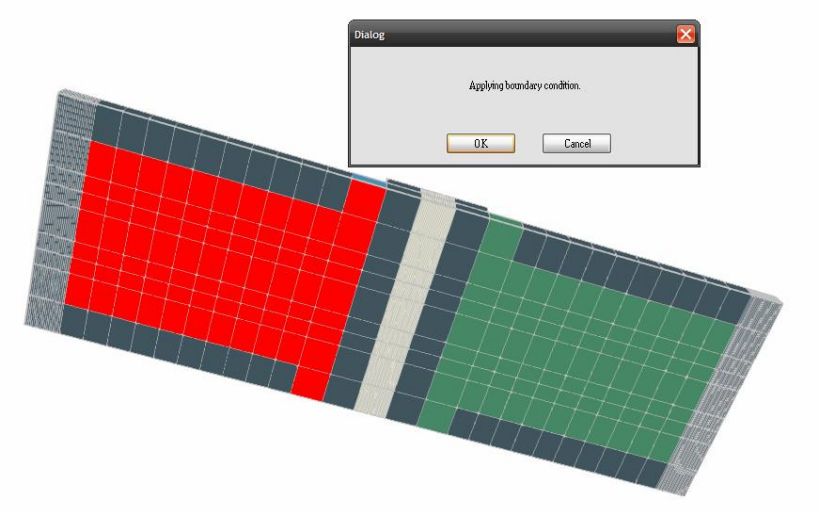

Figure 4.8: Boundary assignment which is shown in red for TEM

4.3.2.4 Loads

Loads are used to provide electrical information of the model for the simulation tool to integrate into the analysis. Due to the use of only electrostatic actuation, voltage loads are only required. With this information, the analysis can then be able to provide a resultant force of the electrostatic plates. Figure 4.9 shows the application of a voltage to an entity on the RF MEMS switch.

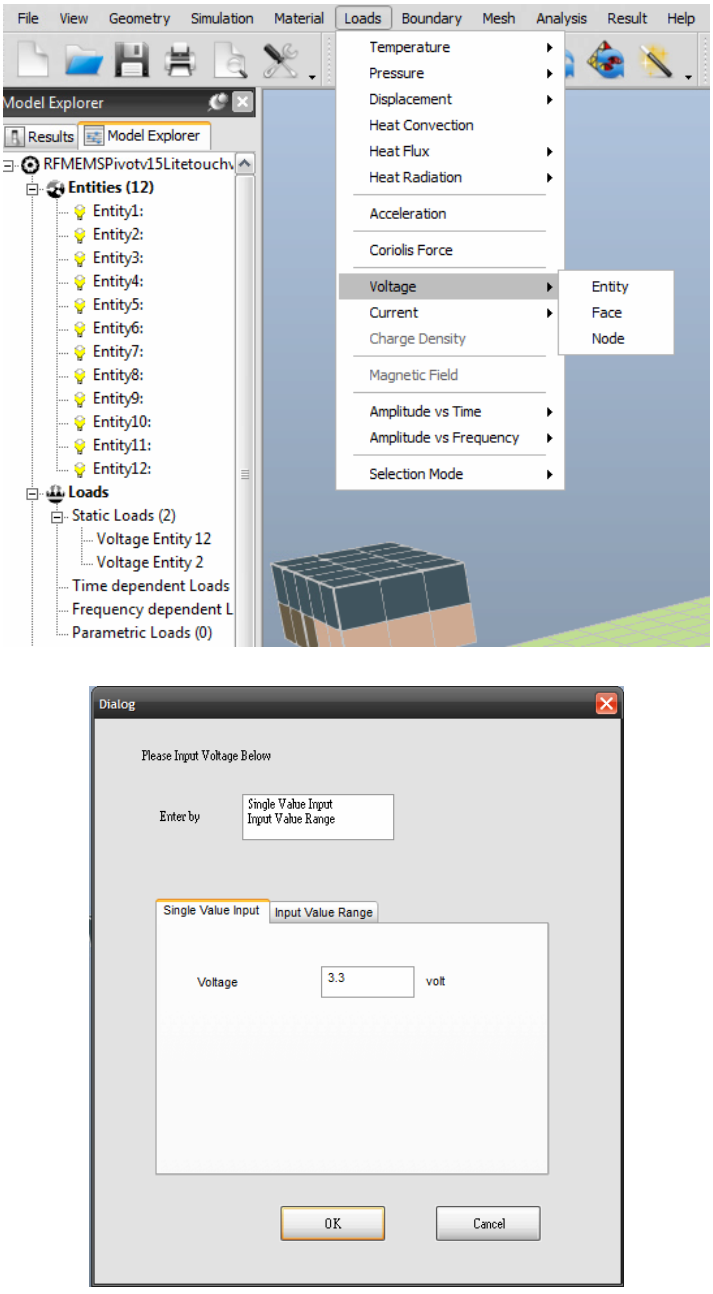

Figure 4.9: Applying loads to the switch for TEM simulation

4.3.3 Simulation Processes

To understand the structure of the device, a set of simulation tests (also known as simulation processes) are required to ascertain the behaviour of the structure during operating conditions and to see if the design functions correctly.

These simulation processes are characterised as:

- Static Simulation
- Modal Simulation
- Dynamic Contact Release
- Electromagnetic Simulations

4.3.3.1 Static Simulation with Contact Analysis

Static simulation is a type of simulation that is not time based but iteration based of the structure in one direction with the use of a single electrostatic pair of plates. Using this simulation method allows a way to obtain the pull-in voltage of the switch, which demonstrates the voltage requirement. The simulation needs to run a broad voltage range to identify approximately what the pull-in voltage is for the device. Further to this, the simulation needs to take into account the closing of the contacts, and so contact analysis is needed to be enabled to identify when the switch closes. Once the switch has closed the simulation results can display them in video or graphical form to determine the pull-in voltage used to achieve it. Advantages of this type of simulation is an expedient method for finding results it also allows pull-in voltages to be configured in a range format. A disadvantage is that the simulation is not presented in the time domain, which does not allow dynamic movement to occur.

Firstly, the simulation would need to be configured with all its parameters such as material information, where parts of the device are fixed the reason for this is to identify a reference point of the switch from which the design can operate and permit the simulation to identify the moving and fixed components of the switch. Next would

be to identify the electro static plates and where the contacts will occur to apply contact analysis on the faces of the component.

Once all parameters are completed the simulation setting are then identified, for static simulation. The calculation type is then set to ‘Static’ and analysis type is set to ‘ThermoElectroMechanical Relaxation’. This analysis type is used, because it incorporates a trilogy of Thermal, Electrical and Mechanical parameters including displacement and stress. Displacement setting is set to large in order to filter the minute movements, which would use more processing time thus slowing down the simulation. As for the ‘Convergence Definition’, ‘Iteration’ is set to an optimum value of 20 and an ‘Iteration Accuracy’ of 0.001. These are the optimum values to reach a result, which converges within a reasonable time-period with sufficient accuracy. Also, ‘Contact Analysis’ is enabled which incorporates slip/stick analysis of the contacts. These simulation settings are shown in Figure 4.10.

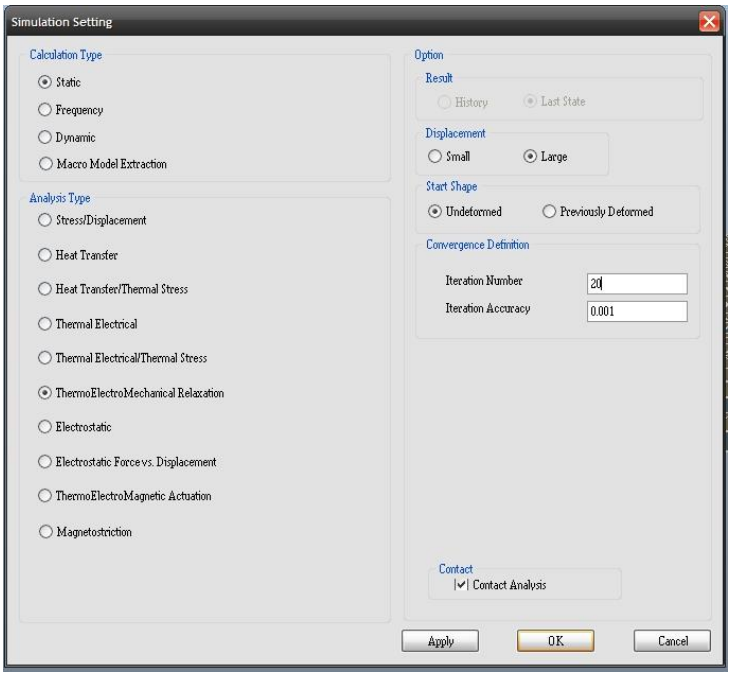

Figure 4.10: Static Simulation Settings

4.3.3.2 Modal Simulation

Modal simulation is used for analysing the closing and opening of the contacts. This approach is implemented by using a Reduced Order Macro (ROM) model. Intellisuite SYNPLE which is a multi-scale system-level simulation tool is used to achieve this, and is explained in Appendix A.

The processing of modelling contact dynamic behaviour in SYNPLE has the following steps:

- Non-contact macro model extraction
- Determining the "pull-in" voltage
- Determining the maximum contribution under "pull-in" condition
- Constructing the system circuit and run simulations in SYNPLE

The following procedure describes the steps to run the macro model contact dynamic analysis.

4.3.3.2.1 System model extraction

In order to understand the dynamic behaviour of the contacts, a macro model needs to be extracted using Intellisuite TEM simulation tool. Once the results are extracted, they can then be implemented to Intellisuite SYNPLE package, where the dynamic movement of the contacts can then be analysed.

A number of simulations are required to be carried out on TEM, in order to be ready for simulating on SYNPLE, the following simulation results are required:

- Maximum Mode contribution analysis (with contact analysis option enabled)
- Non-Contact Macro Model which includes modal contribution analysis
- Strain Energy Calculation
- Electrostatic energy analysis

4.3.3.2.1.1 Finding the pull-in voltage (Maximum Mode contribution analysis)

To reach the contacts, the actuation voltage is required. Using Static analysis with contact analysis enabled, which is shown in Figure 4.11, it is possible to find the

voltage required to pull the switch closed. This is also commonly known as the pull-in voltage. During static analysis simulation, a range of voltages are applied. Once the simulation is complete, results can be shown on a voltage vs displacement graph shown in Figure 4.12, which shows the voltage at which the switch closes.

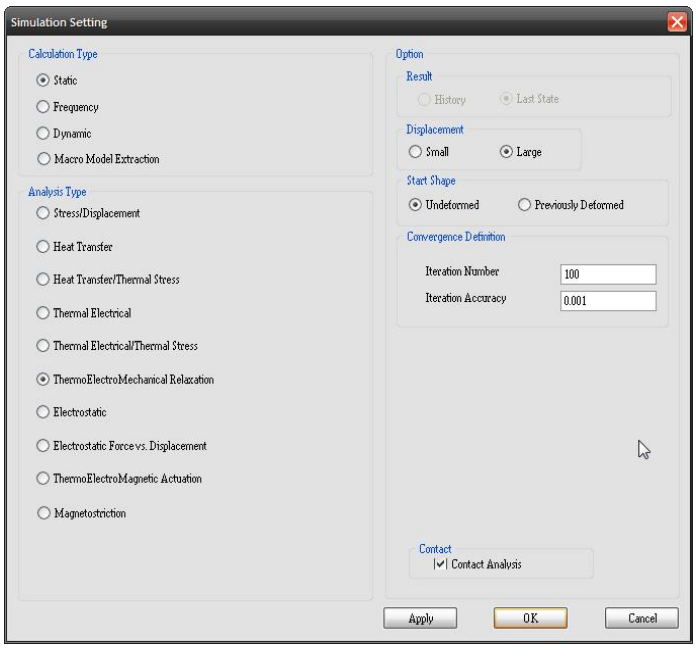

Figure 4.11: Simulation Set Up of Static Analysis with Contact analysis enabled

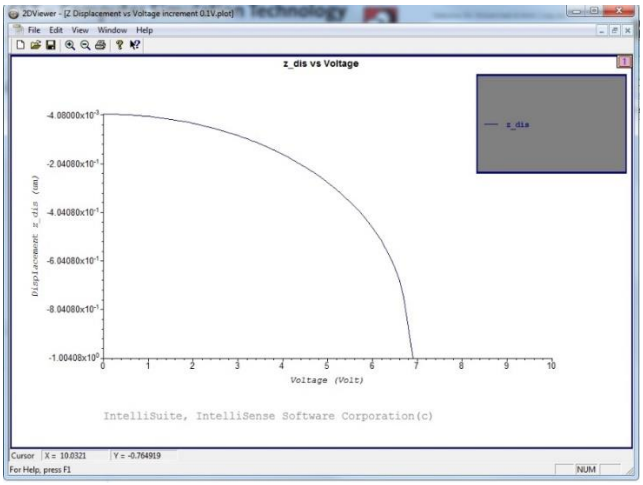

Figure 4.12: Z axis Displacement vs Voltage (Result shown using 2DViewer)

4.3.3.2.1.2 Finding the maximum mode contributions at Pull-in

To find the maximum mode contribution at the pull-in voltage, contact modal contribution analysis with pull-in voltage is needed to be performed, this is shown in

Figure 4.13. This sets the maximum limit of the contact distance for Intellisuite SYNPLE to calculate.

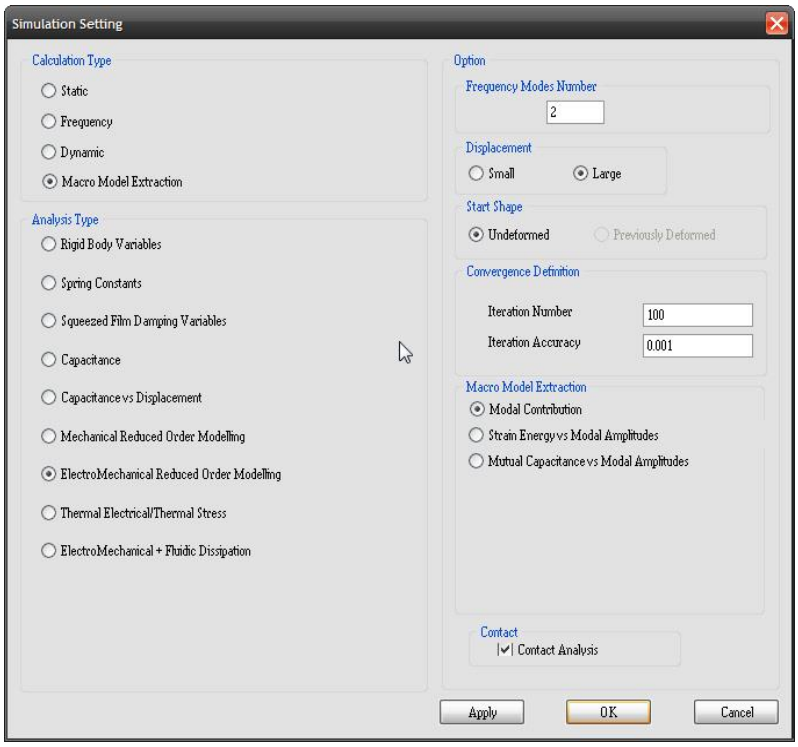

Figure 4.13: Simulation Set Up for maximum mode contribution at the pull-in voltage

4.3.3.2.1.3 Strain Energy calculation

After modal contribution analyses are completed, the next stage is to find the strain of the switch, this shows the minute movements of the contacts, shown in Figure 4.14 and Figure 4.15, with two modes of scaling factor used. The first mode uses the scaling factor similar to the distance of the airgap (e.g. if the air gap is 2.7µm then the scaling factor would be 2.7) the second mode uses the scaling factor that is 1000 times smaller from the air gap (e.g. if the air gap is 2.7µm then the scaling factor would be 0.003).

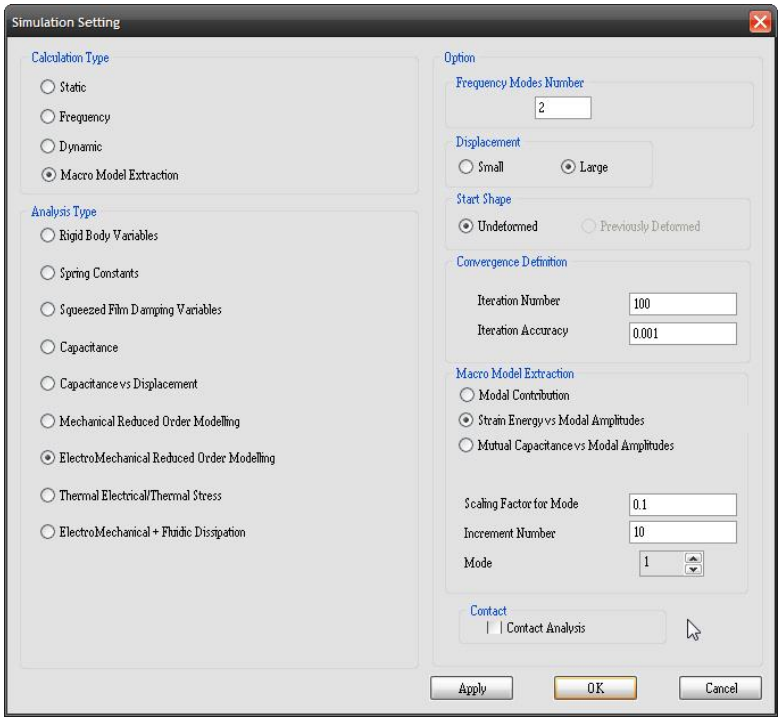

Figure 4.14: Setting of strain energy calculation for mode 1

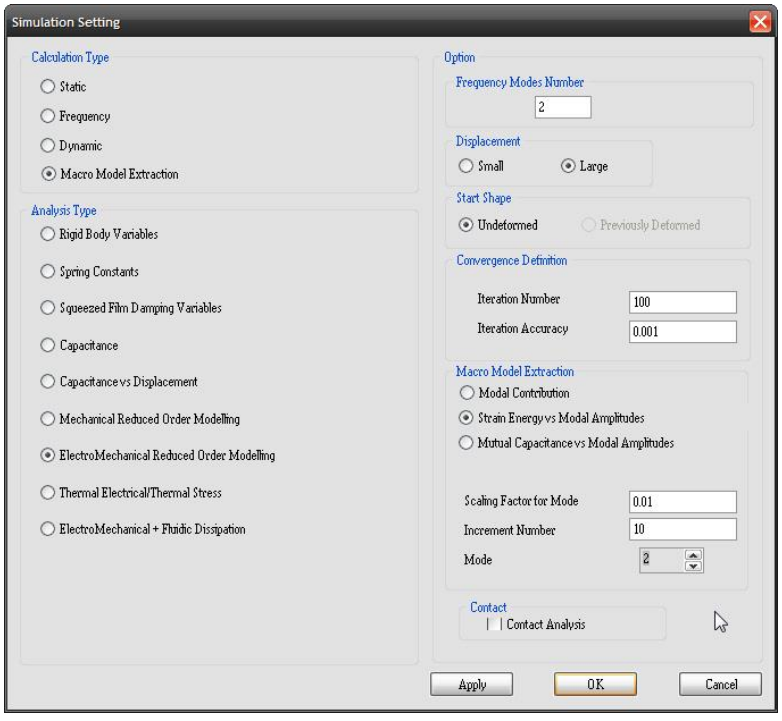

Figure 4.15: Setting of strain energy calculation for mode 2

4.3.3.2.1.4 Capacitance (Electrostatic energy) analysis

The capacitance analysis is used to provide electrostatic information of the switch for SYNPLE, shown in Figure 4.16.

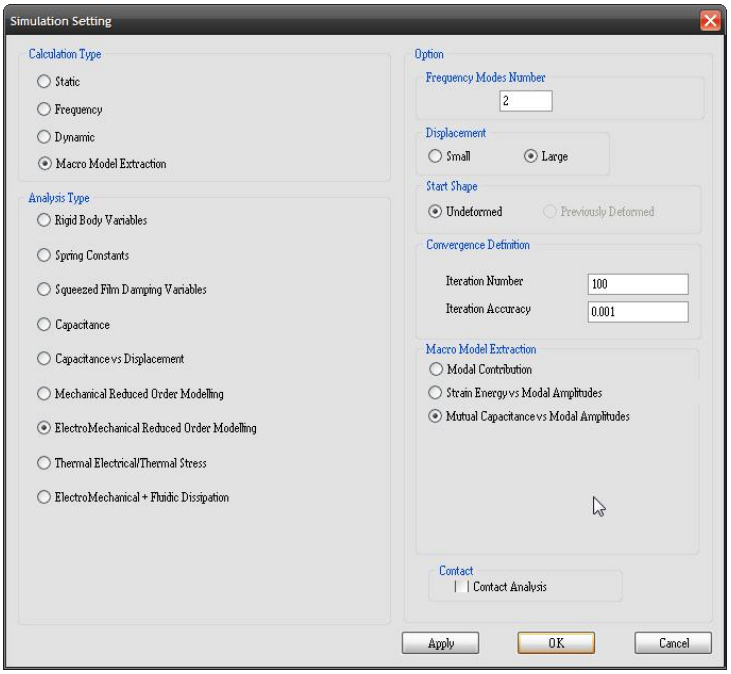

Figure 4.16: Simulation Set Up of Capacitance Analysis

4.3.3.2.2 Simulation in SYNPLE

4.3.3.2.2.1 Information for Template of Macromodel of TEM

The elements of Macromodel of TEM can be easily accessed from MEMS Devices in the Devices Box. There are several versions of macromodel elements. 'MacromodelII' is a template for "mems_rom 10m5c5p", which indicate for the Macromodel which can handle up to 10 modes, 5 conductors and 5 represent nodes.

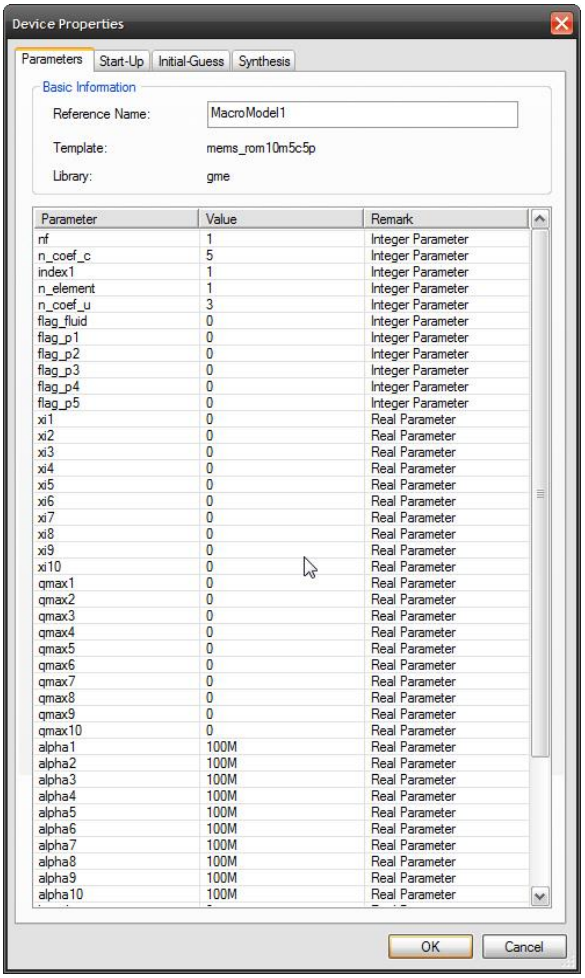

Figure 4.17: Device property

In Figure 4.17, it includes the parameters of qmax1, qmax2, alpha1, alpha2, beta1, beta2 etc. for the contact model given in Equation 0.3 in Appendix A.

The macro model template has following parameters:

xi1, *xi2*, *xi3*, *xi4*, *xi5*, *xi6*, *xi7*, *xi8*, *xi9*, and *xi10* are the damping ratio for each of the 10 modes. The default value for these parameters respectively is 0.

qmax1, *qmax2*, *qmax3*, *qmax4*, *qmax5*, *qmax6*, *qmax7*, *qmax8*, *qmax9*, *qmax10* are the maximum modal contributions. The default value is 0. These parameters would need to be modified and with use of only qmax1 and qmax2 and optionally qmax3; other qmax's are not required during simulation and are set to 0 to disable them. Qmax1 and qmax2 parameters are set with the values extracted from the TEM analysis. Note that parameters, which are not used, are left to its default values in order for simulation to continue.

4.3.3.2.2.2 Wiring the circuit

In the SYNPLE simulator, on the left-hand-side, a list of available elements, categorized into Electrical Elements, Mechanical Elements, MEMS Elements, are shown in the element library.

On the right-hand-side, the 2D grid for the schematic is displayed, which shown in Figure 4.18.

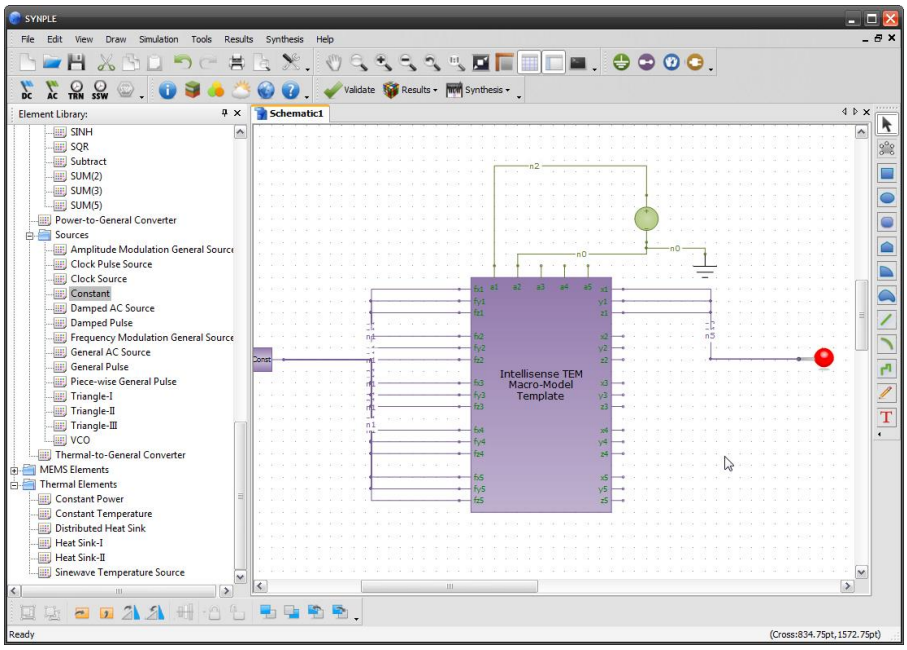

Figure 4.18: Wiring A circuit

If the wires are connected correctly, as shown in Figure 4.18, a name will automatically appear for the wire. The name can then be changed by double clicking on the wire. Click and Drag between the nodes on the respective elements to connect them with a wire.

For the “Constant” elements, the default values (0) are left alone for c, c1 and c2. This sets the forces on all 5 representative nodes as 0.

4.3.3.2.2.3 Transient DC Analysis Simulation

To show the hysteresis effect in DC sweep analysis of the contact modelling forward and backward voltage sweeping is required. However, the DC analysis would become difficult to converge around the pull-in voltage, once the flag of contact node is set as non-zero value.

An alternative way, is to use a slow varying triangular waveform input voltage in a transient simulation. This method will achieve the simulation goal. Other options include the use a trapezoidal waveform which also archives the simulation goal without a high voltage peak.

To start the simulation a time setup is required to analyse the contact for a given time. Once completed, the OK button is pressed and simulation starts, which is shown in Figure 4.19.

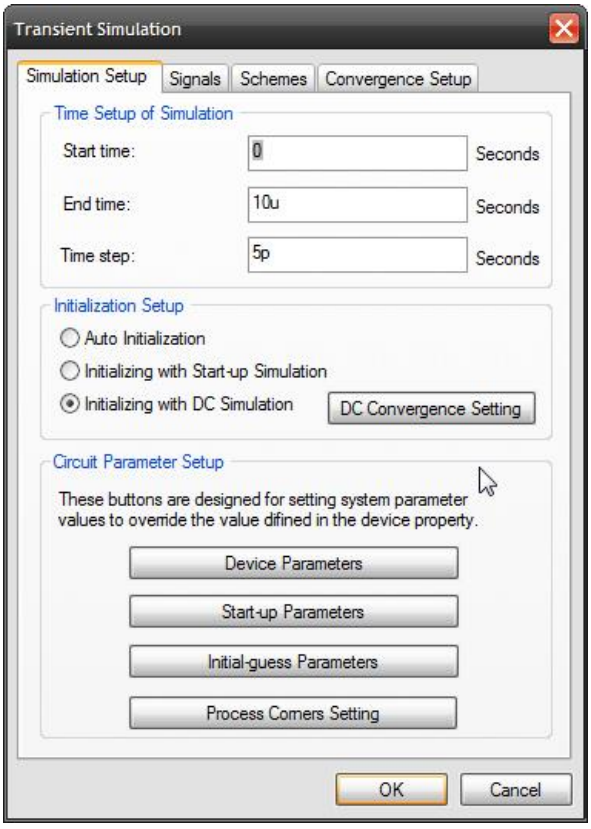

Figure 4.19: Simulation Setup (Press OK button to start simulation)

To show the displacement vs voltage hysteresis effect or better management curves, WaveRunner is used to show the results graphically. Shown in Figure 4.20 and Figure 4.21. Alternatively, the data can be exported to Microsoft Excel to graphically display the data.

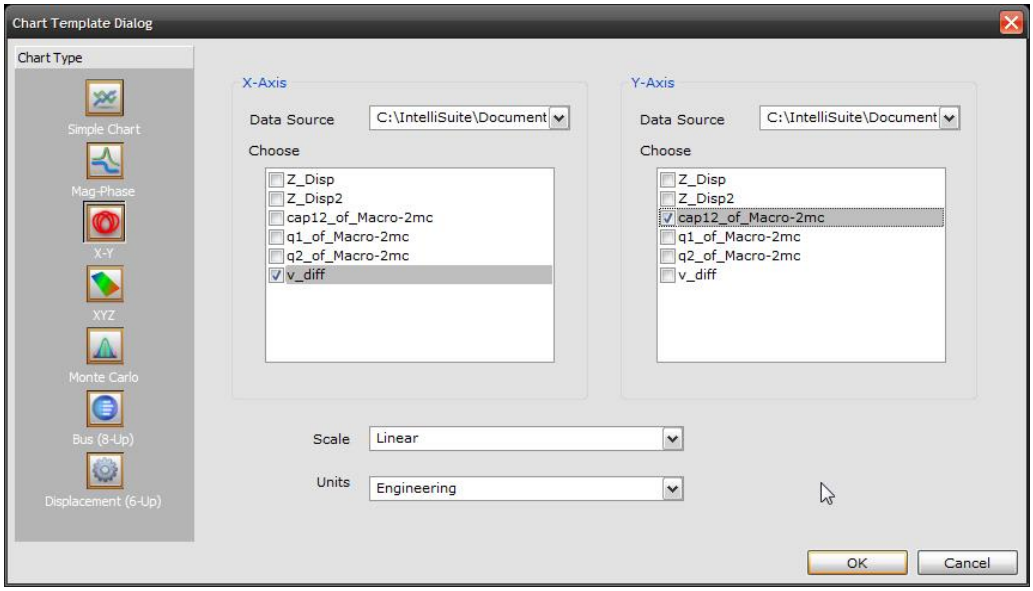

Figure 4.20: Chart Template Set Up

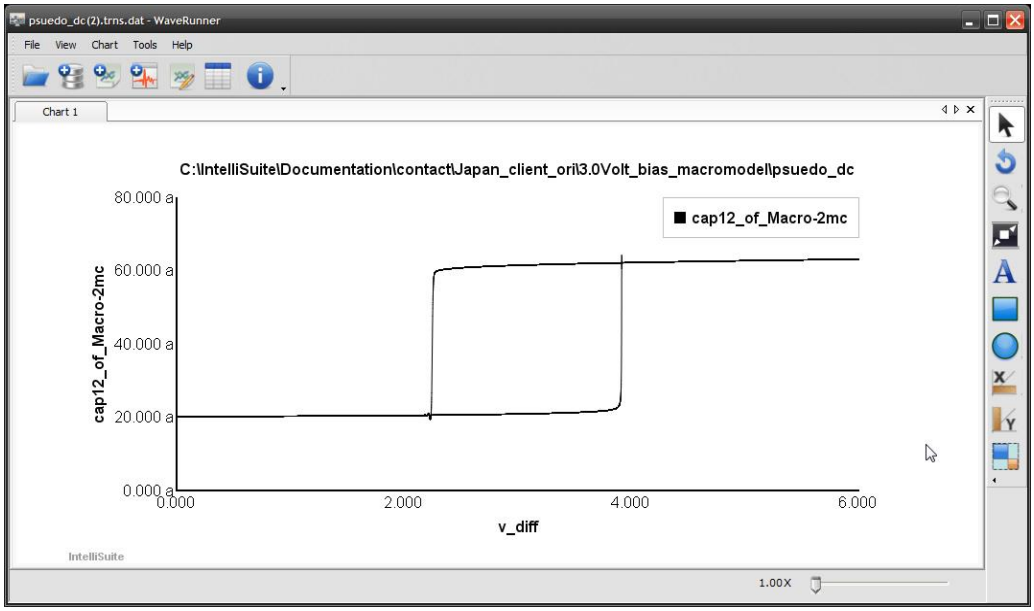

Figure 4.21: Capacitance vs Voltage

This example shows the hysteresis effect of displacement vs voltage result. The pull-in voltage is about 3.9 volts.

This macromodel template has the capability of contact modelling and has been developed within the SYNPLE element library. The design flow of system-model-extraction, in the TEM tool and system simulation within SYNPLE, has been shown in this chapter. This chapter is an example of the MEMS switch design using a combination of Intellisuite's TEM and SYNPLE packages.

4.3.3.3 TEM Contact Release Simulation with Contact Analysis

This is used when simulating the design when its initial state is on, prior to releasing it to its off state. This is also known as 'Elastic Recovery', as it is the recovery rate of which the beam returns to its original state using the beams elastic properties. It is a dynamic simulation, which is time dependant and shows the switch's characteristics during its progress to its off state. This shows if the design has any issues such as ringing due to insufficient dampening.

A disadvantage to this simulation is that it cannot show contact analysis, as the contacts touch each other. However, the simulation can be shown when the contacts are being released. An advantage to this simulation is that it shows how quickly the device can switch off and stay at its steady off-state. With this analysis, it can show the characteristics of the elastic recovery of the switch.

4.3.3.3.1 Frequency response of the switch

In order to start with contact release simulation, the natural frequency *(f)* (Equation 4.1) of the device needs to be acquired. This is to identify the time (T) required for the switch to complete a single cycle.

(Simple Harmonic motion: http://physics.bu.edu/~duffy/py105/SHM.html accessed 21-01-2018).

Equation 4.1

$$T = \frac{1}{f}$$

Where:

T = Period (Seconds)

f = Frequency (Hertz)

The cycle can then be used to set the Time Period for Dynamic analysis and provide a set range in which the switch can be released within the time period. In order to implement frequency response analysis, the simulation settings need to be set to 'Frequency' with the Analysis type set to 'ThermoElectroMechanical Relaxation', with the displacement set to large and iteration Number set to 10 and 0.001 for iteration

accuracy (the iteration number is the number of times the simulation is carried out to reach convergence and the iteration accuracy set to the specified value). The ThermoElectroMechanical Relaxation analysis calculates the natural frequencies of the switch, taking into consideration the form of the structure, with any external or electrostatic forces effecting the switch including thermal effects. The analysis takes into account the residual stress around the device while considering six degrees of freedom for every node on the mesh.

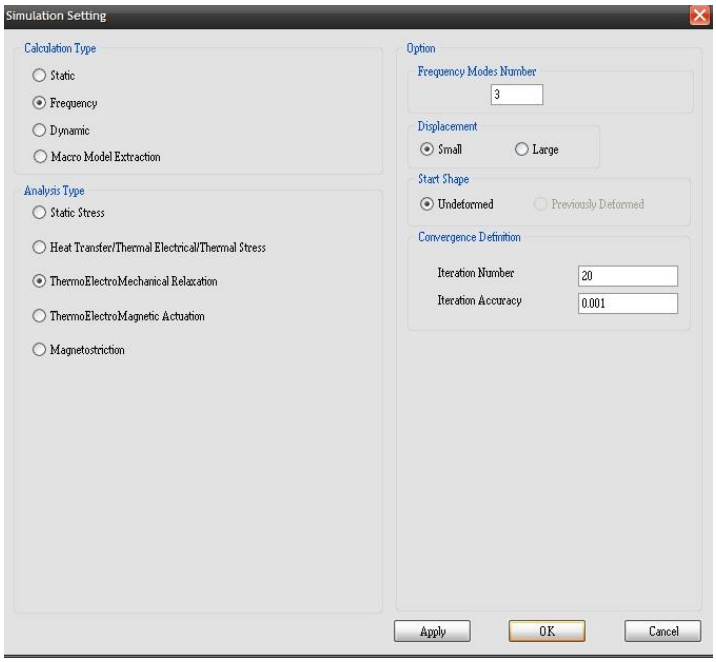

Figure 4.22: Simulation Setting for Frequency Response

Once analysis of the structure is complete, the results are then shown by clicking on 'Result' tab, a drop-down menu appears with the option of selecting 'Natural Frequency'. Once clicked, Intellisuite TEM simulation tool displays in tabular format the modes of frequencies. Using Mode 1, provides the natural frequency of the switch.

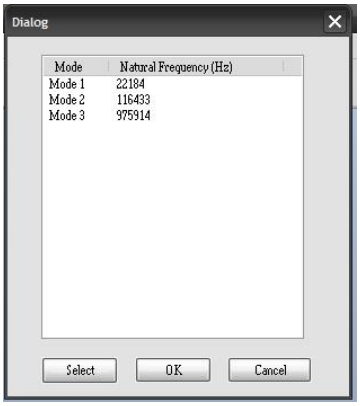

Figure 4.23: Example of Natural Frequency Result Displayed in Intellisuite

With the use of Mode 1 the estimated time for the switch to stabilise back to its off-state from when the switch was active. This is calculated using Equation 4.1. Although this is an estimation of the switch-off time, it may not be accurate if the design has a spring effect, and so extra time may be needed for the switch to stabilise (i.e. due to contact bounce) at its off-state. This then requires the data to be manually checked to see if it reaches the off-state, and if not, to extend the simulation time-period, in order to take this effect into consideration.

4.3.3.3.2 Contact Release Simulation

Once the estimated time-period has been identified, using the frequency response analysis, the next stage is to set the simulation setting and parameters for contact release simulation. In order to start contact release (also known as elastic recovery), it is important to know that the simulation is a dynamic analysis and so careful consideration of the implementation of the electrostatic plates and contact pairs parameters.

Here the settings need to be applied as a dynamic simulation with ‘Stress/Disp./Electrostatic (Direct Integration). Using this analysis type allows the simulation software to solve Electro-Mechanical cases using a direct integration method with implicit methods based on Hilber-Hughes-Taylor operator (Hilber et al. 1977). This implicit method uses implicit time integration in order to calculate the dynamic transients of the system. Next part of the simulation settings is to select the options for displacement type, start shape, convergence definition, dynamic

capacitance, Dynamic time-period and contact analysis. For Displacement type the choice is preferably to take notice of small movements and so ‘Small’ should be selected for accurate convergence of the analysis and is taken into consideration from design to design. The start shape is set to ‘Undeformed’. This is to make sure that the simulation starts at the point where the switch is at its rested state, and that no external forces are enabling the switch at the beginning. As for the convergence definition, the ‘iteration number’ would ideally be set initially to 20 but if convergence fails set to a higher iteration number, such as 30. Also, the ‘iteration accuracy’ is left as default at 0.001. As for dynamic capacitance option, it is selected to ‘Update’, as it allows the capacitance to change as the switch moves dynamically over time. For ‘Dynamic’ option selected to Transient (Fixed Time Increment), to allow the option for a time-period for which the total amount of cycles can be inputted. With ‘Increment Number’ set to 100, (increment number is used to split the number of frames there is within a time-period, with higher increment number it allows for improved resolution of the total time of the simulation, which therefore provides a smoother animation of the results. Also, if simulation fails the time period is increased, but it will extend the duration of the simulation). Last of all, is to enable the contact analysis, as the contacts will be touching one another. These ‘Simulation Settings’ provides the optimum parameters for the analysis, allowing for fast simulation turn around without compromising accuracy of the analysis.

The electrostatic plates would need to be set to static 0 volts, with a dynamic voltage being applied to the positive plates, enabling the switch to respond dynamically (this will allow for the voltage to change during the simulation), which is shown in Figure 4.24. For Dynamic contact analysis of the contact simulation to work, the initial time at 0 seconds needs to be an enabled voltage, which requires the switch to stay down for a brief time. After the brief time, it is then required to set the dynamic voltage to 0 volts. This allows for the device to recover to its off-state. If the time-period of the simulation setting is sufficient, then the results of the simulation can be proven by enabling the results of the beams movement from the displacement axis and then selecting ‘Node Curve’, Magnitude on the result tab, and then selecting a node at the end of the beam, which corresponds to the most movement. Intellisuite TEM displays the results on a graph, with Displacement of the named axis vs Time.

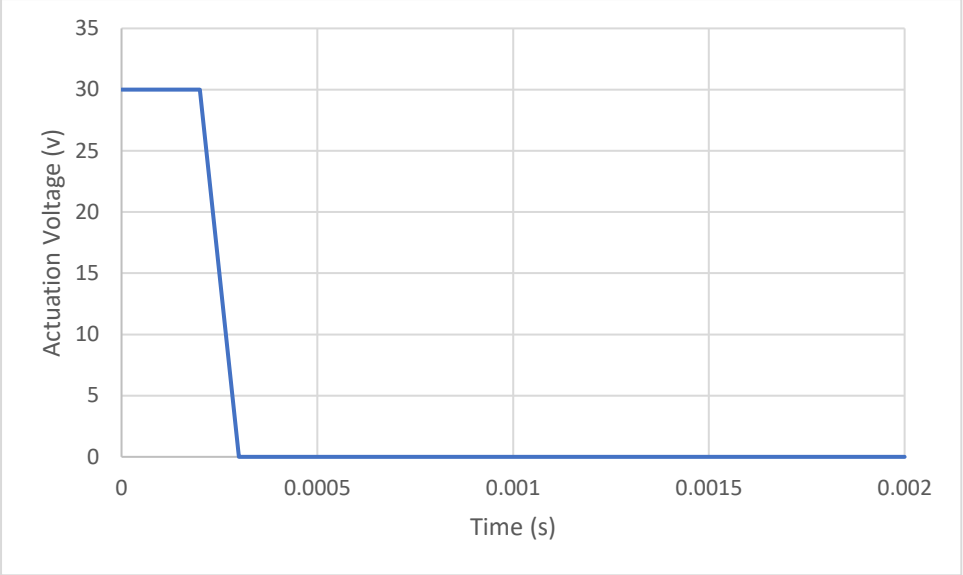

Figure 4.24: Graphical representation of dynamic voltage used for contact release simulation

The sequence of the process is:

- Set dynamic simulation settings (shown in Figure 4.25)

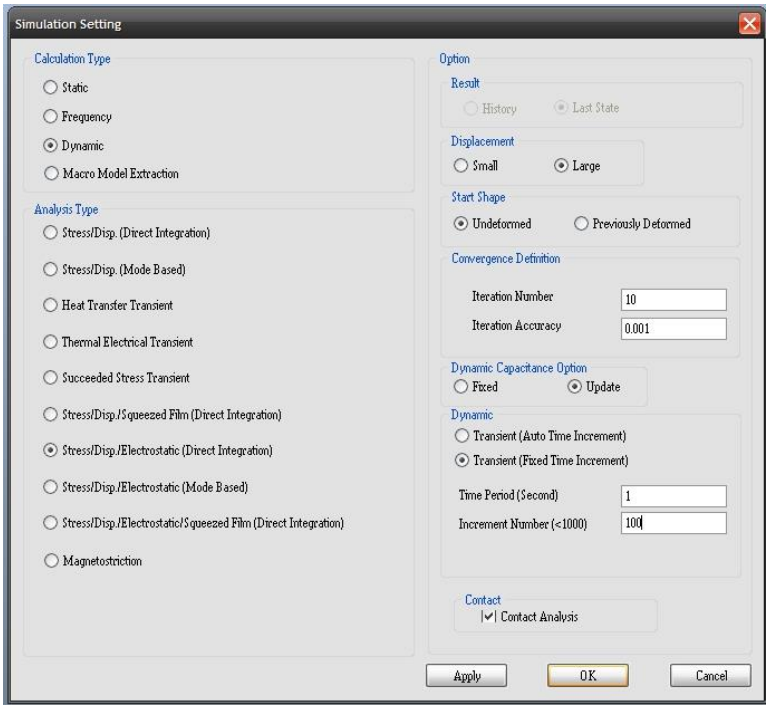

Figure 4.25: Simulation Setting for Dynamic Contact Release

- Then apply static loads all plates used to 0V

- Then apply Amplitude vs Time Tabular Load on to each of the electrostatic plates except for the ground.

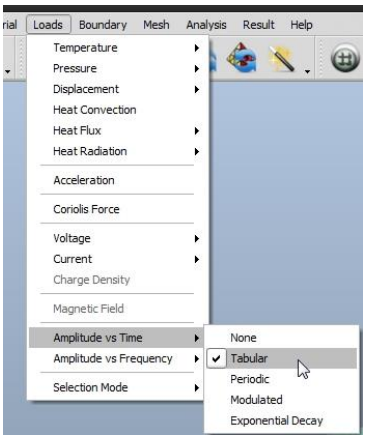

Figure 4.26: Tabular Voltage selection

- Set the multiple Tabular Loads from 0 seconds to 0.02 seconds as a voltage on one plate

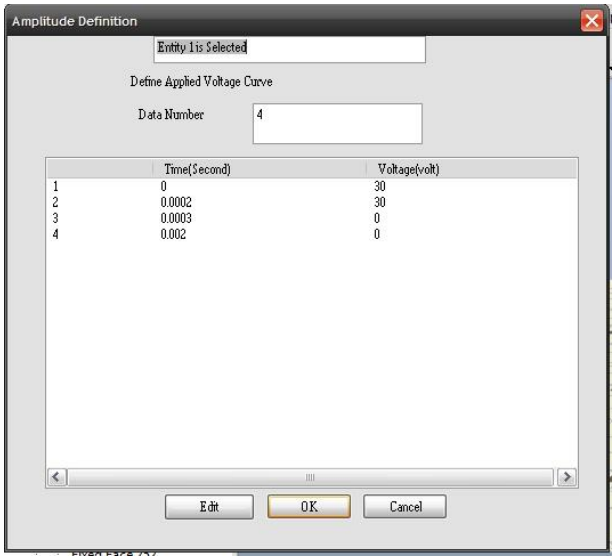

Figure 4.27: Setting the Tabular Voltages

- Run the simulation and check using VisualEase

4.3.3.4 CST EM Simulation Analysis

CST (Computer Simulation Technology) electromagnetic analysis is a Finite Element analysis, which provides s-parameters of a device.

In order to use CST two options can be used, with either waveguide port analysis or discrete port analysis, which both can run on frequency domain calculations.

Waveguide port analysis enables a port to stimulate an infinitely long waveguide, connected to a structure. The waveguide modes travel out of the structure and towards the boundary planes, which in turn decreases the reflection levels.

The general use of waveguide ports is required to enclose the entire field including the transmission line with the port area. The simulation uses eigenmode solver, which can calculate the port's exact mode with enclosed boundaries.

Discrete port analysis provides an alternative option to feed the calculation domain with power. Three different types of discrete ports are available, depending of the requirement of voltage, current or impedance elements, which absorbs power and enables S-parameter calculations.

Discrete ports can also be attached from one existing object to another. This only allows to create a single port connection between both ends. The discrete port is shown as a blue line, which represents a perfectly conducting wire and the red conical arrow displays the direction of flow. Unfortunately, a second port of the same end to end could not be included.

For discrete port analysis, using S-parameters, the port type is modelled around a lumped element also known as 'Lumped Network Elements'. A lumped element is considered to represent a simple electronic network. This includes the use of either series or parallel RLC (Resistor, Inductor and Capacitor) network. Alternatively, it can be implemented with a diode network or a combination of all component elements. A discreate port consists of a current source with an internal parallel impedance that excites and absorbs power. Also, the impedance values are specified within the setting of the discreate port.

4.3.3.4.1 CST EM Simulation

4.3.3.4.1.1 Modelling

In order to start with the simulation, it is firstly required a model to simulate on. There are two options on creating a model the first option is to use an existing model used from Intellisuite TEM simulation package and exporting out to a ASIC file with extension identifier ending with SAT. This option allows the importing of the same model without having to recreate it but proves a disadvantage due to the design already pre-meshed in TEM. When imported to CST simulation software the TEM mesh then identifies each block as an individual and would require time to group them back. Also, higher probability of errors may occur during EM simulation, as CST uses hexahedral and tetrahedral unstructured grid meshes as oppose to the structured hexahedron shape of the mesh imported from Intellisuite. Importing to CST does not have to be just ASIC files, as CST has broad range of design files it can translate from other modelling tools can be used, if it agrees to the import files CST can translate from.

The other option for modelling is by using the integrated modelling tool. If the dimensions of the device structure are known, then with the modeller the design can be recreated accurately. This reduces the CST design file considerably as the part may not need to be split or imported with previous the meshing involved. Also, the simulation is more compatible, as import errors are non-existent and therefore decrease simulation time. A disadvantage to using the modeller is that it is not user intuitive and requires careful consideration of placing and designing of component as it is coordinate based. A flow diagram of CST's simulation process is shown in Figure 4.28.

Once the model has been created and the components of the model has been grouped together, the next stage of the setup is to apply the material information of the components. The material information is assigned according to the switch's specification, this is to understand the switching characteristics the components in which the RF communication would travel. This information is included into the simulation to provide an accurate electromagnetic result.

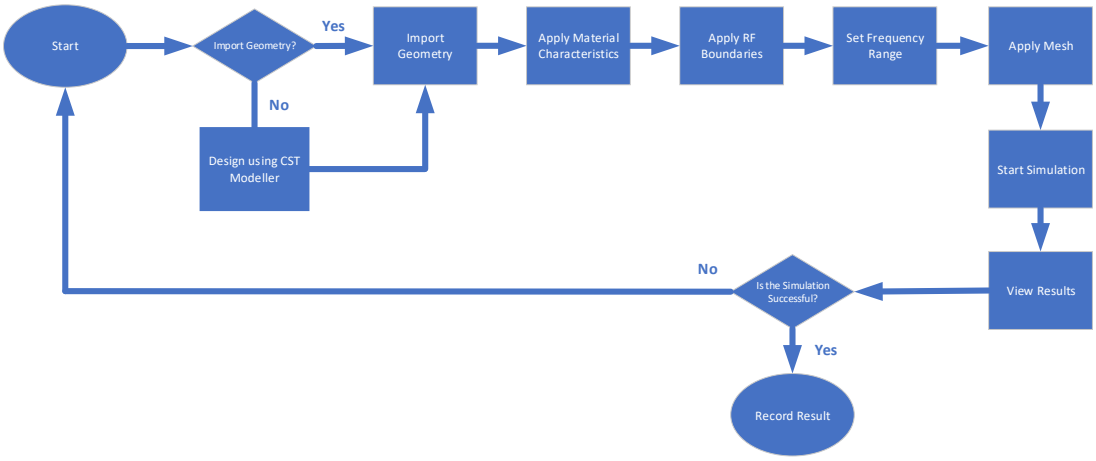

Figure 4.28: Flow Diagram of the CST Simulation Process

4.3.3.4.1.2 Simulation Setup

After the modelling is completed, the simulation setting is then applied. Firstly, it is to set the 'Problem Type' located on the 'Home' tab ribbon, which is then set to 'High Frequency' due to the nature of the simulation.

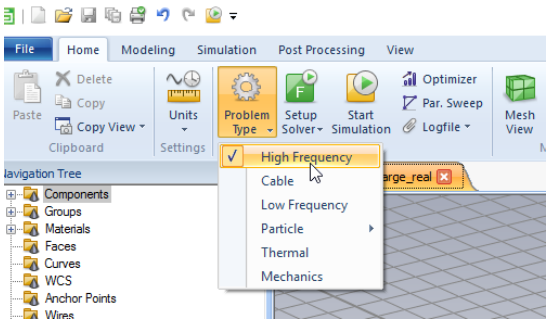

Figure 4.29: Setup of the simulation for High Frequency

Next, is the solver setup, which is then required to be set to 'Frequency Domain Solver'. The 'Frequency Domain Solver' uses a form of Maxwell's equations for electromagnetic fields (Maxwell 1982). The parameters for the 'Frequency Domain Solver' are set to default with the exception of selecting to 'Normalize S-parameter to' 50 Ohms. This is to normalise the ports to a reference impedance, in order for the s-parameters to be calculated with fixed impedance of the ports. The mesh type is set to Tetrahedral as default mesh with adaptive mesh refinement enabled in order to improve the mesh using multiple passes to correct the mesh.

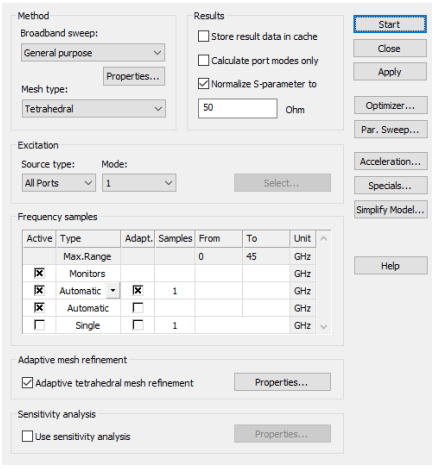

Figure 4.30: Frequency Domain Solver Parameters

Once the simulation solver and problem type is setup, the frequency range for the simulation is required to be set, this is done by selecting the 'Frequency' button located in the Simulation tab ribbon,

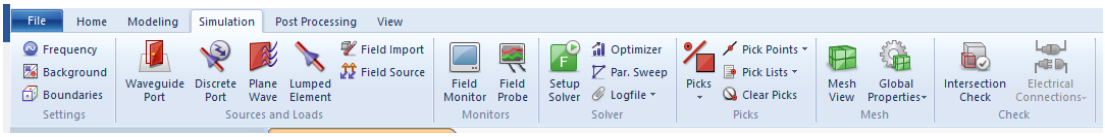

Figure 4.31: Simulation setting options available on the Simulation tab ribbon

Once the frequency range is set, CST simulation runs a broad set of analyses across the set range of frequencies.

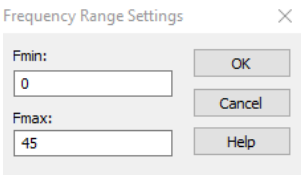

Figure 4.32: Frequency Range Settings for CST to run analysis within

The next setup is to set the area around the switch, also known as the 'Background', the background can be set from the icon named 'Background' shown in Figure 4.31. The material type is set to normal; this is ideal as the default setting for normal is a vacuum. The 'Surrounding Space' setting are set to the values shown on Figure 4.33.

Also, the boundaries of the background are set to ‘open’ in all directions, which is shown in Figure 4.33.

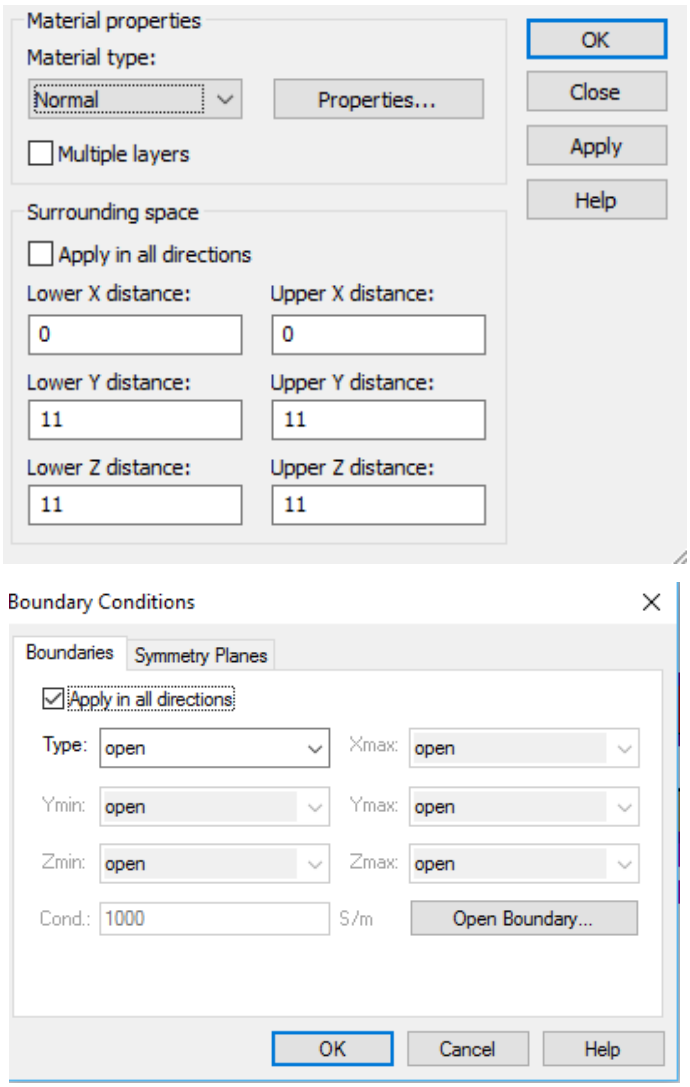

Figure 4.33: Background Properties (left) and Boundary Conditions (right) used for all designs

For these set of simulations, the type of ports which is to be used are ‘Waveguide Ports’. This type of port is available in the simulation tab ribbon as shown in Figure 4.31. Compared to discrete ports, which is used to simulate the area directly within the air gap. The waveguide port is used at each end of the switch, allowing for analysis to take into consideration the entire switch. The waveguide ports are set on one axis with two ports setup as positive and negative on the same axis. The ports’ axes are set at the connecting ends of the switch, enabling the microstrip, connecting the contacts, to be excited. The setting of the ports is shown in Figure 4.34.

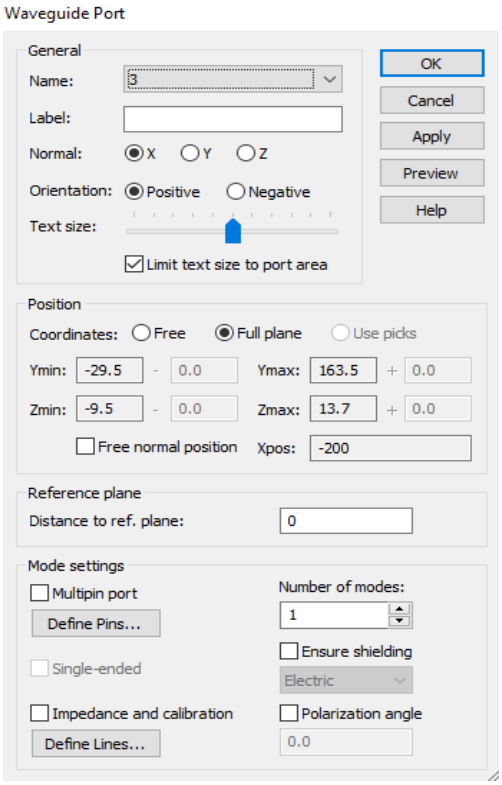

Figure 4.34: Waveguide Port setup window

Once all setup is complete, it is then required to set the E-field monitors. This is to set the frequency points of interests, which allows to see the results in 3D format of the way the EM radiated from the ports, after analysis is completed. To access setup of the E-field monitors, it is accomplished by clicking on ‘Field Monitor’ shown on Figure 4.31. The Type should be selected as E-Field with ‘Specification’ set to ‘Frequency’ with a step width (linear) set between minimum and maximum frequency. The setup is shown in Figure 4.35.

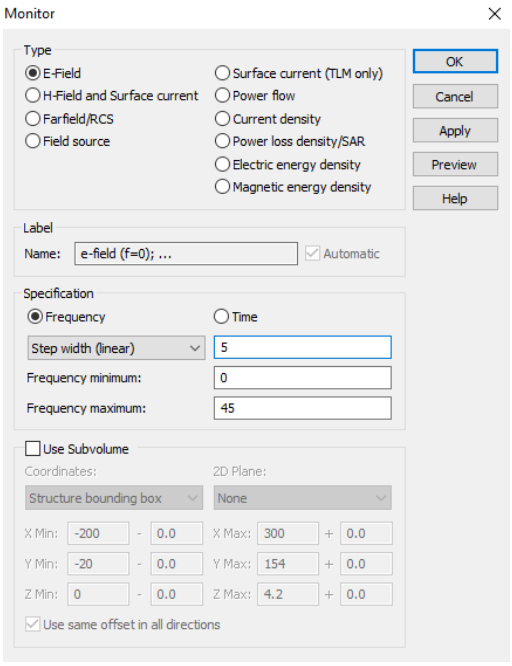

Figure 4.35: Setting up E-Field monitors using the Field Monitor setup window

4.3.3.4.1.3 Visualising the Results on CST

Once simulation settings are set, the analysis can start by clicking on the 'Start Simulation' button located in the 'Home' tab ribbon. When simulation starts, CST initially runs meshing of the design, before stimulating the ports for EM analysis. After analysis is complete, folders appear on the navigational tree, known as '1D Results' and '2D/3D Results'. Within the '1D Results', results are presented in graph form, which includes the s-parameters. In the '2D/3D Results' folder, 'Port Modes', 'E-Field' and 'Electrical Energy Density' is displayed as a visual representation, directly on the switch itself. The resulting images and graphs can be exported out for further representations of the results on to other media.

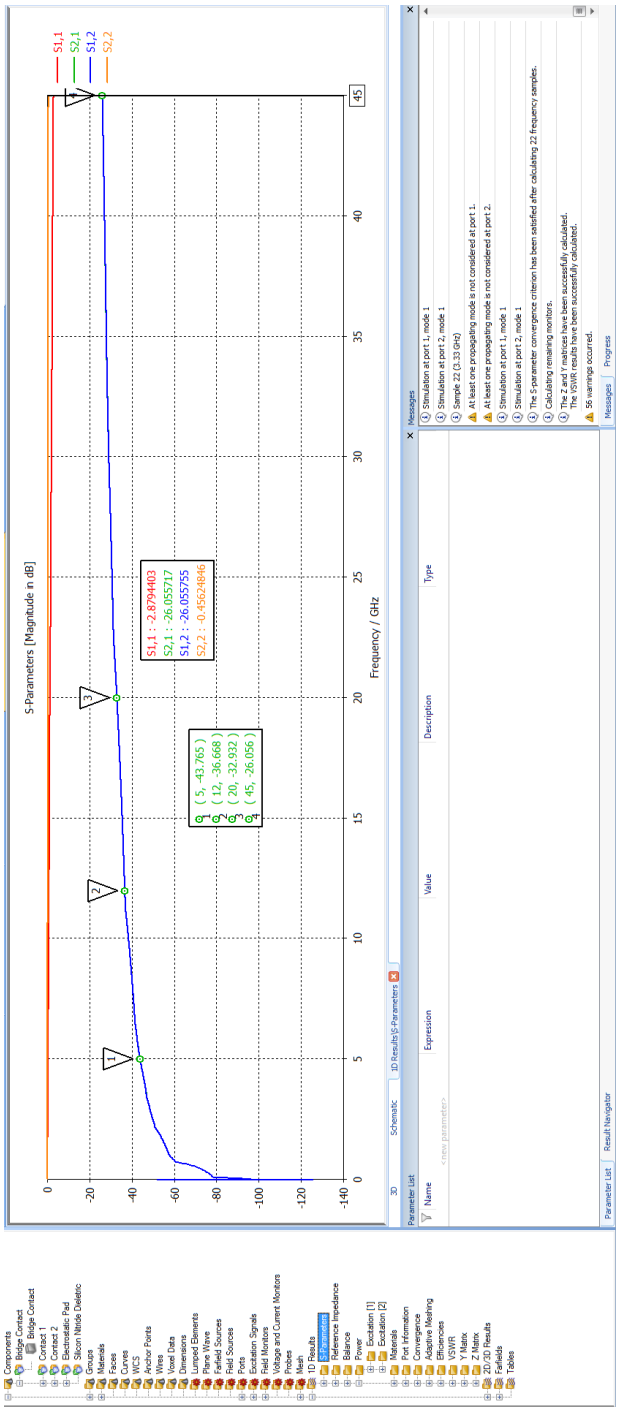

Figure 4.36: Example of Results from CST S-Parameters

To summarise, this chapter describes both the selection process and the modelling of an RF MEMS switch, using Intellisense (Intellisuite) for electro mechanical simulations, to provide results for stress, voltage, force and displacement in graphical format. CST is used to determine the electromagnetic characteristics of the switch, i.e. the scatter parameters, which include the isolation and reflection.

Chapter 5

5 RF MEMS Switch Design

This chapter describes the development of the RF MEMS switch from the original HRL Cantilever developed by Daniel Hyman (Hyman et al. 1999) from Hughes Research Laboratories. This is used as a benchmark from which advancements were made, to achieve a unique design, when used in mobile telecommunication systems. It also describes the stages which made a significant impact to the performance of the switch and provides a background of the development of RF MEMS technology, with information about the switches advantages and disadvantages.

5.1 RF MEMS

World War II spurred the use of RF technology for communication using thermionic valves, also known as 'vacuum tubes, these were used for high power transmission systems and radar, which were then followed, commercially, in radios and televisions. After vacuum tubes, the progression to integrated circuits (IC) appeared with the first known transistor amplifier, which was developed and patented in 1949 by the German physicist and engineer Werner Jacobi (Jacobi Werner 1949). By 1958 Jack Kilby of Texas Instruments created the first prototype IC and commercialised them and was filled for patent by 1959 (KILBY JACK S 1964) . In accordance with Moore's Law (Gordon E. Moore, 1965, 2006 reprint) the communication system started to be more powerful and decreased in size. Although ICs are becoming smaller and smaller the disadvantage is the leakage current between contacts, which in turn consumes more power. Researchers found an alternative way to overcome this obstacle by using a mechanical switch with a physical disconnect. This alleviates the problem of current leakage, by using electrostatic actuation voltages that are innately voltage driven. RF MEMS switching technology was invented by Professor Larry Larson in 1990 in conjunction with Hughes Research Laboratory with DARPA funding (L. E. Larson et al. 1991) . The varactor, which Professor Laray Larson created, operated from DC to 50 GHz, which then inspired Rockwell Science Center, in 1995, to develop a metal-

to-metal contact type switch suitable for DC to 60 GHz and Texas Instruments also developed the capacitive contact type switch suitable for 10 to 120 GHz. Since then, the typical actuation voltages for subsequent RF MEMS switches have ranged from 20 to 80 V, which is shown in Table 5.1.

Table 5.1: Performance Characteristics of RF MEMS, PIN Diodes and FETs referenced from Gabriel M. Rebeiz, RF MEMS Theory, Design and Technology, p 5 (Rebeiz 2003)

Parameter	**RF MEMS**	**PIN**	**FET**
Voltage (V)	20 -80	± 3 - 5	3 – 5
Current (mA)	0	3 – 20	0
Power Consumption [note 1] (mW)	0.05 – 0.1	5 – 100	0.05 – 0.1
Switching Time	1 -300 μs	1 -100 ns	1 -100 ns
C_{up} (Series) (fF)	1 – 6	40 – 80	70 – 140
R_s (Series) (Ω)	0.5 – 2	2 – 4	4 - 6
Capacitance Ratio [note 2]	40 – 500 [note 2]	10	n/a
Cut-off Frequency (THz)	20 – 80	1 - 4	0.5 – 2
Isolation (1 – 10 GHz)	Very High	High	Medium
Isolation (10 – 40 GHz)	Very High	Medium	Low
Isolation (60 – 100 GHz)	High	Medium	None
Loss (1 – 100 GHz)	0.05 – 0.2	0.3 – 1.2	0.4 – 2.5
Power Handling (W)	< 1	< 10	< 10
Third-order intercept point (dBm)	+ 66 - 80	+ 27 - 45	+ 27 - 45

Note 1: Includes Voltage upconverter or drive circuity

Note 2: Capacitive switch only. A ratio of 500 is achieved with high-ε_r dielectrics

5.1.1 RF MEMS within Mobile Systems Communication: Advantages and Disadvantages

RF MEMS is used in mobile system communication due to it high isolation from DC to 100 GHz. with a low insertion loss. From the Table 5.1 it can be seen that the power consumption between an RF MEMS switch, and a FET is similar, however the RF MEMS power also includes the peripheral drive circuity to step up the voltage. By eliminating the drive circuit, the power consumption would be significantly reduced. In addition, the series resistance of the RF MEMS switch is low due to its ohmic direct contact and the capacitance is also low due the high isolation. All the parameters described above are RF MEMS advantages over FET technology. The disadvantages of RF MEMS switches are; low power handling, High Voltage actuation and long switching times, however the architecture for power handling can be rearranged to overcome this flaw. As for the switching time, this is dependent on the application of the switch. If the device is used to swap modes, the requirement of switching is irrelevant oppose to T/R Switching (Transmit / Receive Switching) with regards to the actuation voltage. One of the aims of this research is to reduce the actuation voltage to minimise the requirement of peripheral drive circuity such as, boost, charge pump and up converters. With the development of smart phone technology and the need for better performance, research on RF MEMS switches has increased, making them compatible and a catalyst to the growth of mobile communication systems.

Although the advantages of RF MEMS isolation cover DC – 100 GHz, mobile telecommunication systems practical frequency ranges from DC to 6 GHz, which includes the use of Wi-Fi.

5.1.2 Real World use of RF MEMS Switches

RF MEMS switches are used in radio frequency communication and microwave devices.

For example:

- Transmitters
- Receivers
- Transceivers
- Mode Selection switchers
- Antenna switching

These switches operate at RF to millimetre wave frequencies (100 MHz to 100 GHz).

A Transceivers contains both a transmitter and a receiver to connect to a single input/output antenna. This is achieved by using a Single-Pole Double-Throw (SPDT) switch, examples of this is shown in Figure 5.1 of a Radant MEMS manufactured switch (RadantMEMS 2014).

Mode Selection switches are capable of selecting from multiple inputs to a single output in order to switch between protocols such as; 2G, 3G, 4G, GSM, Bluetooth, Wi-Fi, etc. These are known as Single-Pole Multi-Throw (SPxT) switches, shown in Figure 5.2 of a Radant MEMS manufactured switch.

Mode selection and switching switches can either be used for antenna switching. An example of the RF MEMS switch used in a transceiver setup incorporating mode selection and transmit and receive switching is shown in the block diagram of Figure 5.3.

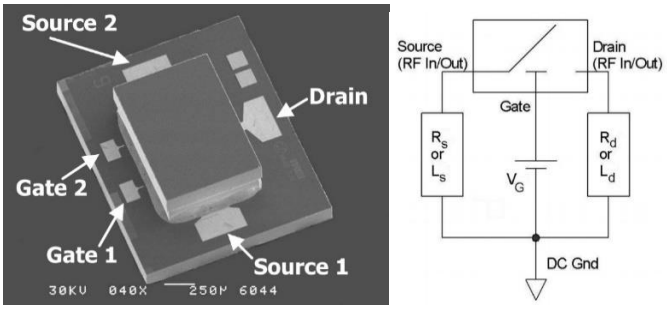

Figure 5.1: Radant MEMS RMSW221 SPDT switch DC to 20 GHz

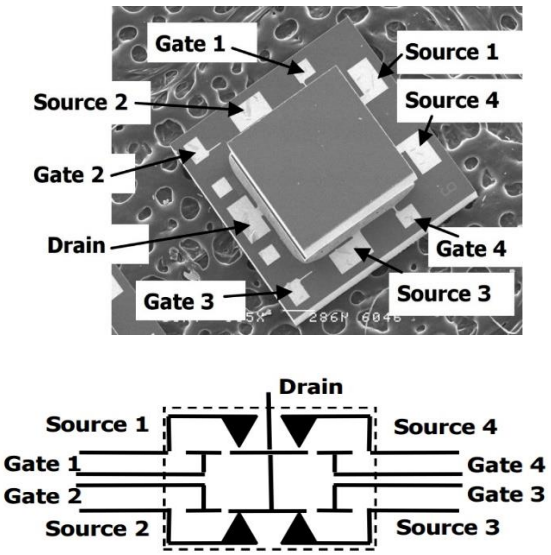

Figure 5.2: Radant MEMS RMSW240 SP4T Switch DC to 20 GHz

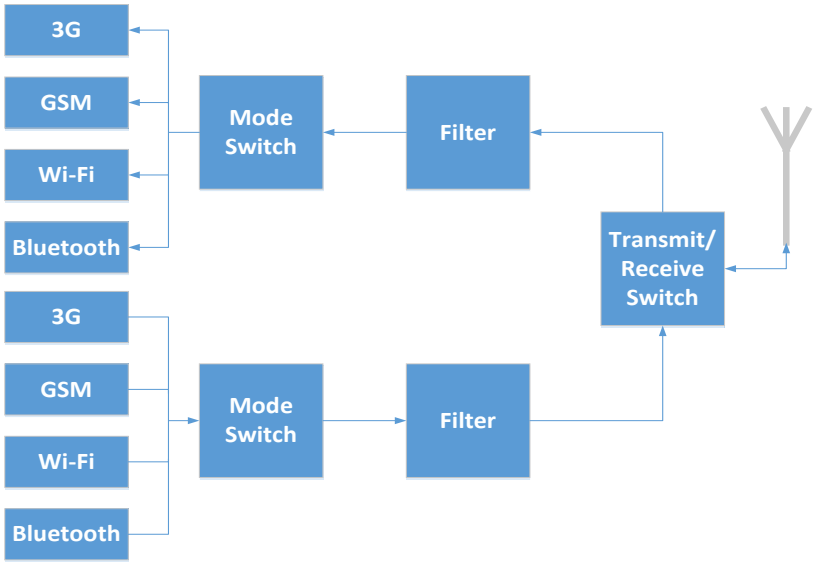

Figure 5.3: Simplified Block Diagram of a transceiver setup

5.2 Initial Design

After considering a number of research papers and books (Rebeiz 2003) the following type of RF MEMS switch was chosen for further investigation due its simple design, which allowed the expedient analysis of the design using Intellisuite simulation in order to verify the feasibility of the design via validation. Although the design is simple it was considered to have a great deal of potential for further development.

The performance of an existing cantilever beam (Fig 5.4) switch is verified using Intellisuite software. To prove the design, the simulation considered the dimensions

of the whole switch, including the size of the electrostatic plates, contact size, beam length and thickness, air gap and switch materials. Once all the parameters were set, the simulation provided results for a specific actuation voltage which were then verified against the actuation voltage specified in the literature (Gabriel M. Rebeiz, RF MEMS Theory, Design and Technology, 2003, p 135), to achieve contact within the set voltage range.

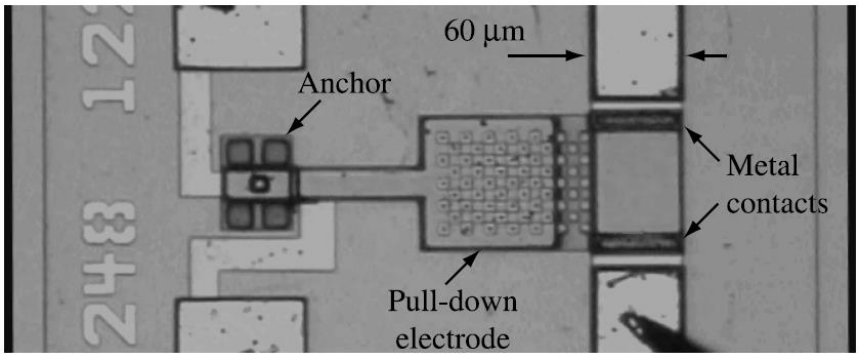

Figure 5.4: HRL RF MEMS Switch from Gabriel M. Rebeiz, RF MEMS Theory, Design and Technology, 2003, p 135

The parameters used in the experiment were:

- Actuation Voltage: 30V
- Air Gap: 1.5 µm
- Area of Electrostatic Plate: 100 x 100 µm
- With dimensions of shown in Figure 5.5

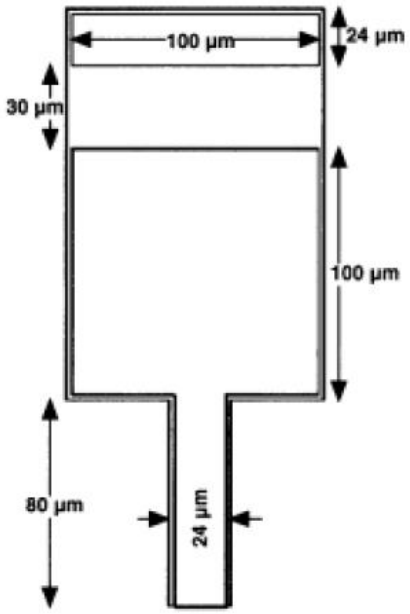

Figure 5.5: Daniel Hyman et al, 1999, HRL Cantilever SPST Switch

- Materials: Gold and Silicon Nitride PECVD
  - Gold Young's Modulus = 74.48 GPa
  - PECVD Young's Modulus = 300 GPa
- Thickness of the beam:
  - PECVD Layer 1 = 0.8 µm
  - Gold layer = 1 µm
  - PECVD Layer 2 = 0.8 µm

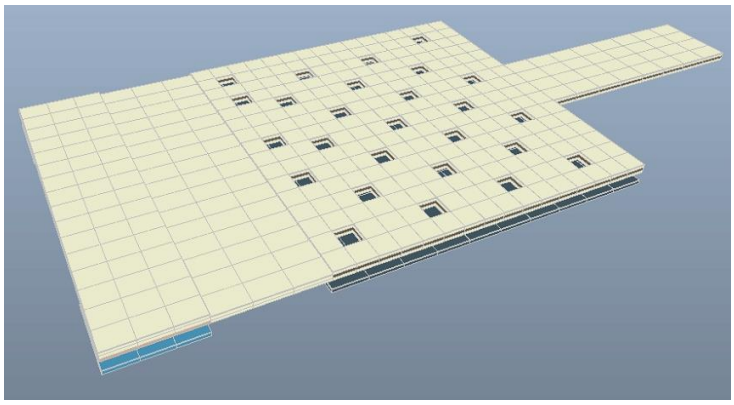

Figure 5.6: Modelled on Intellisuite TEM Simulation tool

The HRL cantilever design shown in Figure 5.6 was simulated with an actuation voltage of 30 V and the switch was able to displace the contacts by 1.5 µm.

Using the mathematical analysis for displacement, described in Chapter 3, the theoretical maximum displacement for this design is 2.374 µm. The mathematical displacement is in accordance with the simulated result and the air gap specified in the literature.

Although this is a functional RF MEMS switch, 20V is not a desirable voltage to be used in mobile communication systems. A more suitable voltage range to be used would be from 5V or less. This can be integrated into portable devices with reduced peripheral components.

The displacement is dependent on the pulling force which is created by the actuation voltage. The pulling force is inversely proportional to the square of the distance between the electrostatic plates. Therefore, by reducing this distance, i.e. the air gap, a significant decrease in actuation voltage can be achieved.

In order to reduce the actuation voltage, the HRL cantilever deign would need to be modified. The parameters that can be modified are; the area of the electrostatic plates, the distance between them, the thickness of the beam and the type of material.

Initially, a new design was created by scaling down the HRL cantilever by 10 times. The reason for this was to demonstrate via simulation that the smaller the design becomes the lower the actuation voltage. Thus, reducing the air gap by a factor of 10 increases the force by a factor of 100. However, this reduced scale would not be manufacturable with today's manufacturing techniques.

The HRL cantilever, although novel in its design, has disadvantages such as, allowing only single pole single throw actuation, with relatively high von mises stress, which reaches up to 690 MPa and requires voltages of up to 25 to 30V during operation.

5.3 Straight Pivot Seesaw RF MEMS Switch

To overcome the disadvantages described in the initial design chapter, the design had to be altered. To overcome this issue, the moving component would need to be designed with a more flexible structure and minimal movement to allow lower actuation voltages. By taking into consideration the scaled down cantilever (in the nano scale), it was realised that the beam was more flexible due to the thinner structure. The structure was then rotated by 90 degrees and reduced in length to 1.3 µm to become a pivot. Two pivots are used over one larger pivot to increase flexibility of the pivot area as shown in Table 5.2, which shows the voltage requirement of a single pivot (Figure 5.7 (Left)) and a split pivot (Figure 5.7 (Right)). Also, an additional rigid beam was attached to the pivots from its centre point to become a seesaw design.

A number of tests with different pivot materials and thicknesses were conducted to find the optimum flexibility, the results of which are shown in Figure 5.8 and Figure 5.9.

Table 5.2: Comparison of Actuation Voltage Requirement of Single and Split, Straight Pivot Seesaw, DPDT Switch

Switch Type	Actuation Voltage (V)
Straight Single Pivot Seesaw DPDT Switch	22
Straight Split Pivot Seesaw DPDT Switch	14

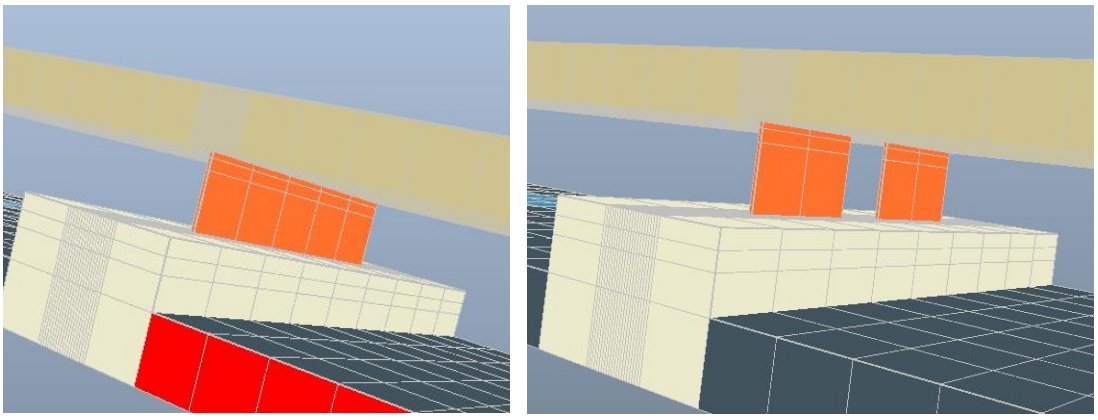

Figure 5.7: (Left) Single Straight Pivot Seesaw DPDT Switch with pivot width of 5 µm, (Right) Split Pivot Seesaw DPDT Switch with Pivot width 2 µm each and a spacing of 1 µm between them

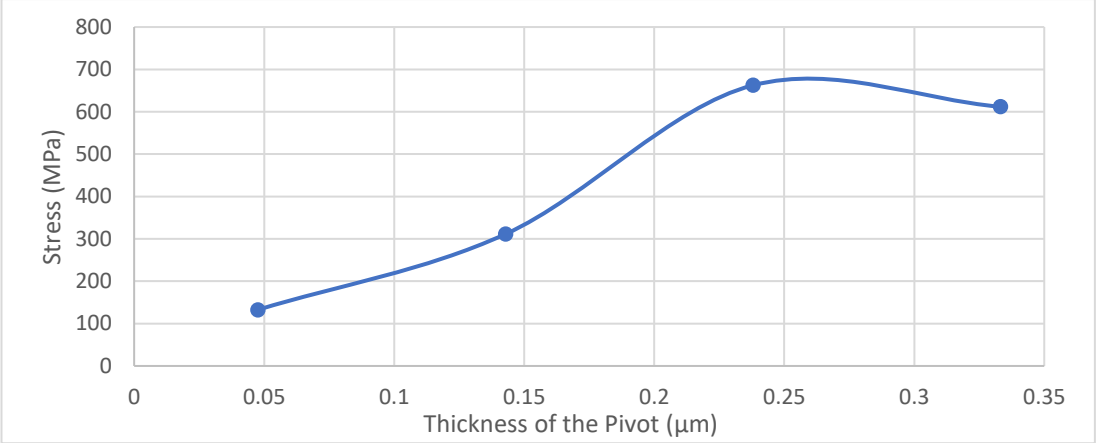

Figure 5.8: Stress for various pivot thicknesses to achieve a 1 µm displacement

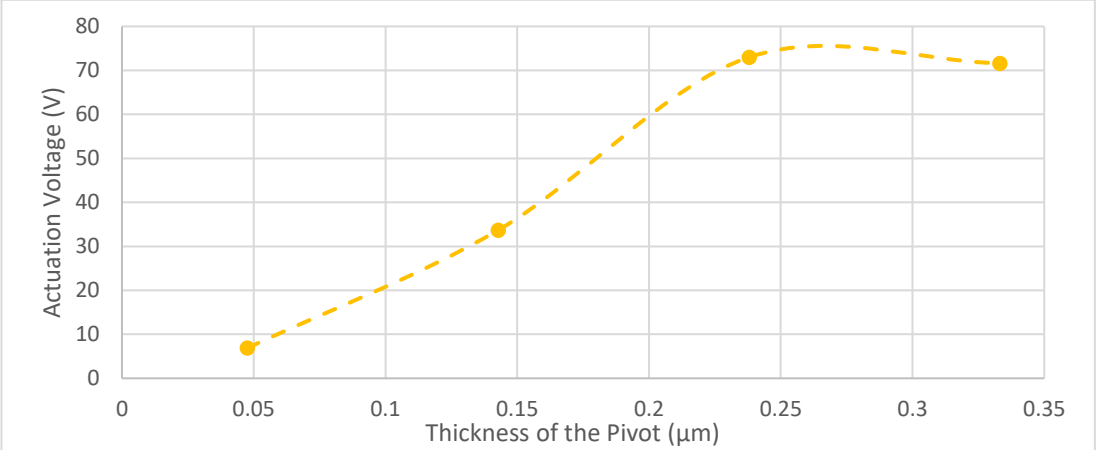

Figure 5.9: Actuation Voltage for various pivot thicknesses to achieve a 1 µm displacement

The materials gold (Au) and aluminium (Al) were originally considered, but as can be seen in Table 4.2 of Chapter 4 (Engineering Design Process), pure gold is ductile and pure aluminium has a very low yield strength. Therefore, these materials were eliminated as a pivot material. However, copper has a yield strength of 70 MPa, which allows the materials to withstand more stress during bending before deforming and the results shown in Figure 5.8 and Figure 5.9 indicates this.

The stress for copper at its minimum thickness was still too high (i.e. 132 MPa, with pivot thickness of 47.62 nm), as shown in Figure 5.8. Therefore, to reduce stress on the pivot, it would need to be lengthened. However, this would cause other problems whereby the distance between the electrostatic plates would be increased, causing the actuation voltage levels to be increased as well.

It was realised that the beam can move in two directions, allowing the option of providing an SPDT (Single-Pole, Double-Throw) switch. To take advantage of the space envelope, additional contacts can be utilised above the beam as shown in Figure 5.10. This allowed the switch to become a DPDT (Double-Pole, Double-Throw) switch.

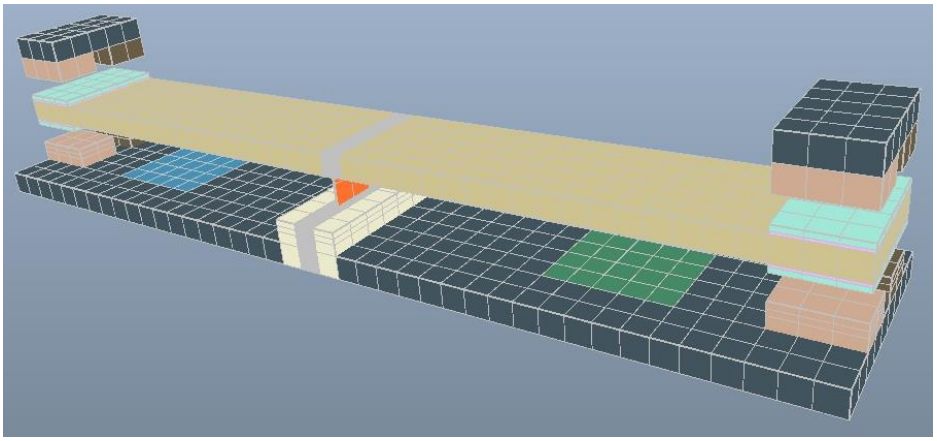

Figure 5.10: Model of the Straight Pivot Seesaw RF MEMS Switch v1

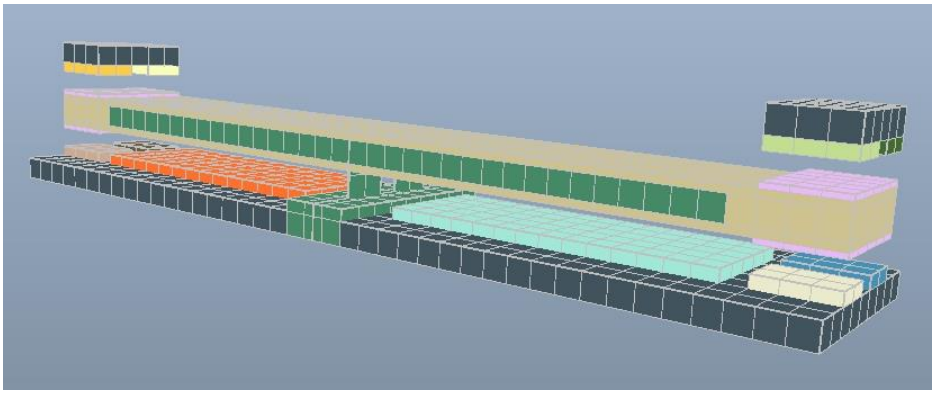

Figure 5.11: Model of the Straight Pivot Seesaw RF MEMS Switch v2

This Straight Pivot Seesaw RF MEMS Switch v1 was an improvement over the HRL cantilever in a few areas such as:

- A reduction of stress from 694.498 MPa down to 132 MPa
- A reduction in actuation voltage from 30 V down to 14 V
- Increased connectivity from SPST to DPDT

A disadvantage to this design is still the stress at the pivot. Knowing that the yield strength of copper is 70 MPa, the stress created at the pivot goes beyond this, at 132 MPa. Increasing the pivot length can reduce the stress at the pivot but from the parallel plates force equation, increasing the length of the pivot would increase the distance between the two plates, this in turn would increase the voltage requirement.

5.4 'S' Shaped Pivot Seesaw RF MEMS Switch

The disadvantage of the Straight Pivot Seesaw RF MEMS Switch can be overcome by lengthening the pivot but without increasing the distance between the electrostatic plates. To do this, the pivot design would need to be compressed into an 'S' shape (Serpentine). This would allow the pivot to distribute the stress along each segment of the links, as shown in Figure 5.12.

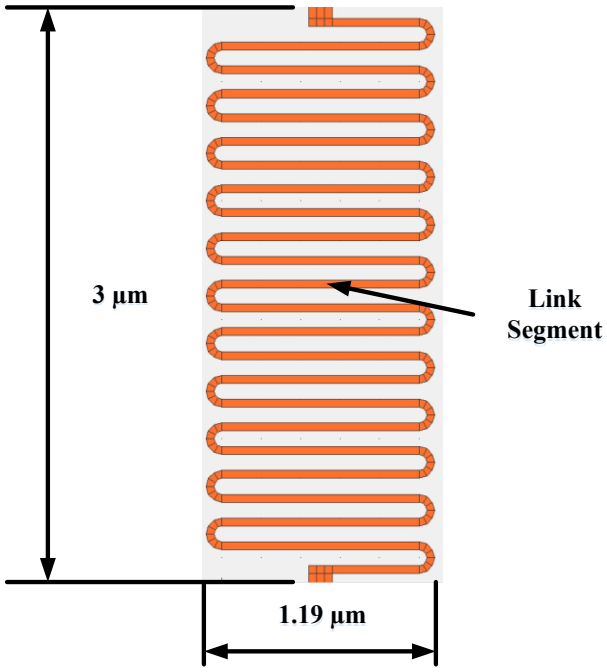

Figure 5.12: 'S' Shaped Spring Pivot showing the Link Segments

The design of the 'S' Shaped pivot is created on its side shown in Figure 5.13. In order to facilitate the serpentine shape, it would need to be set on its side, because of its complex shape.

As stress is distributed along all the links, this allows a reduction of total stress on the pivot (i.e. 21 MPa). Also, due to the increase flexibility of the pivot, the actuation

voltage required to achieve the displacement of 1 µm, from the original seesaw, can now be increased to 2.7 µm, which in turn provides improved isolation of the contacts; this is an improvement over the HRL cantilever which was 2.2 µm.

With the improvements of the pivot, the actuation voltage requirements have been significantly reduced from 14 V, with an air gap of 1 µm (from the straight pivot seesaw), down to 7 V, with an air gap of 2.7 µm.

Although both the 'S' shaped and straight pivots provide greater advantages over the HRL cantilever, the designs still have a disadvantage. When the beam is pulled and the contacts connect, the low contacts have greater contact force but the upper set do not. This is due to the angle the pivots move, as it draws closer to the plates it's been pulled to.

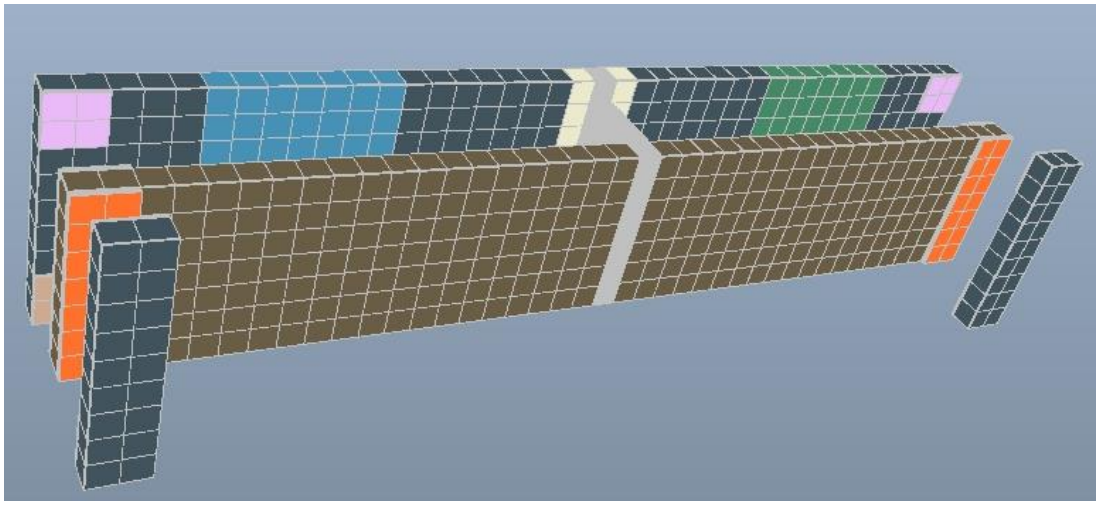

Figure 5.13: 'S' Shaped Pivot Seesaw RF MEMS Switch

5.5 'S' Shaped Pivot with Delta Electrostatic Plates RF MEMS Switch

To decrease the actuation voltage, so that the switch can be used with common voltage levels used in mobile telecommunication systems (i.e. voltages below 5V). The area of the electrostatic plates would need to be increased in size, without working outside the space envelope. The area can be increased by using another set of electrostatic plates above the beam. This solves the problem encountered by the previous seesaw designs and ensures that the upper contacts connect fully.

With the angled electrostatic plates, shown in Figure 5.14, the maximum force is created. The triangular shaped electrostatic plates shown in Figure 5.14, enable the force to be increased at the beam, as the plates get closer to each other.

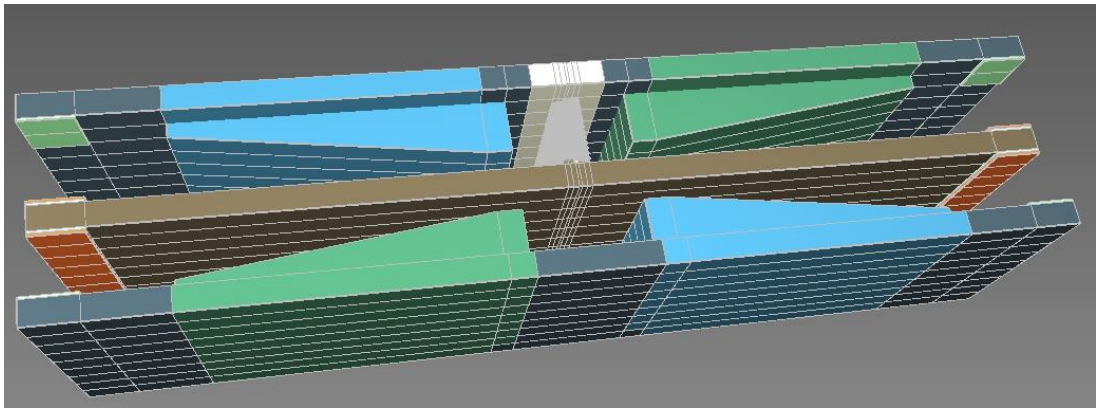

Figure 5.14: ‘S’ Shaped Pivot with Delta Electrostatic Plates RF MEMS Switch

The ‘S’ Shaped Pivot with Delta Electrostatic Plates RF MEMS Switch enables very low voltages to be used.

The ‘S’ Shaped Pivot with Delta Electrostatic Plates RF MEMS Switch, overcomes the disadvantages of the previous designs, such as:

- The latest design enables lower actuation voltages to be used over previous designs, by the increased area of the delta plates.
- The disadvantages of the straight pivot and the ‘S’ Shaped pivots seesaw switches were the upper bridging contacts not reaching the upper set of contacts. For this to be overcome, the forces are balanced by using two sets of electrostatic delta plates.
- The stress is similar to the first ‘S’ Shaped pivot seesaw design, this is due to the displacement and angle of movement being the same. Therefore, the von mises stresses for both the ‘S’ Shaped and delta plate switches are better than the straight pivot and the HRL cantilever switches.

The extra layers for this design would be more expensive but the benefits outweigh the cost. The development of the nano scaled, ‘S’ shaped serpentine spring pivot, would be a challenge using todays manufacturing techniques, requiring a minimum

feature size of 47nm and less, however manufacturing techniques are being improved upon.

5.6 ‘S’ Shaped Split Pivot with Delta Electrostatic Plates RF MEMS Switch

To take the voltage down further the implementation of splitting the single ‘S’ shaped pivot to two with a 1 μm gap provided a further reduction. By taking advantage of the principles of the straight pivot being split, the pivot flexibility can be increased.

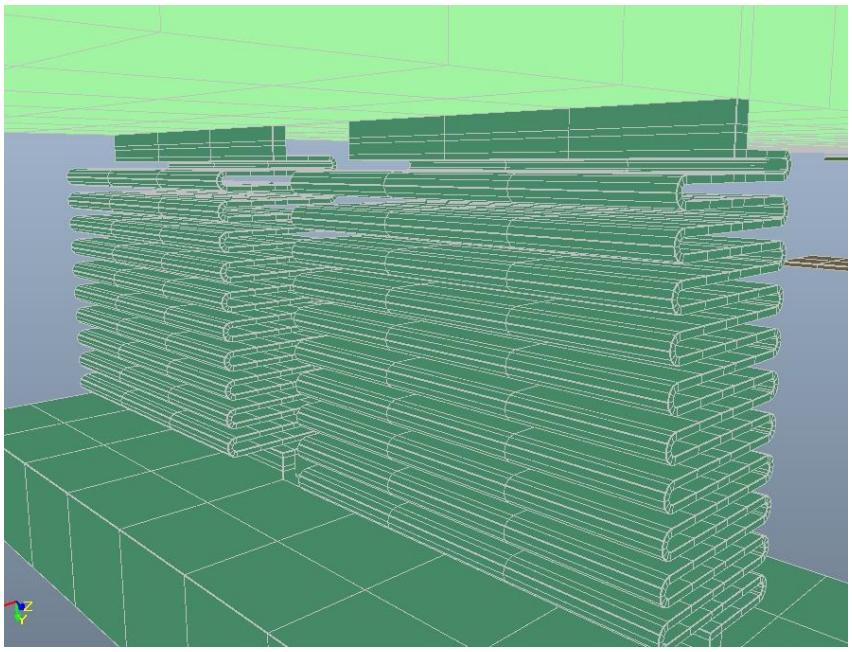

Figure 5.15: 'S' Shaped Split Pivot View

To summarise, this chapter describes the initial design of a cantilever SPST switch, which was then developed into a DPDT, Seesaw type switch with lower von mises stress on the pivot. This enabled the actuation voltage to be decreased for improved performance.

Chapter 6

6 Results and Validation

This chapter provides the initial validation of Grid Independency and mathematical analysis of the HRL cantilever. The chapter then follows on with the results of the unique designs, which reveals the finding from Intellisuite TEM simulation tool and CST EM simulation tool.

The chapter provides results data for the following analyses:

- Grid Independency
- Maths Equations vs Simulations
- The practical HRL cantilever vs the simulated version
- Designs described in chapter 5 and its Stress, Electrostatic and EM Characteristics

This data contributes to the analysis employed in Chapter 7 (Discussion and Results Analysis)

6.1 Grid Independency

The grid independency is conducted using two electrostatic plates, spaced at 1 µm apart, with one plate grounded at 0 V and the other charged at voltages of 1, 5, 10, 15, 20, 25 and 30 volts. The grid independency is then conducted with mesh sizes being applied at 50, 20, 10, 5, 2.5 and 1 µm. The two plates are fixed in place with the size of each plate being 100 µm x 100 µm with thickness of 3 µm. Both plates are parallel to each other.

For this test, the six mesh sizes were used to demonstrate the discrepancy between the finer mesh up to the coarser meshes. The results of this is shown in Table 6.1.

Table 6.1: Results of the average force applied between two plates

	Forces (N) for Different Distances Between Plates					
Applied Voltage	**50 µm**	**20 µm**	**10 µm**	**5 µm**	**2.5 µm**	**1 µm**
1V	4.27754E-08	4.56328E-08	4.64038E-08	4.75091E-08	4.75091E-08	4.82121E-08
5V	1.30019E-06	1.14082E-06	1.16009E-06	1.17401E-06	1.20584E-06	1.2053E-06
10V	4.27754E-06	4.56328E-06	4.60452E-06	4.69602E-06	4.75091E-06	4.82121E-06
15V	9.62445E-06	1.02674E-05	1.04409E-05	0.000010566	1.06896E-05	1.08477E-05
20V	1.71102E-05	1.82531E-05	1.85615E-05	1.87841E-05	1.90037E-05	1.92849E-05
25V	2.67347E-05	2.85205E-05	2.90024E-05	2.93501E-05	2.96782E-05	2.96932E-05
30V	3.8498E-05	4.10695E-05	4.17634E-05	4.22642E-05	4.27582E-05	4.33909E-05

6.2 Simulation Against Mathematical Analysis

The following simulations were carried out and subsequently compared with mathematical equations for these parameters:

- Electrostatic Force
- Displacement of the beam
- Resonant frequency

Using established mathematical theories for electrostatic force, displacement of the beam and resonant frequency were calculated for a set of given dimensions as shown in Figure 6.1. These were also used for the simulation to prove the accuracy of the simulation against the mathematical calculation.

In each test, a simple design was chosen, to reduce the complexity of both the simulation and the mathematics, which also allows for simpler management of the results and direct validation of the test, without the risk of other variables interfering with the results. For example, fringe capacitance, complex shapes and damping.

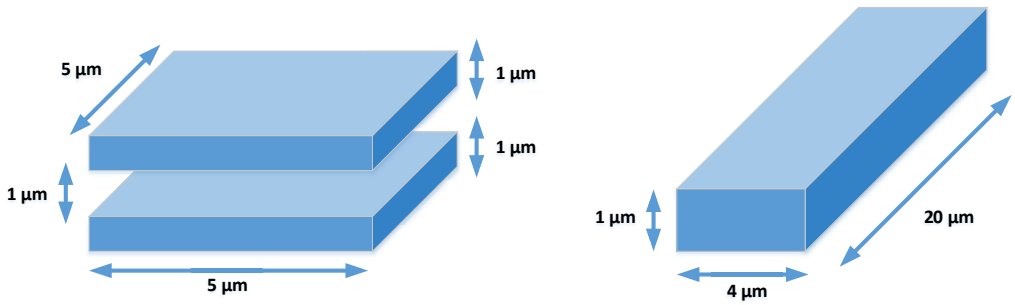

Figure 6.1: Diagram of the electrostatic plates and its dimensions (Left) and the beam and its dimensions (Right)

6.2.1 Electrostatic Force

This section is to prove that the simulation from Intellisuite is in accordance to the mathematical modelling. The stages of testing used two fixed parallel plates with fixed size and spacing between them.

The first test used the average force between the plates from simulation and compare it to the mathematical results.

The second test used four-centre nodes and gets an average force between them and compares it to the maths model.

To verify the electrostatic force between two parallel plates. Two fixed parallel plates, shown in Figure 6.2, were simulated, using Intellisuite TEM simulation tool, with a range of actuation voltages from 1V to 30V. The simulated and calculated results are then compared. The results of which are shown in Table 6.2.

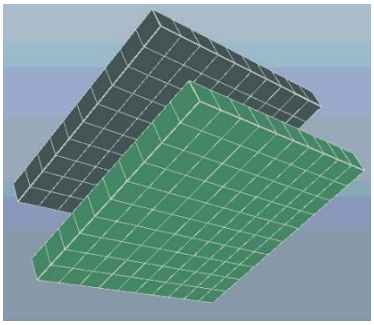

Figure 6.2: Fixed Electrostatic plates on Intellisuite TEM

Table 6.2: Comparison of simulated and calculated forces

Actuation Voltage (V)	Simulated Average Force on the Centre Node of the plates (N)	Simulated with Average Face Plate Force (N)	Calculated Force of the Parallel Plates (N)
1	4.560000E-08	4.640380E-08	4.430000E-08
5	1.141000E-06	1.160090E-06	1.107000E-06
10	4.564000E-06	4.604520E-06	4.427000E-06
15	1.015000E-05	1.044090E-05	9.961000E-06
20	1.805000E-05	1.856150E-05	1.771000E-05
25	2.820500E-05	2.900240E-05	2.767000E-05
30	4.061500E-05	4.176340E-05	3.984000E-05

Note: The dimensions of the parallel electrostatic plates are with a width and length of 5 µm with a thickness of 1 µm. and an airgap of 1 µm.

6.2.2 Displacement of the Beam

The displacement of the beam is used to calculate the distance of the beam as it bends from its original position with a given force. This is calculated using Equation 6.1. Where Young's Modulus and the dimensions of the beam is taken into consideration. The equation can then be compared against the simulated design to validate the relationship between the mathematical model and the analysis.

The displacement, delta (δ), of a beam, is defined by the two following equations where Equation 6.1 is the moment of inertia and Equation 6.2 is the displacement of the beam which integrates moment of inertia (KUBBY, J.A. 2011):

Equation 6.1

$$\boldsymbol{I = \frac{(w * t^3)}{12}}$$

Equation 6.2

$$\boldsymbol{\delta = \left(\frac{L^3}{3 * E * I}\right) * F}$$

Where:

E = Young's Modulus (Pa)

L = Length of the beam (m)

w = Width of the beam (m)

t = Thickness of the beam (m)

Table 6.3: Displacement of the beam Comparison Between Simulation and Mathematical Model

Force (N)	Simulated Displacement (m)	Calculated Displacement (m)
1.0E-06	6.68E-08	6.838E-08
2.0E-06	1.34E-07	1.368E-07
3.0E-06	2.01E-07	2.051E-07
4.0E-06	2.68E-07	2.735E-07
5.0E-06	3.35E-07	3.419E-07
6.0E-06	4.02E-07	4.103E-07
7.0E-06	4.69E-07	4.786E-07
8.0E-06	5.36E-07	5.470E-07
9.0E-06	6.03E-07	6.154E-07
1.0E-05	6.70E-07	6.838E-07

Table 6.4: Copper Beam Parameters

Length of the Beam (L)	20 µm
Width of the Beam (w)	4 µm
Thickness of the Beam (t)	1 µm
Young's Modulus (E)	117 GPa

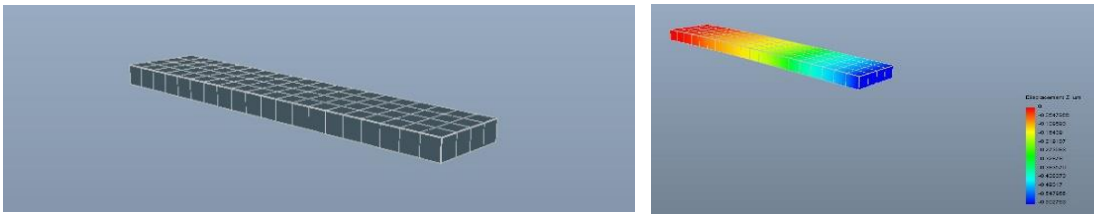

Figure 6.3: (Left) Visual Representation of the model prior to simulation, (Right) Visual representation of the beam model after simulation, with colour coded results information

The results of the beam are shown in Table 6.3, using the parameters from Table 6.4. An example of the structure of the fixed-free beam with colour coded results are shown in Figure 6.3.

6.2.3 Resonant Frequency

The resonant frequency which is also known as the natural frequency, is the vibrational frequency which the structure of the device resonates to. If the amplitude of which the vibration is too great, and the frequency is the same as the natural frequency of the structure, it will eventually cause the damage to the device and eventually break. Therefore, understanding the resonant frequency and comparing the Mathematical equation to the practical simulation would be ideal to prove the validity of the simulation, against proven mathematical equations.

The resonant frequency of the beam, shown in Equation 6.3, f_0, is defined by the following equation (Hyman et al. 1999):

Equation 6.3

$$f_0 = \left(\frac{1}{2 * \pi}\right) * \frac{d}{L^2} * \sqrt{\frac{E}{\rho}}$$

Where:

d = Thickness of the beam (m)

L = Length of the beam (m)

E = Young's Modulus (Pa)

ρ = Density of the material (kg/m^3)

Table 6.5: Resonant Frequency of the beam with simulated and mathematical results

Length of the Beam (μm)	**Simulated Frequency Response (Hz)**	**Mathematical Frequency Response (Hz)**
10	5.99E+06	5.76E+06
11	4.94E+06	4.76E+06
12	4.15E+06	4.00E+06
13	3.53E+06	3.41E+06
14	3.04E+06	2.94E+06
15	2.65E+06	2.56E+06
16	2.32E+06	2.25E+06
17	2.06E+06	1.99E+06
18	1.83E+06	1.78E+06
19	1.64E+06	1.60E+06
20	1.48E+06	1.44E+06

For this test, the width and thickness of the beam were kept constant at 4 μm and 1 μm, respectively. The length of the beam was increased in increments of 1 μm, from 10 μm to 20 μm. In each case, the resonant frequency was calculated and simulated prior to being compared with each other. This is shown in Table 6.5 and in graphical format in Figure 7.10.

6.3 Validation of the HRL Cantilever Against Simulation

6.3.1 Validation of Experimental Results Against Simulation

The paper (Wiley - RF MEMS Theory, Design and Technology by Gabriel M. Rebeiz, p.134, 2003) referenced, contains a practical experiment of the HRL cantilever beam RF MEMS switch. The specifications from this paper are as follows:

- Actuation Voltage: 30 V
- Air Gap (Displacement the beam moved): 1.5 µm
- Materials used: Silicon Nitride PECVD and Gold
- Dimension of the beam (see Figure 6.4)

Using these specifications and associated parameters, a simulation of voltage verses displacement was carried out to verify the results from the paper. The results of these simulations are shown in
Table 6.6. The displacement of the beam was taken from Intellisuite TEM Simulation results.

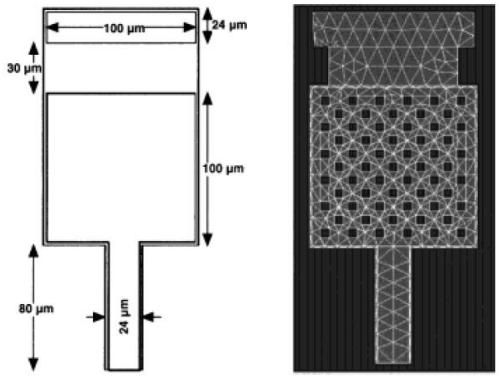

Figure 6.4: Dimension of the HRL cantilever beam from Daniel Hyman et al, 1999

Table 6.6: Voltage verses displacement of HRL Cantilever beam switch

Voltage (V)	Displacement (µm)
0	-0.0213928
1	-0.0225837
2	-0.0261641
3	-0.0321574
4	-0.0406032
5	-0.0515584

6	-0.0650993
7	-0.0813234
8	-0.100353
9	-0.122386
10	-0.147553
11	-0.176118
12	-0.208377
13	-0.244702
14	-0.285572
15	-0.331602
16	-0.383866
17	-0.443181
18	-0.511361
19	-0.591459
20	-0.687805
21	-0.80984
22	-0.985362
23	-1.49718
24	-1.4982
25	-1.49927
26	-1.50009
27	-1.50084
28	-1.50163
29	-1.50246
30	-1.50334

A summary of the simulated results and the results from the paper are shown in Table 6.7 for the purpose of comparison.

Table 6.7: Characteristics of practical verses simulated results

Parameter of the Switch	**Experimental HRL Cantilever Result from Paper**	**Simulated Result Using Intellisuite**
Actuation Voltage	30 Volts	30 Volts
Resonant Frequency	30 kHz (Approximately)	28.1197 kHz
Displacement	1.5 μm	1.5 μm

Note: The HRL Cantilever paper states that the resonant frequency of the switch is an approximation, which explains the difference between the experimental and simulated result in the table.

6.4 Design Results

The following sets of results were obtained from the experimental methodology described in Chapter 3 (Theoretical Background and Engineering Design Process), which are broken down into two parts.

The first part combines the results for actuation voltage, displacement and von mises stress, including elastic recovery results, which shows the variation of displacement with time; the second part provides the results of the electromagnetics of isolation and reflection when the switch is off for each of the designs.

6.4.1 Stress and Electrostatic Characteristics

6.4.1.1 Actuation Voltage, Displacement and Von Mises Stress

The results in Table 6.8 show the actuation voltage, displacement and Von Mises stress of each of the RF MEMS designs.

Table 6.8: Results of the different types of RF MEMS switches (rounded to the closest 1 MPa)

RF MEMS Design	Actuation Voltage (V)	Displacement (µm)*Note 1	Von Mises Stress (MPa)
HRL Cantilever SPST Switch	30*Note 2	1.5 *Note 3	694
Scaled Down version of HRL Cantilever SPST Switch by 10 times	2.3	0.15	690
Straight Pivot Seesaw DPDT Switch, v1	14	1	123
Straight Pivot Seesaw DPDT Switch, v2	7	1	135
‘S’ Shaped Pivot Seesaw DPDT Switch	4	2.7	16
‘S’ Shaped Pivot with Delta Angled Electrostatic Plates DPDT Switch	1.23 *Note 4	2.7	15
‘S’ Shaped Split Pivot with Delta Angled Electrostatic Plates DPDT Switch	1.13 *Note 4	2.7	15

*Note 1: The displacement is equal to the air gap of the switch.

*Note 2: The actuation voltage for the HRL Cantilever SPST Switch is stated to actuate between 25V, which was also verified at 30 V.

*Note 3: The displacement value of the HRL Cantilever SPST Switch was calculated from the material thicknesses provided by the document (Hyman et al. 1999).

*Note 4: The ‘S’ Shaped Pivot with Delta Angled Electrostatic Plates DPDT Switch has an adjustable voltage range depending on the voltage requirement by changing the angle of the electrostatic plates.

6.4.1.2 Displacement vs Voltage

The displacement verses voltage simulation is used to find the point of which the switch contact closes. The tables shown in Appendix C use simulation voltage levels for activating the electrostatic parallel plates for the switch, which shows the displacement at each set.

6.4.1.3 Contact Analysis

The contact analysis for the switches are run by Intellisuite SYNPLE simulation tool, the methodology of running SYNPLE and acquiring results is shown in chapter 4.3.3.2 (Modal Simulation using SYNPLE and TEM).

Due to the amount of data for each iteration being large. The data is, instead, provided on request. The data size can range from 1500 increments to 50,000. Therefore, the data is shown in graphical form in the Discussion and Results Analysis chapter, within the Contact Analysis section.

6.4.1.4 Resonant Frequency

The resonant frequency is the natural frequency of the device. Using Intellisuite TEM simulation tool, the resonant frequencies of the devices are extracted and are presented in Table 6.9.

Table 6.9: Resonant Frequency of the RF MEMS switches

Switch Design	Resonant Frequency (Hz)
HRL Cantilever SPST Switch	28117.9
Scaled Down version of HRL Cantilever SPST Switch by 10 times	285108.0
Straight Pivot Seesaw DPDT Switch, v1	17615.7
Straight Pivot Seesaw DPDT Switch, v2	20568.2
‘S’ Shaped Pivot Seesaw DPDT Switch	6069.34
‘S’ Shaped Pivot with Delta Angled Electrostatic Plates DPDT Switch	3535.39
‘S’ Shaped Split Pivot with Delta Angled Electrostatic Plates DPDT Switch	3273.69

6.4.1.5 Elastic recovery

In this subchapter, the simulation for elastic recovery also known as spring constant, is presented, for six major iterations of the switch, the methodology of extracting the elastic recovery of the switches are explained in the 'TEM Contact Release Simulation with Contact Analysis' chapter. The result tables for this subchapter are located in Appendix C under the heading Elastic Recovery.

6.4.2 EM Characteristics

6.4.2.1 Isolation (S21) and Insertion Loss (S11) Parameters

The CST simulation is run using the contact criteria used for the six designs. Although the designs for both the straight pivot seesaw and both the 'S' shaped pivot seesaw switches contact are identical, the results of each EM simulation are the same, therefore a single common contact design for each is chosen.

Table 6.10: CST Comparison of results for the different designs at S21

Types of Switch	**S21 (dB) at 5 GHz**	**S21 (dB) at 12 GHz**	**S21 (dB) at 20 GHz**	**S21 (dB) at 45 GHz**
Paper Modelled Results	-43.00	-35.00	-29.00	-24.00
Paper Measured Results	-47.00	-36.00	-32.00	-26.00
Design 1*	-43.77	-36.67	-32.93	-26.06
Design 2**	-61.44	-57.99	-53.41	-44.85
Design 3***	-117.16	-109.48	-104.51	-97.18
Design 4****	-122.28	-116.68	-114.48	-110.33
Design 5 *****	-106.59	-103.17	-101.58	-100.22

Table 6.11: CST Comparison of results for the different designs at S11

Types of Switch	**S11 (dB) at 5 GHz**	**S11 (dB) at 12 GHz**	**S11 (dB) at 20 GHz**	**S11 (dB) at 45 GHz**
Design 1*	-0.33	-0.76	-1.20	-2.88
Design2**	-0.29	-0.50	-0.91	-2.68
Design 3***	-0.00	-0.01	-0.01	-0.03
Design 4****	-0.17	-0.40	-0.69	-1.54
Design 5 *****	-0.01	-0.02	-0.03	-0.07

* Design 1 is the contact structure of the ‘HRL cantilever SPST switch’

** Design 2 is the contact structure of the ‘scaled down version of the HRL cantilever SPST switch by 10 times’

*** Design 3 is the contact structure of both the ‘Straight Seesaw DPDT Switch v1’ and the ‘Straight Seesaw DPDT switch, v2’

**** Design 4 is the contact structure of both the ‘‘S’ Shaped Pivot Seesaw DPDT Switch’ and the ‘‘S’ Shaped Pivot with Delta Angled Electrostatic Plates DPDT Switch’

***** Design 5 is the contact structure of both the ‘‘S’ Shaped Pivot Seesaw DPDT Switch’, the ‘‘S’ Shaped Pivot with Delta Angled Electrostatic Plates DPDT Switch’ and the ‘‘S’ Shaped Split Pivot with Delta Angled Electrostatic Plates DPDT Switch’ which are set on its side

To summarise, the data presented in this chapter covers:

- Grid independency
- Mathematical analysis
- Simulation data of a HRL cantilever
- Stress and electrostatic characteristics for the different designs
- EM characteristics for the different designs

This data is further explained and analysed in the next chapter (Discussion and Results Analysis)

Chapter 7

7 Discussion and Results Analysis

This chapter analyses the data provided in Chapter 6 (Results and Validation) and provides a detailed explanation of the methodologies employed and describes the advantages of the different RF MEMS switches over the HRL cantilever switch. It also shows the contributing factors on reducing the actuation voltages of the designs.

7.1 Validation

The validation of the experiment is the first step to identifying the accuracy of the results. Initial validation is conducted in order to identify the discrepancy of the mesh for simulation, this is known as 'Grid Independency' or also known as 'Grid Sensitivity'. The next stage of validation is identifying the accuracy of the simulation against established mathematical equations. Once completed, the simulation is then validated against experimental design from a paper. This allows the comparison between the switch design characteristics made on simulation using the same characteristics reported in the paper and evaluating the results of both.

With these sets of validations, it can show the accuracy of the simulation tool against real world designs.

7.1.1 Grid Independency

Grid Independency, also known as 'Grid Sensitivity', is a test to provide an understanding of the error rate within the grid, and to aim to reach an error rate close to zero, as more nodes are added to the independent grid without any increase to the accuracy of the results. Achieving a true independent grid is a timely issue which encompasses the maximum system resources, causing detrimental performance issues during simulation.

The grid independency test is conducted using a variable size mesh on the same structure and analysing the variation of the results. If the variation from the results are low this would show that the grid sensitivity is low, and the simulation is reaching to grid independence. If the variation is great, it would mean that the mesh needs to be finer in order to create an accurate result.

As the mesh size decreased, the node value (shown in Table 7.1) increased. This in turn increased the load on the simulation tool. This was more noticeable when the mesh size for the parallel plates decreased down to 2.5 µm and 1 µm with the simulation software beginning to struggle to display the plates when observing the design before simulation starts.

Table 7.1: Node requirement for the test per mesh size

Mesh Size	Nodes
50 µm	128
20 µm	560
10 µm	1920
5 µm	7040
2.5 µm	28160
1 µm	169600

The grid independency test results have shown that the variations are minimal and are kept at a tight tolerance within 11.3% as shown on the percentage difference in Table 7.2. Having more nodes increases the resolution of the mesh, which in-turn increases accuracy of the simulation results. However, having higher resolution is detrimental to the time taken for a simulation to be completed. Therefore, an optimum number of nodes is chosen as a compromise between simulation accuracy and simulation time.

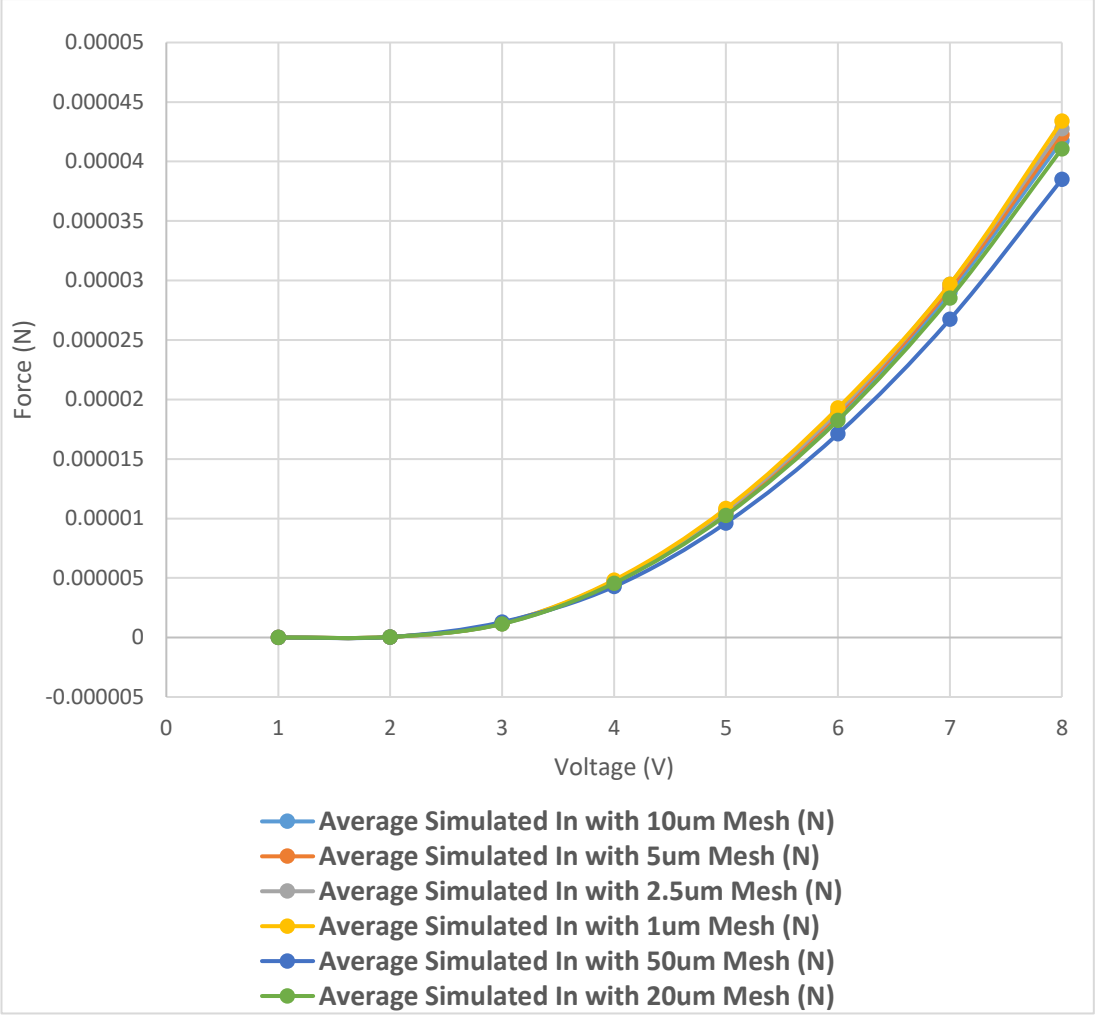

Figure 7.1: Grid Independency comparison of different mesh sizes

Table 7.2: Percentage difference of accuracy from 50 µm

Mesh vs Mesh	Percentage Difference
20 µm vs 50 µm	6.26%
10 µm vs 50 µm	7.82%
5 µm vs 50 µm	8.91%
2.5 µm vs 50 µm	9.96%
1 µm vs 50 µm	11.28%

When the simulation starts, for the finer mesh designs, the speed the analysis completes is far longer than the coarser meshes, which causes an issue with analysis times to be greater. Therefore, with the grid independency mesh sizes between 1 µm and 10 µm, provides a close percentage difference. Thus, using a mesh size of ten

times smaller than the total size of the structure, it is a reasonable resolution for the structure while optimising the simulation speed.

7.1.2 Validation of Simulation against Mathematical Analysis

The next stage of validation is the validation of the simulation tool against known established mathematical equations. The models of the equations and the simulation tools used are simple in design. This reduces the complexity of the calculation while reducing the risk of other fringe calculations, being implemented during the analysis of the simulation software. Other advantages include the rapid calculation time required to provide a result from the simulation software, with a direct validation of both the simulation software and mathematical analysis. The following validations were carried out on: the electrostatic force of two parallel plates, the displacement of a beam and the resonant frequency of a beam.

7.1.2.1 Electrostatic Force

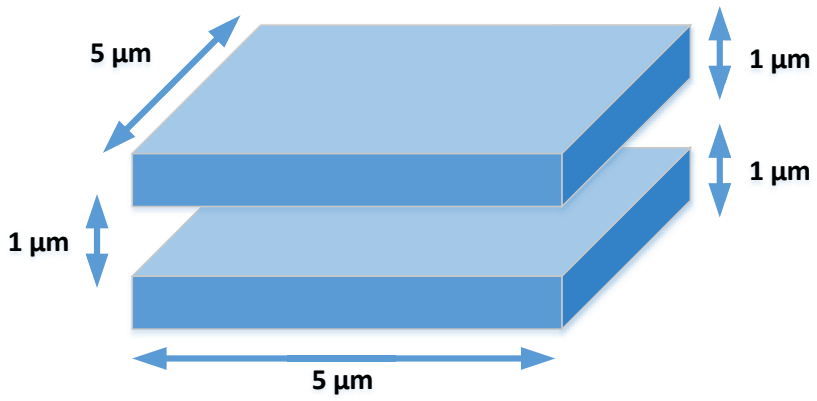

Figure 7.2: Dimensions of two parallel electrostatic plates

The electrostatic force validation is to find out the voltage required to achieve a given amount of force for the plates to attract each other, allowing the beam to be pulled. Intellisuite's Thermo-Electro-Mechanical (TEM) simulation tool was used for this experiment running a static simulation using the ThermoElectroMechanical Relaxation analysis option.

Two sources of results were collected from the TEM simulation tool, the first was the total average force of the faces of the two plates. The second result was taken using 4 centre nodes of the plates and averaging them. The nodes were collected from the plate faces, which were facing each other. This is to avoid fringe capacitance that occurs at the edges of the plates, which in turn affects the force.

The force developed between the two parallel electrostatic plates, shown in Figure 7.3, depends upon the area (A) of the plates, the potential difference (voltage V) across the plates, the distance between the two plates (g) and the dielectric material between them (ε0). Therefore, the force (F) can be defined by the following equation (Rebeiz 2003):

Equation 7.1

$$\boldsymbol{F = \left(\frac{\left(\varepsilon_0 * V^2 * (Aw * Al) \right)}{2 * g^2} \right)}$$

Where:

ε_0 = is the dielectric constant of air (F/m)

V = Actuation voltage (V)

Aw = Width of the electrostatic plates (m)

Al = Length of the electrostatic plates (m)

g = Distance between two plates (m)

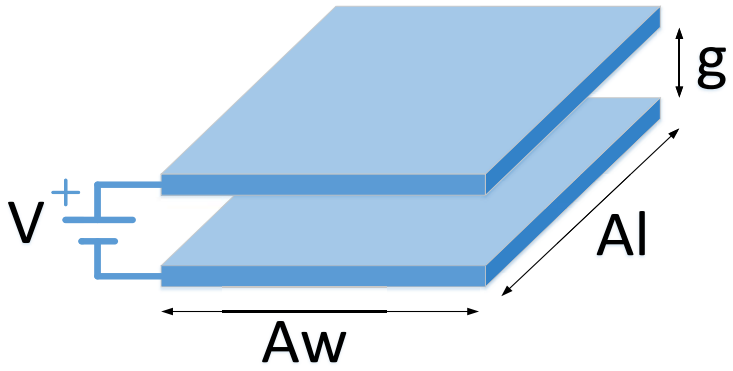

Figure 7.3: 3D Representation of two parallel plates

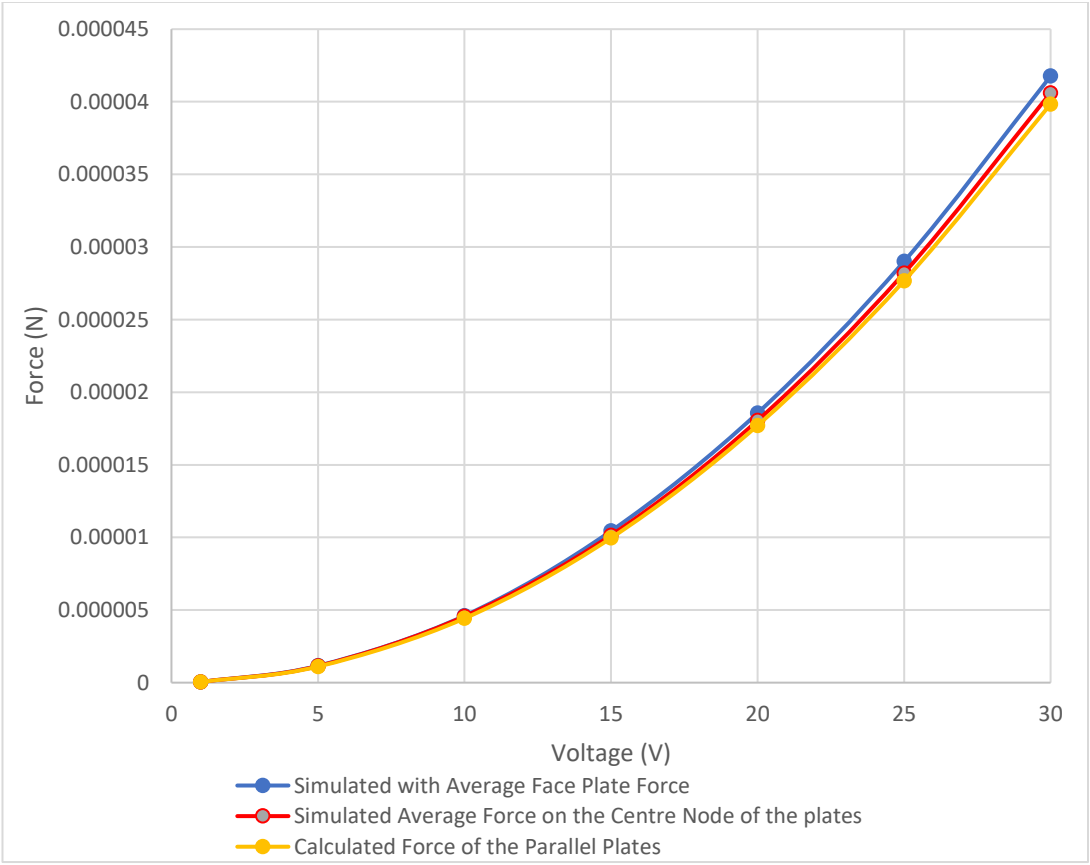

Figure 7.4: Electrostatic Force Equation vs Simulated Average force on face vs Simulated average force on centre nodes on face

For validation, the dimensions of the plates shown in Figure 7.2 were used. Figure 7.4 shows a graphical result of the calculated electrostatic force equation and the simulated results. The results for the calculated electrostatic force equation are slightly lower in force compared to the simulation, but the simulated results taken from the centre nodes is shown to have a closer relationship to the calculated results compared to the average force of the plates. This is due to the fringe capacitance force, exerted from the outer edge of the face. This is shown in Table 7.3 and displayed graphically on Figure 7.5.

Table 7.3: Pressure exerted at the centre nodes along the X and Y axis

Node Point	X axis (MPa)	Y axis (MPa)
1	4.46E-03	4.46E-03
2	4.31E-03	4.31E-03
3	4.14E-03	4.14E-03
4	4.12E-03	4.12E-03
5	4.11E-03	4.11E-03
6	4.10E-03	4.10E-03
7	4.11E-03	4.11E-03
8	4.12E-03	4.12E-03
9	4.14E-03	4.14E-03
10	4.31E-03	4.31E-03
11	4.46E-03	4.46E-03

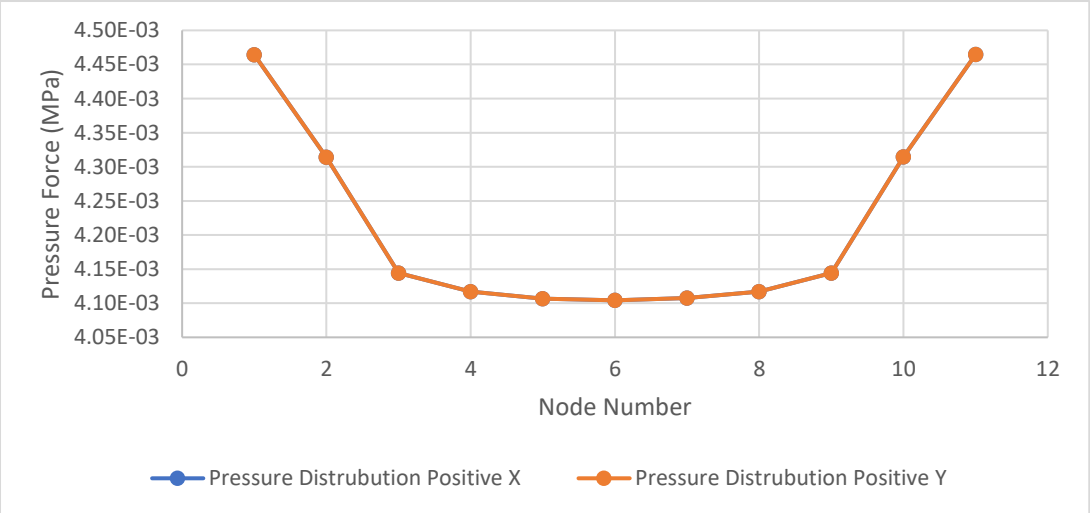

Figure 7.5: Force Pressure distribution though the cross section of X and Y axis

Note: The Pressure Distribution Positive X and Y graphs are identical and is the reason why only the Y graph can be seen (i.e. it lies on top of the X graph)

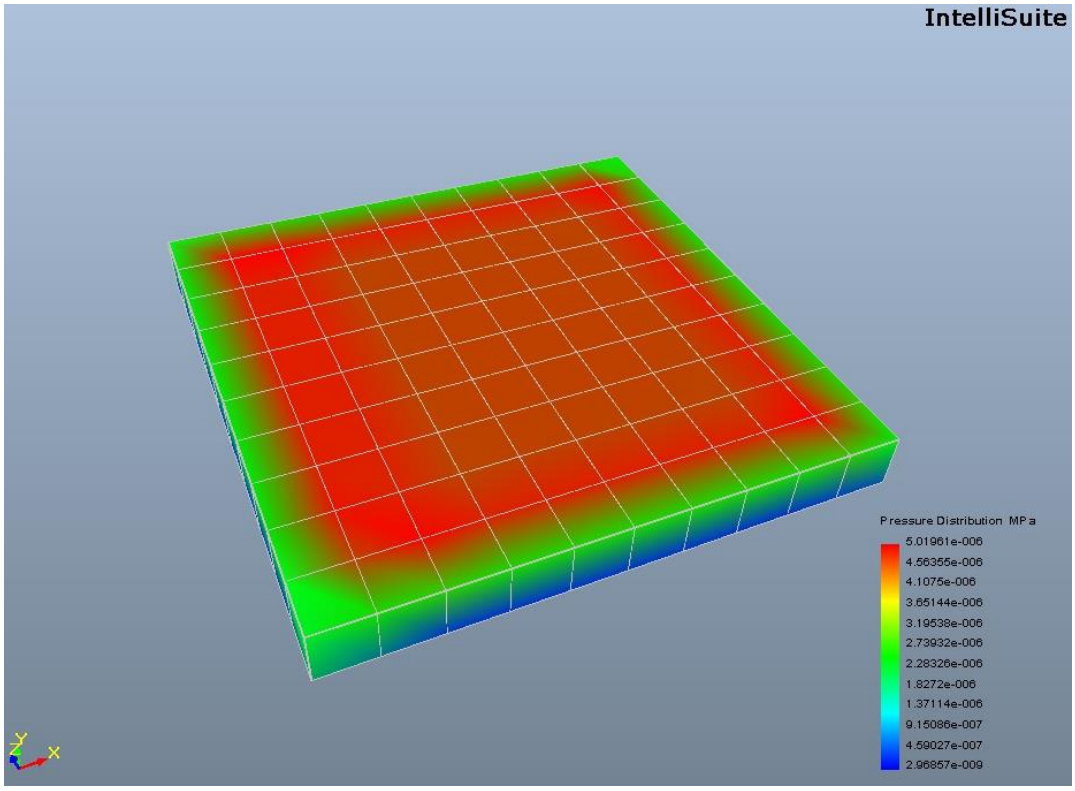

Figure 7.6: Pressure distribution of force in MPa on one side of the plate

On Figure 7.6, it shows an example of the result, displaying the colour coded pressure force distribution across the face of the plate. The higher-pressure distribution is shown in red with the colour changing down to blue for lower pressure distributions.

When the average force of the plates is calculated, the lower pressure of force is included in the sum, causing the overall average to be slightly higher. Whereby taking the nodes in the middle, which do not take into consideration the fringe differences, provides a closer result with the calculated equations.

7.1.2.2 Displacement of a Beam

The displacement of the beam is an important factor to identify the distance of the beam, from its original unaltered position to its bent position with a given force. The calculation for beam displacement is given using Equation 7.3, with the inclusion of Equation 7.2 (KUBBY, J.A. 2011).

Equation 7.2

$$\boldsymbol{I = \frac{(w * t^3)}{12}}$$

Equation 7.3

$$\boldsymbol{\delta = \left(\frac{L^3}{3 * E * I}\right) * F}$$

Where:

E = Young's Modulus (Pa)

L = Length of the beam (m)

w = Width of the beam (m)

t = Thickness of the beam (m)

I = Moment of Inertia of the beam (m^4)

The simulation and mathematical designs were modelled to be a simple beam design, with one side being fixed in all axis positions and the other left free, for a given force to be applied, this is also known as a fixed-free beam and is the common criteria for cantilever switch designs.

The simulation was run on Intellisuite TEM simulation tool using static analysis and ThermoElectroMechanical Relaxation analysis option selected. The force was applied on the edge of the free side of the beam, with a mesh size set at 1 µm. The force was then set at 1 µN and increased in increments from 1 µN up to 10 µN.

As for the mathematical analysis, the equation and its variables were inputted into PTC MathCAD, with a result provided immediately. The dimensions of the beam used for the simulations and for the calculations are shown in Figure 7.7. Copper material is used for both simulation analysis and mathematical calculation with a Young's Modulus of 117 GPa.

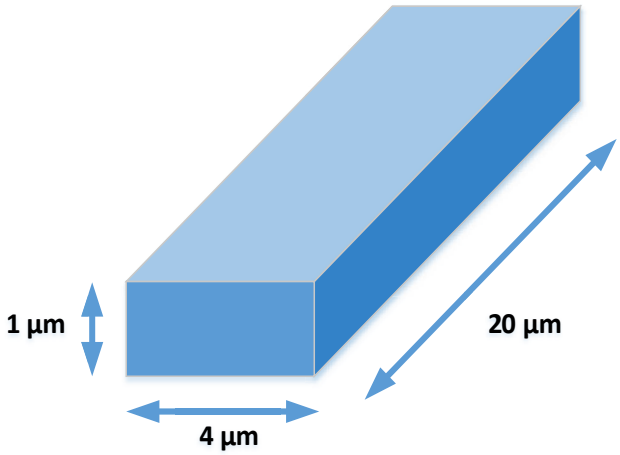

Figure 7.7: Dimensions of the Fixed-Free Beam used for the 'Displacement of a Beam' Simulation

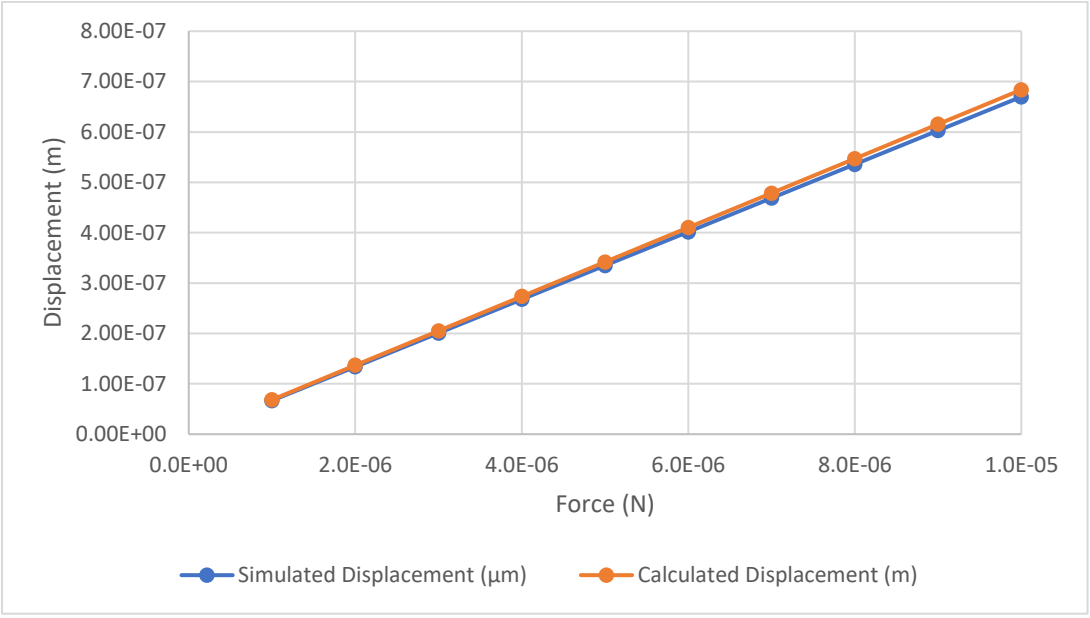

Figure 7.8: Results of the 'Displacement of a Beam' Simulation verses Mathematical

The experiment was to show the validation of the simulation against mathematical analysis. As shown in Figure 7.8, the results, of both the simulation and the mathematical equation, displays a close relationship to the forces of 4 μN and below. But as the forces increase, the results between both, begin to diverge. The reason for the increased divergence, as forces increase, is due to the simulation taking into consideration the second order of displacement. As the force increases the second order method for displacement begins to increase in effect. Due to the beam displacement equation being linear, the mathematics does not take into consideration the non-linear aspects of the bending of the beam and so the equation becomes less accurate as larger forces are applied. Whereas the simulation takes the non-linear nature into consideration. Although the mathematical equation may become increasingly inaccurate as forces increase, this is due to the equation being a first order beam displacement equation rather than taking into consideration second order effects. Therefore, some understanding of the flexibility of the material is required with forces being applied conservatively, to not exaggerate the bend of the beam too much. As most cantilever designs have an air gap, which varies up to 3 μm, allowing the equation to be accurate for designs with smaller air gaps. This in turn allows the equation to be the best form for calculating the beam deformation, and validating designs with small air gaps, or designs which have beams that have small displacement values.

7.1.2.3 Resonant Frequency

The resonant frequency, known as the natural frequency, is the vibrational waveform the structure of the device resonates to. When the amplitude of the set waveform in increased the device will respond more vigorously causing the structure of the design to deform and lead to breaking. Consequently, if the device structure is cycled in a repetitive motion, causing the device to move at the speed of the structure's resonance, this too would lead to the device failure and breakage to the structure. It is useful to understand the resonance of the structure in order to overcome such issues.

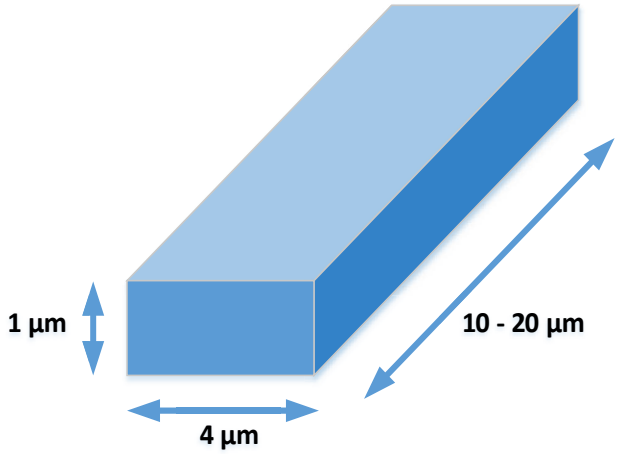

Figure 7.9: Fixed-Free Beam Dimensions with variable length from 10 µm to 20 µm

The model used for both the simulation and mathematical analysis consisted of a beam with 4 µm width and 1 µm thickness, the length of the beam was altered from 10 µm to 20 µm using increments of 1 µm. Intellisuite TEM simulation tool was used to analyse the beam using frequency type calculation. With the first mode providing the natural frequency of the beam. As for the mathematical analysis, the equation shown in Equation 6.3 was used and implemented on PTC MathCAD for fast response of the results. The results are tabulated in the previous chapter (Results and Validation) on Table 6.5.

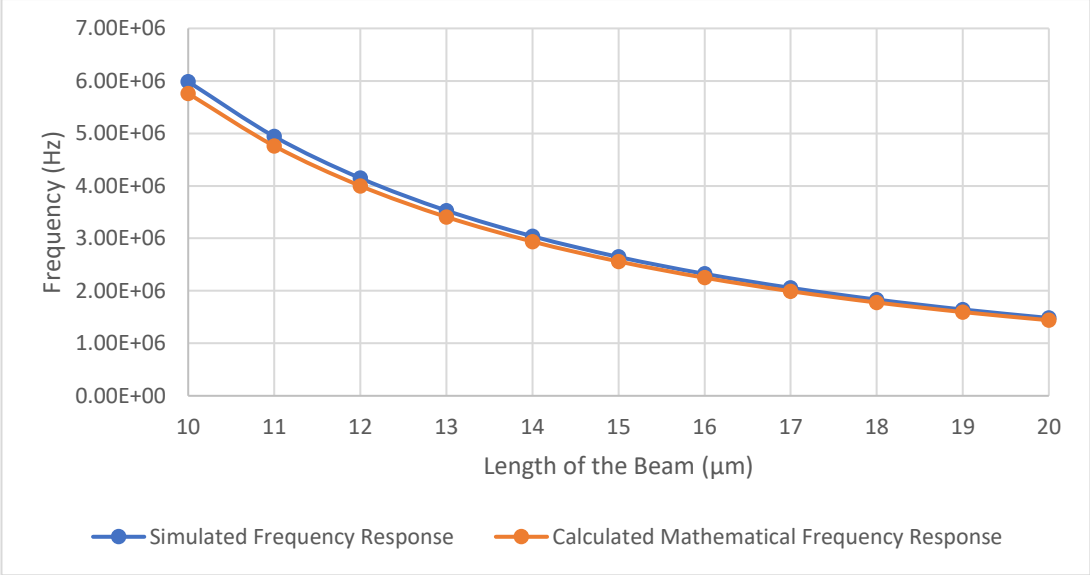

Figure 7.10: Simulated verses Mathematical Frequency response of a beam with varied length

The results have been graphically displayed in Figure 7.10, from the results of Table 6.5. It shows that the frequency response of both the simulation and the mathematics has a discrepancy when the length of the beam was short (at 10 µm) but begins to converge on similar results as the length of the beam is increased. This is because the mathematical equation is purely based on a 2D model and does not take the width of the beam into account. However, as the beam gets shorter the 3D effect becomes significant. This is the reason for the difference between the mathematical and simulated models.

7.1.3 Validation of Simulation against Experimental Results

After the validation of the Electrostatic Force, Displacement of the Beam and Resonant Frequency between simulation and mathematics was completed, the next stage was to prove the validity against an existing practical design. The Hughes Research Laboratories Cantilever Single-Pole Single-Throw switch created by Daniel Hyman (later shortened to the HRL Cantilever SPST Switch in this thesis), was the ideal platform to validate the simulation software, due to it being the first SPST cantilever created in which other researchers based their cantilever designs from and the design being simple to implement. The first stage before initial experimentations, was to model the HRL Cantilever SPST switch on Intellisuite 3DBuilder and then passing it on to Intellisuite TEM simulation tools where all boundaries, material and voltage characteristics were applied, ready for simulating.

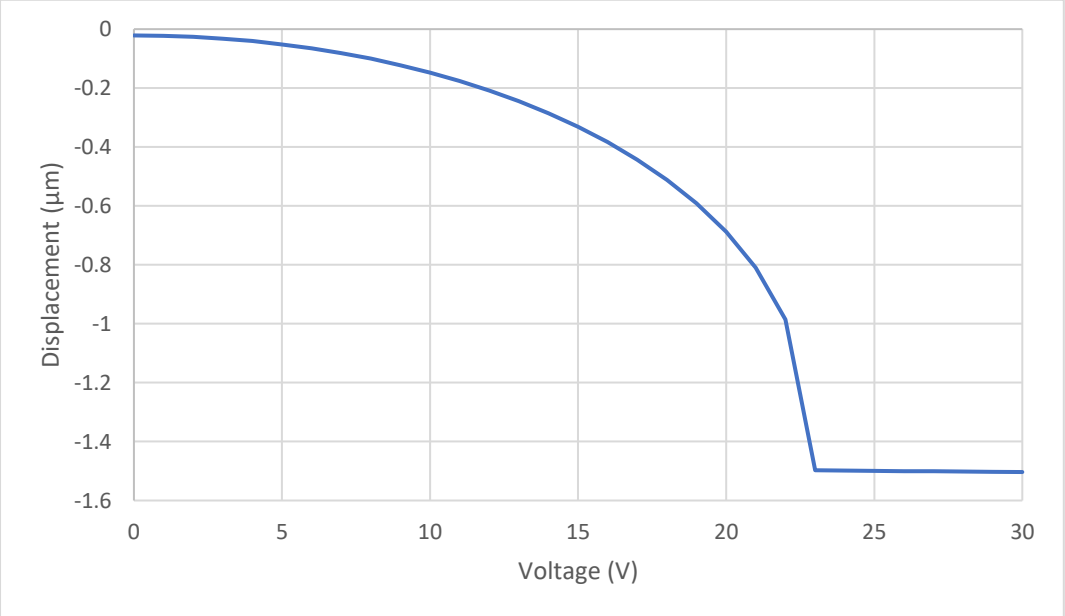

Figure 7.11: Displacement vs Voltage of HRL Cantilever Beam Switch

The first experiment for validation was to prove the HRL Cantilever SPST switch closes at the documented voltage level of 30V. Using Intellisuite TEM Simulation tool the analysis was run as a Static Simulation with ThermoElectroMechanical Relaxation analysis option selected. With the graph shown in Figure 7.11, the simulation proved

that the switch was able to close at 30V. The second test of validation was to achieve a similar resonant frequency of the switch as that proposed in the paper.

Table 7.4: Comparison of Resonant Frequency of the HRL Cantilever SPST Switch-Experimental Verses Simulated

	Resonant Frequency (kHz)
Experimental Resonant Frequency	30
Simulated Resonant Frequency	28.1197

Experimental document reports the typical resonant frequency of the HRL Cantilever SPST Switch to be 30 kHz. Between the simulation and the practical design, the difference was only 1.8803 kHz. This proves to be a marginal difference of the natural frequency of the HRL Cantilever SPST switch. The experimental report of the resonant frequency is shown to be an approximation, whereby the simulation provided an exact value.

7.2 Design Result Analysis

Using the experimental methodology explained in Chapter 4.3.3 (Simulation methods), the results used two types of simulation packages. The first package dealt with the electro-mechanical aspects of the RF MEMS switch design using Intellisense's Intellisuite design and simulation tool package. The second dealt with the Electromagnetic aspects of the switch using CST (Computer Simulation Technologies, as of 2017 is now part of Dassault Systemes) design and simulation tool package. This section and its sub chapters discusses the different iterations of the design and explains the advantages and disadvantages while explaining the improvements made over the previous iteration.

7.2.1 Stress and Electrostatic Characteristics

7.2.1.1 Actuation Voltage, Displacement and Von Mises Stress

The first set of results are tested on models using those created from Intellisuite's 3DBuilder and then simulated on Intellisuite's TEM simulation software. The results of actuation voltage, displacement and von mises stress are all accessed from the single simulation and the actuation voltage applied provides the results for displacement and the stress at the beam. This information can be obtained in the Results tab in Intellisuite's TEM simulation tool, once the simulation has been completed.

The results are tabulated in Table 6.8. and displayed graphically in Figure 7.12, Figure 7.13 and Figure 7.14.

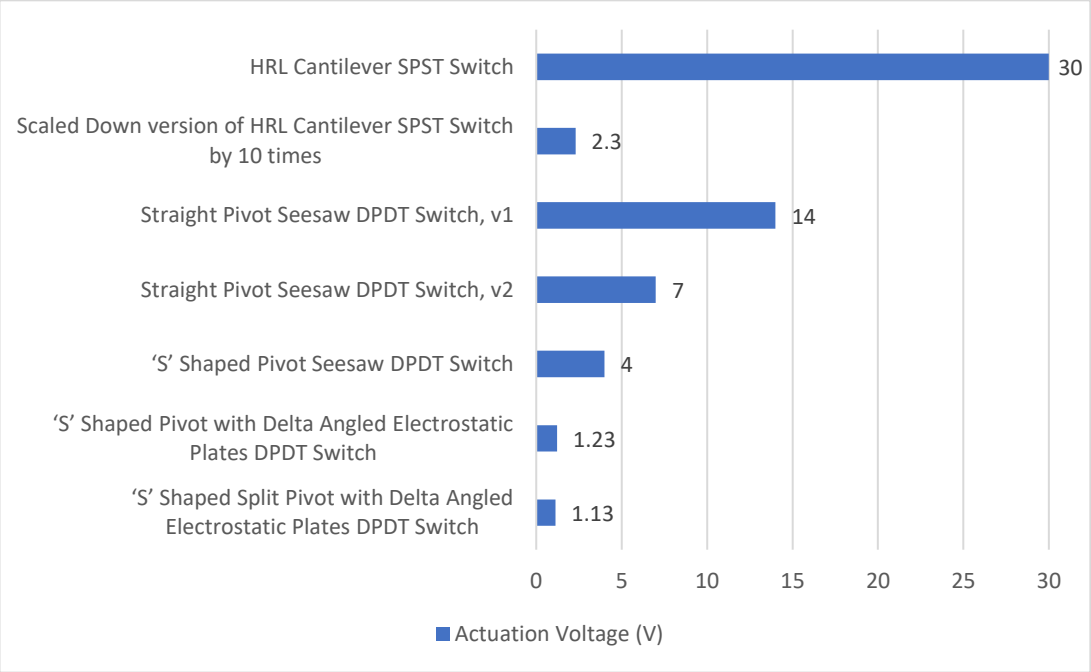

Figure 7.12: Bar Graph Results of the Actuation Voltage of the switches

The results show that the initial design of the HRL Cantilever SPST switch, on which the other designs are based on, establishes the voltage levels from which to improve on. After scaling down the HRL Cantilever SPST Switch by 10 times of its original design, it had shown that the switch can accommodate far lower voltage levels and provided a sub 3-volt actuation voltage. Also, due to the design being the same as the HRL Cantilever SPST switch, with the only difference being its size, the switch takes advantage of the same design process. On the condition that manufacturing techniques

can implement layer thicknesses of a minimum of 0.8 nm with feature sizes of 2.4 µm and dimple sizes of 0.6 µm, then the design can be implemented. This fabrication process detail is not available at the moment and is therefore not possible in existing manufacturing.

Although, providing such great voltage performance, the disadvantage of the switch was its functionality only providing the SPST switching. Therefore, designs were adapted to accommodate further switching, and keeping the design within the microscale. With the use of the DPDT type switches, connectivity functionality of the switch has been achieved.

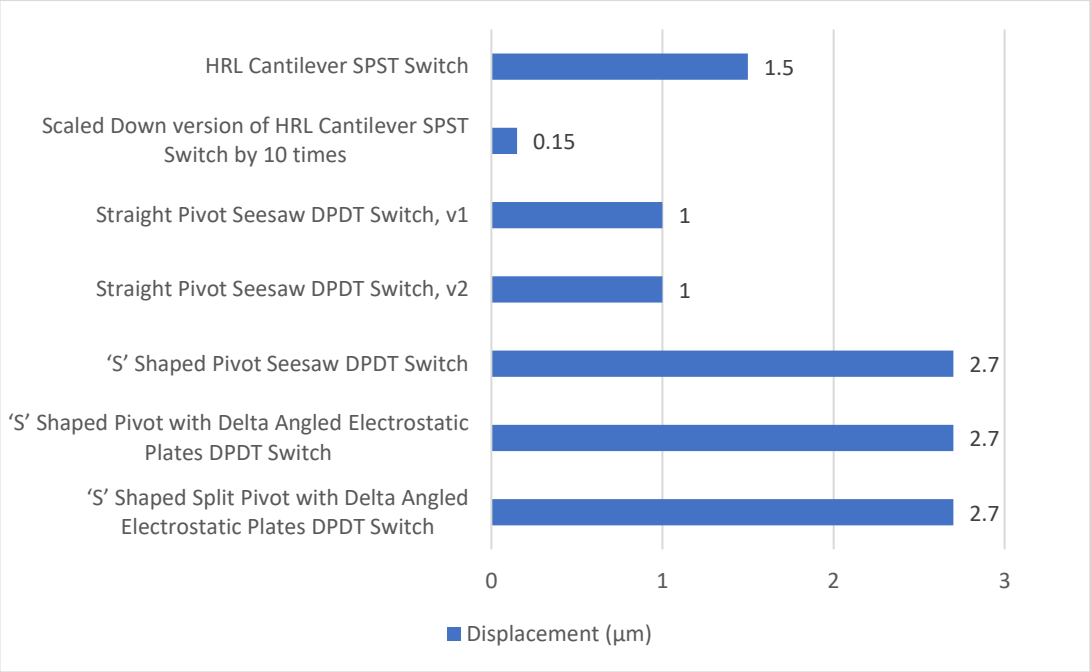

Figure 7.13: Bar Graph Results of the Displacement of the switches for total Air Gap

Although the scaled down version of the HRL cantilever switch provided lower voltage levels than all the designs, it proved a fatal flaw, due to its size. This limits the design's air gap, which potentially reduces the physical disconnection of its off-state, causing isolation of the off-state to be reduced.

With the implementation of the straight pivot type DPDT switch, the air gap was increased over the scaled down version of the HRL cantilever, from 0.15 µm to 1 µm. However, the overall air gap is still half the distance of the base design (HRL

Cantilever SPST Switch). With this realisation, the progression to the 'S' shaped pivot seesaw switches provided improved flexibility, without compromising the air gap. This in turn enabled the air gap to be increased even further than the base design. The flexibility of the pivot provided a further advantage of lowering the actuation voltage.

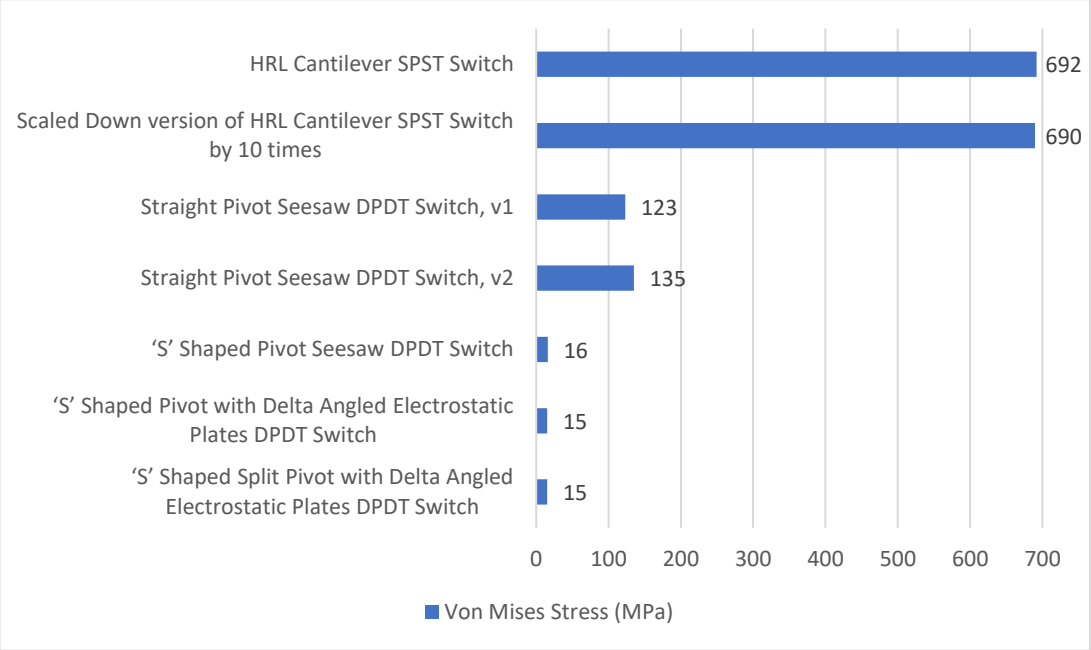

Figure 7.14: Bar graph of von mises Stress of the switches (rounded to the closest 1 MPa)

With both types of HRL cantilevers, resulting in similar stress levels, it was apparent that the levels of stress were quite high. Both designs implemented the use of gold (Au), which is known to be both malleable and ductile, in which silicon nitride PECVD is used to sandwich the gold to stiffen the cantilever and retain elastic recovery. With the pivot type switches, the requirement of a thinner pivot is necessary, which in turn requires a single material that can retain its elastic recovery, by not exceeding its yield strength and deforming. Copper (Cu) was chosen to replace gold for all seesaw designs due to its excellent electrical conductivity and better yield strength over gold. This however requires designs which are hermetically sealed, as oxidisation of copper will occur. Although the straight pivot seesaws were able to keep von mises stresses low, the stress levels went over the yield strength of copper, but provided focus on where improvements were needed, such as the pivot itself.

With the ‘S’ Shaped pivot seesaws, the improvements were concentrated on the reduction of stress at the pivot and increasing the air gap while requiring low pulling forces to provide low actuation voltages. This was realised with the implementation of a ‘S’ shaped spring pivot. With the use of the ‘S’ shaped pivot, the stress was distributed along each linked segment, which reduced the stress through the pivot, compared to the straight pivots, where stress was concentrated to the upper half. This is shown in Figure 7.17 and Figure 7.18.

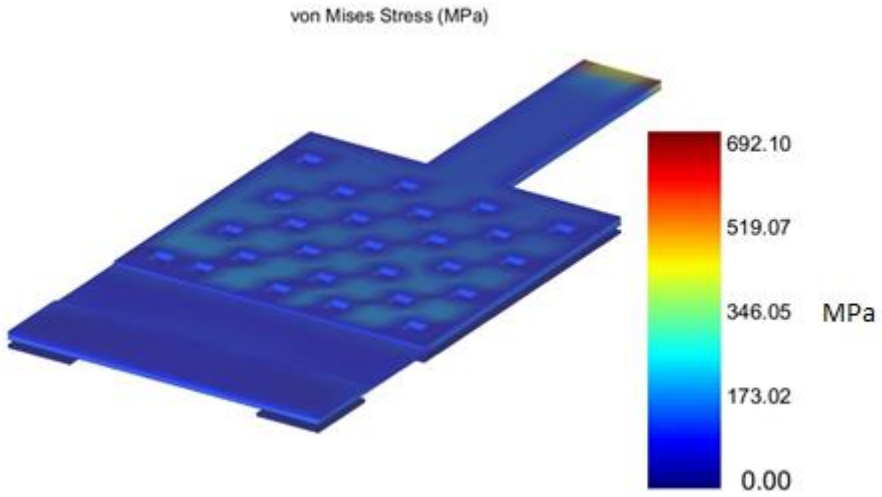

Figure 7.15: von Mises Stress for HRL Cantilever SPST Switch

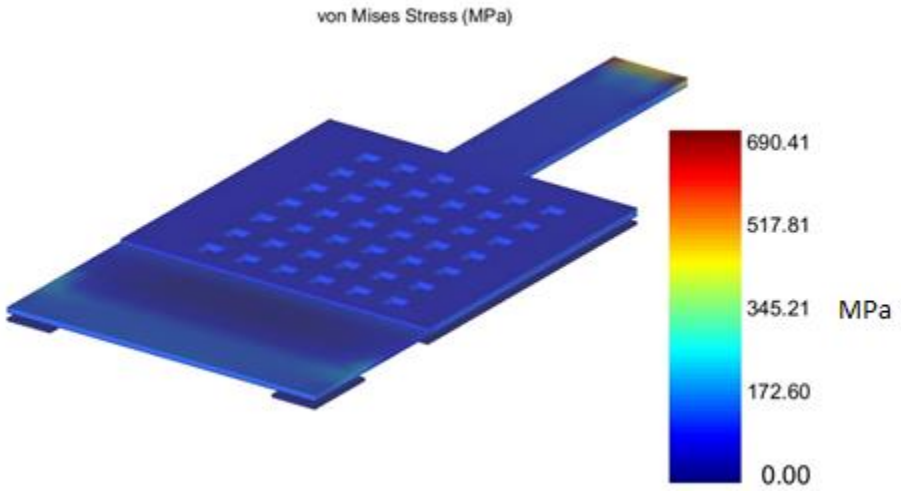

Figure 7.16: von Mises Stress for Scaled Down Version of the HRL Cantilever SPST Switch

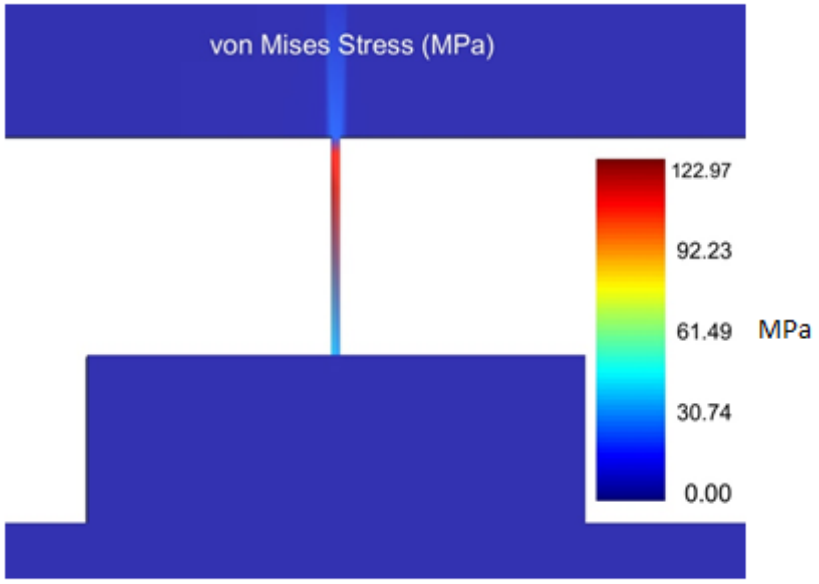

Figure 7.17: von Mises Stress for Straight Pivot Seesaw Switch DPDT Switch v1

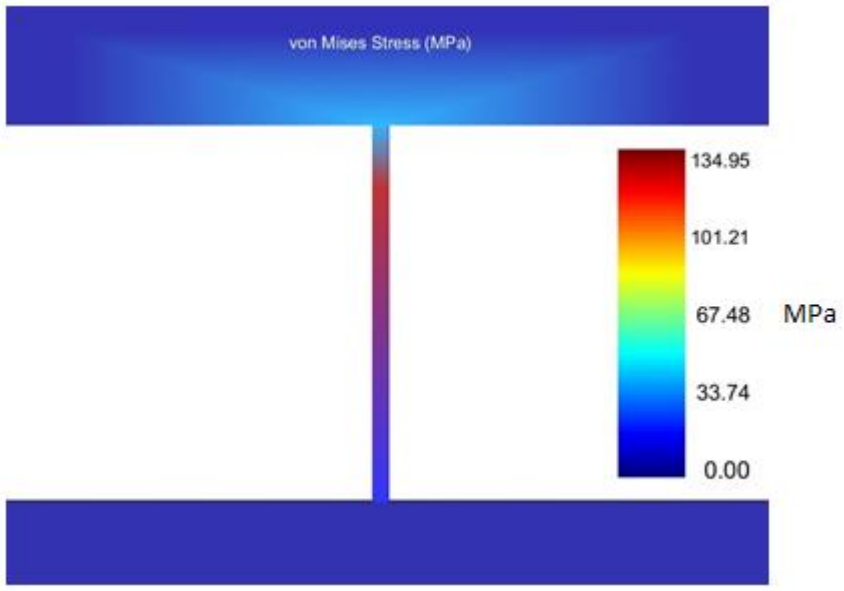

Figure 7.18: von Mises Stress for Straight Pivot Seesaw DPDT Switch v2

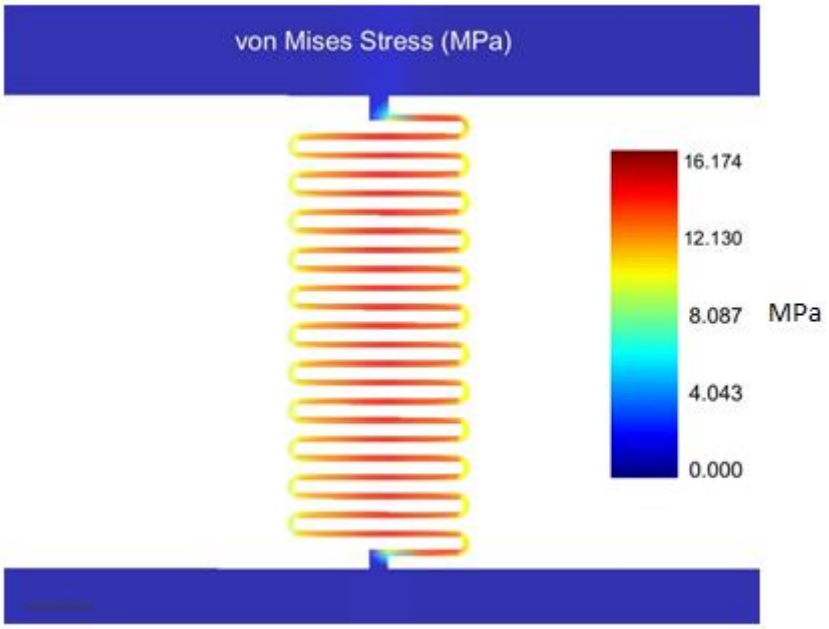

Figure 7.19: von Mises Stress for 'S' Shaped Pivot Seesaw DPDT Switch

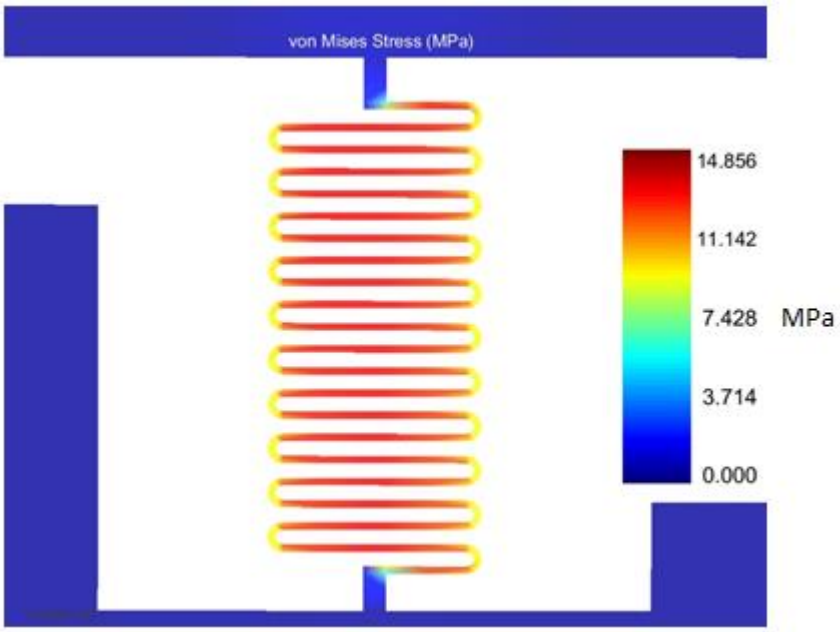

Figure 7.20: von Mises Stress for 'S' Shaped Pivot Seesaw DPDT Switch with Delta Plates

With each iteration of the design, from the base design (the HRL Cantilever SPST switch) to the final design (the ‘S’ Shaped Pivot Seesaw DPDT type Switches), significant improvements have been made in all three areas (i.e. Voltage, Air Gap and

von mises stress). The final design iteration provides a very low von mises stress over the original HRL cantilever switch, with a reduction in von mises stress of 46 times. Also, the 'S' Shaped Pivot Seesaw DPDT Switch actuation voltage levels are closer to the standard voltage levels used in mobile technologies today (from 1V to 5V). With alterations to the electrostatic plates, including the delta plates implemented on the final design iteration, the voltage levels can be reduced or increased, allowing flexibility of the design to be implemented for custom voltage requirements, without compromising the switches' RF isolation, due to the space of the air gap being unchanged.

7.2.1.2 Displacement vs Voltage

The displacement verses voltage simulation analysis is used to understand the characteristics of the switch when a given actuation voltages are applied. This is used to find out the actuation voltage that the switch closes for contact. Figure 7.21, Figure 7.22, Figure 7.23, Figure 7.24, Figure 7.25 and Figure 7.26 provide graphical representations of the switch, from its off-state to when the contacts close.

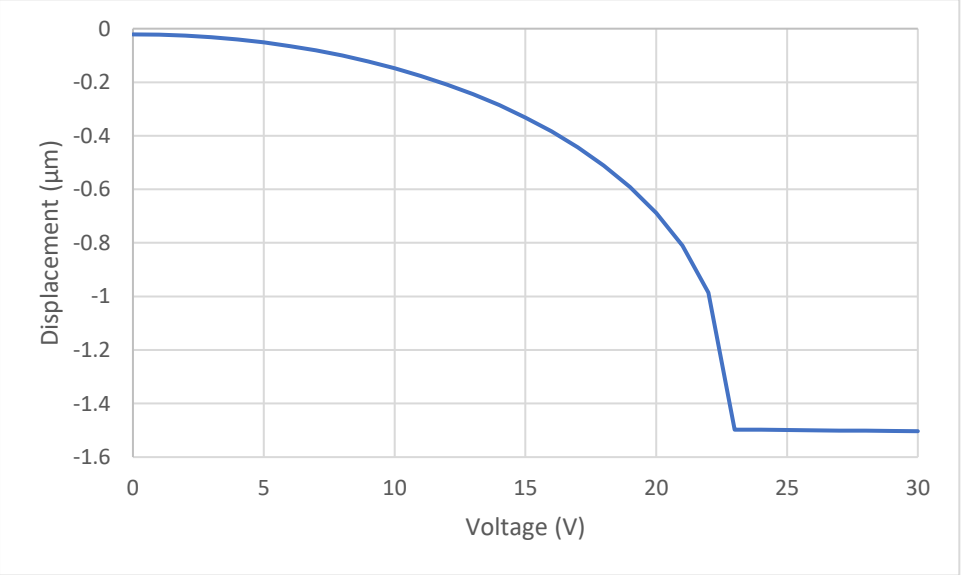

Figure 7.21: Graph form representation of the Voltage vs Displacement of HRL Cantilever SPST Switch

It can be seen from Figure 7.21, the HRL cantilever switch is capable of contacting at 23 volts. However, for validation, the design is pushed further to 30 volts. This verifies the documented actuation voltages carried out by Daniel Hyman et al (Hyman et al. 1999) in their experiments. As can be seen, the HRL Cantilever switch displaces just shy of 1.5 µm at 23 volts but as the voltage is increased the contacts settle at 1.5 µm.

This is due to the beam compensating with the excessive force induced as the voltages are increased. As the electrostatic plates force increases, the middle section of the cantilever begins to straighten, causing the contacts to close. The same can be said for the scaled down version (Figure 7.22), which also has the same characteristics. Therefore, it can be said that the characteristics of the switch does not change as it gets smaller.

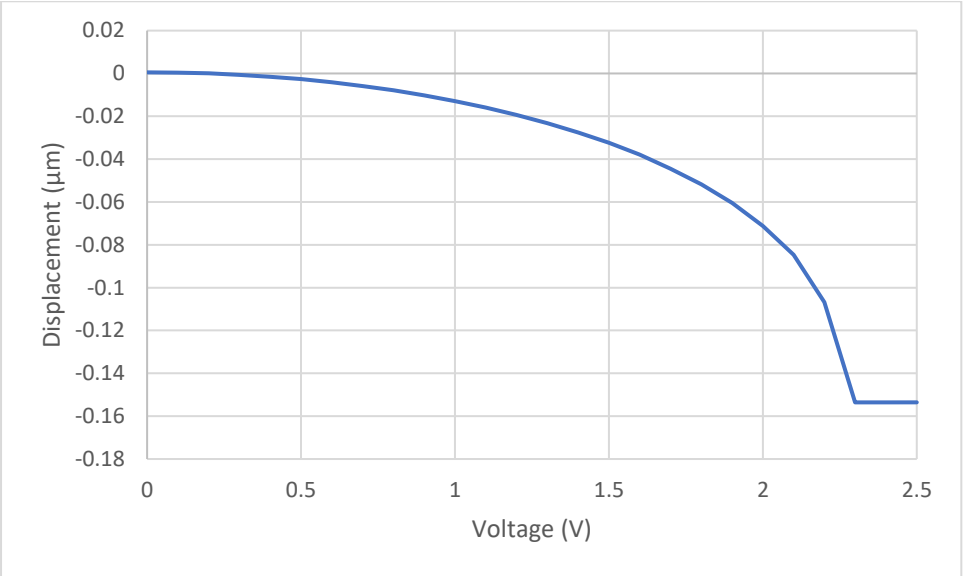

Figure 7.22: Graph form representation of the Voltage vs Displacement of Scaled Down version of HRL Cantilever SPST Switch by 10 times

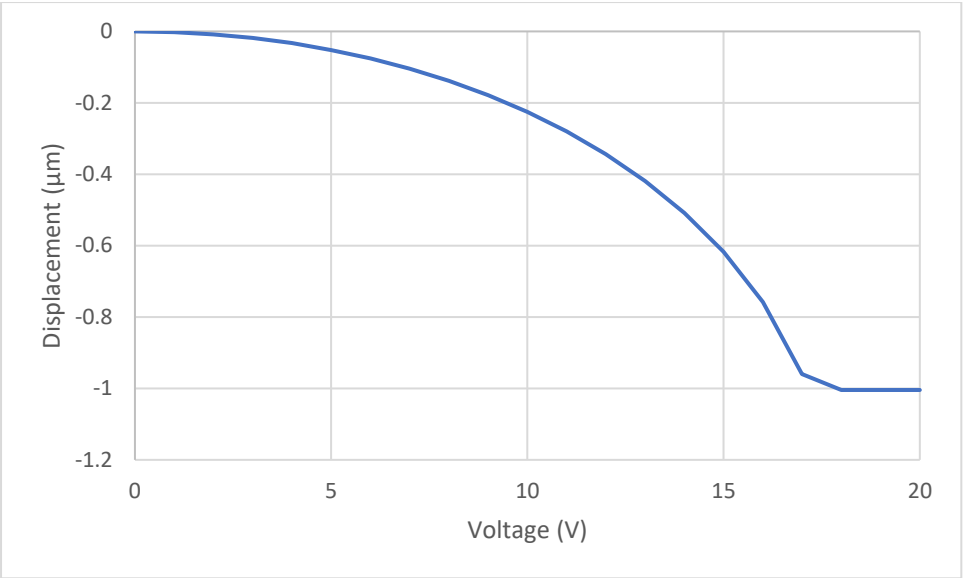

Figure 7.23: Graph form representation of the Voltage vs Displacement of Straight Pivot Seesaw DPDT Switch v1

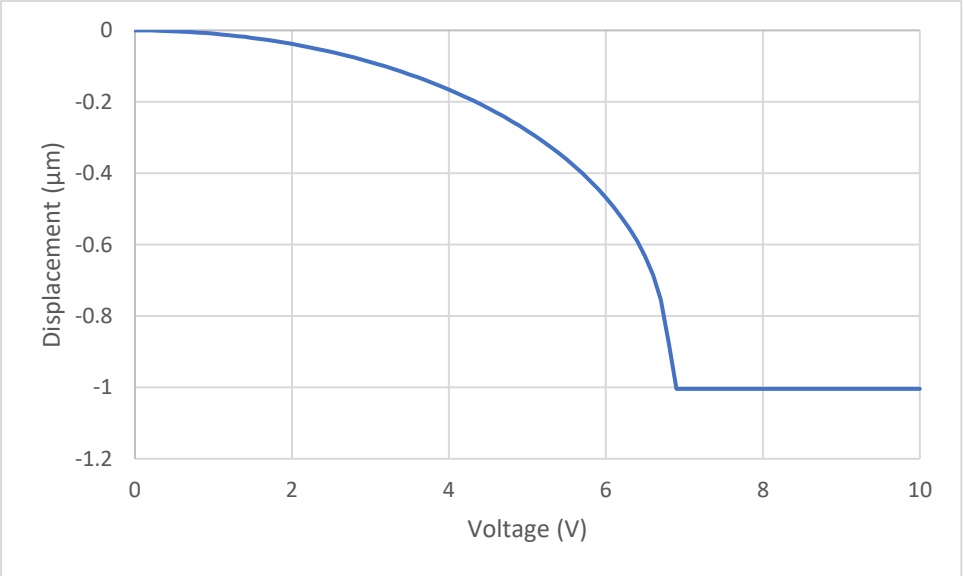

Figure 7.24: Graph form representation of the Voltage vs Displacement of Straight Pivot Seesaw DPDT Switch v2

Between the two-straight pivot seesaw switches, v1 (Figure 7.23) shows to have a slower pace of displacement than v2 (Figure 7.24). This is due to the sizes of the parallel electrostatic plates, which is proportional to the area. This also shows that with larger areas, the reaction with increased actuation voltage causes the beam to displace rapidly. Although the dimensions of the pivots for both v1 and v2 were the same (with

thickness of 42.62 nm), the spring constants are similar. Thus, proving the larger the area, the greater the force, the parallel electrostatic plates will pull.

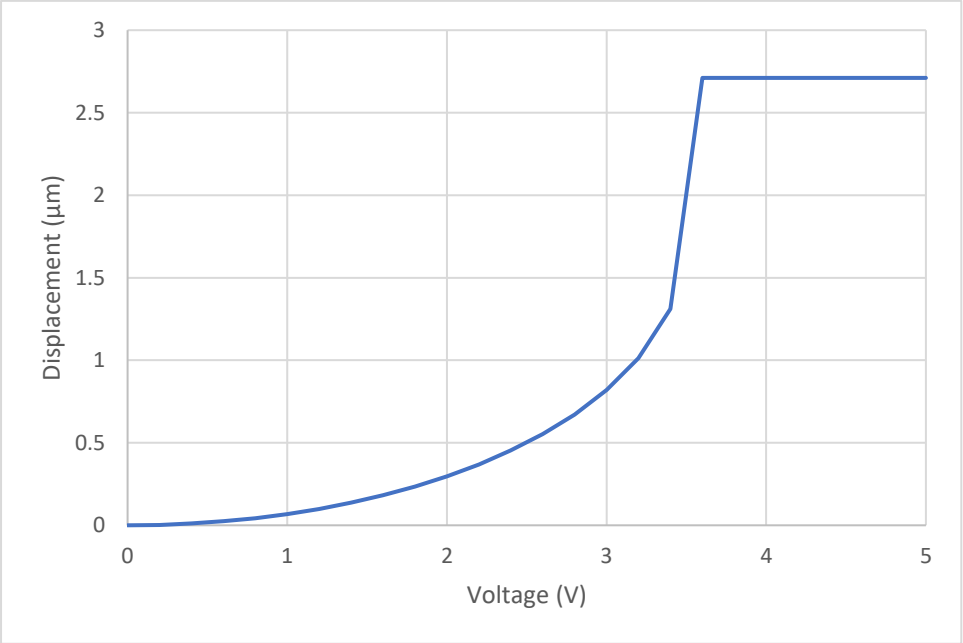

Figure 7.25: Graph form representation of the Voltage vs Displacement of 'S' Shaped Pivot Seesaw DPDT Switch

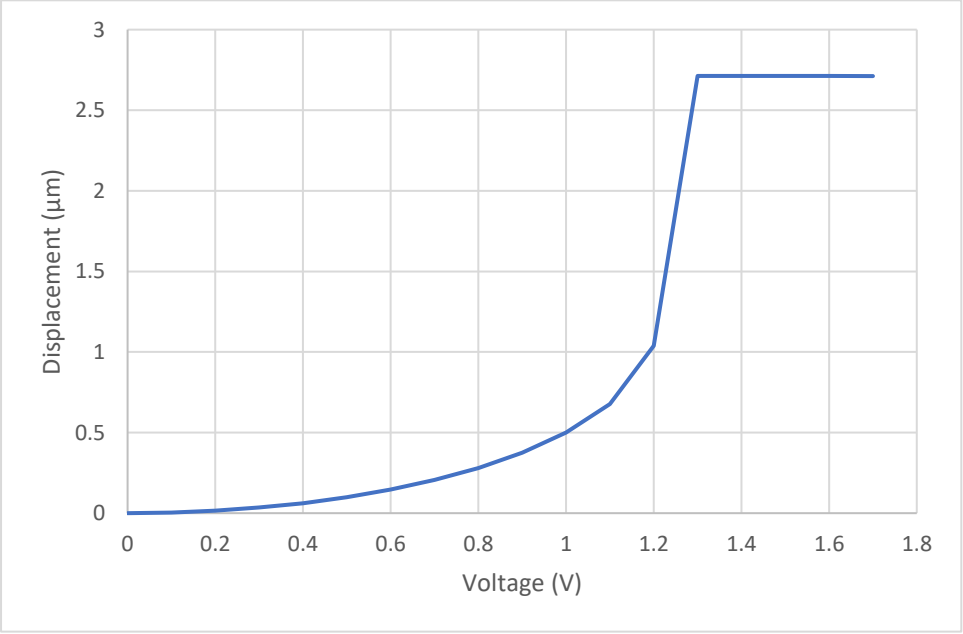

Figure 7.26: Graph form representation of the Voltage vs Displacement of 'S' Shaped Pivot with Delta Angled Electrostatic Plates DPDT Switch

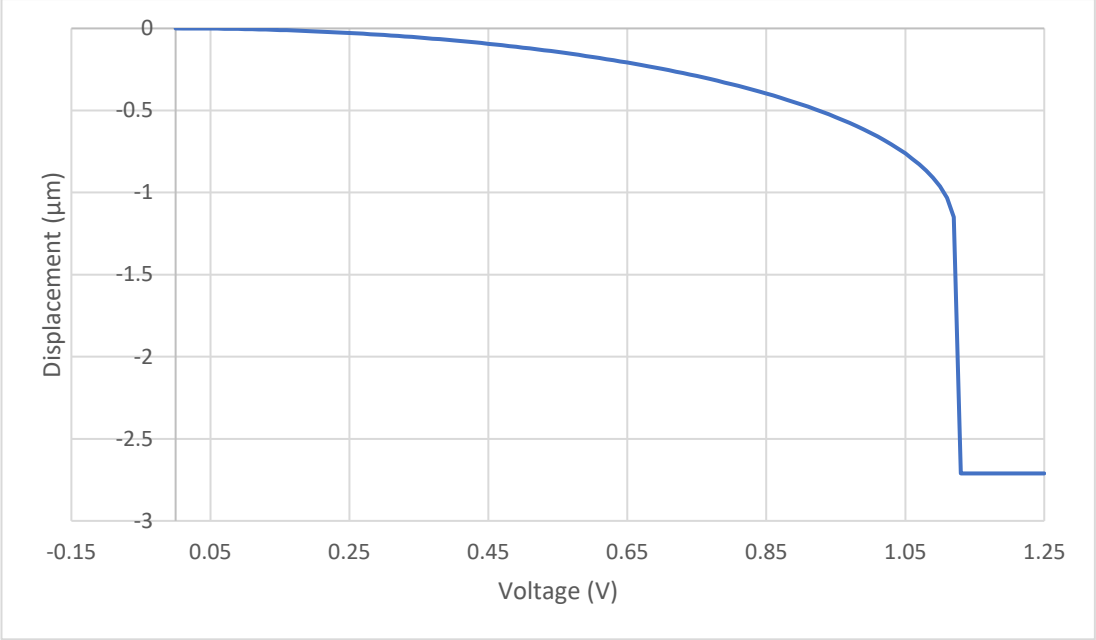

Figure 7.27: Graph form representation of the Voltage vs Displacement of 'S' Shaped Split Pivot with Delta Angled Electrostatic Plates DPDT Switch

With each iteration of the design, the voltage requirements have been decreased. The graphs Figure 7.21, Figure 7.22, Figure 7.23 and Figure 7.24 show that the characteristics for the HRL type cantilever switches and the straight pivot type seesaw switches have similar progressive curves, until the contacts close. However, for the 'S' Shaped type pivot seesaw switches (Figure 7.25, Figure 7.26 and Figure 7.27) it is a different matter, when the beams of these switches displace after 1 µm, there is a rapid approach to contact closure. This is due to the flexibility of the 'S' shaped pivot, which requires less force for the beam to displace. Also, as distance of the plates begin to get closer, the force increases, which aids in pulling the beam to the on-state.

7.2.1.3 Contact Analysis

The contact analysis of the switches was not able to be shown in the 'Results and Validation' chapter due to the data being very large. Instead, the data is provided in an excel file, with the graphical form represented in Figure 7.28, Figure 7.29, Figure 7.30, Figure 7.31, Figure 7.32, Figure 7.35 and Figure 7.36. The contact analysis shown in those Figures, include both contact and release analysis in higher detail than that shown in elastic recovery. Compared to Intellisuite's TEM simulation tool, Intellisuite SYNPLE simulation is a modal type simulation, which provides higher resolution of results with in a relatively short time. Although SYNPLE is fast in analysis, macro models need to be extracted from the TEM simulation for each switch design.

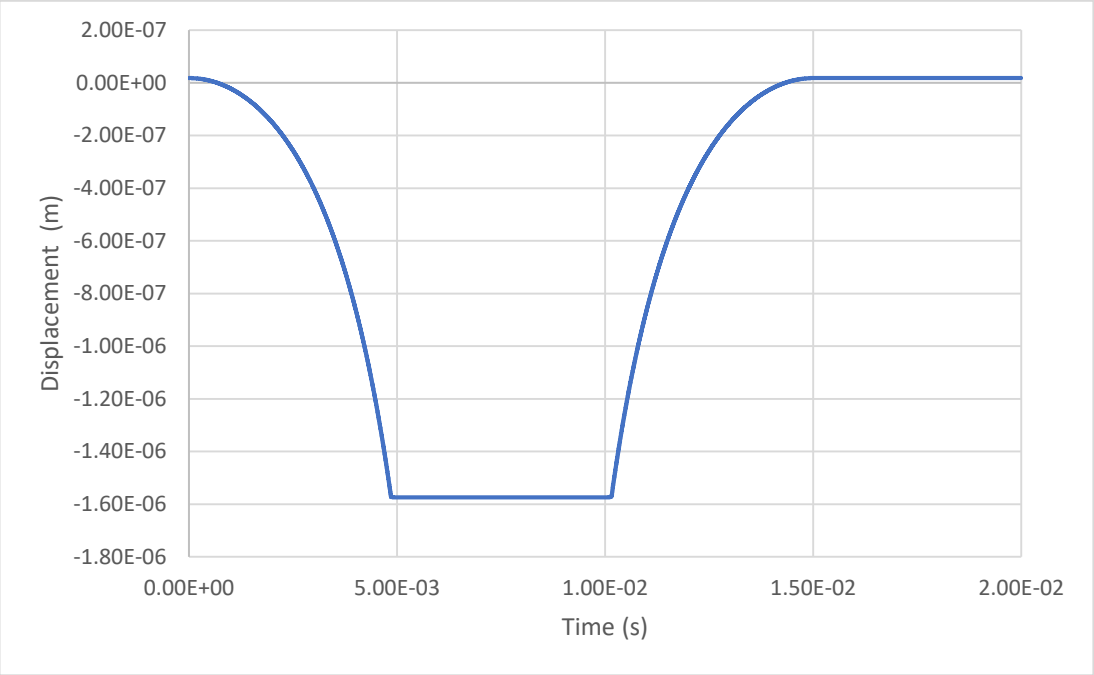

Figure 7.28: Contact Analysis for the HRL Cantilever SPST Switch

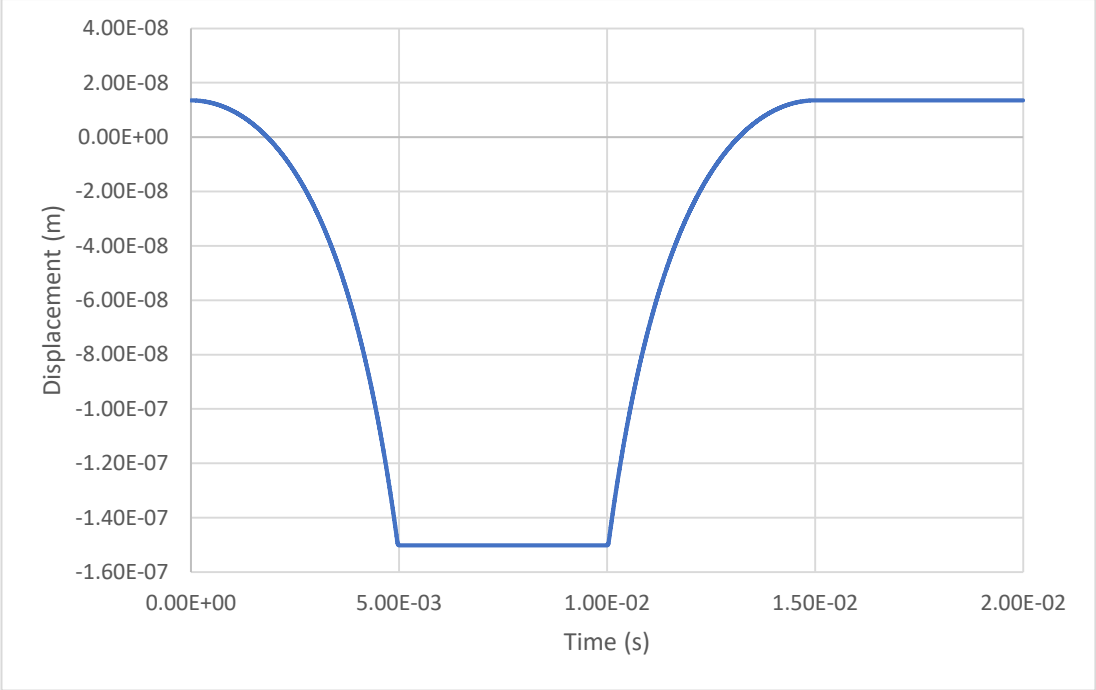

Figure 7.29: Contact Analysis for the Scaled Down version of HRL Cantilever SPST Switch by 10 times

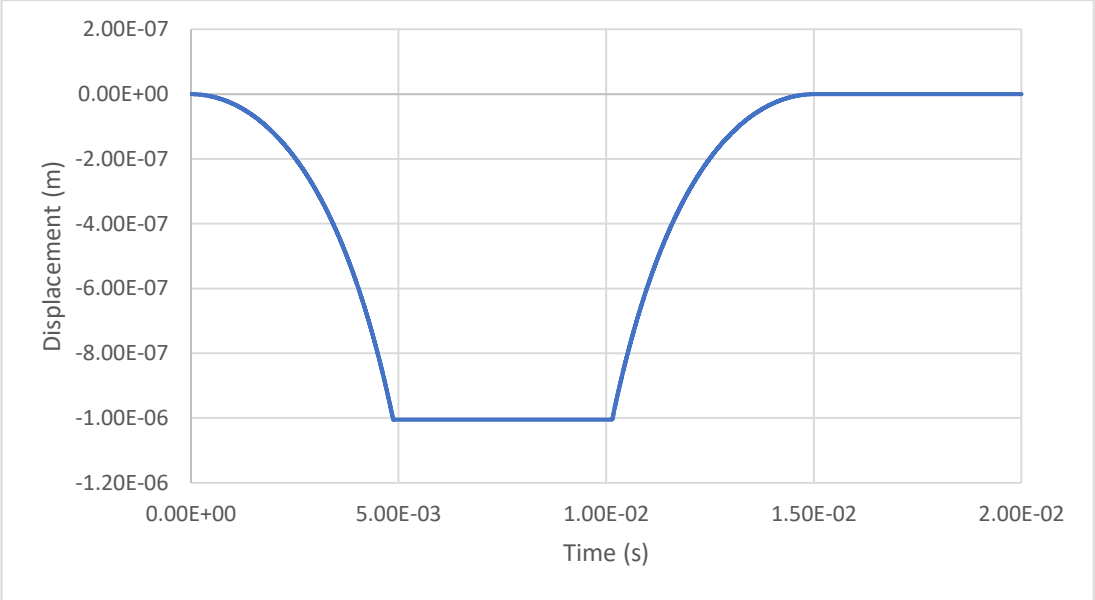

Figure 7.30: Contact Analysis for the Straight Pivot Seesaw DPDT Switch, v1

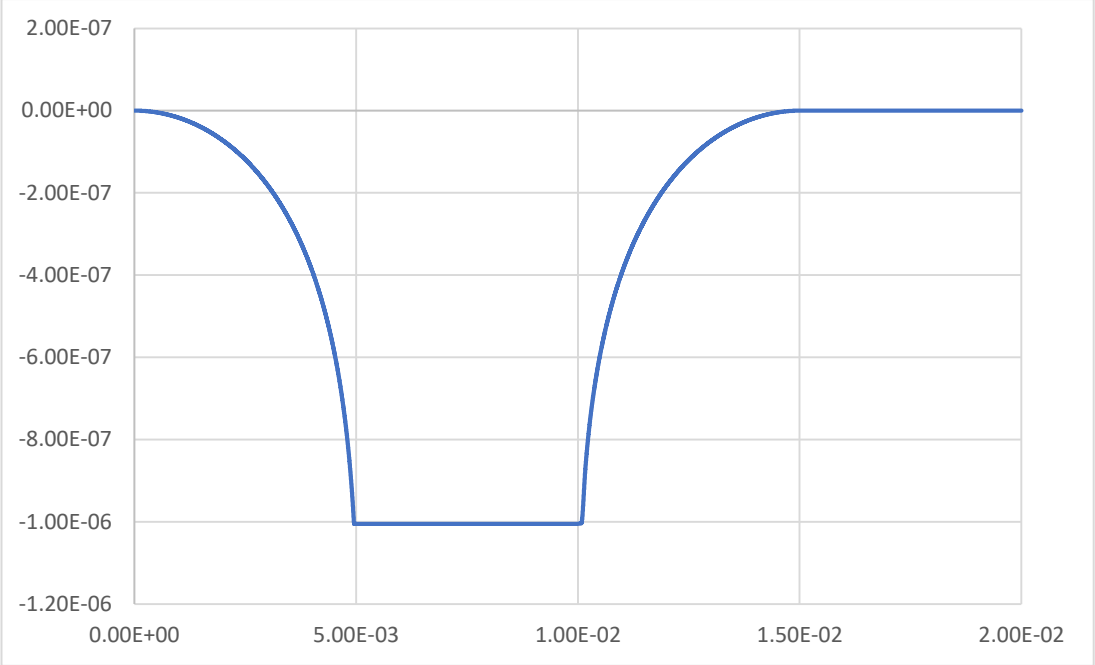

Figure 7.31: Contact Analysis for the Straight Pivot Seesaw DPDT Switch, v2

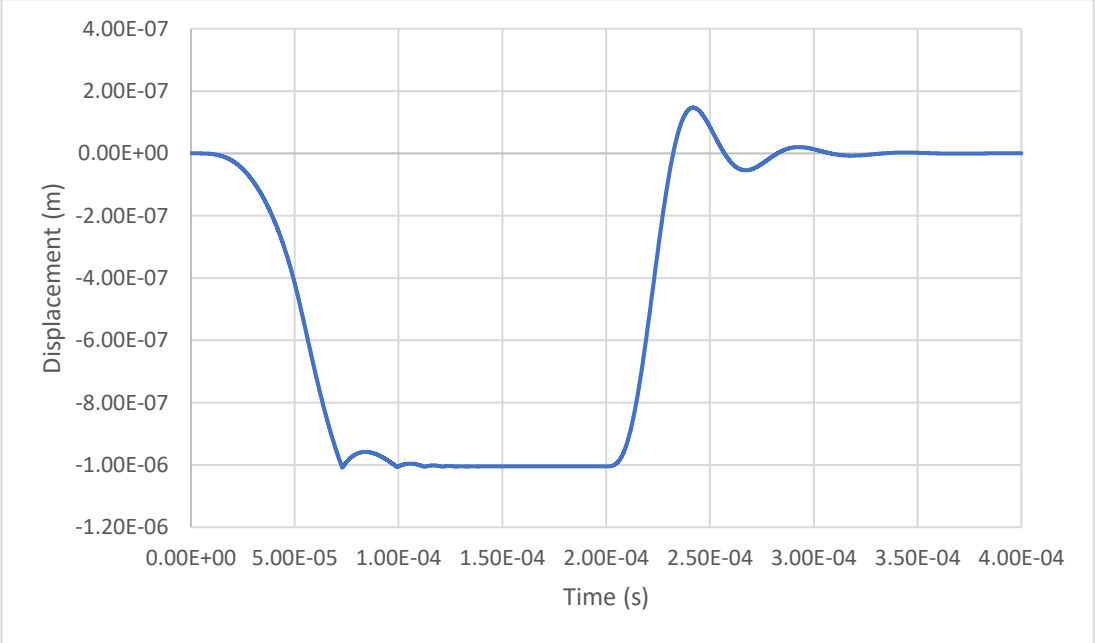

Figure 7.32: Contact Analysis for the Straight Pivot Seesaw DPDT Switch, v2, with shorter reaction time

With reference to Figure 7.32, it can be seen that there is an overshoot and an undershoot when the contacts are released, which gradually fades away. The period between the peaks is 5.1 $x10^{-5}$ seconds which relates to a frequency of 19.61 kHz, which is in close proximity to the resonant frequency of the switch that was simulated at 20.5682 kHz.

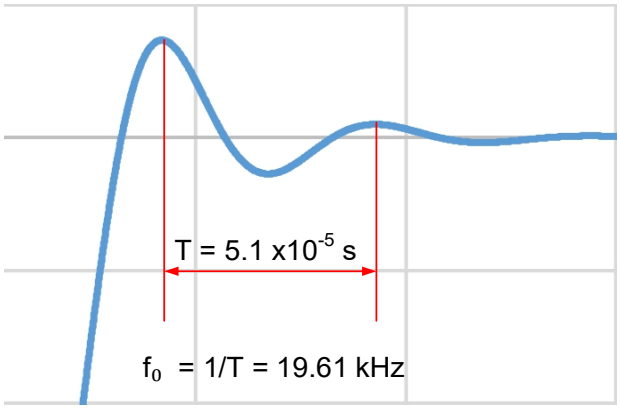

Figure 7.33: Zoomed in overshoot and undershoot from Figure 7.32

When the switch is closed this undershoot and overshoot is limited by the contacts and produces contact bounce as shown in Figure 7.32 and closely in Figure 7.34. The time taken for contact bounce to settle is 66.9 µs.

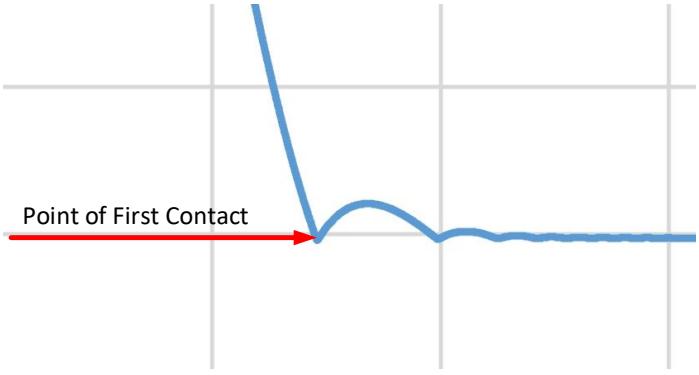

Figure 7.34: Zoomed in contact bounce from Figure 7.32

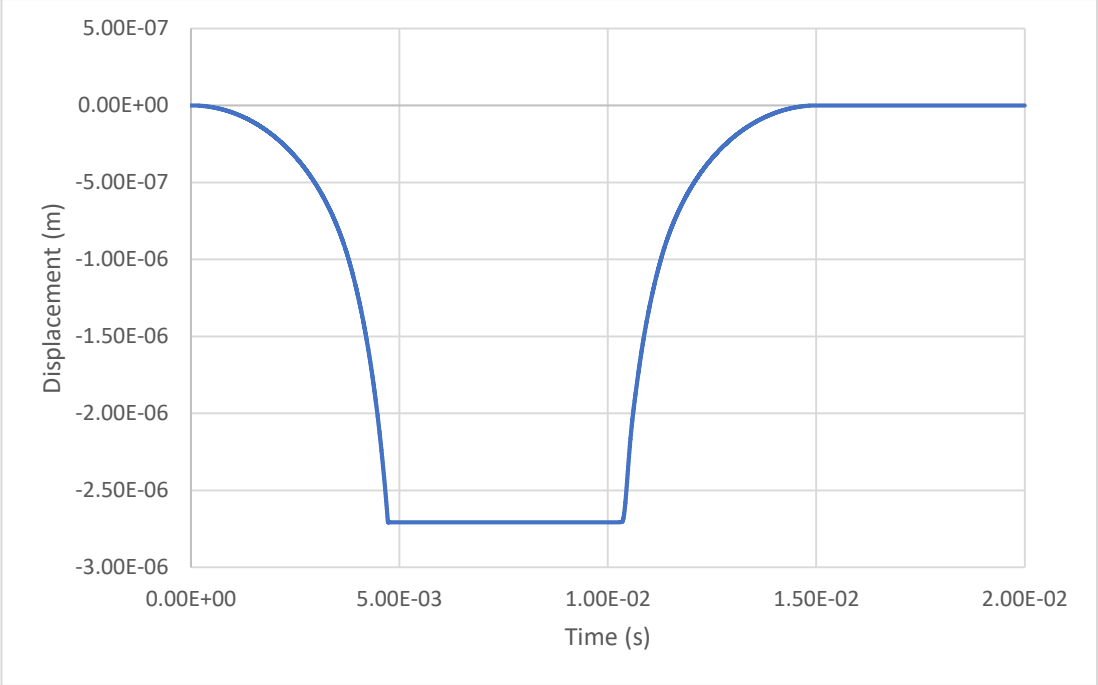

Figure 7.35: Contact Analysis for the ‘S’ Shaped Pivot Seesaw DPDT Switch

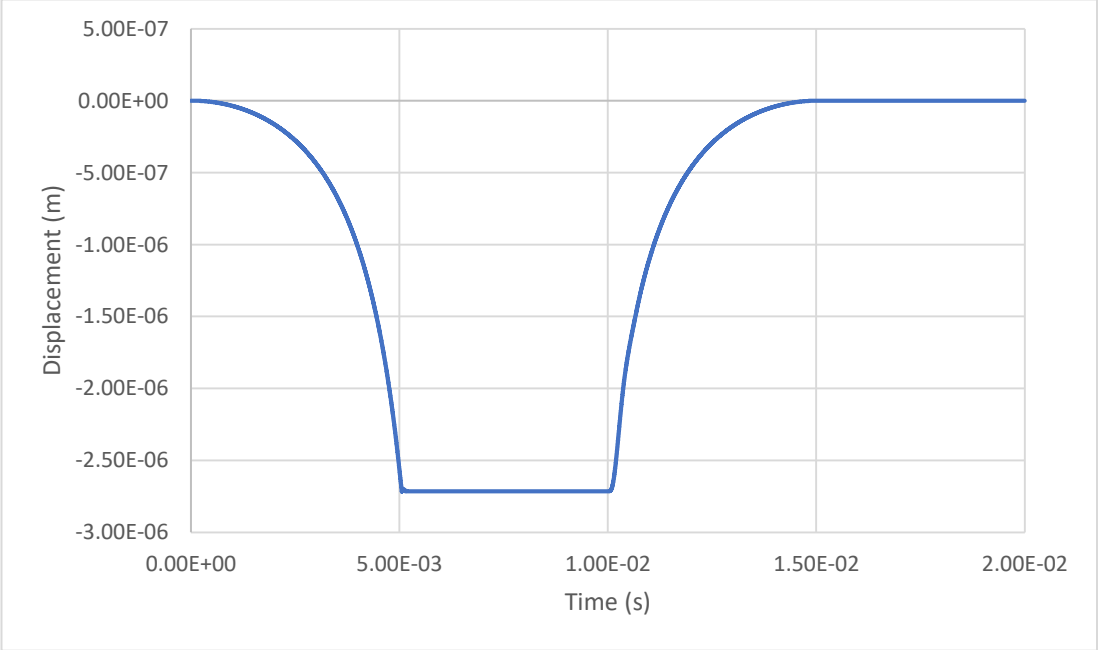

Figure 7.36: Contact Analysis for the ‘S’ Shaped Pivot with Delta Angled Electrostatic Plates DPDT Switch

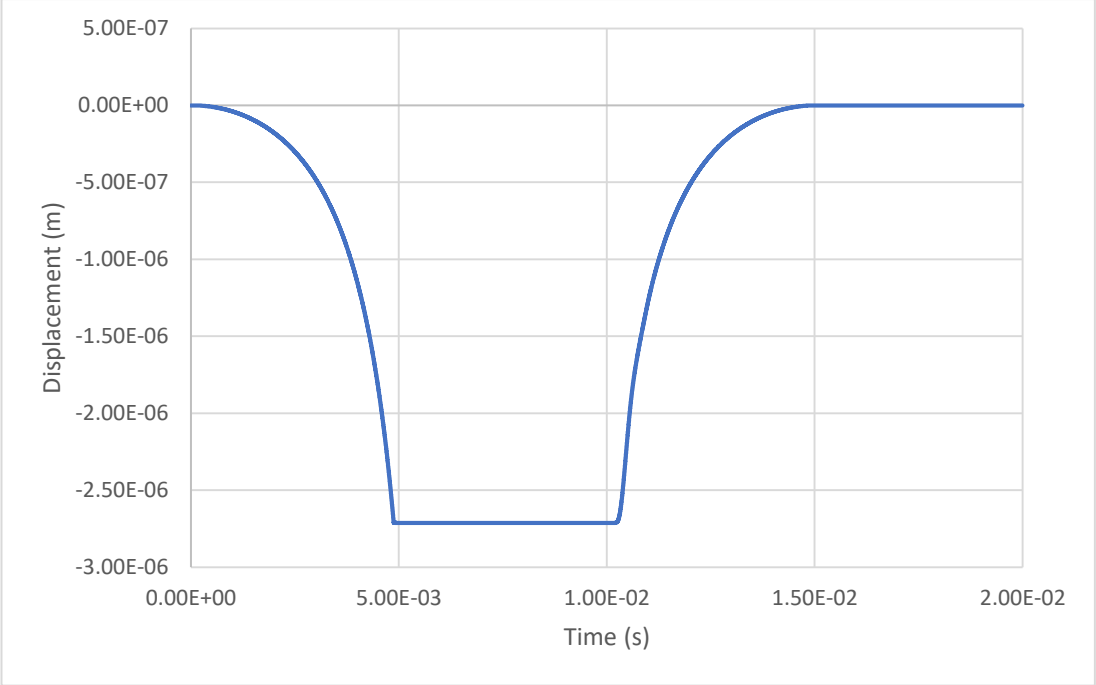

Figure 7.37: Contact Analysis for the 'S' Shaped Split Pivot with Delta Angled Electrostatic Plates DPDT Switch

With the contact analysis, it has shown that the design, which is scaled down, exhibits contact bounce with ringing when the design is switched off. Although small, it is noticeable, even though the voltage applied was the minimum required for the switch to close, the contact bounce was still noticeable. This is due to the force at which the contacts are closed. With the straight pivot v2, there was an increase in mass applied to the beam, with this the pivot had extra mass in which the substrate would cause the contact bouncing and ringing effect as it switches off. As the design progressed towards the final iteration, contact bounce was eliminated. This was achieved by reducing the mass of the beam by decreasing the amount of substrate used.

To settling time of the contact bounce for the scaled down version of HRL Cantilever is 9 µs, whereby the settling time for the contact bounce for the straight pivot seesaw v2 is 66.9 µs. The difference between the settling times is due to the size of the switch, whereby the smaller the switch the faster it reacts.

Table 7.5, shows the speed at which the switches reach their on-states from their off-states and vice versa.

Table 7.5: Switches activation and deactivation speed

Switch Design	Switch ON (s)	Switch OFF (s)
HRL Cantilever SPST Switch	4.85×10^{-3}	4.8×10^{-3}
Scaled Down version of HRL Cantilever SPST Switch by 10 times	4.97×10^{-3}	4.9×10^{-3}
Straight Pivot Seesaw DPDT Switch, v1	4.86×10^{-3}	5.4×10^{-3}
Straight Pivot Seesaw DPDT Switch, v2	0.109×10^{-3}	0.146×10^{-3}
'S' Shaped Pivot Seesaw DPDT Switch	$4.72\ 10^{-3}$	4.6×10^{-3}
'S' Shaped Pivot with Delta Angled Electrostatic Plates DPDT Switch	5.05×10^{-3}	4.9×10^{-3}
'S' Shaped Split Pivot with Delta Angled Electrostatic Plates DPDT Switch	4.87×10^{-3}	4.7×10^{-3}

7.2.1.4 Elastic Recovery

The elastic recovery was used to identify the speed at which the switch releases the contacts and reach its off-state. Whereby contact analysis with SYNPLE identified the on-state and off-state, elastic recovery identifies the off-state using FEA. In order to identify the characteristics of the switches' release to off-state, the switch would need to start the simulation with an active voltage, at which the beam is forced to contact. The simulation is then set to a dynamic analysis with 'Stress/Disp/Electrostatic (Direct Integration)' analysis type set. This provides simulations with results, which are set as movement and time. Figure 7.38 shows the set timing for the experiment with active voltage being changed to the appropriate voltage requirement for each switch.

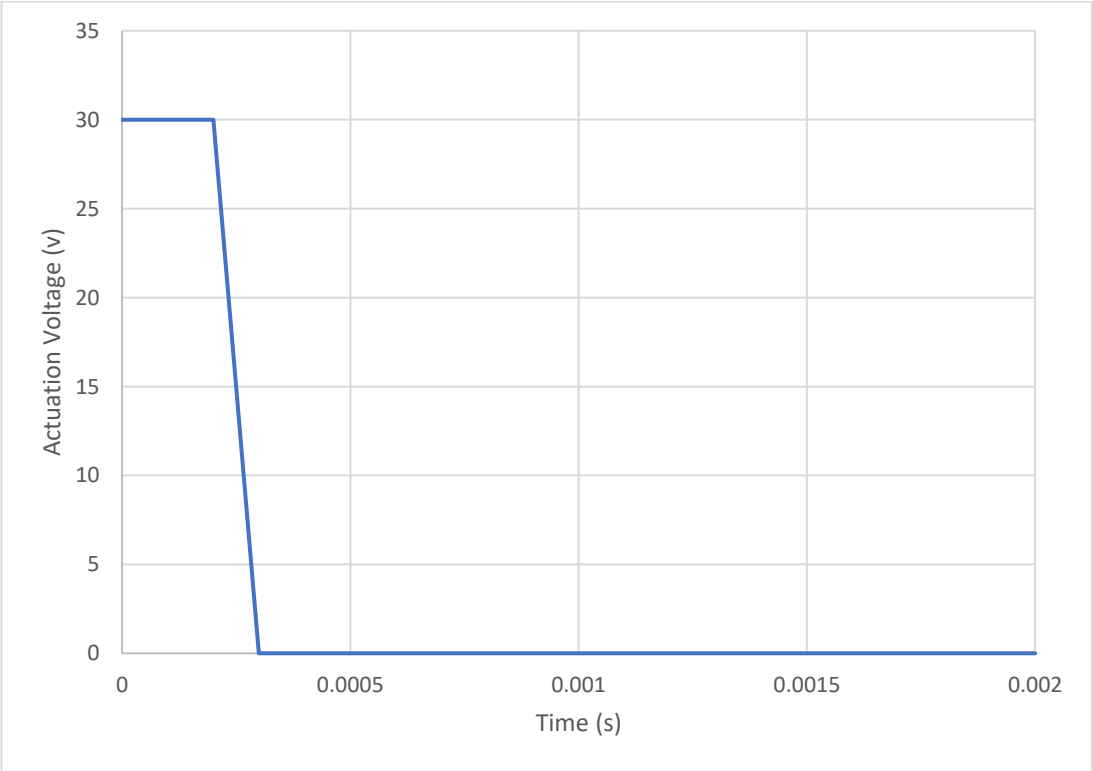

Figure 7.38: Example of Set Timing for the Elastic Recovery Experiment

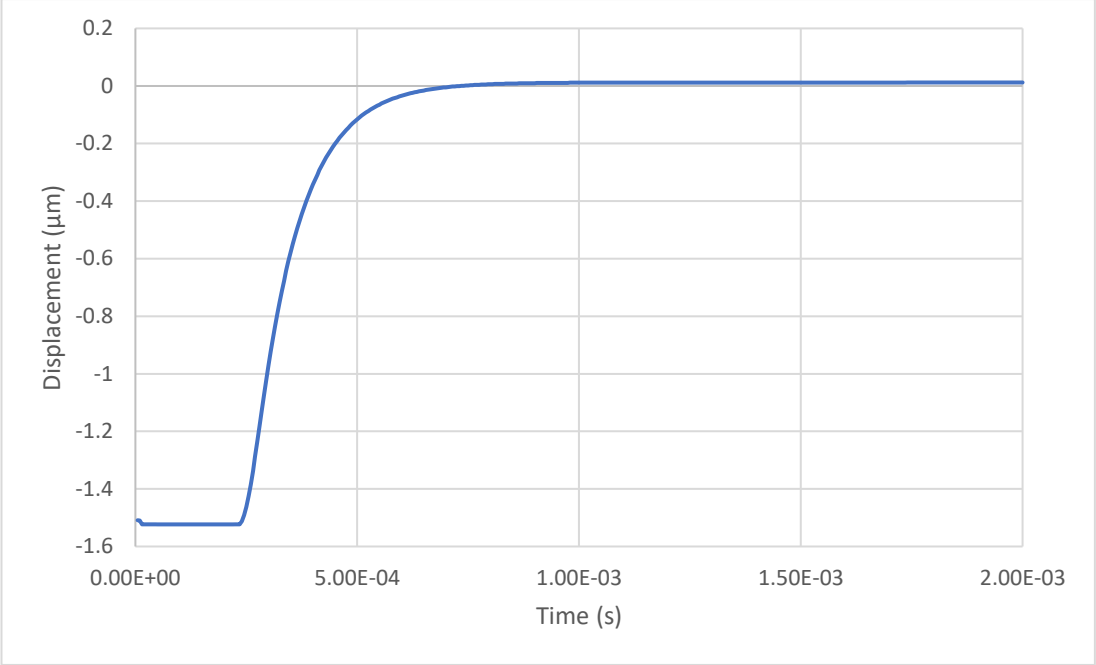

Figure 7.39: Elastic Recovery analysis result for the HRL Cantilever SPST Switch

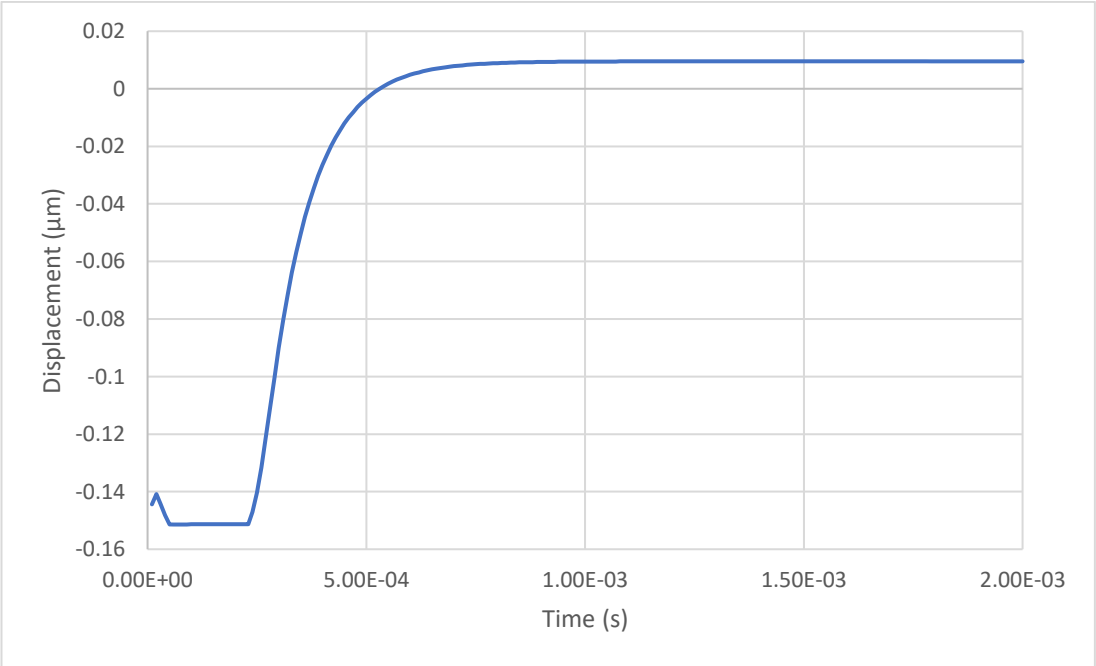

Figure 7.40: Elastic Recovery analysis result for the Scaled Down version of the HRL Cantilever SPST Switch by 10 times

For Figure 7.40, the off-state goes over 0, this is due to the selected node of the switch, which is taken at the edge of the cantilever beam and the design is not set on the true centre axis of the simulation. Therefore, this offsets the results.

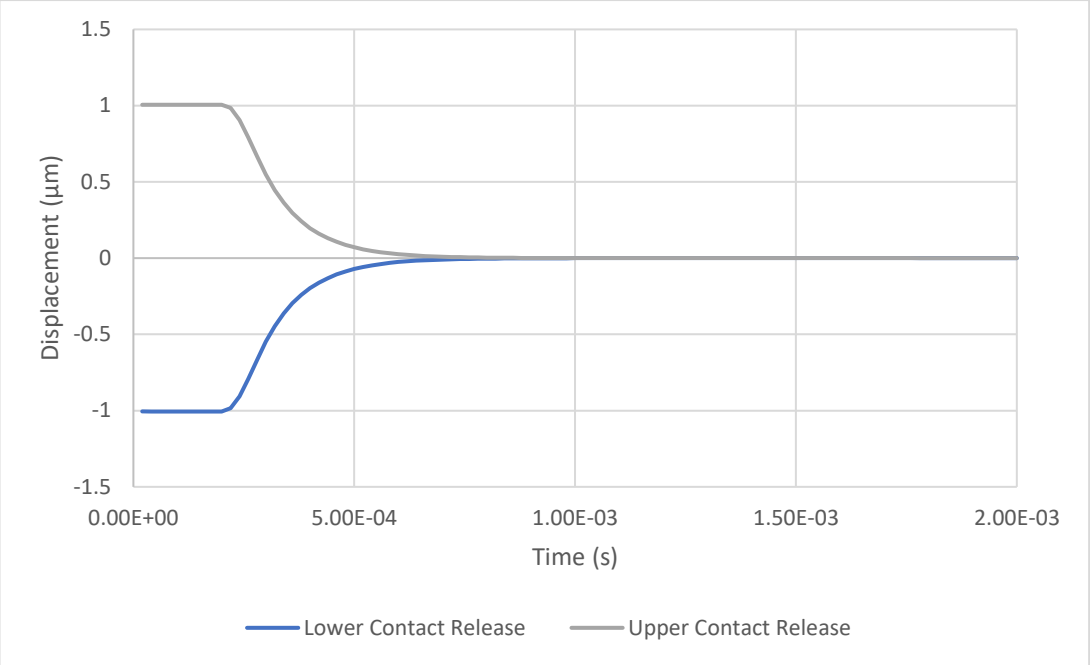

Figure 7.41: Elastic Recovery analysis result for the Straight Pivot Seesaw DPDT Switch, v1, with upper and lower contact release

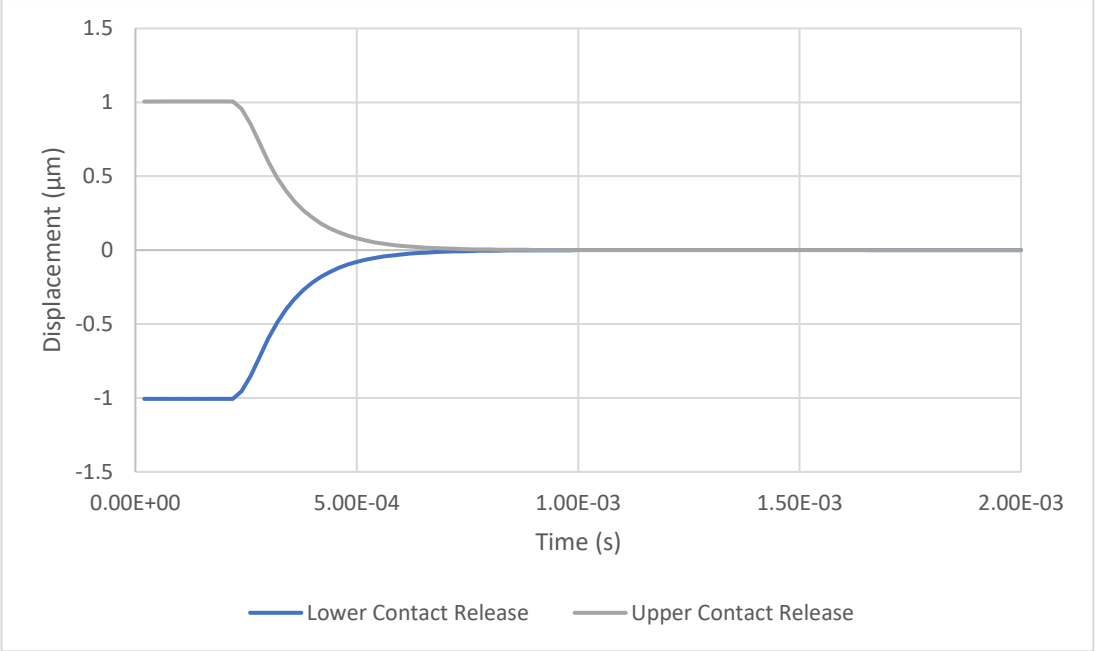

Figure 7.42: Elastic Recovery analysis result for the Straight Pivot Seesaw DPDT Switch, v2, with upper and lower contact release

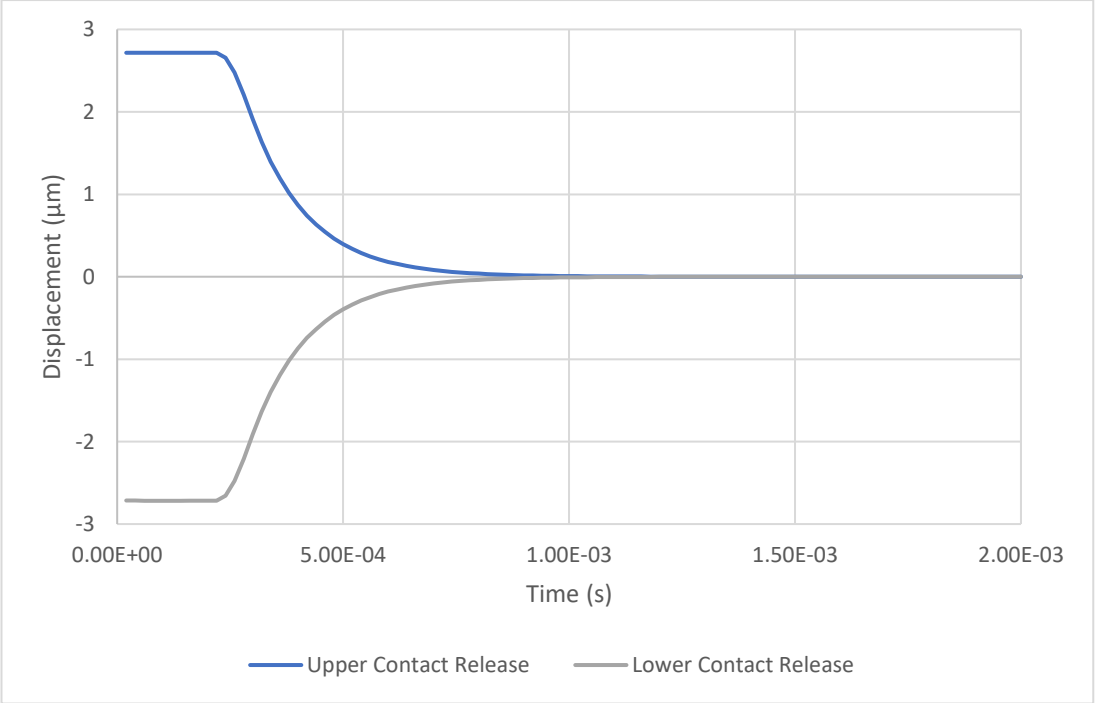

Figure 7.43: Elastic Recovery analysis result for the ‘S’ Shaped Pivot Seesaw DPDT Switch with upper and lower contact release

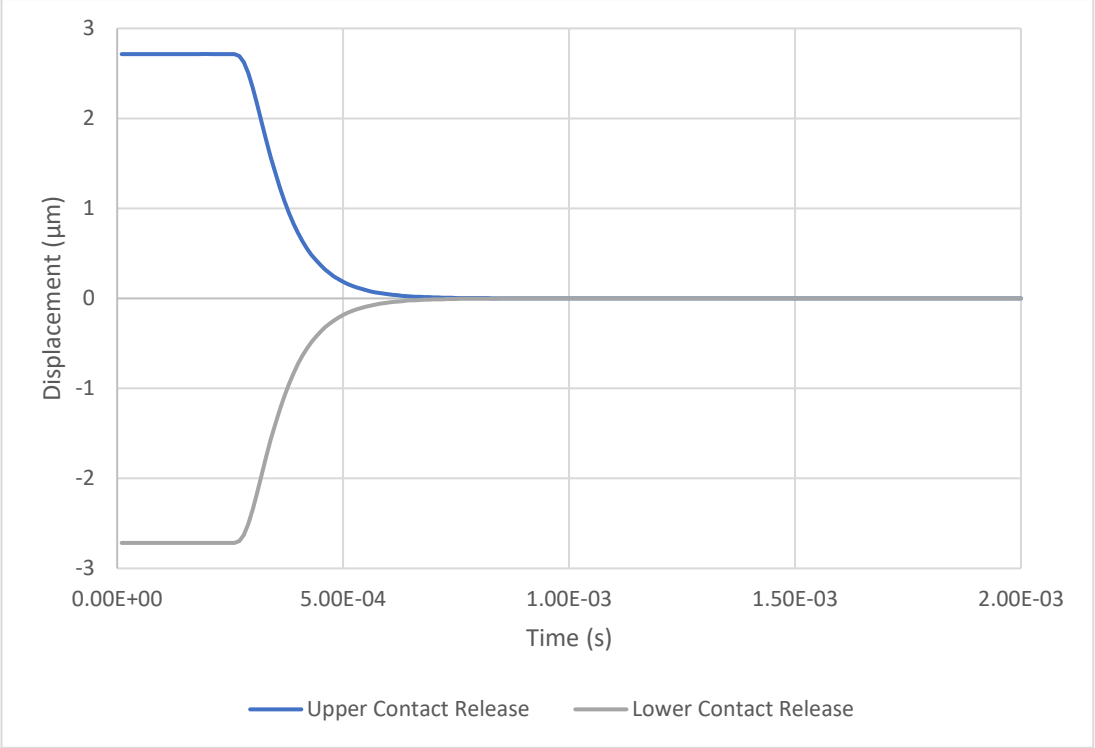

Figure 7.44: Elastic Recovery analysis result for the 'S' Shaped Pivot with Delta Angled Electrostatic Plates DPDT Switch with upper and lower contact release

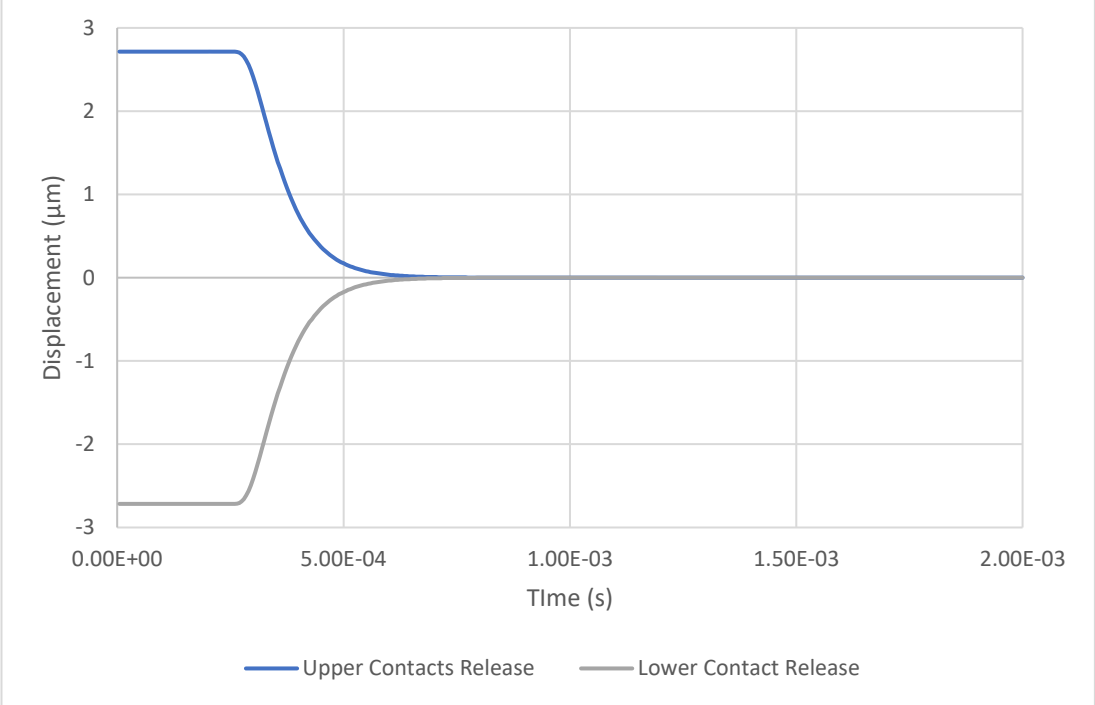

Figure 7.45: Elastic Recovery analysis result for the 'S' Shaped Split Pivot with Delta Angled Electrostatic Plates DPDT Switch with upper and lower contact release

It is shown that the elastic recovery of both HRL cantilevers provide similar switching speeds when the timings are set at the same (Figure 7.39 and Figure 7.40). This is also true for the 'Straight Pivot Seesaw DPDT Switch, v1' (Figure 7.41) with similar switch-off times of 8.8 $x10^{-4}$ seconds. However, the 'Straight Pivot Seesaw DPDT Switch, v2' (Figure 7.42) had a longer recovery time due to the thicker layer of silicon (0.3 µm) and shorter length of the copper with each end being reduced by 4 µm and replacing it with silicon. As for the ''S' Shaped Pivot Seesaw DPDT Switch' (Figure 7.43), it too had a similar recovery time as v2; this was due to the distance of the electrostatic plates, which in turn makes the switch react slower, but with the addition of the delta plates (Figure 7.44), the recovery time of the switch was greatly improved with a recovery time of 8.2 $x10^{-4}$ seconds. The delta plates were able to provide greater recovery time due to the angle of the plates, allowing them to be as close to each other on each side of the beam. However, when the 'S' Shaped Split Pivot version (Figure 7.45) was created, with a gap of 1 µm through the middle of the pivot, it provided the advantage of reducing the voltage from 1.23 V to 1.13 V, but sacrificed the switching recovery.

7.2.1.5 Resonant Frequency

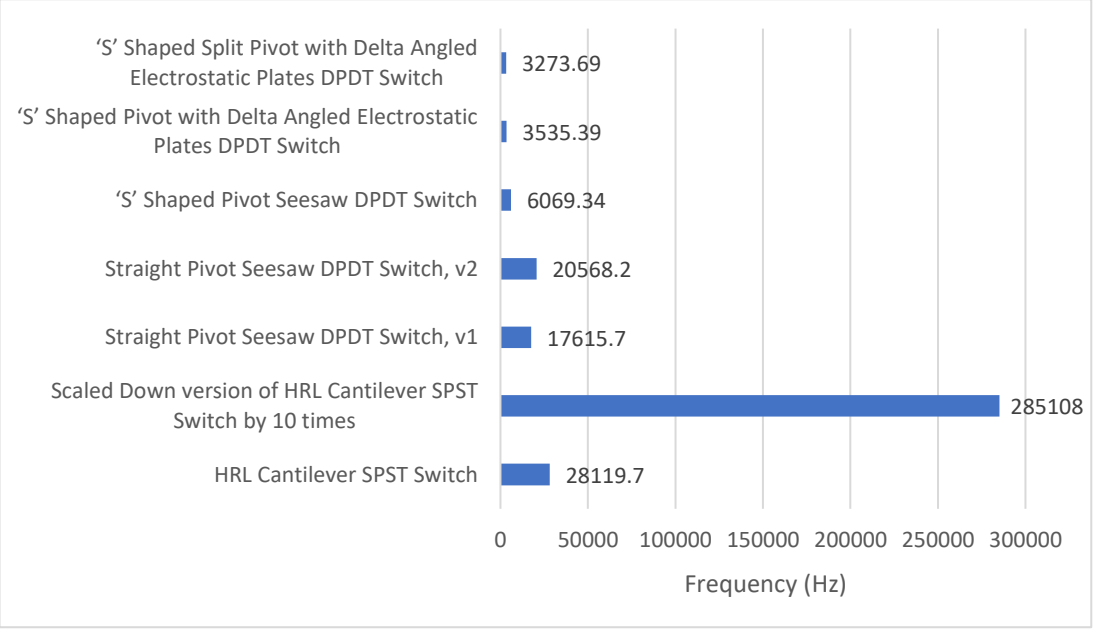

Figure 7.46: Resonant Frequencies of the different types of switches

The resonant frequency depends upon the components within the resonant frequency equation (Equation 3.14). The scaled down version of the HRL cantilever switch has a much higher resonant frequency of 285.108 kHz than that of the base design (HRL cantilever switch). This is because its mass is much smaller due to its reduced dimensions. However, the same could not be said about the straight pivot seesaw switches, which have resonant frequencies of 17.6157 kHz and 20.5682 kHz, respectively. These are lower than those of the HRL cantilever switch. This is due to the structure of the design being different from the HRL cantilever. Also, the beam of v1 has a slightly different layout to the beam of v2, which changes its resonant characteristics.

As for the ‘S’ Shaped and ‘S’ Shaped Split pivots with their delta angled electrostatic plates, the beams are identical except that the split pivot has a section removed. This shows a 261.7 Hz difference just by removing a section of mass. Also, due to its spring like nature, the split type ‘S’ shaped pivot is more flexible than the single ‘S’ shape. This in turn reduces the resonant frequency. The natural frequencies (resonant frequencies) of these designs, determine the maximum speeds at which the switches can operate.

7.2.2 Electromagnetic Characteristics

7.2.2.1 Isolation (S21) and Insertion Loss (S11) Parameters

The electromagnetic characteristics of the switch focused on the isolation and comparison was made with experiments contained in Daniel Hyman et al (Hyman et al. 1999) paper. For the EM simulation CST simulation software was used with the same simulation characteristics, to validate the results.

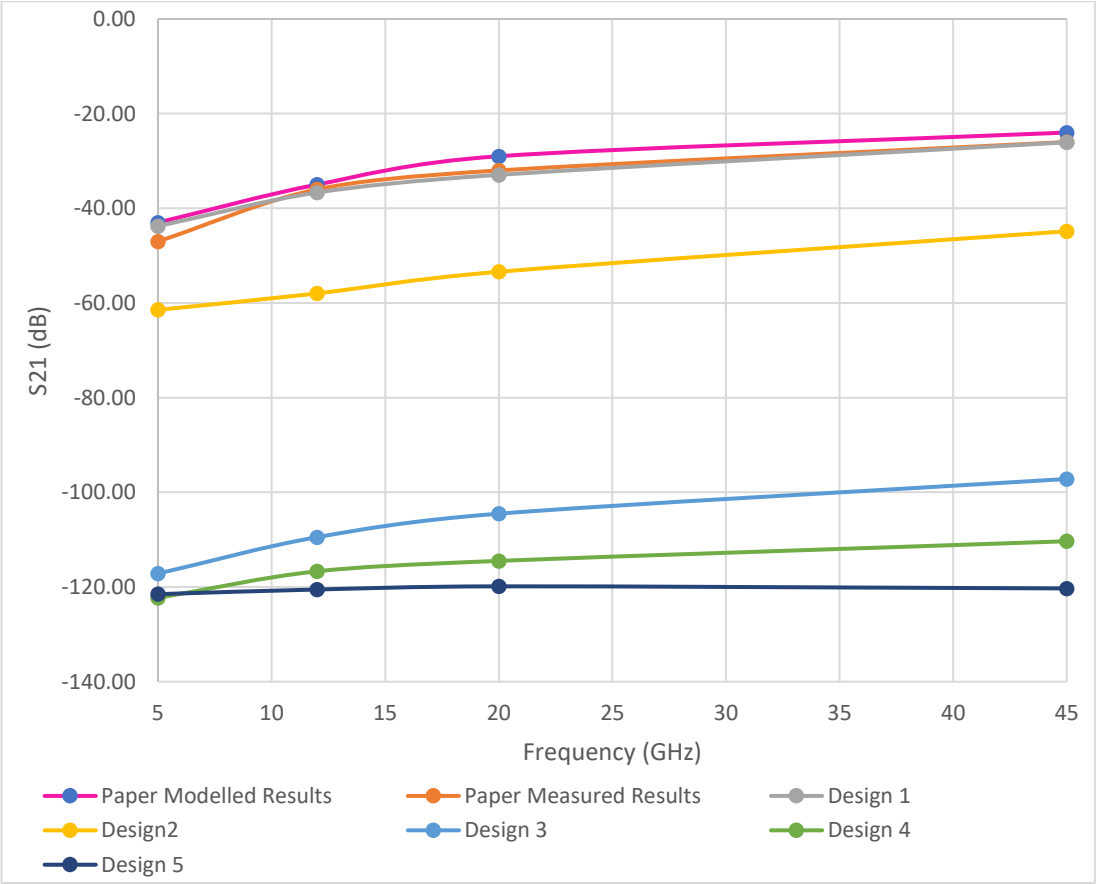

Figure 7.47: CST simulation S21 parameter analysis result for switch contacts

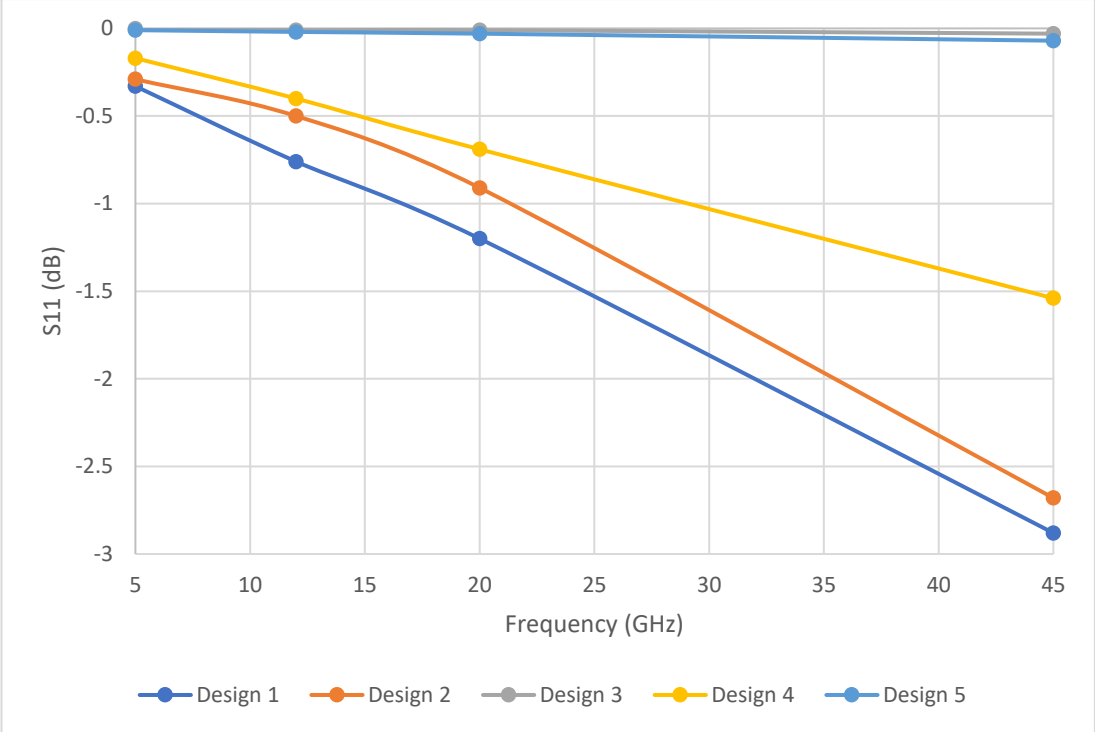

Figure 7.48: Graph of the S11 simulated results from CST for the different designs

Table 7.6: Error comparisons between simulations of the HRL Cantilever contacts against the measured

Types of Switch	S21 (dB) at 5 GHz	S21 (dB) at 12 GHz	S21 (dB) at 20 GHz	S21 (dB) at 45 GHz
Paper Modelled Results	-43	-35	-29	-24
Paper Measured Results	-47	-36	-32	-26
Design 1	-43.77	-36.67	-32.93	-26.06
Paper Modelled Simulation difference with Respect to Measured Results	8.51%	2.78%	9.38%	7.69%
Design 1 Simulation difference with Respect to Paper Measured Results	6.87%	1.86%	2.91%	0.23%

The comparison between the results from (Hyman et al. 1999) results and design 1 are closely related, which validates the results for the HRL cantilever switch. With the same simulation settings used for the HRL cantilever, designs 2, 3 and 4 followed the same design parameters in order to reduce variance of the analysis boundaries. Figure 7.47 shows that designs 2, 3 and 4 improves the isolation of the switch with each iteration. Although, Design 2 (which is the scaled down version of the HRL cantilever

switch) provided a smaller improvement of isolation over the base switch, its mechanical (contact bounce and ringing) and functionality (only SPST) issues did not provide the best option. However, design 3 which is based on the straight pivot type seesaw switches provided far greater isolation, with more functionality of the switch using an air gap of 1 µm. With design 4, the air gap was increased to 2.7 µm, the isolation was able to be improved further, and provided the best isolation out of all the designs. As shown in Table 7.6, Design 1 (which is the HRL cantilever) is accurate from 0.23 % to 6.87 %, compared to the simulation model research by (Hyman et al. 1999) which has an accuracy of 2.78 % to 9.38 %. Design 4 and 5 are both based on the 'S' shaped cantilever pivot. Design 4 was set in the same position as design 1, 2 and 3 for direct comparison of performance of the switch. However, it was not the true orientation of the contacts. Design 5 provided the true orientation of the switch, which did greater performance compared to Design 4. However, Design 5 still provided greater performance benefit over Design 1 and 2, with similar frequency isolation for 5 GHz against Design 4 but better isolation overall compared to all other designs.

As for the insertion loss of the switch, Figure 7.48 shows the straight pivot types (Design 3) and the spring pivot types (on its side) (Design 5) have improved insertion loss compared to the HRL cantilever, which provides minimal loss of signal when the contacts are closed.

Figure 7.49, Figure 7.50, Figure 7.51, Figure 7.52, Figure 7.53, Figure 7.54, Figure 7.55, Figure 7.56, Figure 7.57 and Figure 7.58, shows the contact designs modelled in CST simulation tool.

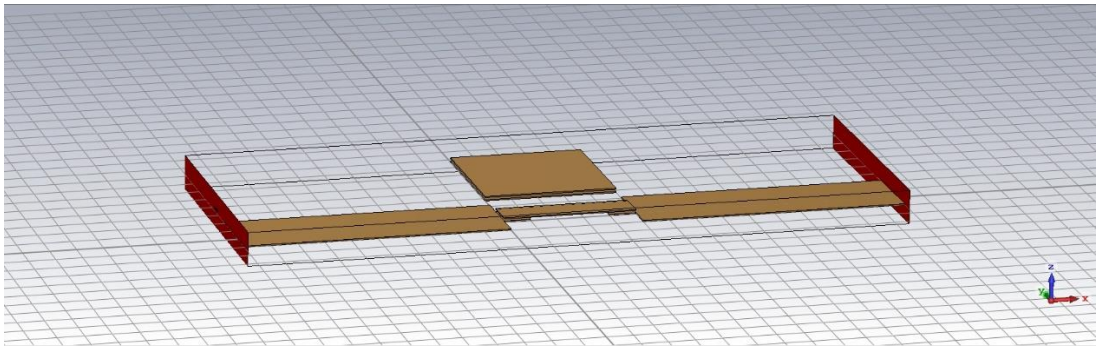

Figure 7.49: Overall contact model view of Design 1

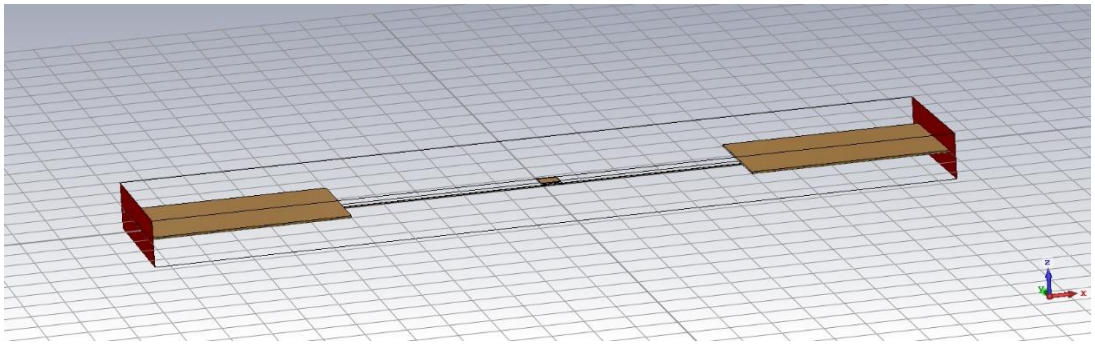

Figure 7.50: Overall contact model view of Design 2

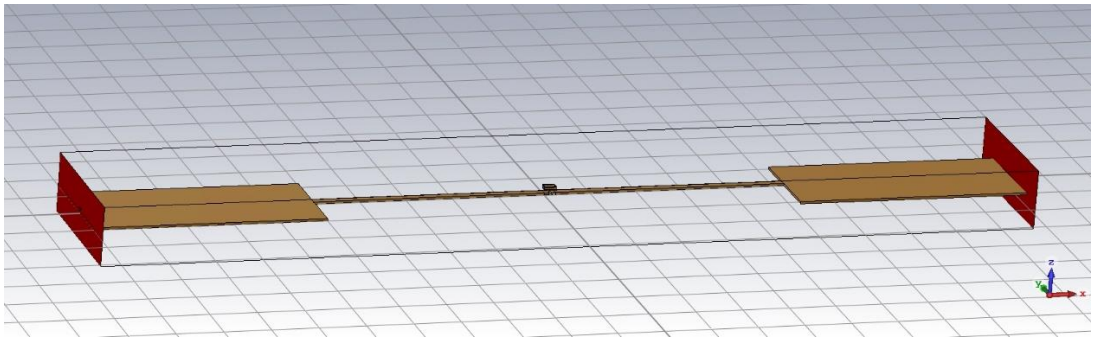

Figure 7.51: Overall contact model view of Design 3

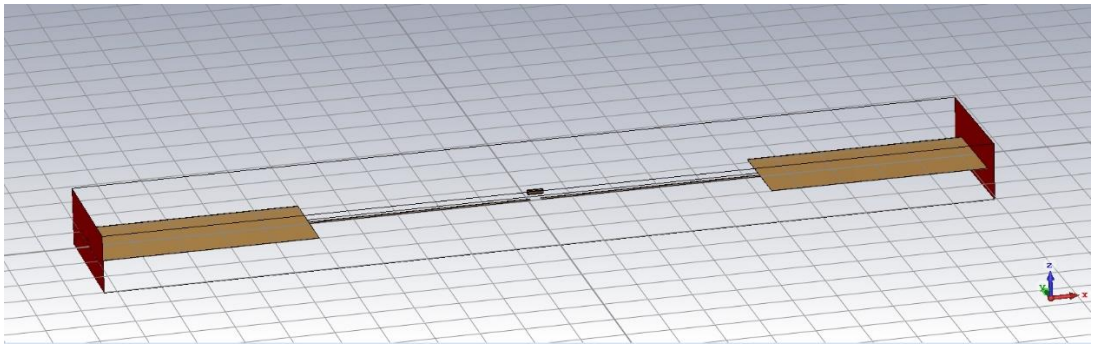

Figure 7.52: Overall contact model view of Design 4

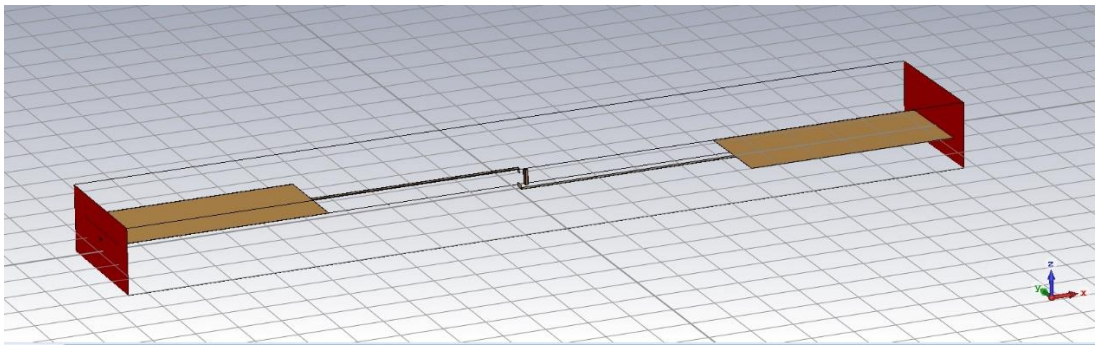

Figure 7.53: Overall contact model view of Design 5

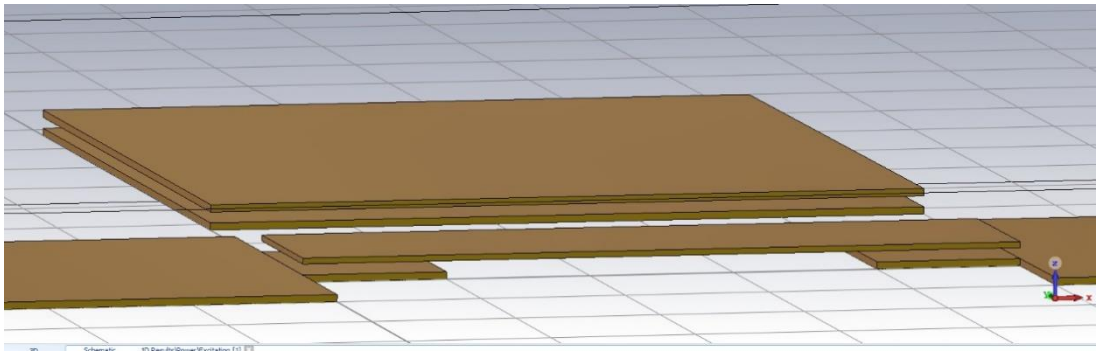

Figure 7.54: Close up view of Design 1

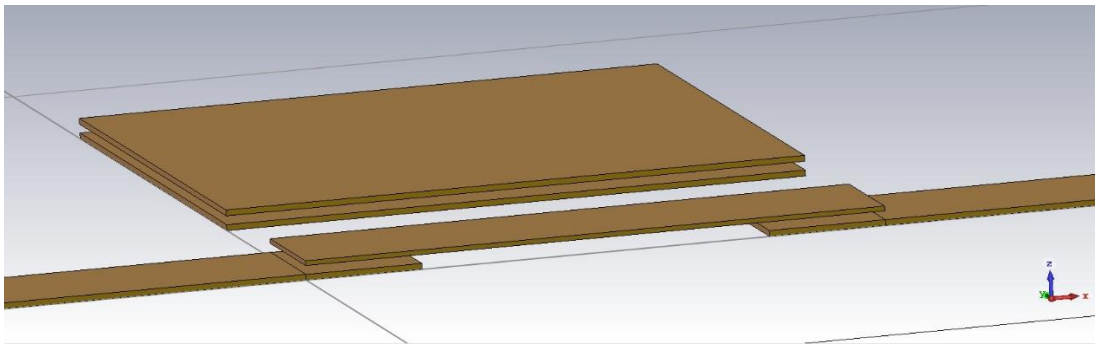

Figure 7.55: Close up view of Design 2

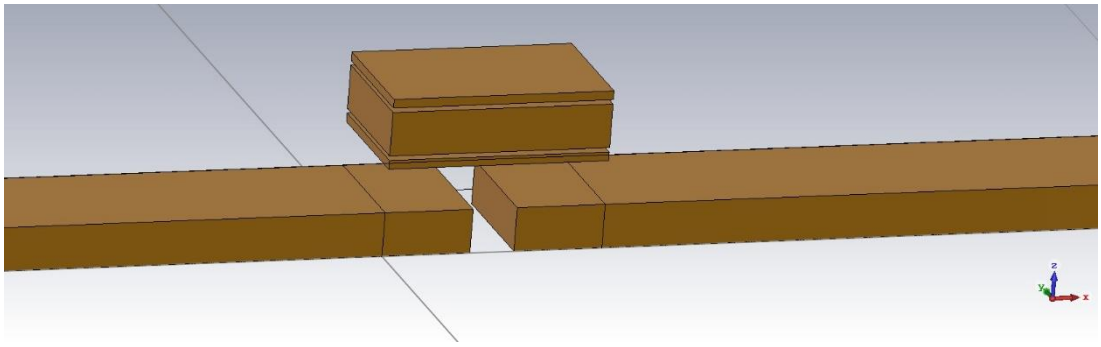

Figure 7.56: Close up view of Design 3

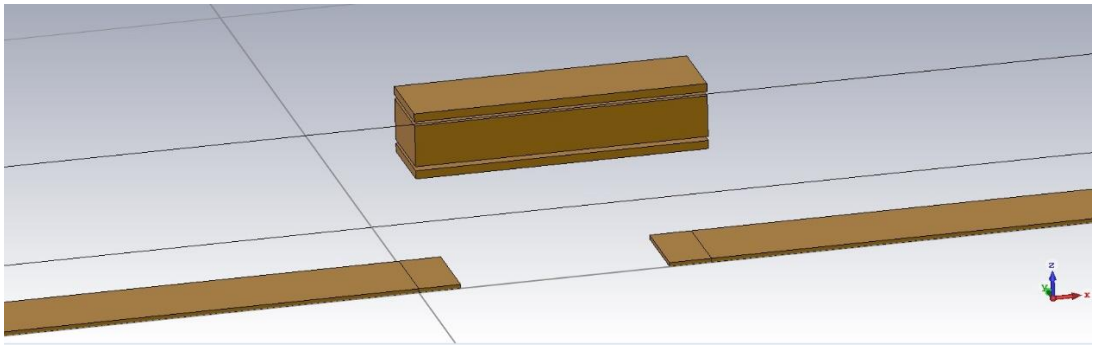

Figure 7.57: Close up view of Design 4

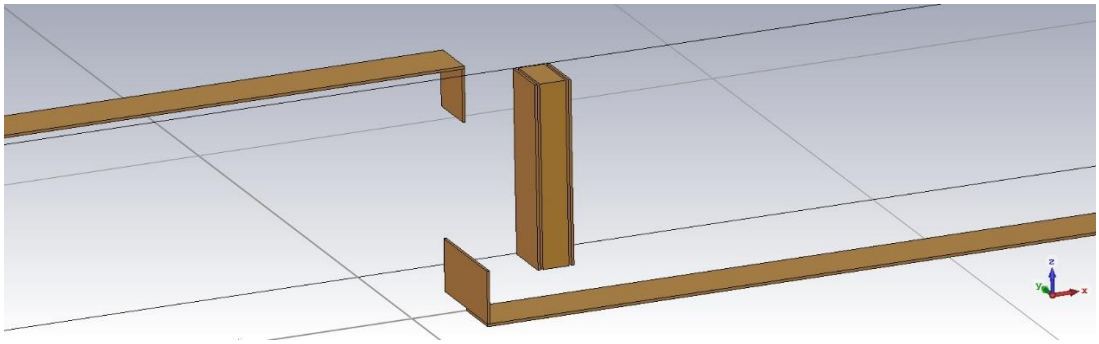

Figure 7.58: Close up view of Design 5

The work carried out on grid independency provides evidence that the simulation software is highly accurate between the sizes of 1 µm and 10 µm. However, a smaller mesh size dramatically increases simulation time. Therefore, a compromise must be made between the mesh size and the simulation time. Using a mesh size ten smaller than the design itself proved to be the optimum combination. Also, the mathematical equations and experimental results are a close match to the simulated results.

Furthermore, the ‘S’ Shaped Split pivots switch, with delta angled electrostatic plates, provided the best performance of all the designs, in terms of electromechanical and electromagnetic characteristics.

Chapter 8

8 Conclusion

This thesis identified a number of research questions described in Thesis Structure, Section 1.7. These following research questions have been addressed as follows:

- **What are the reasons for using RF MEMS switches in mobile communications?**

  Within Chapters 1, 2 and 5, the research identified the advantages of RF MEMS switches over solid states switches for use in general and mobile telecommunication systems. For example, RF MEMS switches are innately linear, consume less power with better isolation than PIN and FET switches (Table 5.1).

- **What are the challenges in existing MEMS switches?**

  This thesis addressed this question in Chapter 5 by identifying the disadvantages of RF MEMS switches. For example, they require high actuation voltages, which depend on auxiliary DC to DC converter components. The RF MEMS switches also have high stress on their components due to them being mechanically moving parts. The research found solutions to overcome their high actuation voltages by using unique seesaw designs, which enable the switches to actuate with common mobile phone voltage levels, while reducing the stress on their components.

- **Can the proposed methodology be used to validate the hypothesis?**

  The hypothesis has been validated in Chapter 7 with the Grid Independency providing an optimum value of 10 times smaller than the total size of the

structure, which is an optimum value for simulation speed and accuracy. The chapter goes on further to validate the known mathematical equations of a cantilever beam and compares them to the simulation results; thus, providing a close match between the two. The final validation (also explained in Chapter 7) is the comparison of the simulations (on Intellisuite and CST) to a practical experiment carried out by Daniel Hyman (Hyman et al. 1999) and shows the simulation packages providing very similar results to the practical outcomes, with higher accuracy compared to the simulated results that Daniel Hyman reported.

- **What is the practical frequency range for use of RF MEMS with mobile communications?**

  Section 5.1.1 describes the practical frequency ranges used for RF MEMS in mobile communications, which includes the use of Wi-Fi and other protocols.

- **What are the required driving voltages of RF MEMS Switches?**

  In this thesis it was found that industry today has no standard driving voltage for RF MEMS switches. However, the research has shown that an actuation driving voltage of less than 5V is desirable, as it reduces the number of auxiliary components, such as DC-DC converters, which simplifies the integration of RF MEMS switches. The driving voltages are explained in the Introduction (Chapter 1) and is a common goal throughout this thesis to connect the RF MEMS switches to common mobile telecommunication voltage levels, such as 1.5V, 1.8V, 3.3V and 5V.

Table 8.1, provides a list the objectives set in Section 1.5 and the locations of where the objectives have been achieved.

Table 8.1: List of Objectives linked to Achievements addressed in Chapters and Sections

Objectives Numbers (Located in 'Aims and Objectives' Section 1.5)	**Chapters or Sections where the objectives have been addressed**
1	Chapter 2 (Literature Review)
2	Chapter 2 (Literature Review)
3	Chapter 2 (Literature Review)
4	Chapter 3 is the theory with 6 and 7 for simulated results
5	Chapter 3 is the theory with 6 and 7 for simulated results
6	Section 4.1
7	Chapter 4 shows the process with Chapter 5 describing the design and Chapter 6 showing the results with Chapter 7 analysing them
8	Sections 4.3.2 and 4.3.3
9	Sections 4.3.2 and 4.3.3
10	Sections 7.1.2 and 7.1.3
11	Chapter 7
12	Section 7.2

This research investigated RF MEMS switching technology and the results were specifically focused on ohmic metal-to-metal type contact switches. An analysis of their performance was conducted by optimising an HRL cantilever switch. RF MEMS ohmic type switches are known to have issues, such as low reliability, high actuation voltages and require complementary components such as DC-DC converters.

The initial stage of the research validated an HRL cantilever, ohmic type, SPST switch (Hyman et al. 1999). The electromechanical and electromagnetic aspects of the HRL cantilever switch were compared against Daniel Hyman's documented results (Hyman et al. 1999). The software tools used for these validations were Intellisuite (for the electromechanical) and CST (for the electromagnetic). The percentage difference between the CST simulations and Daniel Hyman's practical tests were within a range from 0.23% to 6.87% (Figure 7.47). The percentage difference between Daniel Hyman's simulations and his practical tests were within a range from 2.78% to 9.38% (Figure 7.47). Thus, Table 7.6 shows that the CST simulations were more accurate than Daniel Hyman's simulations (Hyman et al. 1999), with respect to his practical

tests, over a frequency range from 5 GHz to 45 GHz. The settings and boundary conditions were used for evaluating the optimised designs.

By optimising the HRL cantilever, SPST ohmic type switch, the following five distinct advancements were achieved:

1. A scaled down version of the HRL SPST cantilever switch, provided an actuation voltage (2.9 V), which is 10 times lower than the initial HRL cantilever, with an average EM isolation improvement of 56% over a frequency range of 5 GHz to 45 GHz.
2. Optimised Straight Pivot, Seesaw DPDT type switches, provided 4 times more functionality over the HRL cantilever SPST switches by implementing a set of contacts, above and below the beam at each end. The actuation voltage was reduced to 7 V (v2) and 14 V (v1), and the von mises stress reduced to 123 MPa (v1) and 135 MPa (v2) compared to the HRL cantilever von mises stress of 692 MPa. Both these improvements are due to the increased flexibility of the pivot with nano scaled thickness. The switches provided an average increased isolation of 207%, against the HRL SPST cantilever switch over a frequency range of 5 GHz to 45 GHz, due to the significant reduction in the area of the contacts.
3. An Optimised ‘S’ Shaped Pivot Seesaw DPDT Switch, also increased functionality by 4 times. The actuation voltage of the switch was reduced from 30 V to 4 V, while decreasing the von mises stress down to 16 MPa. The design has a von mises stress, which is far below the yield strength threshold for copper, while allowing the switch to recover to its original state (OFF-state) without deformation. Also, the air gap was increased to 2.7 μm compared to the HRL cantilever’s 1.5 μm air gap, with a larger isolation over all other designs, including the HRL cantilever. All these improvements are due to the characteristics of the ‘S’ shaped pivot, which distributes the stress along the pivot links with increased flexibility. The switch gives an average isolation improvement of 246% over a frequency range of 5 GHz to 45 GHz.
4. This optimisation was the addition of the electrostatic delta plates, which takes advantage of the changing angle of the beam. The beam and the delta plates become more parallel as they become closer to each other. Thus, making more efficient use of the pulling forces between them. This enabled the ‘S’ Shaped

Pivot DPDT switch to be operated with a lower actuation voltage of 1.23 V, which enabled the beam to be evenly pulled from both sides, ensuring contact is made simultaneously on both ends. Von mises stress was further reduced to 15 MPa (the switch is named ‘S’ Shaped Pivot Seesaw DPDT RF MEMS).

5. The final optimisation was the use of a split pivot, which provided a great advantage for the straight pivot type seesaws as they were able to reduce the voltage down from 22 V to 14 V (Figure 5.7). This was due to the pivots providing more flexibility as a portion of the pivot is removed. The same was applied for the ‘S’ shaped pivot, providing a 0.1 V decrease in actuation voltage, with minor change to the switching speed (Figure 7.37 and Figure 7.45) (the switch is named ‘S’ Shaped Split Pivot Seesaw DPDT RF MEMS).

The final iteration named the ‘S’ Shaped Pivot Seesaw DPDT Switch, with delta plates, provided best performance characteristics over all the switches, by surpassing actuation voltage requirements below 2 V, while keeping von mises stress of the switch well below the yield strength of copper. This will allow this switch to be used for ultra-low voltage mobile devices. Depending on the voltage requirements of the system, designers and engineers, can refine the actuation voltage to suit their needs by changing the area of the electrostatic plates, without compromising the isolation of the switch with minimal impact to von mises stress.

8.1 Future Work

The research undertaken on this this thesis, has identified a number or areas for future work, which is listed out as follows:

- Standardisation: RF MEMS technology, in general, does not have a universal method of characterising performance. Therefore, researches need to take common characteristics of the switches into account, so that they can adhere to them.
- Nano Scaled Manufacturing for large Aspect Ratios: The current manufacturing limitations prevent fabrication of nano scaled MEMS components. Future research would enable designs, which are in the micrometre scale, to include nanometre components. The research can go further by creating nano block accuracy. This will open up a broad range of options for manufacturing structural designs for RF MEMS switches, enabling them to take advantage of nano component structures.
- Converting Seesaw Switches to Capacitive Contacts: During this research, RF MEMS 'S' shaped and straight pivots, seesaw types, are used with ohmic contacts. The switches can be converted to those with captative contacts for high RF power to be passed through. The pivot is a ground and since the beam is attached to it, the beam also becomes a ground and is used to divert the RF signal when the switch is closed. There is no physical metal-to-metal contact, due to a substrate of silicon being placed between the contacts. Therefore, metal fusion and stiction is greatly reduced.
- Minimising Actuation Voltage Further: Future research can be carried out to develop the delta plates for increasing the electrostatic pulling forces of the seesaw type switches. In addition, the pivots could be improved for greater flexibility to obtain actuation voltages below 1 V.
- High Power Ohmic Contact Switching: Further research could be carried out to analyse the contacts to prevent stiction and fusion in order to enable high power RF switching.
- 802.11ad Wi-Fi at 60 GHz: Further research into increasing the frequency bandwidth of the seesaw switches could be carried out to include operation 802.11ad Wi-Fi protocol at 60 GHz.

References

A. Akiba, S. Mitarai, S. Morita, K. Ikeda, S. Kurth, S. Leidich, A. Bertz, M. Nowack, J. Froemel and T. Gessner. A fast and low actuation voltage MEMS switch for mm-wave and its integrationAnonymous *2010 International Electron Devices Meeting*, 2010.

A. Broue, J. Dhennin, P. L. Charvet, P. Pons, N. B. Jemaa, P. Heeb, F. Coccetti and R. Plana. Multi-Physical Characterization of Micro-Contact Materials for MEMS SwitchesAnonymous *2010 Proceedings of the 56th IEEE Holm Conference on Electrical Contacts*, 2010.

A. F. Malik, M. Shoaib, S. Naseem and S. Riaz. Modeling and designing of RF MEMS switch using ANSYSAnonymous *2008 4th International Conference on Emerging Technologies*, 2008.

A. Fukuda, H. Okazaki, S. Narahashi, T. Hirota and Y. Yamao. A 900/1500/2000-MHz triple-band reconfigurable power amplifier employing RF-MEMS switchesAnonymous *IEEE MTT-S International Microwave Symposium Digest, 2005.*, 2005.

A. Hariri, J. Zu and R. Ben Mrad, 2007. Modeling of Wet Stiction in Microelectromechanical Systems (MEMS). *Journal of Microelectromechanical Systems*, vol. 16, no. 5, pp. 1276-1285 ISSN 1057-7157. DOI 10.1109/JMEMS.2007.904349.

A. Menz and R. Hper. Micromechanical silicon RF switch with electroplated solid contacts for high reliabilityAnonymous *2012 7th European Microwave Integrated Circuit Conference*, 2012.

A. Tazzoli, V. Peretti and G. Meneghesso, 2007. Electrostatic Discharge and Cycling Effects on Ohmic and Capacitive RF-MEMS Switches. *IEEE Transactions on Device and Materials Reliability*, vol. 7, no. 3, pp. 429-437 ISSN 1530-4388. DOI 10.1109/TDMR.2007.907422.

AKIBA, A., S. MITARAI, S. MORITA, K. IKEDA, S. KURTH, S. LEIDICH, A. BERTZ, M. NOWACK, J. FROEMEL and T. GESSNER. A fast and low actuation voltage MEMS switch for mm-wave and its integrationAnonymous *Electron Devices Meeting (IEDM), 2010 IEEE International*, 2010.

ANSARI, M.Z. and CHO, C., 2009. Deflection, Frequency, and Stress Characteristics of Rectangular, Triangular, and Step Profile Microcantilevers for Biosensors. *Sensors (Basel, Switzerland)*, vol. 9, no. 8, pp. 6046-6057 PMC. ISSN 1424-8220. DOI 10.3390/s90806046.

ASHBY, M.F., 2000. *Multi-objective optimization in material design and selection.* Available from: http://www.sciencedirect.com/science/article/pii/S1359645499003043 ISBN 1359-6454. DOI //dx.doi.org/10.1016/S1359-6454(99)00304-3.

BOLDEIU, G., D. VASILACHE, V. MOAGAR, A. STEFANESCU and G. CIUPRINA. Study of the von Mises stress in RF MEMS switch anchorsAnonymous , 2015.

C. A. Muley and S. A. Naveed. Modelling of cantilever based MEMS RF switchAnonymous *2013 Fourth International Conference on Computing, Communications and Networking Technologies (ICCCNT)*, 2013.

C. Do, M. Hill, M. Lishchynska, M. Cychowski and K. Delaney. Modeling, simulation and validation of the dynamic performance of a single-pole single-throw RF-MEMS contact switchAnonymous *2011 12th Intl. Conf. on Thermal, Mechanical & Multi-Physics Simulation and Experiments in Microelectronics and Microsystems*, 2011.

C. Palego, S. Hadler, B. Baloglu, Z. Peng, J. C. M. Hwang, H. F. Nied, D. I. Forehand and C. L. Goldsmith. Microwave intermodulation technique for monitoring the mechanical stress in RF MEMS capacitive switchesAnonymous *2008 IEEE MTT-S International Microwave Symposium Digest*, 2008.

C. T. C. Nguyen. RF MEMS in wireless architecturesAnonymous *Proceedings. 42nd Design Automation Conference, 2005.*, 2005.

CABRAL, J.M. and A.S. HOLMES. A novel seesaw-type RF MEMS switchAnonymous *Electrotechnical Conference, 2006. MELECON 2006. IEEE Mediterranean*, 2006.

CHUANG, W., HU, Y., LEE, C., SHIH, W.and CHANG, P., 2009. *Electromechanical behavior of the curled cantilever beam.* ISBN 1932-5150.

D. Peyrou, F. Coccetti, F. Pennec, H. Achkar, P. Pons and R. Plana. A New Methodology For RF MEMS Contact SimulationAnonymous *EuroSimE 2008 - International Conference on Thermal, Mechanical and Multi-Physics Simulation and Experiments in Microelectronics and Micro-Systems*, 2008.

DE LOS SANTOS, H., 2004. *Introduction to Microelectromechanical Microwave Systems.* 2nd ed. Norwood: Artech House Books, Sep 30, ISBN 9781580538718.

E. Ogawa, K. Masunishi, T. Ikehashi, T. Saito, H. Yamazaki, Y. Tomizawa and Y. Sugizaki. A long-term reliability analysis of a creep-immune RF-MEMS tunable capacitorAnonymous *2011 16th International Solid-State Sensors, Actuators and Microsystems Conference*, 2011.

F. Ivaldi, T. Bieniek, P. Janus, J. Zajac, P. Grabiec, W. Majstrzyk, D. Kopiec and T. Gotszalk. New approach for a multi-cantilever arrays sensor system with advanced MOEMS readoutAnonymous *2016 46th European Solid-State Device Research Conference (ESSDERC)*, 2016.

F. Souchon, B. Reig, C. Dieppedale, L. Thouy, A. Koszewski, H. Sibuet and G. Papaioannou. Key improvements of the MEMS switch lifetime thanks to a dielectric-free design and contact reliability investigations in hot/cold switching operationsAnonymous *2013 IEEE International Reliability Physics Symposium (IRPS)*, 2013.

G. E. Moore, 2006. Cramming more components onto integrated circuits, Reprinted from Electronics, volume 38, number 8, April 19, 1965, pp.114 ff. *IEEE Solid-State Circuits Society Newsletter*, vol. 11, no. 5, pp. 33-35 ISSN 1098-4232. DOI 10.1109/N-SSC.2006.4785860.

G. Piazza, R. Abdolvand and F. Ayazi. Voltage-tunable piezoelectrically-transduced single-crystal silicon resonators on SOI substrateAnonymous *The Sixteenth Annual*

International Conference on Micro Electro Mechanical Systems, 2003. MEMS-03 Kyoto. IEEE, 2003.

H. C. Nathanson, W. E. Newell and R. A. Wickstrom. A resonant gate silicon bandpass transistorAnonymous *1965 International Electron Devices Meeting*, 1965.

H. C. Nathanson, W. E. Newell, R. A. Wickstrom and J. R. Davis, 1967. The resonant gate transistor. *IEEE Transactions on Electron Devices*, vol. 14, no. 3, pp. 117-133 ISSN 0018-9383. DOI 10.1109/T-ED.1967.15912.

H. H. Yang, A. Yahiaoui, H. Zareie, P. Blondy and G. M. Rebeiz, 2015. Symmetric and Compact Single-Pole Multiple-Throw (SP7T, SP11T) RF MEMS Switches. *Journal of Microelectromechanical Systems*, vol. 24, no. 3, pp. 685-695 ISSN 1057-7157. DOI 10.1109/JMEMS.2014.2344694.

H. Jaafar, F. L. Nan and N. A. M. Yunus. Design and simulation of high performance RF MEMS series switchAnonymous *2011 IEEE Regional Symposium on Micro and Nano Electronics*, 2011.

HRANAC, R., 2005. Return Loss. *SCTE Technical Coloumns,* [e-journal] <http://www.scte.org/TechnicalColumns/05-10-01%20return%20loss.pdf>.

Hee-Chul Lee, Jae-Yeong Park and Jong-Uk Bu, 2005. Piezoelectrically actuated RF MEMS DC contact switches with low voltage operation. *IEEE Microwave and Wireless Components Letters*, vol. 15, no. 4, pp. 202-204 ISSN 1531-1309. DOI 10.1109/LMWC.2005.845689.

HILBER, H.M., HUGHES, T.J.R. and TAYLOR, R.L., 1977. Improved numerical dissipation for time integration algorithms in structural dynamics. *Earthquake Engineering & Structural Dynamics*, July, vol. 5, no. 3, pp. 283-292 ISSN 0098-8847. DOI 10.1002/eqe.4290050306.

HYMAN, D., LAM, J., WARNEKE, B., SCHMITZ, A., HSU, T.Y., BROWN, J., SCHAFFNER, J., WALSTON, A., LOO, R.Y., MEHREGANY, M. and LEE, J., 1999. Surface-micromachined RF MEMs switches on GaAs substrates. *International Journal of RF and Microwave Computer-Aided Engineering*, vol. 9, no. 4, pp. 348-361 ISSN 1099-047X. DOI AID-MMCE6>3.0.CO;2-K.

Hyouk Kwon, Dong-June Choi, Jae-Hyoung Park, Hee-Chul Lee, Yong-Hee Park, Yong-Dae Kim, Hyo-Jin Nam, Young-Chang Joo and Jong-Uk Bu. Contact materials and reliability for high power RF-MEMS switchesAnonymous *2007 IEEE 20th International Conference on Micro Electro Mechanical Systems (MEMS)*, 2007.

I. C. Ghosekar, A. V. Rewatkar, M. S. Panse and S. D. Mhaske. SPMT, MPST RF MEMS switch using multiplexer approachAnonymous *2015 International Conference on Communications and Signal Processing (ICCSP)*, 2015.

I. Reines, B. Pillans and G. M. Rebeiz. A Stress-Tolerant Temperature-Stable RF MEMS Switched CapacitorAnonymous *2009 IEEE 22nd International Conference on Micro Electro Mechanical Systems*, 2009.

IEEE., 2013. *https://www.microwaves101.com/encyclopedias/mems-for-microwaves#ohmic.* October, Available from: http://www.microwaves101.com/encyclopedias/920-mems-for-microwaves#ohmic.

Intel and Mistry, K., 2017. *Intel - Kaizad Mistry on Intel's 10 nm Technology*. [online] Available at: <https://newsroom.intel.com/newsroom/wp-content/uploads/sites/11/2017/03/Kaizad-Mistry-2017-Manufacturing.pdf> [Accessed: 04/02/2018].

J. Bryzek, K. Peterson and W. McCulley, 1994. Micromachines on the march. *IEEE Spectrum*, vol. 31, no. 5, pp. 20-31 ISSN 0018-9235. DOI 10.1109/6.278394.

J. C. M. Hwang. Reliability of Electrostatically Actuated RF MEMS SwitchesAnonymous *2007 IEEE International Workshop on Radio-Frequency Integration Technology*, 2007.

J. Lin. The ultra-wideband RF MEMS single-pole-four-throw switchAnonymous *2016 International Symposium on Antennas and Propagation (ISAP)*, 2016.

J. M. Cabral and A. S. Holmes. A novel seesaw-type RF MEMS switchAnonymous *MELECON 2006 - 2006 IEEE Mediterranean Electrotechnical Conference*, 2006.

J. Oberhammer and G. Stemme, 2006. Active Opening Force and Passive Contact Force Electrostatic Switches for Soft Metal Contact Materials. *Journal of Microelectromechanical Systems*, vol. 15, no. 5, pp. 1235-1242 ISSN 1057-7157. DOI 10.1109/JMEMS.2006.882810.

J. Pal, Y. Zhu, J. Lu, D. Dao and F. Khan, 2016. High Power and Reliable SPST/SP3T RF MEMS Switches for Wireless Applications. *IEEE Electron Device Letters*, vol. 37, no. 9, pp. 1219-1222 ISSN 0741-3106. DOI 10.1109/LED.2016.2592539.

J. T. Huang and S. Y. Li. Using Residual Stresses to Develop CMOS-compatible RF MEMS SwitchesAnonymous *2006 International Conference on Electronic Materials and Packaging*, 2006.

J. T. Huang, Y. K. Hsu, Y. C. Lo, K. Y. Lee, C. K. Chen and T. C. Tsai. Design and fabrication of low-insertion loss and high-isolation CMOS-MEMS switch for microwave applicationsAnonymous *2010 5th International Microsystems Packaging Assembly and Circuits Technology Conference*, 2010.

Jacobi Werner., 1949. *Halbleiterverstaerker.* SIEMENS AG ed., Germany: .

Jaewoo Lee, Chang Han Je, Sungweon Kang and Chang-Auck Choi, 2005a. A low-loss single-pole six-throw switch based on compact RF MEMS switches. *IEEE Transactions on Microwave Theory and Techniques*, vol. 53, no. 11, pp. 3335-3344 ISSN 0018-9480. DOI 10.1109/TMTT.2005.855746.

Jaewoo Lee, Chang-Han Je, Seongweon Kang and Chang-Auck Choi. A single-pole 6-throw (SP6T) antenna switch using metal-contact RF MEMS switches for multi-band applicationsAnonymous *IEEE MTT-S International Microwave Symposium Digest, 2005.*, 2005b.

JEDEC., 2007a. *ADDENDUM No. 5 to JESD8 - 2.5 V 0.2 V (NORMAL RANGE), AND 1.8 V TO 2.7 V (WIDE RANGE) POWER SUPPLY VOLTAGE AND INTERFACE STANDARD FOR NONTERMINATED DIGITAL INTEGRATED CIRCUIT.* Sep, Available from: https://www.jedec.org/document_search?search_api_views_fulltext=jesd8-5A-01.

JEDEC., 2007b. *INTERFACE STANDARD FOR NOMINAL 3.0 V/3.3 V SUPPLY DIGITAL INTEGRATED CIRCUITS.* Sep, Available from: https://www.jedec.org/document_search?search_api_views_fulltext=jesd8c-01.

Jongseok Kim, Sangwook Kwon, Hong Youngtack, Heemoon Jeong and Sanghoon Lee. Variable pivot seesaw actuated RF MEMS switch for reconfigurable system applicationAnonymous *Micro Electro Mechanical Systems, 2007. MEMS. IEEE 20th International Conference on*, 2007a.

Jongseok Kim, Sangwook Kwon, Youngtack Hong, Heemoon Jeong, Sanghoon Lee, Cheheung Kim, Kyongsoo Lee, Byeongkwon Ju and Insang Song. Variable pivot seesaw actuated RF MEMS switch for reconfigurable system applicationAnonymous *2007 IEEE 20th International Conference on Micro Electro Mechanical Systems (MEMS)*, 2007b.

K. Said, H. Alun and B. Jim. Testing and characterization of a MEMS micro-cantilever systemAnonymous *2016 IEEE 59th International Midwest Symposium on Circuits and Systems (MWSCAS)*, 2016.

K. Y. Chan and R. Ramer. RF MEMS Switch with low stress sensitivity and low actuation voltageAnonymous *2009 IEEE Antennas and Propagation Society International Symposium*, 2009.

KILBY JACK S, inventor; Miniaturized electronic circuits. USA patent US3138743A. 1964 Jun 23,.

Kofsky, I.L., 1951. Atwood's Machine and the Teaching of Newton's Second Law. *American Journal of Physics*, [e-journal] 19 (6), pp.354-356. 10.1119/1.1932825. <https://doi.org/10.1119/1.1932825>.

Kubby, J.A., 2011. *A guide to hands-on MEMS design and prototyping.* 1. publ. ed. Cambridge [u.a.]: Cambridge Univ. Press. ISBN 1107645794.

L. E. Larson, R. H. Hackett, M. A. Melendes and R. F. Lohr. Micromachined microwave actuator (MIMAC) technology-a new tuning approach for microwave integrated circuitsAnonymous *IEEE 1991 Microwave and Millimeter-Wave Monolithic Circuits Symposium. Digest of Papers*, 1991a.

L. E. Larson, R. H. Hackett and R. F. Lohr. Microactuators for GaAs-based microwave integrated circuitsAnonymous *Solid-State Sensors and Actuators, 1991. Digest of Technical Papers, TRANSDUCERS '91., 1991 International Conference on*, 1991b.

L. Liu. High Performance RF MEMS Series Contact Switch - Design and SimulationsAnonymous *2007 Proceedings 57th Electronic Components and Technology Conference*, 2007.

L. Vietzorreck. EM Modeling of RF MEMSAnonymous *EuroSime 2006 - 7th International Conference on Thermal, Mechanical and Multiphysics Simulation and Experiments in Micro-Electronics and Micro-Systems*, 2006.

LEONDES, C.T., 2006. *Mems/Nems.* New York, NY: Springer ISBN 978-0-387-25786-0.

LI, X., S. KIYAWAT and C.J. KIM. High-Aspect-Ratio Electroplated Structures with 2mm BeamwidthAnonymous *ASME Int. Mechanical Engineering Congress and Exposition*, Nov. 1999.

Lingbo Zhu, Jianwen Xu, Zhuqing Zhang, D. W. Hess and C. P. Wong. Lotus effect surface for prevention of microelectromechanical system (MEMS) stictionAnonymous *Proceedings Electronic Components and Technology, 2005. ECTC '05.*, 2005.

M. Asaduzzaman, S. Peik and M. S. R. Shoaib. Electro-thermal and mechanical analysis of a MEMS switchAnonymous *International Conference on Electrical & Computer Engineering (ICECE 2010)*, 2010.

M. L. Ya, A. N. Nordin and N. Soin. Design and analysis of a low-voltage electrostatic actuated RF CMOS-MEMS switchAnonymous *RSM 2013 IEEE Regional Symposium on Micro and Nanoelectronics*, 2013.

M. L. Ya, N. Soin and A. N. Nordin. Theoretical and simulated investigation of dielectric charging effect on a capacitive RF-MEMS switchAnonymous *2016 IEEE International Conference on Semiconductor Electronics (ICSE)*, 2016.

M. Niessner, J. Iannacci, G. Schrag and G. Wachutka. Experimental analysis and modeling of the mechanical impact during the dynamic pull-in of RF-MEMS switchesAnonymous *The Eighth International Conference on Advanced Semiconductor Devices and Microsystems*, 2010.

M. Spasos, N. Charalampidis, K. Tsiakmakis and R. Nilavalan. Analysis and design of an all metal in line series ohmic RF MEMS switch for microwave applicationsAnonymous *2010 Symposium on Design Test Integration and Packaging of MEMS/MOEMS (DTIP)*, 2010.

M. Wietstruck, M. Kaynak, W. Zhang and B. Tillack. Electro-thermo-mechanical analysis of a BiCMOS embedded RF-MEMS switch for temperatures from -55C to + 125CAnonymous *2013 IEEE 13th Topical Meeting on Silicon Monolithic Integrated Circuits in RF Systems*, 2013.

MAFINEJAD, Y., M. ZARGHAMI, A.Z. KOUZANI and K. MAFINEZHAD. Impact of carbon material on RF MEMS switchAnonymous , 2013.

MAXWELL, J.C., 1831-1879., 1982. *A dynamical theory of the electromagnetic field.* 2013 Reprint of 1865 Edition ed. United States: Wipf and Stock Publishers Available from: http://catalog.hathitrust.org/Record/009925033 ISBN 9781579100155.

MCGRUER, N.E., G.G. ADAMS, L. CHEN, Z.J. GUO and Y. DU. Mechanical, Thermal, and Material Influences on Ohmic-Contact-Type MEMS Switch OperationAnonymous , 2006.

Mingxin Song, Jinghua Yin, Xunjun He and Yue Wang. Design and analysis of a novel low actuation voltage capacitive RF MEMS switchesAnonymous *2008 3rd IEEE International Conference on Nano/Micro Engineered and Molecular Systems*, 2008.

N. Saba, N. Soin and K. N. Khamil. Simulation and analysis of actuation voltage of electrostatically actuated RF MEMS cantilever switchAnonymous *2015 International Conference on Smart Sensors and Application (ICSSA)*, 2015.

Nielsen, C.V., Alves, L.M., Bay, N., Martins, P.A.F. and Zhang, W., 2013. *Modeling of Thermo-Electro-Mechanical Manufacturing Processes.* 1. Aufl. ed. London: Springer Verlag London Limited. Available through: <http://ebooks.ciando.com/book/index.cfm/bok_id/372291>1447146425

NIU, C. and G.M. REBEIZ. A miniature RF MEMS metal-contact switch with high biaxial and stress-gradient toleranceAnonymous , 2012.

P. G. Steeneken and O. Wunnicke. Performance limits of MEMS switches for power electronicsAnonymous *2012 24th International Symposium on Power Semiconductor Devices and ICs*, 2012.

PARSEDIYA, D.K. Deflection and stresses of effective micro-cantilever beam designs under low mass loadingAnonymous , 2016.

PENNEC, F., D. PEYROU, A. BROUÉ, J. DHENNIN, P. PONS, R. PLANA and F. COURTADE. RF MEMS electrical contact resistance calculation using mechanical contact simulations and analytical modelsAnonymous , 2009.

PRANONSATIT, S., G. HONG, A.S. HOLMES and S. LUCYSZYN. Rotary RF MEMS Switch Based on the Wobble Motor PrincipleAnonymous *Micro Electro Mechanical Systems, 2006. MEMS 2006 Istanbul. 19th IEEE International Conference on*, 2006.

PRATAP, R. and ARUNKUMAR, A., 2007. Material selection for MEMS devices. *Indian Journal of Pure & Applied Physics*, April, vol. 45, pp. 358-367. Available from: http://nopr.niscair.res.in/bitstream/123456789/2328/1/IJPAP%2045%284%29%2035 8-367.pdf.

R. Behielt, T. Knzig and G. Schrag. Long-term investigations of RF-MEMS switches on failure mechanisms induced by dielectric chargingAnonymous *2014 Symposium on Design, Test, Integration and Packaging of MEMS/MOEMS (DTIP)*, 2014.

R. Feynman, 1993. Infinitesimal machinery. *Journal of Microelectromechanical Systems*, vol. 2, no. 1, pp. 4-14 ISSN 1057-7157. DOI 10.1109/84.232589.

R. Mahameed and G. M. Rebeiz, 2011. RF MEMS Capacitive Switches for Wide Temperature Range Applications Using a Standard Thin-Film Process. *IEEE Transactions on Microwave Theory and Techniques*, vol. 59, no. 7, pp. 1746-1752 ISSN 0018-9480. DOI 10.1109/TMTT.2011.2135376.

R. P. Feynman, 1992. There's plenty of room at the bottom [data storage]. *Journal of Microelectromechanical Systems*, vol. 1, no. 1, pp. 60-66 ISSN 1057-7157. DOI 10.1109/84.128057.

R. Raman and T. Shanmuganantham. Design and analysis of RF MEMS switch with p-shaped cantilever beam for wireless applicationsAnonymous *2016 International Conference on Emerging Technological Trends (ICETT)*, 2016.

RadantMEMS., 2014. *Radant MEMS Products.* Available from: http://www.radantmems.com/radantmems/products.html.

REBEIZ, G.M., 2003. *RF MEMS: Theory, Design, and Technology.* New York, NY, USA: John Wiley & Sons, Inc ISBN 0471201693.

S. B. Asutkar and P. Ghutke. A novel approach for optimized design of RF MEMS capacitive switchAnonymous *2016 2nd International Conference on Advances in Electrical, Electronics, Information, Communication and Bio-Informatics (AEEICB)*, 2016.

S. C. Roy and K. J. Rangra. Design Optimization of RF MEMS SP4T and SP6T SwitchAnonymous *2010 3rd International Conference on Emerging Trends in Engineering and Technology*, 2010.

S. Kang, H. C. Kim and K. Chun. See-saw Type RF MEMS Switch with Fine Gap Vertical CombAnonymous *2006 IEEE International Conference on Semiconductor Electronics*, 2006.

S. Lakshmi, S. Rao, P. Manohar and P. N. Sayanu. Design and simulation of multi-beam RF MEMS varactorAnonymous *International Conference on Circuits, Communication, Control and Computing*, 2014.

S. Pranonsatit, A. S. Holmes, I. D. Robertson and S. Lucyszyn, 2006. Single-Pole Eight-Throw RF MEMS Rotary Switch. *Journal of Microelectromechanical Systems*, vol. 15, no. 6, pp. 1735-1744 ISSN 1057-7157. DOI 10.1109/JMEMS.2006.883578.

S. Sangameswaran, J. De Coster, V. Cherman, P. Czarnecki, D. Linten, M. Scholz, S. Thijs, G. Groeseneken and I. De Wolf. Behavior of RF MEMS switches under ESD stressAnonymous *Electrical Overstress/Electrostatic Discharge Symposium Proceedings 2010*, 2010.

SEKI, T., J. YAMAMOTO, A. MURAKAMI, N. YOSHITAKE, K.-. HINUMA, T. FUJIWARA, K. SANO, T. MATSUSHITA, F. SATO and M. OBA. An RF MEMS switch for 4G Front-EndsAnonymous *Microwave Symposium Digest (IMS), 2013 IEEE MTT-S International*, 2013.

SHARPE, W.N., Jr, HEMKER, K.J. and EDWARDS, R.L., 2004. *Mechanical Properties of MEMS Materials.*, Mar Available from: http://www.dtic.mil/docs/citations/ADA422530.

SHEA, H.R. Reliability of MEMS for space applicationsAnonymous , Jan 21, 2006.

Simple harmonic motion. [on-line] Available at: <http://physics.bu.edu/~duffy/py105/SHM.html> [Accessed: 21-01-2018].

STANIMIROVIĆ, Z. and STANIMIROVIĆ, I., 2009. Mechanical Properties of MEMS Materials. In: K. TAKAHATA ed., *Micro Electronic and Mechanical Systems* Rijeka: InTech, pp. Ch. 11 DOI 10.5772/7010.

Sungchan Kang, Hyeon Cheol Kim and Kukjin Chun. Single pole four throw RF MEMS switch with double stop comb driveAnonymous *2008 IEEE 21st International Conference on Micro Electro Mechanical Systems*, 2008.

T. Kim, Z. Marinkovic, V. MarkoviC, M. Milijic, O. Pronic-Rancic and L. Vietzorreck. Efficient modelling of an RF MEMS capacitive shunt switch with artificial neural networksAnonymous *2013 International Symposium on Electromagnetic Theory*, 2013.

T. Sharma and A. Tyagi. Review of Mechanical Modelling of Fixed-Fixed Beams in RF MEMS SwitchesAnonymous *2013 Third International Conference on Advanced Computing and Communication Technologies (ACCT)*, 2013.

UR RAHMAN, H., K.Y. CHAN and R. RAMER. Investigation of residual stress effects and modeling of spring constant for RF MEMS switchesAnonymous , 2009.

VARADAN, V.K., JOSE, K.A. and VINOY, K.J., 2003. *RF MEMS and their applications.* Reprinted ed. Chichester [u.a.]: Wiley ISBN 9780470843086.

W. Bacher, W. Menz and J. Mohr, 1995. The LIGA technique and its potential for microsystems-a survey. *IEEE Transactions on Industrial Electronics*, vol. 42, no. 5, pp. 431-441 ISSN 0278-0046. DOI 10.1109/41.464604.

W. N. Sharpe. Mechanical properties of MEMS materialsAnonymous *2001 International Semiconductor Device Research Symposium. Symposium Proceedings (Cat. No.01EX497)*, 2001.

Y. Gong, F. Zhao, H. Xin, J. Lin and Q. Bai. Simulation and Optimal Design for RF MEMS Cantilevered Beam SwitchAnonymous *2009 ETP International Conference on Future Computer and Communication*, 2009.

Y. Huang, M. Osterman and M. Pecht. A novel electrostatic Radio Frequency Micro Electromechanical Systems (RF MEMS) with Prognostics functionAnonymous *2012 IEEE 62nd Electronic Components and Technology Conference*, 2012.

Y. Mafinejad, A. Z. Kouzani, K. Mafinezhad and H. Nabovatti. Design and simulation of a low voltage wide band RF MEMS switchAnonymous *2009 IEEE International Conference on Systems, Man and Cybernetics*, 2009.

Yonghua Zhang, Guifu Ding, Xiaofeng Shun, Xueping Li and Bingchu Cai. Design and analysis of the micromechanical structure for an electromagnetic bistable RF MEMS switchAnonymous *2005 Asia-Pacific Microwave Conference Proceedings*, 2005.

Z. Jiang, Z. Gong and Z. Liu. Copper-based multimetal-contact RF MEMS switchAnonymous *2016 17th International Conference on Electronic Packaging Technology (ICEPT)*, 2016.

Zhenyin Yang, LICHTENWALNER, D.J., MORRIS, A.S., KRIM, J. and KINGON, A.I., 2009. Comparison of Au and Au-Ni Alloys as Contact Materials for MEMS Switches. *Journal of Microelectromechanical Systems*, vol. 18, no. 2, pp. 287-295. Available from: http://ieeexplore.ieee.org/document/4770198 CrossRef. ISSN 1057-7157. DOI 10.1109/JMEMS.2008.2010850.

Self-Publications

Al-Amin, M. A. et al., 2017. Development of a double-pole double-throw radio frequency micro electro-mechanical systems switch using an ‘S’shaped pivot. *International Journal of System Assurance Engineering and Management,* 8(1), pp. 173-179.

Al-Amin, M., Yousef, S. & Morris, B., 2013. RF MEMS DPDT switch using novel simulated seesaw design. *International symposium on microelectronics,* 2013(1), pp. 000831-000835.

Al-Amin, M., Yousef, S. & Morris, B., 2014. Simulation of an RF MEMS Double-Pole Double-Throw Switch Using Novel Seesaw Design. *The International Conference on Computing Technology and Information Management (ICCTIM),* p. 381.

Al-Amin, M., Yousef, S., Morris, B. & Shirvani, H., 2014. Simulated RF MEMS Double-Pole Double Throw. *International Journal of Computer Engineering & Technology (IJCET),* 5(7), pp. 73-84.

Appendix A

Equations implemented to Intellisuite SYNPLE

The regular Intellisuite SYNPLE, Reduced Order Macro-model (ROM) cannot capture the dynamic behaviour once the electrodes contact each other over an insulated layer.

In the regular modal summation method, the following equation is integrated:

Equation 0.1

$$m_i \frac{\partial^2 q_i}{\partial t^2} + 2\xi_i \omega_i m_i \frac{\partial q_i}{\partial t} + \frac{\partial U_m(q_i)}{\partial q_i} = \frac{1}{2}\sum_r \frac{\partial C_{ks}(q_i)}{\partial q_i} \cdot (V_k - V_s)^2 + \sum_{j=1}^{n} \Phi_i^j F_j$$

Where:

q_i = time dependent modal amplitude (scaling factor of modal coordinates)

m_i = ith mode generalized mass

ξ_i = linear modal damping ratio

ω_i = ith eigen frequency

Φ_i = ith modal shape function (the displacement vector for the ith mode)

U_m = strain energy

C_{ks} = capacitance between two electrodes

V = voltage on the electrode

The deformation state of the structure is given by nth nodal displacement.

Where $\sum_{j=1}^{n} \Phi_i^j F_j$ is the sum, over the representative nodes of the external node force, weighted by the mode shape.

With the contact condition, two things will change:

a) While integrating the above equation, an extra constraint is obeyed by knowing which point is likely to have the largest displacement on the topology of the structure. A constraint can be identified at the point in terms of modal coordinates. This provides a unilateral constraint which cannot be avoided in

a contact situation. This constraint involves the variables state of the dynamic simulation, therefore in the integration ensures that the plate does not penetrate the substrate below.

b) The sum of the total forces is equal to zero. Before the contact happens:

$$Fe(q) = Fm(q)$$

In other words, the mechanical force is equal to the electrostatic force. Once the contact occurs:

$$Fe(q) = Fm(q) + Fr(q)$$

A repulsive force generated from solid-state compression in the materials comprising the dielectric layer and the substrate should be added to balance the electrostatic force.

The dynamic equation has been modified to its new form as shown below in order to model the condition of the contact.

Equation 0.2

$$m_i \frac{\partial^2 q_i}{\partial t^2} + 2\xi_i \omega_i m_i \frac{\partial q_i}{\partial t} + \frac{\partial U_m(q_i)}{\partial q_i} = \frac{1}{2}\sum_r \frac{\partial C_{ks}(q_i)}{\partial q_i} \cdot (V_k - V_s)^2 + \sum_{j=1}^{n} \Phi_i^j F_j + \sum_{l=1}^{s} \Phi_i^l R_i^l$$

Where:

R_i = contact repulsive force at the contact node l

s = the number of contact nodes $s \in n$ (to it limiting number) (i.e. s is an element of n)

The strong repulsive force is expressed as the following:

Equation 0.3

$$R_i = \left(e^{-[\alpha_i (q_i - qmax_i)]^{\beta_i}} - 1\right) u\,(qmax_i - q_i)$$

$qmax_i$ is the maximum modal contribution. It is the maximum of normalized displacement scaling factor.

The term $\sum_{l=1}^{s} \Phi_i^l R_i^l$ takes into account the repulsive force on the contacted nodes that occurs when the moving element strikes the fixed element, and transfers this force into

modal coordinates. The step function *u(x)* is employed to guarantee that the repulsive force occurs only when the modal shape node of the moving electrode penetrates the fixed electrode. The exponential mathematical expression of such force has been chosen to model its extreme variation as a function of position, while maintaining continuity of the total force acting on the moving plate and its derivative. The continuity of the force and its derivative is a necessary condition to have a stable numerical solution of the equation. The value of the parameters α and β determines the steepness of the variation of the repulsive force as a function of the modal position and so the default values are 10^8 and 3, respectively.

Appendix B

MEMS Fabrication Techniques

This section describes a brief introduction to fabrication techniques which are commonly used in three-dimensional MEMS designs.

Conventional IC Fabrication process

Conventional IC fabrication process uses both chemical and photolithography etching.

The stages of the process are to cover the wafer with thin-film such as Silicon Oxide (SiO_2) for silicon technology process or Silicon Nitride (Si_3N_4) for Gallium Arsenide technology process on which a pattern created.

The second stage is to coat the thin-film with a photoresist which is a light sensitive material.

The third stage is to apply a photomask over the wafer, where the photoresist is exposed through the mask using a high powered ultraviolet (UV) light wherever the oxide needs to be removed.

The photoresist is developed similar to how order nary photographic film technique for the final stage. The parts which have been exposed to the UV light can affect differently depending on the polarity of the photoresist. If the resist is positive the part which have been exposed to the UV light will be washed away and expose the SiO_2. If the resist is negative, the exposed area will be hardened and the remaining parts will be washed away.

Conventional IC fabrication process are designed for 2D wafer fabrication. However, MEMS are 3D structures which requires extra layers which can be carried via bulk Micromachining and surface Micromachining (W. Bacher et al. 1995).

Bulk Micromachining

Bulk micromachining is a mature technology which was developed in the late 1950s for the production of silicon pressure sensors. Later techniques emerged to aim for 3D MEMS structures, such LIGA (RoentgenLIthographie, Galvanik, Abformung which is a German acronym for X-Ray lithography, Galvanic and Moulding) Mechanical structures can be addressed by bulk micromachining via wafer bulk. The technology is based on photolithography and etching, which is used in IC batch processing, to provide the ability for creating complex system designs.

Bulk micromachining uses a combination of anisotropic (highly directional) with isotropic (non-directional) etchants and the orientation of the wafer's crystals. The rates of the etching can be manipulated to create a wide variety of mechanical structures within the wafer bulk.

It is possible to form deep cavities using heavily doped regions which etched slowly using PN junctions to stop the etching process. Deep cavities provide an essential role for specific MEMS devices such as diaphragms for pressure sensors and speakers, and electromechanical capacitive bridge switches.

Wafer crystallographic planes determines the maximum aspect ratios and restricts the geometry to relatively large structures compared to other micromachining technologies which is a limitation of bulk micromachining.

Surface Micromachining

For surface micromachining patterned layers of thin-film materials are deposited onto the wafer substrate and are called 'sacrificial material'. On the other hand, the material remaining is considered as 'structural material' in order to create a circuit. To create a micromachined structure on the surface of the wafer, a combination of thin-film deposition, wet and dry etching is applied.

During the 1960's and 70's, scientist and engineers at Westinghouse Electric Corporation at Pennsylvania, created MEMS switches and electronic filters which used resonant mechanical thin-film metal structures. While at IBM Corporation,

electrostatically actuated MEMS switches and sensors were development using thin-film oxide structures.

1967 the paper “The Resonant Gate Transistor” (H. C. Nathanson et al. 1967) describes using sacrificial materials to allow the gate of a transistor to be released. This demonstrated the use of silicon fabrication techniques to remove mechanical systems from a silicon substrate. The next stage in development was the use of polysilicon as a structural material, and silicon dioxide as the sacrificial material using hydrofluoric acid for etching.

This paved the way for developing free moving mechanical gears, spring, sliding structures and balanced beams, which used polysilicon structures with silicon dioxide sacrificial materials. As MEMS application requires an interface with electronic circuity, integration of both technologies (mechanical and electronic systems) were to be created simultaneous. The most successful foundry process for surface micromachining is known as Multi-user MEMS processes (MUMPs). An alternative approach to silicon substrate material was the use of gallium arsenide (GaAs) for surface micromachining technique in creating microwave MEMS devices for use with MMICs (Monolithic Microwave Integrated Circuits) this resulted in process for creating a microwave actuator (MIMAC) (L. E. Larson et al. 1991b) . Later research in cost reduction of manufacturing process for microwave integrated circuits focused on alumina based substrates which possessed low loss properties(De Los Santos 2004) .

Fusion Bonding

Other approaches to create complex systems on bulk micromachining is to create each layer of the system and bond it together. Fusion bonding technique integrates the use of multiple wafers and relies on the atomic bonds between each wafer either directly or indirectly via thin film such as silicon dioxide, in order to fuse the layers together. The technique originally helped to atomically bond two monocrystalline layers to produce similar mechanical and electrical characteristics to a single layer.

The technique requires high temperatures, such as silicon would need 1100 ºC in order for fusion bonding to occur and is necessary to form the bonding process before any

electrical IC processing in order to avoid problems in the doping profiles and any metallization. Although fusion bonding is an emerging technology process compared to the processes explained in this thesis, it provides great commercial potential for sensors, resonators and accelerometers systems.

Other processes such as silicon-on-insulator (SOI) is used for applications which require stress-free and high mechanical quality, of a single-crystal silicon in order to achieve improved device performance (G. Piazza et al. 2003).

LIGA and Sacrificial LIGA

The process for LIGA is to create a mold of the structure and release of the substrate surface, this in turn allows the creation of the desired three-dimensional structure using the following process:

The first step is to apply a thick layer of photoresist over the metal substrate, where the mask will be patterned and developed using exposure of high energy X-Ray radiation, the pattern created from the exposure of the photoresist, would then be used as a mold plate. Lastly the molds themselves can be either conductive or magnetic, which is used to affect the way the molded structure is created using reactive, thermoplastic or emboss molding methods. Polymers like polyimide, polymethyl methacrylate are usually used by these molds.

The LIGA process provides high resolution allowing very thin vertical structures to be formed, but the process is limited due to the requirement of a synchrotron X-ray equipment. Although a compromise has been devised combining features of LIGA with surface micromachining, which alleviate the requirement of X-ray exposure (J. Bryzek et al. 1994). one named process was called sacrificial LIGA (Li et al. Nov. 1999), which replaces the use of a thick photoresist by using a polyimide as an electroplating mold. This allowed compatibility with conventional IC batch processing.

Appendix C

Result Tables

Displacement vs Voltage

Table 9.1: HRL Cantilever SPST Switch

Voltage	Displacement
0	-0.0213928
1	-0.0225837
2	-0.0261641
3	-0.0321574
4	-0.0406032
5	-0.0515584
6	-0.0650993
7	-0.0813234
8	-0.100353
9	-0.122386
10	-0.147553
11	-0.176118
12	-0.208377
13	-0.244702
14	-0.285572
15	-0.331602
16	-0.383866
17	-0.443181
18	-0.511361
19	-0.591459
20	-0.687805
21	-0.80984
22	-0.985362
23	-1.49718
24	-1.4982
25	-1.49927
26	-1.50009
27	-1.50084
28	-1.50163
29	-1.50246
30	-1.50334

Table 9.2: Scaled Down version of HRL Cantilever SPST Switch by 10 times

Voltage	Displacement
0	0.000506852
0.1	0.000380833
0.2	1.94E-06
0.3	-0.000632386
0.4	-0.00152646
0.5	-0.0026865
0.6	-0.00412084
0.7	-0.00584016
0.8	-0.00785787
0.9	-0.0101907
1	-0.0128592
1.1	-0.0158891
1.2	-0.0193119
1.3	-0.0231676
1.4	-0.027507
1.5	-0.0323954
1.6	-0.0379197
1.7	-0.0444553
1.8	-0.0518049
1.9	-0.0604199
2	-0.0711823
2.1	-0.0846754
2.2	-0.106718
2.3	-0.153537
2.4	-0.15354
2.5	-0.153542

Table 9.3: Straight Pivot Seesaw DPDT Switch v1

Voltage	Displacement
0	0
1	-0.00203441
2	-0.00816022
3	-0.018446
4	-0.0330096
5	-0.0520219
6	-0.0757183
7	-0.104475
8	-0.138636
9	-0.178783
10	-0.225644
11	-0.280201
12	-0.344053
13	-0.418941
14	-0.508466
15	-0.617514
16	-0.757965
17	-0.959354
18	-1.00432
19	-1.00432
20	-1.00432

Table 9.4: Straight Pivot Seesaw DPDT Switch v2

Voltage	Displacement
0	0
0.1	-9.28E-05
0.2	-0.000371456
0.3	-0.000836028
0.4	-0.00148688
0.5	-0.00232451
0.6	-0.00334953
0.7	-0.00456262
0.8	-0.0059647
0.9	-0.00755689
1	-0.00934021
1.1	-0.011316
1.2	-0.0134859
1.3	-0.0158514
1.4	-0.0184144

1.5	-0.0211769
1.6	-0.024141
1.7	-0.0273088
1.8	-0.0306834
1.9	-0.0342669
2	-0.0380632
2.1	-0.0420743
2.2	-0.0463045
2.3	-0.0507572
2.4	-0.0554365
2.5	-0.0603467
2.6	-0.0654923
2.7	-0.0708785
2.8	-0.0765103
2.9	-0.0823925
3	-0.0885333
3.1	-0.0949371
3.2	-0.101613
3.3	-0.108567
3.4	-0.115806
3.5	-0.123342
3.6	-0.131184
3.7	-0.139341
3.8	-0.147824
3.9	-0.156645
4	-0.16582
4.1	-0.175489
4.2	-0.185436
4.3	-0.195782
4.4	-0.206551
4.5	-0.217764
4.6	-0.229446
4.7	-0.241623
4.8	-0.254322
4.9	-0.267583
5	-0.281438
5.1	-0.295936
5.2	-0.311122
5.3	-0.327054
5.4	-0.343802
5.5	-0.361721
5.6	-0.380418
5.7	-0.400226
5.8	-0.421292

5.9	-0.443794
6	-0.467965
6.1	-0.494554
6.2	-0.523243
6.3	-0.554944
6.4	-0.591247
6.5	-0.633366
6.6	-0.684791
6.7	-0.754439
6.8	-0.875656
6.9	-1.00408
7	-1.00408
7.1	-1.00408
7.2	-1.00408
7.3	-1.00408
7.4	-1.00408
7.5	-1.00408
7.6	-1.00408
7.7	-1.00408
7.8	-1.00408
7.9	-1.00408
8	-1.00408
8.1	-1.00408
8.2	-1.00408
8.3	-1.00408
8.4	-1.00408
8.5	-1.00408
8.6	-1.00408
8.7	-1.00408
8.8	-1.00408
8.9	-1.00408
9	-1.00408
9.1	-1.00408
9.2	-1.00408
9.3	-1.00408
9.4	-1.00408
9.5	-1.00408
9.6	-1.00408
9.7	-1.00408
9.8	-1.00408
9.9	-1.00408
10	-1.00408
10	-1.00408

Table 9.5: ‘S’ Shaped Pivot Seesaw DPDT Switch

Voltage	Displacement
0	0
0.2	0.00267086
0.4	0.0107132
0.6	0.0242175
0.8	0.043339
1	0.0683067
1.2	0.0994673
1.4	0.137212
1.6	0.182117
1.8	0.234928
2	0.296639
2.2	0.368758
2.4	0.453049
2.6	0.552441
2.8	0.671885
3	0.819415
3.2	1.01278
3.4	1.31182
3.6	2.71099
3.8	2.71099
4	2.71099
4.2	2.71099
4.4	2.71099
4.6	2.71099
4.8	2.71099
5	2.71099

Table 9.6: ‘S’ Shaped Pivot with Delta Angled Electrostatic Plates DPDT Switch

Voltage	Displacement
0	0
0.01	3.76E-05
0.02	0.000150321
0.03	0.000338256
0.04	0.000601429
0.05	0.000939897
0.06	0.00135375
0.07	0.00184308
0.08	0.002408
0.09	0.00304867

0.1	0.00376521
0.11	0.00455783
0.12	0.00542667
0.13	0.00637197
0.14	0.00739402
0.15	0.00849293
0.16	0.0096691
0.17	0.0109227
0.18	0.0122542
0.19	0.0136638
0.2	0.0151519
0.21	0.0167189
0.22	0.018365
0.65	0.174461
0.66	0.180425
0.67	0.186575
0.68	0.192847
0.69	0.199272
0.7	0.205842
0.71	0.212564
0.72	0.219435
0.73	0.226455
0.74	0.233641
0.75	0.240994
0.76	0.248514
0.77	0.25621
0.78	0.26423
0.79	0.272299
0.8	0.280559
0.81	0.289014
0.82	0.297677
0.83	0.306545
0.84	0.315628
0.85	0.324898
0.86	0.334436
0.87	0.344215
0.88	0.354243
0.89	0.364535
0.9	0.375097
0.91	0.38594
0.92	0.39708
0.93	0.408523
0.94	0.420296
0.95	0.432408

0.96	0.444876
0.97	0.457729
0.98	0.470975
0.99	0.484561
1	0.498673
1.01	0.513569
1.02	0.528722
1.03	0.544424
1.04	0.560727
1.05	0.577707
1.06	0.59537
1.07	0.613793
1.08	0.633068
1.09	0.65328
1.1	0.674976
1.11	0.697514
1.12	0.721414
1.13	0.746895
1.14	0.774757
1.15	0.804486
1.16	0.836984
1.17	0.873786
1.18	0.915654
1.19	0.965075
1.2	1.02916
1.21	1.13269
1.22	2.22427
1.23	2.70914
1.24	2.7092
1.25	2.70926
1.26	2.70932
1.27	2.70938
1.28	2.70943
1.29	2.70949
1.3	2.70955
1.31	2.70962
1.32	2.70968
1.33	2.70974
1.34	2.7098
1.35	2.70986
1.36	2.70993
1.37	2.70999
1.38	2.71006
1.39	2.71012

1.4	2.71019
1.41	2.71026
1.42	2.71032
1.43	2.71039
1.44	2.71046
1.45	2.71053
1.46	2.7106
1.47	2.71067
1.48	2.71074
1.49	2.71081
1.5	2.71088
1.51	2.71095
1.52	2.71103
1.53	2.7111
1.54	2.71117
1.55	2.71125
1.56	2.71132
1.57	2.7114
1.58	2.71148
1.59	2.71155
1.6	2.71163
1.61	2.71171
1.62	2.71179
1.63	2.71187
1.64	2.71195
1.65	2.71203
1.66	2.71211
1.67	2.7122
1.68	2.71228
1.69	2.71236
1.7	2.71245
1.71	2.71253
1.72	2.71262
1.73	2.71271
1.74	2.71279
1.75	2.71288
1.76	2.71297
1.77	2.71306
1.78	2.71315
1.79	2.71324
1.8	2.71333

Table 9.7: ‘S’ Shaped Split Pivot with Delta Angled Electrostatic Plates DPDT Switch

Voltage	Displacement
0	0
0.01	-0.000044
0.02	-0.000176
0.03	-0.000396
0.04	-0.000704
0.05	-0.0011
0.06	-0.001585
0.07	-0.002158
0.08	-0.002819
0.09	-0.00357
0.1	-0.004409
0.11	-0.005338
0.12	-0.006356
0.13	-0.007463
0.14	-0.008661
0.15	-0.00995
0.16	-0.011329
0.17	-0.012799
0.18	-0.014361
0.19	-0.016015
0.2	-0.017762
0.21	-0.019601
0.22	-0.021534
0.23	-0.023562
0.24	-0.025684
0.25	-0.027902
0.26	-0.030216
0.27	-0.032627
0.28	-0.035135
0.29	-0.037742
0.3	-0.040448
0.31	-0.043254
0.32	-0.046161
0.33	-0.04917
0.34	-0.052282
0.35	-0.055498
0.36	-0.058818
0.37	-0.062246
0.38	-0.06578
0.39	-0.069423

0.4	-0.073177
0.41	-0.077041
0.42	-0.081018
0.43	-0.08511
0.44	-0.089316
0.45	-0.09364
0.46	-0.098081
0.47	-0.102643
0.48	-0.107333
0.49	-0.112142
0.5	-0.117075
0.51	-0.122143
0.52	-0.127336
0.53	-0.132666
0.54	-0.13813
0.55	-0.143733
0.56	-0.14947
0.57	-0.15535
0.58	-0.161383
0.59	-0.167564
0.6	-0.173899
0.61	-0.180389
0.62	-0.187046
0.63	-0.193849
0.64	-0.200828
0.65	-0.207979
0.66	-0.215308
0.67	-0.222808
0.68	-0.230497
0.69	-0.238378
0.7	-0.246454
0.71	-0.254882
0.72	-0.263374
0.73	-0.272089
0.74	-0.281024
0.75	-0.290189
0.76	-0.299598
0.77	-0.309248
0.78	-0.319117
0.79	-0.329283
0.8	-0.339729
0.81	-0.35046
0.82	-0.36149
0.83	-0.372834

0.84	-0.384507
0.85	-0.396522
0.86	-0.408893
0.87	-0.421645
0.88	-0.434797
0.89	-0.448373
0.9	-0.462395
0.91	-0.476831
0.92	-0.491804
0.93	-0.507657
0.94	-0.523826
0.95	-0.540629
0.96	-0.558113
0.97	-0.576369
0.98	-0.595422
0.99	-0.61537
1	-0.636309
1.01	-0.658786
1.02	-0.682161
1.03	-0.707013
1.04	-0.733538
1.05	-0.762049
1.06	-0.793594
1.07	-0.827643
1.08	-0.866244
1.09	-0.910341
1.1	-0.962745
1.11	-1.03153
1.12	-1.14854
1.13	-2.71102
1.14	-2.71102
1.15	-2.71102
1.16	-2.71102
1.17	-2.71102
1.18	-2.71102
1.19	-2.71102
1.2	-2.71102
1.21	-2.71102
1.22	-2.71102
1.23	-2.71102
1.24	-2.71102
1.25	-2.71102

Elastic Recovery

Table 9.8: HRL Cantilever SPST Switch

Time (s)	Displacement (μm)
5.00E-06	-1.50832
1.00E-05	-1.51043
1.50E-05	-1.52313
2.00E-05	-1.52313
2.50E-05	-1.52313
3.00E-05	-1.52313
3.50E-05	-1.52313
4.00E-05	-1.52313
4.50E-05	-1.52313
5.00E-05	-1.52312
5.50E-05	-1.52312
6.00E-05	-1.52312
6.50E-05	-1.52312
7.00E-05	-1.52312
7.50E-05	-1.52312
8.00E-05	-1.52312
8.50E-05	-1.52312
9.00E-05	-1.52312
9.50E-05	-1.52312
0.0001	-1.52312
0.000105	-1.52312
0.00011	-1.52312
0.000115	-1.52312
0.00012	-1.52312
0.000125	-1.52312
0.00013	-1.52312
0.000135	-1.52312
0.00014	-1.52312
0.000145	-1.52312
0.00015	-1.52312
0.000155	-1.52312
0.00016	-1.52312
0.000165	-1.52312
0.00017	-1.52312
0.000175	-1.52312
0.00018	-1.52312
0.000185	-1.52312

0.00019	-1.52312
0.000195	-1.52312
0.0002	-1.52312
0.000205	-1.52312
0.00021	-1.52312
0.000215	-1.52312
0.00022	-1.52312
0.000225	-1.52313
0.00023	-1.52313
0.000235	-1.52313
0.00024	-1.51188
0.000245	-1.49083
0.00025	-1.46182
0.000255	-1.42585
0.00026	-1.38409
0.000265	-1.33775
0.00027	-1.28801
0.000275	-1.23596
0.00028	-1.18259
0.000285	-1.1288
0.00029	-1.07534
0.000295	-1.02289
0.0003	-0.971983
0.000305	-0.923105
0.00031	-0.876532
0.000315	-0.832281
0.00032	-0.790244
0.000325	-0.750306
0.00033	-0.712362
0.000335	-0.67631
0.00034	-0.642056
0.000345	-0.609509
0.00035	-0.578583
0.000355	-0.549198
0.00036	-0.521277
0.000365	-0.494745
0.00037	-0.469535
0.000375	-0.445579
0.00038	-0.422816
0.000385	-0.401186
0.00039	-0.380633
0.000395	-0.361102
0.0004	-0.342543
0.000405	-0.324907

0.00041	-0.308149
0.000415	-0.292225
0.00042	-0.277093
0.000425	-0.262713
0.00043	-0.249049
0.000435	-0.236064
0.00044	-0.223726
0.000445	-0.212001
0.00045	-0.200859
0.000455	-0.190271
0.00046	-0.18021
0.000465	-0.170649
0.00047	-0.161564
0.000475	-0.15293
0.00048	-0.144726
0.000485	-0.13693
0.00049	-0.129521
0.000495	-0.122481
0.0005	-0.115791
0.000505	-0.109433
0.00051	-0.103392
0.000515	-0.0976511
0.00052	-0.0921956
0.000525	-0.0870114
0.00053	-0.0820849
0.000535	-0.0774033
0.00054	-0.0729545
0.000545	-0.0687269
0.00055	-0.0647095
0.000555	-0.0608918
0.00056	-0.0572639
0.000565	-0.0538164
0.00057	-0.0505402
0.000575	-0.047427
0.00058	-0.0444685
0.000585	-0.0416571
0.00059	-0.0389855
0.000595	-0.0364466
0.0006	-0.034034
0.000605	-0.0317413
0.00061	-0.0295626
0.000615	-0.0274922
0.00062	-0.0255248
0.000625	-0.0236551

0.00063	-0.0218784
0.000635	-0.02019
0.00064	-0.0185855
0.000645	-0.0170608
0.00065	-0.0156119
0.000655	-0.014235
0.00066	-0.0129266
0.000665	-0.0116831
0.00067	-0.0105016
0.000675	-0.00937869
0.00068	-0.00831165
0.000685	-0.00729764
0.00069	-0.00633405
0.000695	-0.00541834
0.0007	-0.00454816
0.000705	-0.00372123
0.00071	-0.00293541
0.000715	-0.00218865
0.00072	-0.001479
0.000725	-0.000804635
0.00073	-0.000163787
0.000735	0.000445207
0.00074	0.00102393
0.000745	0.00157389
0.00075	0.00209651
0.000755	0.00259315
0.00076	0.00306511
0.000765	0.0035136
0.00077	0.00393981
0.000775	0.00434483
0.00078	0.00472972
0.000785	0.00509547
0.00079	0.00544305
0.000795	0.00577335
0.0008	0.00608723
0.000805	0.00638552
0.00081	0.00666897
0.000815	0.00693834
0.00082	0.00719432
0.000825	0.00743757
0.00083	0.00766873
0.000835	0.00788841
0.00084	0.00809716
0.000845	0.00829554

0.00085	0.00848406
0.000855	0.00866321
0.00086	0.00883346
0.000865	0.00899524
0.00087	0.00914898
0.000875	0.00929508
0.00088	0.00943392
0.000885	0.00956585
0.00089	0.00969123
0.000895	0.00981038
0.0009	0.00992361
0.000905	0.0100312
0.00091	0.0101335
0.000915	0.0102306
0.00092	0.010323
0.000925	0.0104107
0.00093	0.0104941
0.000935	0.0105733
0.00094	0.0106486
0.000945	0.0107202
0.00095	0.0107882
0.000955	0.0108528
0.00096	0.0109143
0.000965	0.0109726
0.00097	0.0110281
0.000975	0.0110808
0.00098	0.0111309
0.000985	0.0111785
0.00099	0.0112237
0.000995	0.0112667
0.001	0.0113075
0.001005	0.0113463
0.00101	0.0113832
0.001015	0.0114183
0.00102	0.0114516
0.001025	0.0114832
0.00103	0.0115133
0.001035	0.0115419
0.00104	0.0115691
0.001045	0.0115949
0.00105	0.0116194
0.001055	0.0116427
0.00106	0.0116649
0.001065	0.0116859

0.00107	0.0117059
0.001075	0.0117249
0.00108	0.011743
0.001085	0.0117602
0.00109	0.0117765
0.001095	0.011792
0.0011	0.0118067
0.001105	0.0118207
0.00111	0.0118341
0.001115	0.0118467
0.00112	0.0118587
0.001125	0.0118701
0.00113	0.011881
0.001135	0.0118913
0.00114	0.0119011
0.001145	0.0119104
0.00115	0.0119193
0.001155	0.0119277
0.00116	0.0119357
0.001165	0.0119433
0.00117	0.0119505
0.001175	0.0119573
0.00118	0.0119639
0.001185	0.01197
0.00119	0.0119759
0.001195	0.0119815
0.0012	0.0119868
0.001205	0.0119919
0.00121	0.0119967
0.001215	0.0120013
0.00122	0.0120056
0.001225	0.0120097
0.00123	0.0120136
0.001235	0.0120173
0.00124	0.0120209
0.001245	0.0120242
0.00125	0.0120274
0.001255	0.0120305
0.00126	0.0120333
0.001265	0.0120361
0.00127	0.0120387
0.001275	0.0120412
0.00128	0.0120435
0.001285	0.0120458

0.00129	0.0120479
0.001295	0.0120499
0.0013	0.0120518
0.001305	0.0120536
0.00131	0.0120554
0.001315	0.012057
0.00132	0.0120586
0.001325	0.0120601
0.00133	0.0120615
0.001335	0.0120628
0.00134	0.0120641
0.001345	0.0120653
0.00135	0.0120665
0.001355	0.0120676
0.00136	0.0120686
0.001365	0.0120696
0.00137	0.0120705
0.001375	0.0120714
0.00138	0.0120723
0.001385	0.0120731
0.00139	0.0120738
0.001395	0.0120746
0.0014	0.0120753
0.001405	0.0120759
0.00141	0.0120765
0.001415	0.0120771
0.00142	0.0120777
0.001425	0.0120782
0.00143	0.0120787
0.001435	0.0120792
0.00144	0.0120797
0.001445	0.0120801
0.00145	0.0120805
0.001455	0.0120809
0.00146	0.0120813
0.001465	0.0120817
0.00147	0.012082
0.001475	0.0120823
0.00148	0.0120826
0.001485	0.0120829
0.00149	0.0120832
0.001495	0.0120835
0.0015	0.0120837
0.001505	0.0120839

0.00151	0.0120842
0.001515	0.0120844
0.00152	0.0120846
0.001525	0.0120848
0.00153	0.012085
0.001535	0.0120851
0.00154	0.0120853
0.001545	0.0120855
0.00155	0.0120856
0.001555	0.0120858
0.00156	0.0120859
0.001565	0.012086
0.00157	0.0120861
0.001575	0.0120863
0.00158	0.0120864
0.001585	0.0120865
0.00159	0.0120866
0.001595	0.0120867
0.0016	0.0120868
0.001605	0.0120868
0.00161	0.0120869
0.001615	0.012087
0.00162	0.0120871
0.001625	0.0120871
0.00163	0.0120872
0.001635	0.0120873
0.00164	0.0120873
0.001645	0.0120874
0.00165	0.0120874
0.001655	0.0120875
0.00166	0.0120875
0.001665	0.0120876
0.00167	0.0120876
0.001675	0.0120877
0.00168	0.0120877
0.001685	0.0120878
0.00169	0.0120878
0.001695	0.0120878
0.0017	0.0120879
0.001705	0.0120879
0.00171	0.0120879
0.001715	0.0120879
0.00172	0.012088
0.001725	0.012088

0.00173	0.012088
0.001735	0.012088
0.00174	0.0120881
0.001745	0.0120881
0.00175	0.0120881
0.001755	0.0120881
0.00176	0.0120881
0.001765	0.0120882
0.00177	0.0120882
0.001775	0.0120882
0.00178	0.0120882
0.001785	0.0120882
0.00179	0.0120882
0.001795	0.0120882
0.0018	0.0120883
0.001805	0.0120883
0.00181	0.0120883
0.001815	0.0120883
0.00182	0.0120883
0.001825	0.0120883
0.00183	0.0120883
0.001835	0.0120883
0.00184	0.0120883
0.001845	0.0120883
0.00185	0.0120883
0.001855	0.0120884
0.00186	0.0120884
0.001865	0.0120884
0.00187	0.0120884
0.001875	0.0120884
0.00188	0.0120884
0.001885	0.0120884
0.00189	0.0120884
0.001895	0.0120884
0.0019	0.0120884
0.001905	0.0120884
0.00191	0.0120884
0.001915	0.0120884
0.00192	0.0120884
0.001925	0.0120884
0.00193	0.0120884
0.001935	0.0120884
0.00194	0.0120884
0.001945	0.0120884

0.00195	0.0120884
0.001955	0.0120884
0.00196	0.0120884
0.001965	0.0120884
0.00197	0.0120884
0.001975	0.0120884
0.00198	0.0120884
0.001985	0.0120884
0.00199	0.0120884
0.001995	0.0120884
0.002	0.0120885

Table 9.9: Scaled Down version HRL Cantilever SPST Switch by 10 times

Time (s)	**Displacement (µm)**
1.00E-05	-0.144447
2.00E-05	-0.140868
3.00E-05	-0.144266
4.00E-05	-0.148194
5.00E-05	-0.151372
6.00E-05	-0.151369
7.00E-05	-0.151362
8.00E-05	-0.151357
9.00E-05	-0.151352
0.0001	-0.151347
0.00011	-0.151343
0.00012	-0.151339
0.00013	-0.151336
0.00014	-0.151333
0.00015	-0.15133
0.00016	-0.151328
0.00017	-0.151326
0.00018	-0.151324
0.00019	-0.151322
0.0002	-0.15132
0.00021	-0.151319
0.00022	-0.151326
0.00023	-0.151346
0.00024	-0.147109
0.00025	-0.140439
0.00026	-0.131563
0.00027	-0.12162
0.00028	-0.110936
0.00029	-0.100306
0.0003	-0.0899939

0.00031	-0.0804343
0.00032	-0.0716975
0.00033	-0.063829
0.00034	-0.05671
0.00035	-0.050294
0.00036	-0.044493
0.00037	-0.0392607
0.00038	-0.0345321
0.00039	-0.0302649
0.0004	-0.0264095
0.00041	-0.0229293
0.00042	-0.0197855
0.00043	-0.0169471
0.00044	-0.0143832
0.00045	-0.0120682
0.00046	-0.00997716
0.00047	-0.0080889
0.00048	-0.00638344
0.00049	-0.00484326
0.0005	-0.00345221
0.00051	-0.00219593
0.00052	-0.00106128
0.00053	-3.65E-05
0.00054	0.00088897
0.00055	0.00172485
0.00056	0.0024798
0.00057	0.00316164
0.00058	0.00377746
0.00059	0.00433365
0.0006	0.004836
0.00061	0.0052897
0.00062	0.00569948
0.00063	0.00606958
0.00064	0.00640385
0.00065	0.00670576
0.00066	0.00697845
0.00067	0.00722473
0.00068	0.00744717
0.00069	0.00764808
0.0007	0.00782953
0.00071	0.00799343
0.00072	0.00814145
0.00073	0.00827515
0.00074	0.0083959

0.00075	0.00850497
0.00076	0.00860347
0.00077	0.00869245
0.00078	0.0087728
0.00079	0.00884539
0.0008	0.00891094
0.00081	0.00897015
0.00082	0.00902363
0.00083	0.00907193
0.00084	0.00911555
0.00085	0.00915496
0.00086	0.00919055
0.00087	0.00922269
0.00088	0.00925172
0.00089	0.00927795
0.0009	0.00930163
0.00091	0.00932302
0.00092	0.00934234
0.00093	0.00935979
0.00094	0.00937556
0.00095	0.00938979
0.00096	0.00940265
0.00097	0.00941427
0.00098	0.00942475
0.00099	0.00943423
0.001	0.00944279
0.00101	0.00945052
0.00102	0.0094575
0.00103	0.0094638
0.00104	0.0094695
0.00105	0.00947464
0.00106	0.00947929
0.00107	0.00948348
0.00108	0.00948727
0.00109	0.0094907
0.0011	0.00949379
0.00111	0.00949658
0.00112	0.0094991
0.00113	0.00950138
0.00114	0.00950344
0.00115	0.0095053
0.00116	0.00950698
0.00117	0.00950849
0.00118	0.00950986

0.00119	0.0095111
0.0012	0.00951222
0.00121	0.00951323
0.00122	0.00951414
0.00123	0.00951496
0.00124	0.0095157
0.00125	0.00951638
0.00126	0.00951698
0.00127	0.00951753
0.00128	0.00951802
0.00129	0.00951847
0.0013	0.00951888
0.00131	0.00951924
0.00132	0.00951957
0.00133	0.00951987
0.00134	0.00952014
0.00135	0.00952038
0.00136	0.0095206
0.00137	0.00952079
0.00138	0.00952097
0.00139	0.00952114
0.0014	0.00952128
0.00141	0.00952141
0.00142	0.00952153
0.00143	0.00952164
0.00144	0.00952174
0.00145	0.00952182
0.00146	0.0095219
0.00147	0.00952197
0.00148	0.00952204
0.00149	0.0095221
0.0015	0.00952215
0.00151	0.0095222
0.00152	0.00952224
0.00153	0.00952228
0.00154	0.00952231
0.00155	0.00952235
0.00156	0.00952238
0.00157	0.0095224
0.00158	0.00952242
0.00159	0.00952245
0.0016	0.00952246
0.00161	0.00952248
0.00162	0.0095225

0.00163	0.00952251
0.00164	0.00952252
0.00165	0.00952254
0.00166	0.00952255
0.00167	0.00952256
0.00168	0.00952256
0.00169	0.00952257
0.0017	0.00952258
0.00171	0.00952258
0.00172	0.00952259
0.00173	0.0095226
0.00174	0.0095226
0.00175	0.0095226
0.00176	0.00952261
0.00177	0.00952261
0.00178	0.00952261
0.00179	0.00952262
0.0018	0.00952262
0.00181	0.00952262
0.00182	0.00952262
0.00183	0.00952263
0.00184	0.00952263
0.00185	0.00952263
0.00186	0.00952263
0.00187	0.00952263
0.00188	0.00952263
0.00189	0.00952263
0.0019	0.00952263
0.00191	0.00952263
0.00192	0.00952264
0.00193	0.00952264
0.00194	0.00952264
0.00195	0.00952264
0.00196	0.00952264
0.00197	0.00952264
0.00198	0.00952264
0.00199	0.00952264
0.002	0.00952264

Table 9.10: Straight Pivot Seesaw DPDT Switch v1 (Lower Release Contact)

Time (s)	**Displacement (µm)**
2.00E-05	-1.00613

4.00E-05	-1.00614
6.00E-05	-1.00614
8.00E-05	-1.00614
0.0001	-1.00614
0.00012	-1.00614
0.00014	-1.00614
0.00016	-1.00614
0.00018	-1.00614
0.0002	-1.00614
0.00022	-0.985015
0.00024	-0.905994
0.00026	-0.792749
0.00028	-0.666612
0.0003	-0.547666
0.00032	-0.446374
0.00034	-0.36357
0.00036	-0.296253
0.00038	-0.241414
0.0004	-0.196777
0.00042	-0.160404
0.00044	-0.130777
0.00046	-0.106632
0.00048	-0.0869539
0.0005	-0.0709145
0.00052	-0.057838
0.00054	-0.0471771
0.00056	-0.0384835
0.00058	-0.0313943
0.0006	-0.0256122
0.00062	-0.0208964
0.00064	-0.0170495
0.00066	-0.0139115
0.00068	-0.0113515
0.0007	-0.00926281
0.00072	-0.00755866
0.00074	-0.00616818
0.00076	-0.00503355
0.00078	-0.00410767
0.0008	-0.0033521
0.00082	-0.00273549
0.00084	-0.00223225
0.00086	-0.00182155
0.00088	-0.00148634
0.0009	-0.00121274

0.00092	-0.000989429
0.00094	-0.000807153
0.00096	-0.000658368
0.00098	-0.000536918
0.001	-0.00043778
0.00102	-0.000356853
0.00104	-0.000290789
0.00106	-0.00023686
0.00108	-0.000192834
0.0011	-0.000156893
0.00112	-0.000127552
0.00114	-0.000103598
0.00116	-8.40E-05
0.00118	-6.81E-05
0.0012	-5.50E-05
0.00122	-4.44E-05
0.00124	-3.57E-05
0.00126	-2.86E-05
0.00128	-2.28E-05
0.0013	-1.81E-05
0.00132	-1.42E-05
0.00134	-1.11E-05
0.00136	-8.51E-06
0.00138	-6.41E-06
0.0014	-4.70E-06
0.00142	-3.30E-06
0.00144	-2.15E-06
0.00146	-1.22E-06
0.00148	-4.55E-07
0.0015	1.68E-07
0.00152	6.76E-07
0.00154	1.09E-06
0.00156	1.43E-06
0.00158	1.71E-06
0.0016	1.93E-06
0.00162	2.12E-06
0.00164	2.27E-06
0.00166	2.39E-06
0.00168	2.49E-06
0.0017	2.57E-06
0.00172	2.64E-06
0.00174	2.69E-06
0.00176	2.74E-06
0.00178	2.78E-06

0.0018	2.81E-06
0.00182	2.83E-06
0.00184	2.85E-06
0.00186	2.87E-06
0.00188	2.88E-06
0.0019	2.89E-06
0.00192	2.90E-06
0.00194	2.91E-06
0.00196	2.91E-06
0.00198	2.92E-06
0.002	2.92E-06

Table 9.11: Straight Pivot Seesaw DPDT Switch v1 (Upper Release Contact)

Time (s)	**Displacement (µm)**
2.00E-05	1.00577
4.00E-05	1.00577
6.00E-05	1.00577
8.00E-05	1.00577
0.0001	1.00577
0.00012	1.00577
0.00014	1.00577
0.00016	1.00577
0.00018	1.00577
0.0002	1.00577
0.00022	0.9847
0.00024	0.905867
0.00026	0.792658
0.00028	0.666607
0.0003	0.547654
0.00032	0.44638
0.00034	0.363564
0.00036	0.296256
0.00038	0.241411
0.0004	0.196778
0.00042	0.160402
0.00044	0.130777
0.00046	0.106631
0.00048	0.0869542
0.0005	0.070914
0.00052	0.0578382
0.00054	0.0471768
0.00056	0.0384835
0.00058	0.0313941

0.0006	0.0256123
0.00062	0.0208963
0.00064	0.0170495
0.00066	0.0139115
0.00068	0.0113514
0.0007	0.00926279
0.00072	0.00755866
0.00074	0.00616816
0.00076	0.00503354
0.00078	0.00410766
0.0008	0.00335209
0.00082	0.00273548
0.00084	0.00223225
0.00086	0.00182154
0.00088	0.00148634
0.0009	0.00121274
0.00092	0.000989427
0.00094	0.000807151
0.00096	0.000658366
0.00098	0.000536917
0.001	0.000437779
0.00102	0.000356852
0.00104	0.000290789
0.00106	0.000236859
0.00108	0.000192833
0.0011	0.000156893
0.00112	0.000127551
0.00114	0.000103598
0.00116	8.40E-05
0.00118	6.81E-05
0.0012	5.50E-05
0.00122	4.44E-05
0.00124	3.57E-05
0.00126	2.86E-05
0.00128	2.28E-05
0.0013	1.81E-05
0.00132	1.42E-05
0.00134	1.11E-05
0.00136	8.51E-06
0.00138	6.41E-06
0.0014	4.70E-06
0.00142	3.29E-06
0.00144	2.15E-06
0.00146	1.22E-06

0.00148	4.55E-07
0.0015	-1.68E-07
0.00152	-6.76E-07
0.00154	-1.09E-06
0.00156	-1.43E-06
0.00158	-1.71E-06
0.0016	-1.93E-06
0.00162	-2.12E-06
0.00164	-2.27E-06
0.00166	-2.39E-06
0.00168	-2.49E-06
0.0017	-2.57E-06
0.00172	-2.64E-06
0.00174	-2.70E-06
0.00176	-2.74E-06
0.00178	-2.78E-06
0.0018	-2.81E-06
0.00182	-2.83E-06
0.00184	-2.85E-06
0.00186	-2.87E-06
0.00188	-2.88E-06
0.0019	-2.89E-06
0.00192	-2.90E-06
0.00194	-2.91E-06
0.00196	-2.91E-06
0.00198	-2.92E-06
0.002	-2.92E-06

Table 9.12: Straight Pivot Seesaw DPDT Silicon and Copper v2 (Lower Contact Release)

Time (s)	**Displacement (µm)**
2.00E-05	-1.00614
4.00E-05	-1.00613
6.00E-05	-1.00614
8.00E-05	-1.00613
0.0001	-1.00614
0.00012	-1.00613
0.00014	-1.00614
0.00016	-1.00613
0.00018	-1.00614
0.0002	-1.00613
0.00022	-1.00614
0.00024	-0.95561

0.00026	-0.85337
0.00028	-0.725886
0.0003	-0.59997
0.00032	-0.490723
0.00034	-0.401043
0.00036	-0.327756
0.00038	-0.267891
0.0004	-0.218949
0.00042	-0.17896
0.00044	-0.146271
0.00046	-0.119558
0.00048	-0.0977225
0.0005	-0.0798766
0.00052	-0.0652895
0.00054	-0.053367
0.00056	-0.0436216
0.00058	-0.0356562
0.0006	-0.0291452
0.00062	-0.0238234
0.00064	-0.0194733
0.00066	-0.0159176
0.00068	-0.0130112
0.0007	-0.0106354
0.00072	-0.00869351
0.00074	-0.00710618
0.00076	-0.00580868
0.00078	-0.00474809
0.0008	-0.00388116
0.00082	-0.00317252
0.00084	-0.00259327
0.00086	-0.00211978
0.00088	-0.00173274
0.0009	-0.00141638
0.00092	-0.00115777
0.00094	-0.000946383
0.00096	-0.000773591
0.00098	-0.000632348
0.001	-0.000516893
0.00102	-0.000422519
0.00104	-0.000345375
0.00106	-0.000282316
0.00108	-0.000230771
0.0011	-0.000188637
0.00112	-0.000154196

0.00114	-0.000126043
0.00116	-0.00010303
0.00118	-8.42E-05
0.0012	-6.88E-05
0.00122	-5.63E-05
0.00124	-4.60E-05
0.00126	-3.76E-05
0.00128	-3.07E-05
0.0013	-2.51E-05
0.00132	-2.05E-05
0.00134	-1.68E-05
0.00136	-1.37E-05
0.00138	-1.12E-05
0.0014	-9.17E-06
0.00142	-7.49E-06
0.00144	-6.13E-06
0.00146	-5.01E-06
0.00148	-4.09E-06
0.0015	-3.35E-06
0.00152	-2.74E-06
0.00154	-2.24E-06
0.00156	-1.83E-06
0.00158	-1.49E-06
0.0016	-1.22E-06
0.00162	-9.98E-07
0.00164	-8.16E-07
0.00166	-6.67E-07
0.00168	-5.45E-07
0.0017	-4.46E-07
0.00172	-3.64E-07
0.00174	-2.98E-07
0.00176	-2.43E-07
0.00178	-1.99E-07
0.0018	-1.63E-07
0.00182	-1.33E-07
0.00184	-1.09E-07
0.00186	-8.88E-08
0.00188	-7.26E-08
0.0019	-5.94E-08
0.00192	-4.85E-08
0.00194	-3.97E-08
0.00196	-3.24E-08
0.00198	-2.65E-08
0.002	-2.17E-08

Table 9.13: Straight Pivot Seesaw DPDT Silicon and Copper v2 (Upper Contact Release)

Time (s)	Displacement (µm)
2.00E-05	1.00604
4.00E-05	1.00606
6.00E-05	1.00607
8.00E-05	1.00607
0.0001	1.00607
0.00012	1.00607
0.00014	1.00607
0.00016	1.00607
0.00018	1.00607
0.0002	1.00607
0.00022	1.00606
0.00024	0.95555
0.00026	0.85333
0.00028	0.725865
0.0003	0.599961
0.00032	0.490719
0.00034	0.401042
0.00036	0.327755
0.00038	0.267891
0.0004	0.218948
0.00042	0.17896
0.00044	0.146271
0.00046	0.119558
0.00048	0.0977222
0.0005	0.0798764
0.00052	0.0652893
0.00054	0.0533668
0.00056	0.0436215
0.00058	0.035656
0.0006	0.0291452
0.00062	0.0238233
0.00064	0.0194732
0.00066	0.0159175
0.00068	0.0130111
0.0007	0.0106354
0.00072	0.00869349
0.00074	0.00710616
0.00076	0.00580866
0.00078	0.00474808
0.0008	0.00388115
0.00082	0.00317251

0.00084	0.00259326
0.00086	0.00211977
0.00088	0.00173274
0.0009	0.00141637
0.00092	0.00115777
0.00094	0.00094638
0.00096	0.000773589
0.00098	0.000632346
0.001	0.000516892
0.00102	0.000422517
0.00104	0.000345374
0.00106	0.000282315
0.00108	0.00023077
0.0011	0.000188636
0.00112	0.000154195
0.00114	0.000126042
0.00116	0.00010303
0.00118	8.42E-05
0.0012	6.88E-05
0.00122	5.63E-05
0.00124	4.60E-05
0.00126	3.76E-05
0.00128	3.07E-05
0.0013	2.51E-05
0.00132	2.05E-05
0.00134	1.68E-05
0.00136	1.37E-05
0.00138	1.12E-05
0.0014	9.17E-06
0.00142	7.49E-06
0.00144	6.13E-06
0.00146	5.01E-06
0.00148	4.09E-06
0.0015	3.35E-06
0.00152	2.74E-06
0.00154	2.24E-06
0.00156	1.83E-06
0.00158	1.49E-06
0.0016	1.22E-06
0.00162	9.98E-07
0.00164	8.16E-07
0.00166	6.67E-07
0.00168	5.45E-07
0.0017	4.46E-07

0.00172	3.64E-07
0.00174	2.98E-07
0.00176	2.43E-07
0.00178	1.99E-07
0.0018	1.63E-07
0.00182	1.33E-07
0.00184	1.09E-07
0.00186	8.88E-08
0.00188	7.26E-08
0.0019	5.94E-08
0.00192	4.85E-08
0.00194	3.97E-08
0.00196	3.24E-08
0.00198	2.65E-08
0.002	2.17E-08

Table 9.14: ‘S’ Shaped Pivot Seesaw DPDT Switch (Lower Contact Release)

Time (s)	**Displacement (µm)**
2.00E-05	-2.71558
4.00E-05	-2.71572
6.00E-05	-2.71603
8.00E-05	-2.71614
0.0001	-2.71633
0.00012	-2.71641
0.00014	-2.71653
0.00016	-2.71656
0.00018	-2.71656
0.0002	-2.71656
0.00022	-2.71656
0.00024	-2.65728
0.00026	-2.47823
0.00028	-2.20767
0.0003	-1.91117
0.00032	-1.63515
0.00034	-1.39625
0.00036	-1.19263
0.00038	-1.01875
0.0004	-0.8702
0.00042	-0.743311
0.00044	-0.634928
0.00046	-0.542347
0.00048	-0.463268
0.0005	-0.395719
0.00052	-0.338022

0.00054	-0.288737
0.00056	-0.24664
0.00058	-0.210681
0.0006	-0.179966
0.00062	-0.15373
0.00064	-0.13132
0.00066	-0.112177
0.00068	-0.0958268
0.0007	-0.0818605
0.00072	-0.0699308
0.00074	-0.0597409
0.00076	-0.0510369
0.00078	-0.0436022
0.0008	-0.0372517
0.00082	-0.0318273
0.00084	-0.0271939
0.00086	-0.0232363
0.00088	-0.0198557
0.0009	-0.0169682
0.00092	-0.0145017
0.00094	-0.012395
0.00096	-0.0105954
0.00098	-0.00905834
0.001	-0.0077454
0.00102	-0.00662392
0.00104	-0.005666
0.00106	-0.00484777
0.00108	-0.00414886
0.0011	-0.00355188
0.00112	-0.00304196
0.00114	-0.0026064
0.00116	-0.00223436
0.00118	-0.00191658
0.0012	-0.00164514
0.00122	-0.00141328
0.00124	-0.00121524
0.00126	-0.00104608
0.00128	-0.000901591
0.0013	-0.000778171
0.00132	-0.00067275
0.00134	-0.000582703
0.00136	-0.000505789
0.00138	-0.000440091
0.0014	-0.000383974

0.00142	-0.000336041
0.00144	-0.000295098
0.00146	-0.000260126
0.00148	-0.000230255
0.0015	-0.000204739
0.00152	-0.000182945
0.00154	-0.000164329
0.00156	-0.000148428
0.00158	-0.000134846
0.0016	-0.000123245
0.00162	-0.000113335
0.00164	-0.000104871
0.00166	-9.76E-05
0.00168	-9.15E-05
0.0017	-8.62E-05
0.00172	-8.17E-05
0.00174	-7.78E-05
0.00176	-7.45E-05
0.00178	-7.17E-05
0.0018	-6.93E-05
0.00182	-6.73E-05
0.00184	-6.55E-05
0.00186	-6.40E-05
0.00188	-6.28E-05
0.0019	-6.17E-05
0.00192	-6.08E-05
0.00194	-6.00E-05
0.00196	-5.93E-05
0.00198	-5.87E-05
0.002	-5.82E-05

Table 9.15: ‘S’ Shaped Pivot Seesaw DPDT Switch (Upper Contact Release)

Time (s)	**Displacement (µm)**
2.00E-05	2.71656
4.00E-05	2.71656
6.00E-05	2.71656
8.00E-05	2.71656
0.0001	2.71656
0.00012	2.71656
0.00014	2.71656
0.00016	2.71656
0.00018	2.71656
0.0002	2.71656
0.00022	2.71656

0.00024	2.65703
0.00026	2.47786
0.00028	2.20718
0.0003	1.91067
0.00032	1.63464
0.00034	1.39576
0.00036	1.19217
0.00038	1.01832
0.0004	0.8698
0.00042	0.742948
0.00044	0.634595
0.00046	0.542048
0.00048	0.462998
0.0005	0.395479
0.00052	0.337807
0.00054	0.288546
0.00056	0.246471
0.00058	0.210532
0.0006	0.179834
0.00062	0.153614
0.00064	0.131218
0.00066	0.112089
0.00068	0.0957494
0.0007	0.0817929
0.00072	0.069872
0.00074	0.0596897
0.00076	0.0509925
0.00078	0.0435637
0.0008	0.0372183
0.00082	0.0317984
0.00084	0.027169
0.00086	0.0232147
0.00088	0.0198372
0.0009	0.0169522
0.00092	0.014488
0.00094	0.0123832
0.00096	0.0105854
0.00098	0.00904973
0.001	0.00773805
0.00102	0.00661767
0.00104	0.00566069
0.00106	0.00484328
0.00108	0.00414508
0.0011	0.0035487

0.00112	0.0030393
0.00114	0.0026042
0.00116	0.00223255
0.00118	0.0019151
0.0012	0.00164395
0.00122	0.00141234
0.00124	0.00121451
0.00126	0.00104553
0.00128	0.000901197
0.0013	0.000777913
0.00132	0.000672608
0.00134	0.000582661
0.00136	0.000505832
0.00138	0.000440207
0.0014	0.000384154
0.00142	0.000336275
0.00144	0.000295378
0.00146	0.000260446
0.00148	0.000230609
0.0015	0.000205123
0.00152	0.000183353
0.00154	0.000164759
0.00156	0.000148876
0.00158	0.00013531
0.0016	0.000123722
0.00162	0.000113824
0.00164	0.00010537
0.00166	9.81E-05
0.00168	9.20E-05
0.0017	8.67E-05
0.00172	8.22E-05
0.00174	7.84E-05
0.00176	7.51E-05
0.00178	7.23E-05
0.0018	6.99E-05
0.00182	6.78E-05
0.00184	6.61E-05
0.00186	6.46E-05
0.00188	6.33E-05
0.0019	6.22E-05
0.00192	6.13E-05
0.00194	6.05E-05
0.00196	5.98E-05
0.00198	5.92E-05

0.002	5.88E-05

Table 9.16: ‘S’ Shaped Pivot with Delta Angled Electrostatic Plates DPDT Switch (Upper Contact Release)

Time (s)	Displacement (µm)
1.00E-05	2.71528
2.00E-05	2.71529
3.00E-05	2.7153
4.00E-05	2.7153
5.00E-05	2.71531
6.00E-05	2.71532
7.00E-05	2.71532
8.00E-05	2.71533
9.00E-05	2.71533
0.0001	2.71533
0.00011	2.71534
0.00012	2.71534
0.00013	2.71534
0.00014	2.71535
0.00015	2.71535
0.00016	2.71535
0.00017	2.71535
0.00018	2.71535
0.00019	2.71536
0.0002	2.71536
0.00021	2.71528
0.00022	2.71514
0.00023	2.71496
0.00024	2.71475
0.00025	2.71451
0.00026	2.71426
0.00027	2.6922
0.00028	2.62427
0.00029	2.50456
0.0003	2.34223
0.00031	2.15348
0.00032	1.95432
0.00033	1.75647
0.00034	1.56721
0.00035	1.39063
0.00036	1.22869
0.00037	1.08202
0.00038	0.950393
0.00039	0.833081

0.0004	0.729077
0.00041	0.637246
0.00042	0.55642
0.00043	0.485454
0.00044	0.423269
0.00045	0.368861
0.00046	0.321315
0.00047	0.279807
0.00048	0.243598
0.00049	0.21203
0.0005	0.184522
0.00051	0.160562
0.00052	0.139698
0.00053	0.121534
0.00054	0.105725
0.00055	0.0919679
0.00056	0.0799971
0.00057	0.069582
0.00058	0.0605213
0.00059	0.0526392
0.0006	0.0457829
0.00061	0.0398191
0.00062	0.0346318
0.00063	0.03012
0.00064	0.0261958
0.00065	0.0227828
0.00066	0.0198144
0.00067	0.0172327
0.00068	0.0149874
0.00069	0.0130346
0.0007	0.0113362
0.00071	0.00985915
0.00072	0.00857454
0.00073	0.00745732
0.00074	0.00648567
0.00075	0.00564063
0.00076	0.0049057
0.00077	0.00426654
0.00078	0.00371066
0.00079	0.00322721
0.0008	0.00280675
0.00081	0.00244108
0.00082	0.00212305
0.00083	0.00184646

0.00084	0.00160591
0.00085	0.00139671
0.00086	0.00121475
0.00087	0.00105651
0.00088	0.000918884
0.00089	0.000799188
0.0009	0.000695086
0.00091	0.000604547
0.00092	0.000525803
0.00093	0.000457317
0.00094	0.000397754
0.00095	0.00034595
0.00096	0.000300894
0.00097	0.000261707
0.00098	0.000227625
0.00099	0.000197983
0.001	0.000172201
0.00101	0.000149778
0.00102	0.000130275
0.00103	0.000113313
0.00104	9.86E-05
0.00105	8.57E-05
0.00106	7.46E-05
0.00107	6.49E-05
0.00108	5.64E-05
0.00109	4.91E-05
0.0011	4.27E-05
0.00111	3.71E-05
0.00112	3.23E-05
0.00113	2.81E-05
0.00114	2.44E-05
0.00115	2.13E-05
0.00116	1.85E-05
0.00117	1.61E-05
0.00118	1.40E-05
0.00119	1.22E-05
0.0012	1.06E-05
0.00121	9.21E-06
0.00122	8.01E-06
0.00123	6.97E-06
0.00124	6.07E-06
0.00125	5.28E-06
0.00126	4.59E-06
0.00127	3.99E-06

0.00128	3.47E-06
0.00129	3.02E-06
0.0013	2.63E-06
0.00131	2.29E-06
0.00132	1.99E-06
0.00133	1.73E-06
0.00134	1.51E-06
0.00135	1.31E-06
0.00136	1.14E-06
0.00137	9.93E-07
0.00138	8.64E-07
0.00139	7.52E-07
0.0014	6.55E-07
0.00141	5.70E-07
0.00142	4.96E-07
0.00143	4.31E-07
0.00144	3.75E-07
0.00145	3.27E-07
0.00146	2.84E-07
0.00147	2.48E-07
0.00148	2.16E-07
0.00149	1.88E-07
0.0015	1.63E-07
0.00151	1.42E-07
0.00152	1.24E-07
0.00153	1.08E-07
0.00154	9.38E-08
0.00155	8.17E-08
0.00156	7.11E-08
0.00157	6.19E-08
0.00158	5.39E-08
0.00159	4.70E-08
0.0016	4.09E-08
0.00161	3.56E-08
0.00162	3.10E-08
0.00163	2.70E-08
0.00164	2.35E-08
0.00165	2.05E-08
0.00166	1.79E-08
0.00167	1.56E-08
0.00168	1.36E-08
0.00169	1.18E-08
0.0017	1.03E-08
0.00171	8.98E-09

0.00172	7.82E-09
0.00173	6.82E-09
0.00174	5.95E-09
0.00175	5.18E-09
0.00176	4.52E-09
0.00177	3.94E-09
0.00178	3.44E-09
0.00179	3.00E-09
0.0018	2.62E-09
0.00181	2.28E-09
0.00182	1.99E-09
0.00183	1.74E-09
0.00184	1.52E-09
0.00185	1.32E-09
0.00186	1.15E-09
0.00187	1.01E-09
0.00188	8.80E-10
0.00189	7.69E-10
0.0019	6.71E-10
0.00191	5.87E-10
0.00192	5.12E-10
0.00193	4.48E-10
0.00194	3.91E-10
0.00195	3.42E-10
0.00196	2.99E-10
0.00197	2.62E-10
0.00198	2.29E-10
0.00199	2.00E-10
0.002	1.75E-10

Table 9.17: ‘S’ Shaped Pivot with Delta Angled Electrostatic Plates DPDT Switch (Lower Contact Release)

Time (s)	**Displacement (µm)**
1.00E-05	-2.71656
2.00E-05	-2.71656
3.00E-05	-2.71656
4.00E-05	-2.71656
5.00E-05	-2.71656
6.00E-05	-2.71656
7.00E-05	-2.71656
8.00E-05	-2.71656
9.00E-05	-2.71656
0.0001	-2.71656

0.00011	-2.71656
0.00012	-2.71656
0.00013	-2.71656
0.00014	-2.71656
0.00015	-2.71656
0.00016	-2.71656
0.00017	-2.71656
0.00018	-2.71656
0.00019	-2.71656
0.0002	-2.71656
0.00021	-2.71656
0.00022	-2.71656
0.00023	-2.71656
0.00024	-2.71656
0.00025	-2.71656
0.00026	-2.71656
0.00027	-2.69463
0.00028	-2.62675
0.00029	-2.50699
0.0003	-2.34453
0.00031	-2.15561
0.00032	-1.95626
0.00033	-1.75821
0.00034	-1.56876
0.00035	-1.39198
0.00036	-1.22988
0.00037	-1.08305
0.00038	-0.951289
0.00039	-0.833855
0.0004	-0.729744
0.00041	-0.637818
0.00042	-0.556909
0.00043	-0.485873
0.00044	-0.423626
0.00045	-0.369164
0.00046	-0.321573
0.00047	-0.280025
0.00048	-0.243782
0.00049	-0.212185
0.0005	-0.184652
0.00051	-0.160671
0.00052	-0.139789
0.00053	-0.12161
0.00054	-0.105788

0.00055	-0.0920196
0.00056	-0.0800395
0.00057	-0.0696165
0.00058	-0.0605492
0.00059	-0.0526616
0.0006	-0.0458006
0.00061	-0.0398329
0.00062	-0.0346424
0.00063	-0.0301279
0.00064	-0.0262015
0.00065	-0.0227867
0.00066	-0.0198168
0.00067	-0.0172339
0.00068	-0.0149877
0.00069	-0.0130341
0.0007	-0.0113352
0.00071	-0.00985766
0.00072	-0.00857272
0.00073	-0.00745526
0.00074	-0.00648345
0.00075	-0.00563831
0.00076	-0.00490333
0.00077	-0.00426416
0.00078	-0.0037083
0.00079	-0.00322489
0.0008	-0.0028045
0.00081	-0.00243891
0.00082	-0.00212097
0.00083	-0.00184448
0.00084	-0.00160403
0.00085	-0.00139493
0.00086	-0.00121308
0.00087	-0.00105494
0.00088	-0.000917408
0.00089	-0.000797808
0.0009	-0.0006938
0.00091	-0.00060335
0.00092	-0.000524691
0.00093	-0.000456286
0.00094	-0.000396799
0.00095	-0.000345066
0.00096	-0.000300078
0.00097	-0.000260955
0.00098	-0.000226932

0.00099	-0.000197345
0.001	-0.000171615
0.00101	-0.000149239
0.00102	-0.00012978
0.00103	-0.000112859
0.00104	-9.81E-05
0.00105	-8.53E-05
0.00106	-7.42E-05
0.00107	-6.45E-05
0.00108	-5.61E-05
0.00109	-4.88E-05
0.0011	-4.24E-05
0.00111	-3.69E-05
0.00112	-3.21E-05
0.00113	-2.79E-05
0.00114	-2.43E-05
0.00115	-2.11E-05
0.00116	-1.84E-05
0.00117	-1.60E-05
0.00118	-1.39E-05
0.00119	-1.21E-05
0.0012	-1.05E-05
0.00121	-9.12E-06
0.00122	-7.93E-06
0.00123	-6.90E-06
0.00124	-6.00E-06
0.00125	-5.22E-06
0.00126	-4.54E-06
0.00127	-3.94E-06
0.00128	-3.43E-06
0.00129	-2.98E-06
0.0013	-2.59E-06
0.00131	-2.25E-06
0.00132	-1.96E-06
0.00133	-1.70E-06
0.00134	-1.48E-06
0.00135	-1.29E-06
0.00136	-1.12E-06
0.00137	-9.74E-07
0.00138	-8.47E-07
0.00139	-7.37E-07
0.0014	-6.40E-07
0.00141	-5.57E-07
0.00142	-4.84E-07

0.00143	-4.21E-07
0.00144	-3.66E-07
0.00145	-3.18E-07
0.00146	-2.77E-07
0.00147	-2.40E-07
0.00148	-2.09E-07
0.00149	-1.82E-07
0.0015	-1.58E-07
0.00151	-1.37E-07
0.00152	-1.19E-07
0.00153	-1.04E-07
0.00154	-9.02E-08
0.00155	-7.84E-08
0.00156	-6.82E-08
0.00157	-5.93E-08
0.00158	-5.15E-08
0.00159	-4.48E-08
0.0016	-3.89E-08
0.00161	-3.38E-08
0.00162	-2.94E-08
0.00163	-2.56E-08
0.00164	-2.22E-08
0.00165	-1.93E-08
0.00166	-1.68E-08
0.00167	-1.46E-08
0.00168	-1.27E-08
0.00169	-1.10E-08
0.0017	-9.57E-09
0.00171	-8.32E-09
0.00172	-7.23E-09
0.00173	-6.28E-09
0.00174	-5.46E-09
0.00175	-4.74E-09
0.00176	-4.12E-09
0.00177	-3.58E-09
0.00178	-3.11E-09
0.00179	-2.70E-09
0.0018	-2.35E-09
0.00181	-2.04E-09
0.00182	-1.77E-09
0.00183	-1.54E-09
0.00184	-1.33E-09
0.00185	-1.16E-09
0.00186	-1.01E-09

0.00187	-8.74E-10
0.00188	-7.59E-10
0.00189	-6.59E-10
0.0019	-5.72E-10
0.00191	-4.97E-10
0.00192	-4.31E-10
0.00193	-3.74E-10
0.00194	-3.25E-10
0.00195	-2.82E-10
0.00196	-2.44E-10
0.00197	-2.12E-10
0.00198	-1.84E-10
0.00199	-1.60E-10
0.002	-1.38E-10

Table 9.18: 'S' Shaped Split Pivot with Delta Angled Electrostatic Plates DPDT Switch (Upper Contact Release)

Time (s)	**Displacement (µm)**
5.00E-06	2.71475
1.00E-05	2.71485
1.50E-05	2.71487
2.00E-05	2.71488
2.50E-05	2.7149
3.00E-05	2.71491
3.50E-05	2.71493
4.00E-05	2.71494
4.50E-05	2.71495
5.00E-05	2.71496
5.50E-05	2.71497
6.00E-05	2.71498
6.50E-05	2.71499
7.00E-05	2.715
7.50E-05	2.71501
8.00E-05	2.71502
8.50E-05	2.71503
9.00E-05	2.71504
9.50E-05	2.71504
0.0001	2.71505
0.000105	2.71506
0.00011	2.71506
0.000115	2.71507
0.00012	2.71507
0.000125	2.71508

0.00013	2.71508
0.000135	2.71509
0.00014	2.71509
0.000145	2.7151
0.00015	2.7151
0.000155	2.71511
0.00016	2.71511
0.000165	2.71511
0.00017	2.71512
0.000175	2.71512
0.00018	2.71512
0.000185	2.71513
0.00019	2.71513
0.000195	2.71513
0.0002	2.71513
0.000205	2.71514
0.00021	2.71511
0.000215	2.71507
0.00022	2.71502
0.000225	2.71495
0.00023	2.71488
0.000235	2.71479
0.00024	2.71469
0.000245	2.71459
0.00025	2.71449
0.000255	2.71437
0.00026	2.71426
0.000265	2.71186
0.00027	2.70334
0.000275	2.68538
0.00028	2.65585
0.000285	2.61371
0.00029	2.55896
0.000295	2.49252
0.0003	2.41595
0.000305	2.33125
0.00031	2.24052
0.000315	2.14573
0.00032	2.04854
0.000325	1.95034
0.00033	1.85227
0.000335	1.75523
0.00034	1.65996
0.000345	1.56703

0.00035	1.47688
0.000355	1.38984
0.00036	1.30614
0.000365	1.22596
0.00037	1.14938
0.000375	1.07644
0.00038	1.00716
0.000385	0.941482
0.00039	0.879358
0.000395	0.820699
0.0004	0.765405
0.000405	0.71336
0.00041	0.664441
0.000415	0.618519
0.00042	0.575459
0.000425	0.535127
0.00043	0.497387
0.000435	0.462103
0.00044	0.429145
0.000445	0.398382
0.00045	0.36969
0.000455	0.342946
0.00046	0.318035
0.000465	0.294844
0.00047	0.273266
0.000475	0.253199
0.00048	0.234546
0.000485	0.217215
0.00049	0.20112
0.000495	0.186178
0.0005	0.172312
0.000505	0.159448
0.00051	0.147518
0.000515	0.136458
0.00052	0.126206
0.000525	0.116708
0.00053	0.107908
0.000535	0.099759
0.00054	0.0922134
0.000545	0.0852282
0.00055	0.0787631
0.000555	0.0727806
0.00056	0.0672455
0.000565	0.0621254

0.00057	0.0573898
0.000575	0.0530106
0.00058	0.0489615
0.000585	0.0452182
0.00059	0.0417579
0.000595	0.0385597
0.0006	0.0356041
0.000605	0.032873
0.00061	0.0303495
0.000615	0.0280182
0.00062	0.0258645
0.000625	0.0238752
0.00063	0.0220378
0.000635	0.0203409
0.00064	0.0187739
0.000645	0.0173268
0.00065	0.0159907
0.000655	0.014757
0.00066	0.0136181
0.000665	0.0125666
0.00067	0.011596
0.000675	0.0107
0.00068	0.00987294
0.000685	0.00910958
0.00069	0.00840504
0.000695	0.0077548
0.0007	0.0071547
0.000705	0.0066009
0.00071	0.00608985
0.000715	0.00561825
0.00072	0.00518309
0.000725	0.00478154
0.00073	0.00441104
0.000735	0.00406919
0.00074	0.00375377
0.000745	0.00346276
0.00075	0.00319427
0.000755	0.00294656
0.00076	0.00271804
0.000765	0.00250721
0.00077	0.00231271
0.000775	0.00213328
0.00078	0.00196776
0.000785	0.00181507

0.00079	0.00167421
0.000795	0.00154427
0.0008	0.00142441
0.000805	0.00131385
0.00081	0.00121186
0.000815	0.00111779
0.00082	0.00103101
0.000825	0.000950969
0.00083	0.000877137
0.000835	0.000809036
0.00084	0.00074622
0.000845	0.000688281
0.00085	0.000634839
0.000855	0.000585546
0.00086	0.00054008
0.000865	0.000498145
0.00087	0.000459465
0.000875	0.00042379
0.00088	0.000390884
0.000885	0.000360534
0.00089	0.000332541
0.000895	0.000306722
0.0009	0.000282909
0.000905	0.000260945
0.00091	0.000240686
0.000915	0.000222002
0.00092	0.000204768
0.000925	0.000188873
0.00093	0.000174213
0.000935	0.000160691
0.00094	0.000148219
0.000945	0.000136716
0.00095	0.000126107
0.000955	0.000116321
0.00096	0.000107296
0.000965	9.90E-05
0.00097	9.13E-05
0.000975	8.42E-05
0.00098	7.77E-05
0.000985	7.17E-05
0.00099	6.61E-05
0.000995	6.10E-05
0.001	5.62E-05
0.001005	5.19E-05

0.00101	4.79E-05
0.001015	4.42E-05
0.00102	4.07E-05
0.001025	3.76E-05
0.00103	3.47E-05
0.001035	3.20E-05
0.00104	2.95E-05
0.001045	2.72E-05
0.00105	2.51E-05
0.001055	2.32E-05
0.00106	2.14E-05
0.001065	1.97E-05
0.00107	1.82E-05
0.001075	1.68E-05
0.00108	1.55E-05
0.001085	1.43E-05
0.00109	1.32E-05
0.001095	1.22E-05
0.0011	1.12E-05
0.001105	1.04E-05
0.00111	9.56E-06
0.001115	8.82E-06
0.00112	8.14E-06
0.001125	7.51E-06
0.00113	6.93E-06
0.001135	6.39E-06
0.00114	5.90E-06
0.001145	5.45E-06
0.00115	5.03E-06
0.001155	4.64E-06
0.00116	4.28E-06
0.001165	3.95E-06
0.00117	3.65E-06
0.001175	3.37E-06
0.00118	3.11E-06
0.001185	2.87E-06
0.00119	2.65E-06
0.001195	2.44E-06
0.0012	2.26E-06
0.001205	2.08E-06
0.00121	1.92E-06
0.001215	1.78E-06
0.00122	1.64E-06
0.001225	1.51E-06

0.00123	1.40E-06
0.001235	1.29E-06
0.00124	1.19E-06
0.001245	1.10E-06
0.00125	1.02E-06
0.001255	9.39E-07
0.00126	8.67E-07
0.001265	8.01E-07
0.00127	7.40E-07
0.001275	6.83E-07
0.00128	6.31E-07
0.001285	5.83E-07
0.00129	5.39E-07
0.001295	4.98E-07
0.0013	4.60E-07
0.001305	4.25E-07
0.00131	3.93E-07
0.001315	3.63E-07
0.00132	3.36E-07
0.001325	3.10E-07
0.00133	2.87E-07
0.001335	2.65E-07
0.00134	2.45E-07
0.001345	2.27E-07
0.00135	2.09E-07
0.001355	1.94E-07
0.00136	1.79E-07
0.001365	1.66E-07
0.00137	1.53E-07
0.001375	1.42E-07
0.00138	1.31E-07
0.001385	1.21E-07
0.00139	1.12E-07
0.001395	1.04E-07
0.0014	9.61E-08
0.001405	8.89E-08
0.00141	8.23E-08
0.001415	7.62E-08
0.00142	7.05E-08
0.001425	6.53E-08
0.00143	6.05E-08
0.001435	5.60E-08
0.00144	5.19E-08
0.001445	4.80E-08

0.00145	4.45E-08
0.001455	4.12E-08
0.00146	3.82E-08
0.001465	3.54E-08
0.00147	3.28E-08
0.001475	3.04E-08
0.00148	2.82E-08
0.001485	2.62E-08
0.00149	2.43E-08
0.001495	2.25E-08
0.0015	2.09E-08
0.001505	1.94E-08
0.00151	1.80E-08
0.001515	1.67E-08
0.00152	1.55E-08
0.001525	1.44E-08
0.00153	1.34E-08
0.001535	1.24E-08
0.00154	1.15E-08
0.001545	1.07E-08
0.00155	9.94E-09
0.001555	9.24E-09
0.00156	8.59E-09
0.001565	7.99E-09
0.00157	7.43E-09
0.001575	6.91E-09
0.00158	6.43E-09
0.001585	5.98E-09
0.00159	5.56E-09
0.001595	5.18E-09
0.0016	4.82E-09
0.001605	4.49E-09
0.00161	4.18E-09
0.001615	3.90E-09
0.00162	3.63E-09
0.001625	3.38E-09
0.00163	3.15E-09
0.001635	2.94E-09
0.00164	2.74E-09
0.001645	2.56E-09
0.00165	2.39E-09
0.001655	2.23E-09
0.00166	2.08E-09
0.001665	1.94E-09

0.00167	1.81E-09
0.001675	1.69E-09
0.00168	1.58E-09
0.001685	1.48E-09
0.00169	1.38E-09
0.001695	1.29E-09
0.0017	1.21E-09
0.001705	1.13E-09
0.00171	1.06E-09
0.001715	9.90E-10
0.00172	9.26E-10
0.001725	8.67E-10
0.00173	8.12E-10
0.001735	7.61E-10
0.00174	7.13E-10
0.001745	6.68E-10
0.00175	6.26E-10
0.001755	5.87E-10
0.00176	5.51E-10
0.001765	5.17E-10
0.00177	4.85E-10
0.001775	4.55E-10
0.00178	4.27E-10
0.001785	4.01E-10
0.00179	3.77E-10
0.001795	3.54E-10
0.0018	3.33E-10
0.001805	3.13E-10
0.00181	2.94E-10
0.001815	2.76E-10
0.00182	2.60E-10
0.001825	2.44E-10
0.00183	2.30E-10
0.001835	2.16E-10
0.00184	2.04E-10
0.001845	1.92E-10
0.00185	1.81E-10
0.001855	1.70E-10
0.00186	1.60E-10
0.001865	1.51E-10
0.00187	1.42E-10
0.001875	1.34E-10
0.00188	1.27E-10
0.001885	1.19E-10

0.00189	1.13E-10
0.001895	1.06E-10
0.0019	1.00E-10
0.001905	9.46E-11
0.00191	8.92E-11
0.001915	8.43E-11
0.00192	7.96E-11
0.001925	7.51E-11
0.00193	7.10E-11
0.001935	6.70E-11
0.00194	6.33E-11
0.001945	5.99E-11
0.00195	5.66E-11
0.001955	5.35E-11
0.00196	5.06E-11
0.001965	4.78E-11
0.00197	4.52E-11
0.001975	4.28E-11
0.00198	4.05E-11
0.001985	3.83E-11
0.00199	3.62E-11
0.001995	3.43E-11
0.002	3.24E-11

Table 9.19: ‘S’ Shaped Split Pivot with Delta Angled Electrostatic Plates DPDT Switch (Lower Contact Release)

Time (s)	**Displacement (µm)**
5.00E-06	-2.71656
1.00E-05	-2.71656
1.50E-05	-2.71656
2.00E-05	-2.71656
2.50E-05	-2.71656
3.00E-05	-2.71656
3.50E-05	-2.71656
4.00E-05	-2.71656
4.50E-05	-2.71656
5.00E-05	-2.71656
5.50E-05	-2.71656
6.00E-05	-2.71656
6.50E-05	-2.71656
7.00E-05	-2.71656
7.50E-05	-2.71656
8.00E-05	-2.71656

8.50E-05	-2.71656
9.00E-05	-2.71656
9.50E-05	-2.71656
0.0001	-2.71656
0.000105	-2.71656
0.00011	-2.71656
0.000115	-2.71656
0.00012	-2.71656
0.000125	-2.71656
0.00013	-2.71656
0.000135	-2.71656
0.00014	-2.71656
0.000145	-2.71656
0.00015	-2.71656
0.000155	-2.71656
0.00016	-2.71656
0.000165	-2.71656
0.00017	-2.71656
0.000175	-2.71656
0.00018	-2.71656
0.000185	-2.71656
0.00019	-2.71656
0.000195	-2.71656
0.0002	-2.71656
0.000205	-2.71656
0.00021	-2.71656
0.000215	-2.71656
0.00022	-2.71656
0.000225	-2.71656
0.00023	-2.71656
0.000235	-2.71656
0.00024	-2.71656
0.000245	-2.71656
0.00025	-2.71656
0.000255	-2.71656
0.00026	-2.71656
0.000265	-2.71425
0.00027	-2.7058
0.000275	-2.6879
0.00028	-2.65839
0.000285	-2.61625
0.00029	-2.56149
0.000295	-2.495
0.0003	-2.41837

0.000305	-2.3336
0.00031	-2.24279
0.000315	-2.1479
0.00032	-2.05062
0.000325	-1.95232
0.00033	-1.85415
0.000335	-1.75701
0.00034	-1.66164
0.000345	-1.56861
0.00035	-1.47836
0.000355	-1.39123
0.00036	-1.30745
0.000365	-1.22717
0.00037	-1.15051
0.000375	-1.0775
0.00038	-1.00814
0.000385	-0.942392
0.00039	-0.880201
0.000395	-0.82148
0.0004	-0.766126
0.000405	-0.714026
0.00041	-0.665056
0.000415	-0.619085
0.00042	-0.57598
0.000425	-0.535606
0.00043	-0.497826
0.000435	-0.462506
0.00044	-0.429514
0.000445	-0.39872
0.00045	-0.369998
0.000455	-0.343228
0.00046	-0.318291
0.000465	-0.295077
0.00047	-0.273478
0.000475	-0.253391
0.00048	-0.23472
0.000485	-0.217373
0.00049	-0.201263
0.000495	-0.186307
0.0005	-0.172427
0.000505	-0.159552
0.00051	-0.147611
0.000515	-0.136541
0.00052	-0.126281

0.000525	-0.116774
0.00053	-0.107967
0.000535	-0.0998109
0.00054	-0.0922591
0.000545	-0.0852682
0.00055	-0.078798
0.000555	-0.0728108
0.00056	-0.0672716
0.000565	-0.0621477
0.00057	-0.0574087
0.000575	-0.0530264
0.00058	-0.0489745
0.000585	-0.0452287
0.00059	-0.0417662
0.000595	-0.038566
0.0006	-0.0356086
0.000605	-0.0328759
0.00061	-0.030351
0.000615	-0.0280185
0.00062	-0.0258637
0.000625	-0.0238735
0.00063	-0.0220352
0.000635	-0.0203376
0.00064	-0.0187699
0.000645	-0.0173223
0.00065	-0.0159857
0.000655	-0.0147517
0.00066	-0.0136124
0.000665	-0.0125607
0.00067	-0.0115899
0.000675	-0.0106937
0.00068	-0.00986658
0.000685	-0.00910315
0.00069	-0.00839856
0.000695	-0.00774831
0.0007	-0.00714822
0.000705	-0.00659446
0.00071	-0.00608346
0.000715	-0.00561194
0.00072	-0.00517686
0.000725	-0.00477542
0.00073	-0.00440502
0.000735	-0.00406329
0.00074	-0.003748

0.000745	-0.00345712
0.00075	-0.00318877
0.000755	-0.00294121
0.00076	-0.00271283
0.000765	-0.00250214
0.00077	-0.0023078
0.000775	-0.00212852
0.00078	-0.00196314
0.000785	-0.0018106
0.00079	-0.00166989
0.000795	-0.00154009
0.0008	-0.00142038
0.000805	-0.00130996
0.00081	-0.00120811
0.000815	-0.00111417
0.00082	-0.00102752
0.000825	-0.000947609
0.00083	-0.000873903
0.000835	-0.000805925
0.00084	-0.000743229
0.000845	-0.000685406
0.00085	-0.000632077
0.000855	-0.000582894
0.00086	-0.000537535
0.000865	-0.000495702
0.00087	-0.000457122
0.000875	-0.000421543
0.00088	-0.00038873
0.000885	-0.00035847
0.00089	-0.000330563
0.000895	-0.000304828
0.0009	-0.000281094
0.000905	-0.000259208
0.00091	-0.000239024
0.000915	-0.000220411
0.00092	-0.000203246
0.000925	-0.000187417
0.00093	-0.00017282
0.000935	-0.000159359
0.00094	-0.000146947
0.000945	-0.0001355
0.00095	-0.000124944
0.000955	-0.00011521
0.00096	-0.000106234

0.000965	-9.80E-05
0.00097	-9.03E-05
0.000975	-8.33E-05
0.00098	-7.68E-05
0.000985	-7.08E-05
0.00099	-6.53E-05
0.000995	-6.02E-05
0.001	-5.55E-05
0.001005	-5.12E-05
0.00101	-4.72E-05
0.001015	-4.35E-05
0.00102	-4.01E-05
0.001025	-3.70E-05
0.00103	-3.41E-05
0.001035	-3.15E-05
0.00104	-2.90E-05
0.001045	-2.67E-05
0.00105	-2.47E-05
0.001055	-2.27E-05
0.00106	-2.10E-05
0.001065	-1.93E-05
0.00107	-1.78E-05
0.001075	-1.64E-05
0.00108	-1.51E-05
0.001085	-1.40E-05
0.00109	-1.29E-05
0.001095	-1.19E-05
0.0011	-1.09E-05
0.001105	-1.01E-05
0.00111	-9.30E-06
0.001115	-8.57E-06
0.00112	-7.90E-06
0.001125	-7.29E-06
0.00113	-6.72E-06
0.001135	-6.19E-06
0.00114	-5.71E-06
0.001145	-5.26E-06
0.00115	-4.85E-06
0.001155	-4.47E-06
0.00116	-4.12E-06
0.001165	-3.80E-06
0.00117	-3.50E-06
0.001175	-3.23E-06
0.00118	-2.98E-06

0.001185	-2.75E-06
0.00119	-2.53E-06
0.001195	-2.33E-06
0.0012	-2.15E-06
0.001205	-1.98E-06
0.00121	-1.83E-06
0.001215	-1.68E-06
0.00122	-1.55E-06
0.001225	-1.43E-06
0.00123	-1.32E-06
0.001235	-1.22E-06
0.00124	-1.12E-06
0.001245	-1.03E-06
0.00125	-9.52E-07
0.001255	-8.77E-07
0.00126	-8.08E-07
0.001265	-7.45E-07
0.00127	-6.87E-07
0.001275	-6.33E-07
0.00128	-5.83E-07
0.001285	-5.37E-07
0.00129	-4.95E-07
0.001295	-4.56E-07
0.0013	-4.20E-07
0.001305	-3.87E-07
0.00131	-3.57E-07
0.001315	-3.29E-07
0.00132	-3.03E-07
0.001325	-2.79E-07
0.00133	-2.57E-07
0.001335	-2.37E-07
0.00134	-2.18E-07
0.001345	-2.01E-07
0.00135	-1.85E-07
0.001355	-1.71E-07
0.00136	-1.57E-07
0.001365	-1.45E-07
0.00137	-1.33E-07
0.001375	-1.23E-07
0.00138	-1.13E-07
0.001385	-1.04E-07
0.00139	-9.60E-08
0.001395	-8.84E-08
0.0014	-8.14E-08

0.001405	-7.50E-08
0.00141	-6.90E-08
0.001415	-6.36E-08
0.00142	-5.85E-08
0.001425	-5.39E-08
0.00143	-4.96E-08
0.001435	-4.56E-08
0.00144	-4.20E-08
0.001445	-3.87E-08
0.00145	-3.56E-08
0.001455	-3.28E-08
0.00146	-3.01E-08
0.001465	-2.77E-08
0.00147	-2.55E-08
0.001475	-2.35E-08
0.00148	-2.16E-08
0.001485	-1.99E-08
0.00149	-1.83E-08
0.001495	-1.68E-08
0.0015	-1.55E-08
0.001505	-1.42E-08
0.00151	-1.31E-08
0.001515	-1.20E-08
0.00152	-1.11E-08
0.001525	-1.02E-08
0.00153	-9.34E-09
0.001535	-8.58E-09
0.00154	-7.89E-09
0.001545	-7.25E-09
0.00155	-6.66E-09
0.001555	-6.11E-09
0.00156	-5.62E-09
0.001565	-5.16E-09
0.00157	-4.73E-09
0.001575	-4.35E-09
0.00158	-3.99E-09
0.001585	-3.66E-09
0.00159	-3.36E-09
0.001595	-3.08E-09
0.0016	-2.83E-09
0.001605	-2.59E-09
0.00161	-2.38E-09
0.001615	-2.18E-09
0.00162	-2.00E-09

0.001625	-1.83E-09
0.00163	-1.68E-09
0.001635	-1.53E-09
0.00164	-1.40E-09
0.001645	-1.29E-09
0.00165	-1.18E-09
0.001655	-1.08E-09
0.00166	-9.84E-10
0.001665	-8.99E-10
0.00167	-8.22E-10
0.001675	-7.50E-10
0.00168	-6.85E-10
0.001685	-6.25E-10
0.00169	-5.70E-10
0.001695	-5.20E-10
0.0017	-4.74E-10
0.001705	-4.32E-10
0.00171	-3.93E-10
0.001715	-3.58E-10
0.00172	-3.25E-10
0.001725	-2.96E-10
0.00173	-2.68E-10
0.001735	-2.44E-10
0.00174	-2.21E-10
0.001745	-2.00E-10
0.00175	-1.81E-10
0.001755	-1.64E-10
0.00176	-1.48E-10
0.001765	-1.33E-10
0.00177	-1.20E-10
0.001775	-1.08E-10
0.00178	-9.73E-11
0.001785	-8.73E-11
0.00179	-7.83E-11
0.001795	-7.00E-11
0.0018	-6.25E-11
0.001805	-5.57E-11
0.00181	-4.95E-11
0.001815	-4.38E-11
0.00182	-3.87E-11
0.001825	-3.41E-11
0.00183	-2.99E-11
0.001835	-2.61E-11
0.00184	-2.27E-11

0.001845	-1.96E-11
0.00185	-1.68E-11
0.001855	-1.43E-11
0.00186	-1.21E-11
0.001865	-1.01E-11
0.00187	-8.26E-12
0.001875	-6.64E-12
0.00188	-5.19E-12
0.001885	-3.90E-12
0.00189	-2.76E-12
0.001895	-1.74E-12
0.0019	-8.43E-13
0.001905	-5.20E-14
0.00191	6.42E-13
0.001915	1.25E-12
0.00192	1.78E-12
0.001925	2.23E-12
0.00193	2.62E-12
0.001935	2.96E-12
0.00194	3.24E-12
0.001945	3.47E-12
0.00195	3.67E-12
0.001955	3.82E-12
0.00196	3.95E-12
0.001965	4.04E-12
0.00197	4.10E-12
0.001975	4.15E-12
0.00198	4.17E-12
0.001985	4.17E-12
0.00199	4.16E-12
0.001995	4.13E-12
0.002	4.09E-12